

**DEVELOPMENT OF A SPECTROSCOPIC METHOD FOR THE  
NON-DESTRUCTIVE ANALYSIS OF AUSTRALIAN  
ABORIGINAL OCHRE MATERIALS**



Kate Colyer

A thesis submitted in fulfilment of the requirements of the degree of  
Doctor of Philosophy

School of Chemical and Physical Sciences  
Flinders University, Adelaide, Australia.

May 2015



*for my family...*





i. **Declaration:**

I certify that this thesis does not incorporate without acknowledgment any material previously submitted for a degree or diploma in any university; and that to the best of my knowledge and belief it does not contain any material previously published or written by another person except where due reference is made in the text.

---

Kate Colyer

May 2015



ii. **Acknowledgements:**

On the first day of my PhD, I never could have imagined that the end point would see me here. So much has changed, both personally and academically, and it is quite overwhelming to think that this chapter of my life is closing. I also could never have imagined that out of a full thesis, this page would be the hardest to write! Yet here I am, almost paralysed by the fear that I will forget someone deeply important to the process, and concerned that any words I use will simply be inadequate in expressing my heartfelt thanks. So let me start by firstly sincerely apologising to anyone I may have forgotten – please know that your contribution and support was deeply appreciated.

On a professional level, there are many people to thank. A number of individuals and institutions have shared their knowledge and equipment with me throughout this process, and without them many of the results presented here would not have been possible. Thank you to Associate Research Professor David Beatie from The Ian Wark Research Institute for the use of and assistance with the raman instrument, to Peter Self from the Commonwealth Scientific Industrial Research Organisation for the use of and assistance with in-situ X-ray diffraction experiments, to Professor Jani Matisson and Pamela Solomon, formally from Flinders University, for their assistance with and use of the thermal gravimetric analysis instrument, and Dr Rachel Popelka-Filcoff and all the staff involved with the undertaking of neutron activation analysis at The Australian Nuclear Science and Technology Organisation.

My sincere thanks is also extended to Professor Allan Pring and Dr Keryn Walsh from the Museum of South Australia, and Peter Self from Adelaide Microscopy and The University of Adelaide for their overall guidance with this project. A special mention to Michael Snow from the Museum of South Australia for introducing me to the EFI ES-1000/i1Pro, a handheld colour spectrometer that became instrumental to the progression of this work. Thank you also to Allstone Pty Ltd for the donation of samples.

No project would be possible without the input of supervisors, and I feel very lucky to have been supported by a rather large team. Thank you to Dr Rachel Popelka-Filcoff – the newest member of the team only coming to Flinders University part-way through this project. Thank you for your guidance and input, and for the use of your lab. Your ochre expertise has been invaluable. Thank you to Assoc. Prof Jamie Quinton – my original supervisor – for believing in me from the beginning, for giving me this opportunity, and for your friendship. And finally, I would like to extend my deepest thanks to my primary supervisor, Assoc. Prof Claire Lenehan. Thank you for accepting me as your student part-way through this project when it evolved into a somewhat different direction and it became clear that a different area of expertise was required. Thank you for all your assistance throughout the whole project, and for welcoming me into your group.

As well as supervisors, fellow students shape not only life at university but life outside. I have had the pleasure of being included in a number of groups throughout this project and have worked closely with many students. My heartfelt thanks to you all for the memories we have made along the way. Special mention to Adam Blanch and Anders Barlow, both now Drs, for accepting me as an intruder into the pink room, and to Lauren Hyde for sharing many a Subway lunch with me. A special mention is also necessary for Samuel Wallace – a dear friend from honours and beyond – thank you for the many pizza nights, the laughter and the tears, and for a friendship that will last a lifetime.

As important as friends are in life, family is even more so, and I am eternally grateful for my wonderful family. I have a large immediate and extended family, and the support from all of you has been invaluable. But there are some who deserve special mention, so thank you to my mum for her free babysitting (she made me promise I would write that! But sincerely thank you – my children love you almost as much as I do), and for pushing me to be the best that I can be. To my dad – I know I don't have to, but here is another nice gesture for you – simply thank you. Thank you to my husband Chris, the original Dr Colyer, for everything you have done – I'm sure that I never would have finished this without you by my side.

And finally, to my children, Melanie, Jessica and Benjamin – thank you for giving me a love I never knew existed, for showing me the world through a child's eyes, for putting the triumphs and the failures in perspective, and for giving me three reasons to be the best person and mummy that I can be. This thesis is for you – may it one day inspire you to reach for the stars.

### iii. **Summary:**

This thesis details the work undertaken towards and the results obtained from the development of a portable and non-destructive technique for the analysis of Australian Aboriginal ochre materials. Many of the methods traditionally utilised for analysis are limiting due to their cost, lack of portability, the sample requirements and the destructive nature of analysis. This thesis explores these traditional methods before developing and optimising a spectroscopy based technique that reduces or eliminates many of these and other limitations.

Chapter one explores the historical context of pigments. It investigates what a pigment is chemically and visually, whilst exploring many of the pigments used throughout the ages and their evolution over time across the globe. This chapter then discusses early pigments commonly utilised in Australia, and focuses on ochre as the main pigment used by Aboriginal Australians. This study focuses on the significance of ochre to the Aboriginal culture, the chemistry of ochre and the factors that influence its varied colour, and how the structure of ochre changes with heat treatments. This chapter investigates previous scientific studies conducted on ochre and similar pigments across the globe. It explores the work of others and investigates the analytical methods and instrumentation used for analysis, the results obtained from this work, and the advantages and disadvantages of each technique utilised.

Chapter two focuses on the characterisation of ochre samples via the use of commonly utilised traditional analytical techniques including X-Ray diffraction analysis, neutron activation analysis, infrared analysis, Raman spectroscopy and thermal gravimetric analysis. The analysis concentrates on ten samples obtained by the mining commission chosen because their colour and composition varied, their province was known, they were from a trusted source and they had been used in previous studies thus allowing for accurate comparisons. It details the experimental methods used for the work completed for this project. It denotes the sample type, locality and province studied, the chemical composition of standards, the instrument models used for any analysis, and the modes of operation and specific parameters used. These samples are analysed using the traditional methods of analysis discussed in chapter one, and results are presented.

Chapter three is a preliminary study into the use of a newly emerging instrument known as the X-Rite i1Pro. This instrument is UV-based, portable and non-destructive, and its application to ochre and similar pigments is novel. This chapter discusses the technical aspects of the instrument and the experimental setups utilised before exploring the feasibility of such an application by studying a range of haematite and goethite standards of known mixture compositions. This chapter explores the instruments' ability to detect colour and distinguish between samples of varying colour, before determining the accuracy and reproducibility of these measurements. Experiments then move from standards to the mining samples discussed previously and this chapter presents the results of their analysis with this new and emerging technique. The range of samples is then expanded to include some from an

ethnographic collection, and are also analysed utilising a traditional, laboratory based, bench top grade UV-vis, with the results of the two instruments compared. Work expands to establish a suitable model for the prediction of sample composition, again centring on a range of haematite and goethite standards of known mixture compositions and investigates a number of statistical methods of analysis. Studies include single wave length analysis, a model based on  $\Delta E$ , and multiple linear regression analysis. The results of each model are presented here. This chapter also investigates the effect of a variety of sample preparation methods to explore the suitability of this instrument to artefacts and images of unknown origin. It explores the effect of sample thickness, and application method including the use of a variety of binders. Statistical analysis is completed in this chapter.

Chapter four focuses on the effect of the substrate on the i1Pro results, as it is hypothesised that factors such as surface roughness and colour may influence the spectra obtained. A number of wood and stone based substrates are investigated, and the prediction models developed in chapter three are applied.

Chapter five explores the application of the X-Rite i1-Pro system to a number of well-provenanced raw ochre materials from well-known sites significant to Aboriginal Australians. This chapter aims to determine if the inter-site variation is smaller than the intra-site variation, and if the samples analysed from each site can be statistically linked with the hope that unknowns could be tested and preliminarily provenanced. This chapter presents background information, sample information, experimental methods and the results of the study including statistical analysis. The same raw ochre samples are then analysed utilising neutron activation analysis and the results of the two methods are compared.

Chapter six is a case study focusing on the application of the X-Rite i1-Pro system to toas of cultural significance to Aboriginal Australians. This chapter presents background information on the significance of the toas, sample information, experimental methods and the results of the study. Results include the statistical analysis of the spectra obtained, and comparisons between the ochre found on the toas and material identified as possible source material.

Chapter seven presents the conclusions reached from the research detailed here. It also presents hypotheses for ongoing work, and future directions for this and associated projects.

Appendix A presents a study completed into the formation of haematite via the dehydration of goethite. This is culturally significant as many sources and indeed colours of ochre were held in higher regard than others by Aboriginal Australians, and an understanding into the chemistry of alteration was necessary. This appendix presents background and sample information, as well as experimental techniques and results obtained from the use of both thermal gravimetric analysis studies and X-Ray diffraction analysis.

Appendix B presents a case study into the accumulation of a dust-like particle on the surface of Aboriginal Rock Art at Arkaroo Rock in the Flinders Ranges South Australia. Background information and photographs, experimental techniques and results of the analysis utilising

microscopy, X-ray diffraction, thermal gravimetric analysis and colour analysis with the X-Rite i1pro is presented here, along with subsequent statistical analysis. The results of this appendix were presented at International Symposium on Archaeometry, Tampa, Florida. This work has been published in The Open Journal of Archaeometry.

Appendix C presents supporting data – necessary for the details of the thesis and reference but not specifically relevant to each chapter or section.





iv. **Table of contents:**

<b>1. INTRODUCTION.....</b>	<b>1</b>
<b>1.1. Pigments .....</b>	<b>2</b>
1.1.1. Pigments and their use in artwork throughout history.....	2
<b>1.2. Ochre .....</b>	<b>14</b>
1.2.1. The significance of ochre in Australian Aboriginal culture .....	14
1.2.2. The chemistry of ochre and their varied colours.....	15
1.2.3. Structure of ochre.....	15
1.2.4. Factors that influence the colour of ochre.....	16
1.2.5. The dehydration of goethite to haematite .....	18
<b>1.3. Analysis of ochre.....</b>	<b>18</b>
1.3.1. Analysis of ochre utilising X-ray diffraction analysis and other X-ray based techniques.....	19
1.3.2. Spectroscopic and spectrometric analysis of ochre.....	25
1.3.3. Trace element methods.....	34
1.3.4. Analysis of ochre utilising non-traditional or multidisciplinary based techniques.....	36
<b>1.4. Provenance of ochre .....</b>	<b>40</b>
<b>1.5. Project scope.....</b>	<b>44</b>
<b>2. THE ANALYSIS OF OCHRE UTILISING TRADITIONAL METHODS .</b>	<b>47</b>
<b>2.1. Experimental methods .....</b>	<b>48</b>
2.1.1. X-Ray diffraction.....	48
2.1.2. Raman spectroscopy.....	48
2.1.3. Thermal gravimetric analysis.....	49
2.1.4. Infrared.....	49
2.1.5. Neutron activation analysis.....	49
<b>2.2. Sample Selection.....</b>	<b>49</b>
2.2.1. Natural ochres .....	49
2.2.2. Standards and reference materials .....	50
2.2.3. Sample selection based on techniques .....	50
<b>2.3. Sample preparation .....</b>	<b>51</b>

2.3.1.	X-Ray diffraction .....	51
2.3.2.	Raman spectroscopy .....	51
2.3.3.	Thermal gravimetric analysis .....	51
2.3.4.	Infrared .....	52
2.3.5.	Neutron activation analysis .....	52
<b>2.4.</b>	<b>Results and discussion .....</b>	<b>52</b>
2.4.1.	X-Ray diffraction .....	52
2.4.2.	Raman spectroscopy .....	57
2.4.3.	Thermal gravimetric analysis .....	61
2.4.4.	Infrared .....	65
2.4.5.	Neutron activation analysis .....	67
<b>2.5.</b>	<b>Conclusions .....</b>	<b>81</b>
<b>3.</b>	<b><u>A PRELIMINARY STUDY INTO THE SUITABILITY OF PORTABLE COLORIMETRY FOR THE ANALYSIS OF OCHRE MATERIALS .....</u></b>	<b><u>85</u></b>
<b>3.1.</b>	<b>Background instrumental information .....</b>	<b>86</b>
<b>3.2.</b>	<b>Experimental methods .....</b>	<b>88</b>
3.2.1.	Samples .....	88
3.2.2.	Experimental techniques .....	89
3.2.3.	Data analysis methods .....	90
<b>3.3.</b>	<b>Results and discussion .....</b>	<b>90</b>
3.3.1.	Application of the i1Pro to synthetic ochre standards .....	90
3.3.2.	Determining the reproducibility of results .....	90
3.3.3.	Detecting colour variations .....	96
3.3.4.	Comparison of the i1Pro to bench top grade instrumentation .....	99
3.3.5.	Investigating the effect of varying sample thickness .....	100
3.3.6.	Investigating the effect of varying sample application methods .....	101
3.3.7.	Comparison between ochre made with various pastes .....	104
3.3.8.	Use of i1Pro and derivative spectra to determine the composition of hematite/goethite mixtures .....	104
3.3.9.	Application of the i1Pro to 'real' samples .....	110
<b>3.4.</b>	<b>Conclusions .....</b>	<b>112</b>
<b>4.</b>	<b><u>APPLICATION OF THE I1-PRO AND PREDICTION MODELS TO A VARIETY OF SUBSTRATES .....</u></b>	<b><u>113</u></b>

<b>4.1.</b>	<b>Experimental Methods .....</b>	<b>114</b>
4.1.1.	Samples .....	114
4.1.2.	Experimental techniques .....	114
4.1.3.	Data analysis methods .....	114
<b>4.2.</b>	<b>Determining the instrument accuracy with application to varying substrates 116</b>	
<b>4.3.</b>	<b>Application of the composition prediction models to unknowns on alternate surfaces 119</b>	
4.3.1.	Single wavelength calibration .....	121
4.3.2.	Multiple linear regression analysis.....	124
<b>4.4.</b>	<b>Conclusions .....</b>	<b>129</b>
<b>5.</b>	<b><u>A STUDY INTO THE INTER-SITE AND INTRA-SITE VARIATION AT A NUMBER OF CULTURALLY SIGNIFICANT AUSTRALIAN SITES .....</u></b>	<b><u>131</u></b>
5.1.	Sample sites .....	132
5.2.	Sample preparation .....	133
5.3.	Colour analysis results .....	138
5.3.1.	Moana .....	139
5.3.2.	Wilgie Mia.....	141
5.3.3.	Bookartoo .....	142
5.3.4.	Comparison between all sites.....	143
5.3.5.	Conclusions.....	153
5.4.	Neutron activation analysis .....	154
5.5.	Conclusions .....	164
<b>6.</b>	<b><u>A CASE STUDY WITH THE APPLICATION OF THE i1PRO SYSTEM TO TOAS .....</u></b>	<b><u>167</u></b>
6.1.	Background information .....	168
6.2.	Toas investigated .....	169
6.3.	Experimental methods .....	170
6.4.	Results and discussion .....	171
6.4.1.	Raw ochre samples .....	171
6.4.2.	Toas .....	178
6.4.3.	Comparison between the raw samples and the toas.....	196

6.4.4.	Comparison between the raw material from the Reuther collection and the Bookartoo, Wilgie Mia and Moana samples studied previously .....	202
6.5.	<b>Conclusions .....</b>	<b>202</b>
<b>7.</b>	<b><u>CONCLUSIONS AND FUTURE WORK.....</u></b>	<b><u>205</u></b>
7.1.	Conclusions .....	206
7.2.	Future work .....	210
<b>8.</b>	<b><u>REFERENCES.....</u></b>	<b><u>211</u></b>
<b>9.</b>	<b><u>AN INVESTIGATION INTO THE GOETHITE DEHYDRATION MECHANISM .....</u></b>	<b><u>225</u></b>
9.1.	Background information and motivations .....	226
9.2.	TGA Studies: Variation of temperature.....	226
9.2.1.	Experimental methods .....	226
9.2.2.	Results.....	226
9.3.	X-Ray diffraction .....	227
9.3.1.	Experimental methods .....	227
9.3.2.	Results.....	229
<b>10.</b>	<b><u>ARKAROO ROCK - A CASE STUDY .....</u></b>	<b><u>235</u></b>
10.1.	Site location .....	236
10.2.	Samples .....	237
10.3.	Experimental methods .....	237
10.4.	Results.....	239
10.4.1.	Microscopy.....	239
10.4.2.	X-ray diffraction.....	239
10.4.3.	Thermal gravimetric analysis: .....	240
10.4.4.	Colour analysis utilising the EFI ES-1000:.....	240
10.4.5.	Statistical analysis .....	241
10.5.	Conclusions .....	242
<b>11.</b>	<b><u>SUPPORTING DATA.....</u></b>	<b><u>245</u></b>
11.1.	Results of the XRD analysis of the ten mining samples .....	246
11.2.	Results of the analysis of the ten mining samples utilising the i1Pro, both raw and normalised.....	248

<b>11.3.</b>	<b>Results of the analysis of Moana and Bookartoo ochres utilising both the i1Pro system and the Perkin-Elmer Lambda 950 bench top grade equipment .....</b>	<b>251</b>
<b>11.4.</b>	<b>Results of the analysis of the internal standards utilised in neutron activation analysis .....</b>	<b>252</b>
<b>11.5.</b>	<b>Visual comparisons of spectra obtained for samples of various standard compositions at four known thicknesses utilizing the i1-Pro.....</b>	<b>254</b>



v. **List of abbreviations:**

- AAS** – Atomic Absorption Spectroscopy
- ACIR** – Autocorrelation Infrared
- ANSTO** – Australian Nuclear Science and Technology Organisation
- ATR** – Attenuated Total Reflectance
- ATR-FTIR** – Attenuated Total Reflectance Fourier-Transform Infrared Spectroscopy
- CCDs** – Charge-Coupled Devices
- CHNS** – Carbon, Hydrogen, Nitrogen, Sulphur
- CSIRO** – The Commonwealth Scientific and Industrial Research Organisation
- DRIFT** – Diffuse Reflectance Infrared Fourier Transform Spectroscopy
- DSC** – Differential Scanning Calorimetry
- DTA** – Differential Thermal Analysis
- ED-XRF** – Energy Dispersive X-ray Fluorescence
- EDS** – Energy Dispersive Spectrometers microanalysis
- EDX** – Energy-Dispersive X-rays analysis
- ESEM-EDX** – Environmental Scanning Electron Microscope - Energy-Dispersive X-rays analysis
- FIR** – Far-infrared Spectroscopy
- FTIR** – Fourier Transform Infrared Spectroscopy
- GCMS** – Gas Chromatography Mass Spectrometry
- HPLC** – High Pressure Liquid Chromatography
- ICP-AES** – Inductively Coupled Plasma Atomic Emission Spectroscopy
- ICDD** – International Centre for Diffraction Data
- ICP-AES** – Inductively Couple Plasma Atomic Emission Spectroscopy
- ICP-MS** – Inductively Coupled Plasma Mass Spectrometry
- INAA** – Instrumental Neutron Activation Analysis
- IR** – Infrared
- IRM** – Isothermal Resonance and Magnetic Susceptibility
- LA-ICP-MS** – Laser Ablation Inductively Coupled Plasma Mass Spectrometry
- LD** – Limit of Detection
- Micro-ATR** – Micro-Attenuated Total Reflectance
- MEU** – Minor Early Use
- MLU** – Minor Late Use
- NAA** – Neutron Activation Analysis
- NIPALS** – Nonlinear Iterative Partial Least Squares
- NRA** – Nuclear Reaction Analysis
- PCA** – Principal Component Analysis
- PIGE** – Particle Induced  $\gamma$ -Ray Emission

**FIGME** – Programmed Inert-Gas Multi-Electrode

**PIXE** – Particle Induced X-ray Emission

**RBS** – Rutherford Backscattering Spectrometry

**RQPA** – Rietveld Quantitative Phase Analysis

**SEM** – Scanning Electron Microscopy

**SEM-EDX** – Scanning Electron Microscopy Energy Dispersive X-ray Spectrometry

**SR-XRD** – Synchrotron Radiation X-ray Diffraction

**TGA** – Thermo Gravimetric Analysis

**TOF-SIMS** – Time of Flight Secondary Ion Mass spectrometry

**Unc.** – Uncertainties

**WD-XRF** – Wavelength Dispersive X-ray Fluorescence

**XRF** – X-ray Fluorescence

**XRD** – X-ray Diffraction



vi. **List of figures:**

**Figure 1-1:** (a) Example of an early painting utilizing ochre from a cave at Avignon, France [1]. (b) Example of the use of Egyptian blue in a wall painting from the antiquity time period. 9

**Figure 1-2:** ‘Assumption to Heaven’ artwork from approximately 1518 showing the use of Vermilion as the red based pigment. .... 10

**Figure 1-3:** (a) Ochre samples from Clearwell Caves, Gloucestershire, showing some of the numerous colours that ochres naturally exhibit [63], (b) photographic example of some of the toas contained by The South Australian Museum in the Reuther Collection (A) A6301 (B) A6308 (C) A6178 and (D) A6477. .... 15

**Figure 1-4:** Chemical structure of (a) haematite  $\alpha\text{-Fe}_2\text{O}_3$ , (b) goethite  $\alpha\text{-FeOOH}$ , (c) jarosite  $(\text{KFe}_3(\text{SO}_4)_2(\text{OH})_6)$  and (d) natrojarosite  $(\text{NaFe}_3(\text{SO}_4)_2(\text{OH})_6)$  where sodium polyhedra (A site) are light gray, iron octahedra are dark gray (B site) [67]. .... 16

**Figure 1-5:** Particle diameter of four ochre samples of varied colours as presented by Mortimore et al. .... 17

**Figure 1-6:** The pathways of two beams of X-rays demonstrating the different distances travelled based on atom interactions..... 19

**Figure 1-7:** A simple schematic of a two-beam absorption infrared spectrometer..... 30

**Figure 1-8:** Infrared spectroscopy correlation table showing the bands over which peaks are present and the functional groups responsible within the structures studied. .... 31

**Figure 1-9:** ATR-FTIR spectra showing the variations observed as a result of altering the pH of the aqueous malonate solutions [121]..... 32

**Figure 1-10:** Schematic diagram of Raman spectroscopy. Image from [128]..... 33

**Figure 1-11:** LA-ICP-MS spectra obtained for two ochre samples showing their variation. ... 40

**Figure 1-12:** Location of ochre sources utilised by Mooney et al. [144]..... 42

**Figure 1-13:** IRM acquisitions of various ochre samples from significantly different geographical provenance [144]..... 43

**Figure 2-1:** Photograph of selected mining samples pressed prior to analysis showing the distinct differences in colour. .... 50

**Figure 2-2:** Map of Australia showing the locations of the mining samples (see Table 2-1 for key). .... 51

**Figure 2-3:** XRD Analysis of Ochre 1286 with overlay ICDD Patterns. .... 53

**Figure 2-4:** XRD Analysis of Ochre 1286 at low intensities with overlay ICDD Patterns. .... 53

**Figure 2-5:** XRD Analysis of Ochre 1323 with overlay ICDD Patterns..... 54

**Figure 2-6:** Spectra obtained for the Raman analysis of the ochre standards..... 57

**Figure 2-7:** Spectra obtained for the Raman analysis of the visually yellow ochre samples. 58

**Figure 2-8:** Spectra obtained for the Raman Analysis of the visually yellow ochre samples at low wavenumbers. .... 58

**Figure 2-9:** Spectra obtained for the Raman analysis of the visually red ochre samples. .... 60

<b>Figure 2-10:</b> Spectra obtained for the Raman analysis of the visually red ochre samples at low wavenumbers.....	60
<b>Figure 2-11:</b> TGA weight loss spectra (shown in green) and derivative (shown in blue) of goethite to a maximum of 900°C, showing a transformation temperature of 303.43°C. ....	61
<b>Figure 2-12:</b> TGA weight loss spectra (shown in green) and derivative (shown in blue) of haematite to a maximum of 900°C, showing no significant weight loss.....	62
<b>Figure 2-13:</b> TGA weight loss spectra (shown in green) and derivative (shown in blue) of ochre 1285 to a maximum of 900°C, showing a transformation temperature of 305.90°C. ....	63
<b>Figure 2-14:</b> TGA weight loss spectra (shown in green) and derivative (shown in blue) of ochre 3696 to a maximum of 900°C, showing a transformation temperature of 298.50°C, and a secondary weight loss peak at 118.57°C.....	63
<b>Figure 2-15:</b> TGA weight loss spectra (shown in green) and derivative (shown in blue) of ochre 3742 to a maximum of 900°C, showing a transformation temperature of 294.81°C, and a secondary weight loss peak at 508.01°C.....	64
<b>Figure 2-16:</b> TGA weight loss spectra (shown in green) and derivative (shown in blue) of ochre 1286 to a maximum of 900°C, showing a transformation temperature of 298.50°C, a secondary weight loss peak at 505.55°C, and a small secondary peak at 114.88°C.....	64
<b>Figure 2-17:</b> Results of near-IR analysis for the ten raw ochre mining samples.....	66
<b>Figure 2-18:</b> NAA results for elements detected in all ochre samples at concentrations not exceeding 100mg/kg. ....	79
<b>Figure 2-19:</b> NAA results for elements detected in all ochre samples at concentrations greater than 50mg/kg in at least one sample, but not exceeding 1000mg/kg. ....	79
<b>Figure 2-20:</b> NAA results of all elements detected in all ochre samples at concentrations not exceeding 1000mg/kg. ....	80
<b>Figure 2-21:</b> NAA results for elements detected in all ochre samples at concentrations not exceeding 60000mg/kg. ....	80
<b>Figure 2-22:</b> NAA results for elements detected in all ochre samples at concentrations not exceeding 60000mg/kg. ....	81
<b>Figure 2-23:</b> NAA results for elements detected in all ochre samples at concentrations not exceeding 60000mg/kg, with ochre 1293 omitted for scaling reasons.....	82
<b>Figure 3-1:</b> The EFI ES-1000 hand-held spectrophotometer.....	86
<b>Figure 3-2:</b> (a) Diagram showing a cross section of the internal schematics of the i1 pro instrument, with only the functionally essential elements shown, and (b) an oblique view of the opto-electronic measurement arrangement of the handheld colour measurement device. ..	87
<b>Figure 3-3 :</b> Reflectance Spectra obtained for goethite (yellow) and haematite (red) standards utilising the i1Pro system. ....	91
<b>Figure 3-4:</b> Average Spectra obtained for five separate Goethite Standard samples, each measured twenty times, with the average spectra shown in green.....	95
<b>Figure 3-5:</b> Average Spectra obtained for five separate haematite standard samples, each measured twenty times, with the average spectra shown in green.....	95

<b>Figure 3-6:</b> Absorbance and derivative spectra of a Gaussian band highlighting the effect of first and higher order derivative calculations on the spectra. ....	96
<b>Figure 3-7:</b> Derivatives of the average spectra obtained for five separate goethite and five separate haematite Standard samples, each measured twenty times, with the overall average goethite spectra shown in yellow and haematite spectra in red. ....	97
<b>Figure 3-8:</b> Average spectra obtained for varying goethite and haematite composition samples utilising the EFI ES-1000.....	98
<b>Figure 3-9:</b> First derivatives of the average spectra obtained for varying goethite and haematite composition samples utilising the EFI ES-1000.....	98
<b>Figure 3-10:</b> Comparison of the derivatives of the spectra obtained for (a) Bookartoo ochre 076 and (b) Moana ochre 037 utilising both the i1Pro system (shown in green) and the Perkin-Elmer Lambda 950 (shown in blue).....	99
<b>Figure 3-11:</b> The i1Pro results obtained for the (a) haematite standard, (b) standard containing a 25/75% w/w mixture of goethite and haematite, (c) a 50/50% w/w mixture of goethite and haematite, (d) a 75/25% w/w mixture of goethite and haematite and (e) the goethite standard at four various thicknesses with 20mg shown in blue, 15mg in red, 10mg in green and 5mg in orange. ....	101
<b>Figure 3-12:</b> Derivatives of the spectra obtained for samples of various goethite/haematite composition when applied to paper as (a) a water based paste, (b) an emu oil based paste, and (c) an orchid sap based paste. ....	103
<b>Figure 3-13:</b> Derivatives of the normalised spectra obtained for samples of (a) haematite standard, (b) 25/75 goethite/haematite (w/w%) sample, (c) 50/50 goethite/haematite (w/w%) sample, (d) 75/25 goethite/haematite (w/w%) sample and (e) goethite standard when applied to paper as a water based paste (shown in blue), an emu oil based paste (shown in black), and an orchid sap based paste (shown in purple).....	105
<b>Figure 3-14:</b> The intensity of the derivate of the spectra at 530nm for each sample site with respect to sample composition.....	106
<b>Figure 3-15:</b> The $\Delta E$ value for each sample site with respect to sample composition.....	108
<b>Figure 3-16:</b> Predicted Vs Reference data from the multiple linear regression model.....	109
<b>Figure 3-17:</b> Results obtained for the ten mining samples utilizing the i1Pro. ....	111
<b>Figure 3-18:</b> Derivatives of the results obtained for the ten mining samples utilizing the i1Pro. ....	111
<b>Figure 4-1:</b> Derivatives of the spectra obtained for samples of various goethite/haematite compositions when applied as a water based paste to (a) pine, (b) Australian oak, (c) natural jarrah, (d) natural sandstone, (e) synthetic sandstone, (f) natural slate and (g) synthetic pavers The legend for these figures is presented in (h).....	118
<b>Figure 4-2:</b> Normalised and derivitised i1Pro reflectance spectra obtained for a water based paste when applied to paper (bright blue), pine (black), jarrah (pink), oak (purple), natural sandstone (yellow), synthetic sandstone (deep blue), natural slate (green) and synthetic pavers (red) for the (a) goethite standard, (b) 25/75 goethite/haematite (w/w%) sample, (c)	

50/50 goethite/haematite (w/w%) sample, (d) 75/25 goethite/haematite (w/w%) sample and (e) haematite standard. ....	120
<b>Figure 4-3:</b> Variation between the actual %goethite and the calculate %goethite for the samples of undisclosed composition using the 530nm prediction model.....	123
<b>Figure 4-4:</b> Variation between the actual %goethite and the calculate %goethite for the samples of undisclosed composition using the MLR model on paper. ....	127
<b>Figure 4-5:</b> Predicted Vs Reference data from the Multiple Linear Regression model on Slate. ....	128
<b>Figure 5-1:</b> Map of Australia showing the location of the three sites used in this study. Bookartoo is labelled as site 1, Wilgie Mia as site 2 and Moana as site 3.....	133
<b>Figure 5-2:</b> The normalised and derivative spectra for each colour classification for all Moana samples. The error bars represent a single standard deviation of the average spectra. ....	140
<b>Figure 5-3:</b> Results of principle component analysis for PC1 vs PC2 performed on all Moana samples. ....	140
<b>Figure 5-4:</b> The normalised and derivative spectra for each colour classification for all Wilgie Mia samples. The error bars represent a single standard deviation of the average spectra.....	141
<b>Figure 5-5:</b> Results of principle component analysis for PC1 vs PC2 performed on all Wilgie Mia samples. ....	142
<b>Figure 5-6:</b> The normalised and derivative spectra for each colour classification for all Bookartoo samples. The error bars represent a single standard deviation of the average spectra. ....	143
<b>Figure 5-7:</b> Results of principle component analysis for PC1 vs PC2 performed on all Bookartoo samples.....	144
<b>Figure 5-8:</b> The normalised and derivative spectra for each colour classification for all Wilgie Mia, Bookartoo and Moana samples. The error bars represent a single standard deviation of the average spectra.....	145
<b>Figure 5-9:</b> Results of principle component analysis for PC1 vs PC2 performed on all Wilgie Mia, Bookartoo and Moana samples. ....	146
<b>Figure 5-10:</b> Loadings plot corresponding to the principal component analysis results presented in Figure 5-9. ....	146
<b>Figure 5-11:</b> Results of principle component analysis for PC1 vs PC3 performed on all Wilgie Mia, Bookartoo and Moana samples. ....	147
<b>Figure 5-12:</b> Loadings plot corresponding to the principal component analysis results presented in Figure 5-11. ....	147
<b>Figure 5-13:</b> The normalised and derivative spectra for the ochres classified red in colour for Wilgie Mia (shown in green), Bookartoo (shown in red) and Moana (shown in red) samples. The error bars represent a single standard deviation of the average spectra.....	149

<b>Figure 5-14:</b> Results of PCA for PC1 vs PC2 performed on all Wilgie Mia (shown in black), Bookartoo (shown in bright red) and Moana (shown in dark red) samples classified to be red in colour. ....	150
<b>Figure 5-15:</b> Loadings plot corresponding to the PCA data shown in Figure 5-14. ....	150
<b>Figure 5-16:</b> Ratio calculations for derivative spectral intensity for Bookartoo (shown in red), Moana (shown in blue) and Wilgie Mia (shown in green). The error bars represent a standard deviation. ....	152
<b>Figure 5-17:</b> Results of principle component analysis for PC1 vs PC2 performed on all Wilgie Mia (shown in black), Bookartoo (shown in bright red) and Moana (shown in dark red) samples classified to be red in colour using only wavelengths 530-700nm.....	152
<b>Figure 5-18:</b> Loadings plot corresponding to the PCA data shown in Figure 5-17. ....	153
<b>Figure 5-19:</b> Results of principle component analysis for PC1 vs PC2 performed on the NAA data of all Wilgie Mia (shown in black), Bookartoo (shown in bright red) and Moana (shown in dark red) samples. ....	155
<b>Figure 5-20:</b> Loadings plot corresponding to the PCA results given in Figure 5-19.....	155
<b>Figure 5-21:</b> Results of principle component analysis for PC1 vs PC2 performed on the NAA data of all Wilgie Mia (shown in black), Bookartoo (shown in bright red) and Moana (shown in dark red) samples classified to be red in colour. ....	156
<b>Figure 5-22:</b> Loadings plot corresponding to the PCA results given in Figure 5-21.....	156
<b>Figure 5-23:</b> Results of principle component analysis for PC1 vs PC2 performed on the NAA data of all Wilgie Mia (shown in black), Bookartoo (shown in bright red) and Moana (shown in dark red) samples classified to be red in colour using a reduced number of elements. ....	163
<b>Figure 5-24:</b> Loadings plot corresponding to the PCA results given in Figure 5-23.....	164
<b>Figure 6-1:</b> Map showing the location of the toas collection with respect to Australia and (insert) map of the Lake Eyre region. ....	168
<b>Figure 6-2:</b> Photographic example of some of the toas studied (A) A6301 (B) A6308 (C) A6178 and (D) A6477. ....	170
<b>Figure 6-3:</b> Photographic example of some of the toas studies (A) A40876 (B) A40862 (C) A6190 and (D) A6172. ....	170
<b>Figure 6-4:</b> The average normalised derivative spectra for each of the six raw ochre samples collected by Reuther at the same time as the Toas representing possible source material. ....	172
<b>Figure 6-5:</b> The ratio between the average normalised and derivatised spectra of the six raw ochre samples collected by Reuther at the same time as the toas representing possible source material at 590 and 650nm. ....	172
<b>Figure 6-6:</b> Graphical representation of the average spectra obtained for the raw materials studied with a range and single standard deviation shown. ....	176
<b>Figure 6-7:</b> Principle component analysis results of the six raw materials studied. ....	177
<b>Figure 6-8:</b> Loadings plot generated in conjunction with the PCA results for the six raw materials studied. ....	177

**Figure 6-9:** Each series represents the normalised and derivatised average of a the five measurements taken at a single sample site on Toa A40862, with all four series showing good agreement and allowing for an average to be used for this toa. .... 179

**Figure 6-10:** Series representing the normalised and derivatised average of a the five measurements taken at a single sample site on each of these toas are shown below in Figure H (a), representing toa A6477, H (b), representing toa A40876, and H (c) representing toa A6190. .... 180

**Figure 6-11:** Series representing the normalised and derivatised average of all the measurements taken on each toa, except where statistical averaging was not applicable and multiple series exist per toa. .... 185

**Figure 6-12:** Graphical representation of the average spectra obtained for the yellow areas studied with a range and single standard deviation shown..... 184

**Figure 6-13:** The ratio of the intensities of the peak at 560nm and the minima at 470nm where the spectra underwent normalisation and derivitisation before being averaged to give a single spectra per toa where statistically appropriate. .... 185

**Figure 6-14:** The normalised, derivitised and then averaged spectra for each site for two toas, A6477 shown as (a) and A6195 shown as (b), demonstrating good agreement between all sites studied on each individual toa. .... 187

**Figure 6-15:** Photographic image of toa A40862 and the seven sites studied on this toa. 188

**Figure 6-16:** The normalised, derivitised and averaged spectra for each site on toa A40862, where the number corresponds to the location shown visually in Figure M. .... 188

**Figure 6-17:** The normalised, derivitised and then averaged spectra for the red areas of all toas studied. .... 189

**Figure 6-18:** Graphical representation of the average spectra obtained for the red areas studied with a range and single standard deviation shown..... 193

**Figure 6-19:** Principle component analysis results of the red material on the toas. .... 195

**Figure 6-20:** Loadings plot generated in conjunction with the PCA results for the red material on the toas. .... 196

**Figure 6-21:** The ratio of the peak intensities at 590/650nm of the normalised, derivitised and then averaged spectra for all toas studied..... 196

**Figure 6-22:** Normalised derivative i1Pro spectra for the toas and raw material, overlayed, with the toas all represented in black and the individual raw materials spectra highlighted. 197

**Figure 6-23:** The 590/650nm ratios for the toas (shown in colours) and the toas (shown in pink/purple), with three of the raw materials falling within the range of the toas and three distinctly outside the range. .... 198

**Figure 6-24:** Principal component analysis on the red material on the toas and the raw samples collected as possible sources with the individual sample numbers shown..... 199

**Figure 6-25:** Principal component analysis on the red material on the toas and the raw samples collected as possible sources with the toas shown in red and the sources in blue. ...  
..... 199

<b>Figure 6-26:</b> Loadings plot for principal component analysis on the red material on the toas and the raw samples collected as possible sources.....	200
<b>Figure 6-27:</b> Principal component analysis on the red material on the toas (excluding toa A6153b) and the raw samples collected as possible sources with the individual sample numbers shown. ....	200
<b>Figure 6-28:</b> Principal component analysis on the red material on the toas (exluding toa A6153b) and the raw samples collected as possible sources with the toas shown in red and the sources in blue.....	201
<b>Figure 6-29:</b> Loadings plot for principal component analysis on the red material on the toas (excluding toa A6153b) and the raw samples collected as possible sources. ....	201
<b>Figure 6-30:</b> Principal component analysis on the raw material collected from the Reuther Collection and the Moana, Bookartoo, Wilgie Mia samples. ....	203
<b>Figure 6-31:</b> Loadings plot for the principal component analysis on the raw material collected from the Reuther Collection and the Moana, Bookartoo, Wilgie Mia samples.....	203
<b>Figure 9-1:</b> TGA results obtained from the heating of pure goethite to 900°C in air. ....	227
<b>Figure 9-2:</b> XRD pattern of as-received Hattrick goethite Y163.....	229
<b>Figure 9-3:</b> XRD pattern of as-received Fluka goethite 71063. ....	230
<b>Figure 9-4:</b> XRD patterns of Hattrick goethite Y163 heated at 105°C (shown in black), 150°C (shown in red), 200°C (shown in blue), 250°C (shown in purple) and 300°C (shown in green) for 24 hours in air. ....	230
<b>Figure 9-5:</b> Weight loss of Hattrick goethite Y163 after heating. Heating was in air for a time of 24 hours unless otherwise indicated. The data is plotted on two scales to better show the measured weight loss at temperatures below 250°C. ....	231
<b>Figure 9-6:</b> Spectra obtained (offset) from the heating of goethite, with the original spectra shown in red obtained at room temperature, the second spectra shown in orange obtained as the temperature reached 300°C, and each following spectra being an additional one hour into heating. ....	232
<b>Figure 9-7:</b> Spectra obtained (offset) from the heating of Goethite, with the original spectra shown in red obtained at room temperature, the second spectra shown in orange obtained as the temperature reached 300°C, and each following spectra being an additional one hour into heating, with only theta angles 35 to 45 shown.....	233
<b>Figure 9-8:</b> Spectra obtained (offset) from the heating of Goethite, obtained at room temperature (shown in black), as temp reached 300°C (shown in red), with one and two hours heating (shown in blue and purple), and 16 hours heating (shown in green). Only 2-theta angles 35 to 45 are shown. ....	234
<b>Figure 10-1:</b> Map showing the location of Arkaroo Rock relative to South Australia’s capital city, Adelaide. ....	236
<b>Figure 10-2:</b> Photograph showing the dust- like particles collecting on the surface of the artwork, and the areas where samples were collected both from the rock surface (samples 1-6, 12) and from ground within the protective fence (samples 7-11).....	238

**Figure 10-3:** Photograph taken on medium magnification utilizing a Lietiz orthopol 12 petrographic microscope showing a number of the species present in sample number 5 of the dust like particulate removed from the rock surface. .... 239

**Figure 10-4:** Results of the TGA analysis of the fine particles collected from Arkaroo Rock. The plot shows the derivative weight (percent) as a function of temperature. .... 240

**Figure 10-5:** The derivative of the spectra obtained for all samples collected from both the surface of the rock and the ground within the caged area, using the EFI ES-1000 hand-held spectrophotometer..... 241

**Figure 10-6:** Dendrogram from statistical analysis using the MINITAB software of the derivatives of the spectra obtained for the samples collected (numbering shown in figure 2) and analysed using the EFI ES-1000. .... 242

**Figure 11-1:** XRD analysis of mining sample ochres with ICDD overlap of goethite (green), haematite (purple) and quartz (blue). Samples (a) – (h) appear yellow in colour and (i) -.. 248

**Figure 11-2:** Results of i1Pro analysis of the ten mining samples measured at three spots five times consecutively. .... 250

**Figure 11-3 :** Comparison of the derivatives of the spectra obtained for Bookartoo and Moana ochres utilising both the i1Pro system (shown in green) and the Perkin-Elmer Lambda 950 (shown in blue). .... 252

**Figure 11-4:** Results of the analysis of various composition goethite/haematite standard at four various sample thicknesses, 20mg (shown in purple), 15mg (shown in yellow), 10mg (shown in green) and 5mg (shown in red). Spectra are normalised but not derivitised. .... 256



vii. **List of tables:**

**Table 1-1:** Examples of many of the naturally occurring and synthetic pigments, their colours and their chemical compositions. The pigments presented here are listed based on their chronological order beginning with antiquity though the ages to modern times. This list is indicative and not exhaustive. ....3

**Table 1-2:** A summary of the use of various synthetic and natural pigments throughout time, where MEU represents minor early use and MLU represents minor late use. ....12

**Table 1-3:** Measured content of the major components of four tested ochre samples. Table reproduced from [64].....17

**Table 1-4:** Summary of current research into the analysis of ochre utilizing X-ray based techniques [19, 57, 58, 65, 71, 84-97].....21

**Table 1-5:** Summary of current research into the analysis of ochre utilizing Raman and infrared spectroscopy based techniques [19, 52, 53, 55, 64, 66, 69, 70, 101-111] .....26

**Table 1-6:** Summary of current research into the analysis of ochre utilizing a number of techniques where trace element analysis is the primary aim [58, 84, 87-89, 91, 94, 138]. ...35

**Table 1-7:** Summary of current research into the analysis of ochre utilizing multidisciplinary techniques [60, 61, 93, 97, 99, 140-145].....37

**Table 1-8:** Oxygen Isotope ratios in quartz in a number of ochre samples. The table is reproduced from reference [60].....41

**Table 1-9:** Summary of the elemental composition of eight red ochre samples from Western North America. ....43

**Table 2-1:** A description of the ten Australian mining samples used in this study, their corresponding image number and map location. ....50

**Table 2-2:** Results of XRD analysis showing identified sample components.....55

**Table 2-3:** Results of quantitative phase analysis using Rietveld refinement on a sample of known composition.....56

**Table 2-4:** Results of XRD analysis showing calculated sample compositions, expressed as a %weight. X suggests that analysis was unsuccessful. ....56

**Table 2-5:** Results of autocorrelation analysis on various mining samples.....65

**Table 2-6:** NAA data obtained for ochres 1323, 1337, 3742, 1293 and 1139 for all elements investigated. Data is reported as supplied by ANSTO. ....68

**Table 2-7:** NAA data obtained for ochres 1137, 1150, 1286, 3696 and 1285 for all elements investigated. Data is reported as supplied by ANSTO. ....72

**Table 2-8:** NAA results for all ochres, showing only the elements detected. ....76

**Table 3-1:** Series of standard goethite and haematite samples varying in composition by approximately 5%.....89

**Table 3-2:** Results obtained for two hundred measurements of standard Goethite utilising the EFI ES-1000. ....92

<b>Table 3-3:</b> Results obtained for two hundred measurements of standard haematite utilising the EFI ES-1000.....	94
<b>Table 3-4:</b> Results of analysis of samples of undisclosed composition, with comparison to known composition, using the 530nm prediction model, with values expressed as the percentage of goethite in each sample.....	107
<b>Table 3-5:</b> Results of analysis of samples of undisclosed composition, with comparison to known composition, using the $\Delta E$ prediction model, with values expressed as the percentage of goethite in each sample.....	108
<b>Table 3-6:</b> Results of analysis of samples of undisclosed composition, with comparison to known composition, with values expressed as the percentage of goethite in each sample.	110
<b>Table 4-1:</b> Series of standard goethite and haematite samples varying in composition by approximately 5%.....	115
<b>Table 4-2:</b> Results of analysis of samples of undisclosed composition, with comparison to known composition, with values expressed as the percentage of goethite in each sample, with samples applied to wood and stone surfaces, using the 530nm prediction model. ....	121
<b>Table 4-3:</b> Results of analysis of samples of undisclosed composition, with comparison to known composition, with values expressed as the percentage of goethite in each sample, with samples applied to wood and stone surfaces.....	124
<b>Table 4-4:</b> Results of analysis of samples of undisclosed composition, with comparison to known composition, with values expressed as the percentage of goethite in each sample, with samples applied stone surfaces, calculated utilising a MLR model created on slate.....	128
<b>Table 5-1:</b> Table showing the ochre samples utilised in this study, including their database number, site location, a description of their colour and the corresponding L/A/B colour space values. A description of the sample type is also given where raw stones samples are described based on their sizes with samples less than 2cm in diameter are considered very small, between 2-5cm in diameter small, 6-9cm in diameter medium, 10-15cm in diameter large, and greater than 16cm in diameter extra-large.....	134
<b>Table 5-2:</b> Table showing the ochres utilised in NAA analysis including their database classification number, sample site and visual colour. ....	157
<b>Table 5-3:</b> Descriptive statistics obtained from the NAA analysis of the ochres given in Table 5-2. ....	158
<b>Table 5-4:</b> Elemental average detected and standard deviations (population) for the 34 red samples studied. ....	160
<b>Table 6-1:</b> Table showing the toas used in this study including their museum reference number and the colour components studied.....	169
<b>Table 6-2:</b> Preliminary statistical analysis performed on the average normalised derivative spectra for each of the six raw ochre samples collected by Reuther at the same time as the Toas representing possible source material. ....	173

<b>Table 6-3:</b> Preliminary statistical analysis performed on the average normalised derivative spectra for each of the six raw ochre samples collected by Reuther at the same time as the Toas representing possible source material.....	174
<b>Table 6-4:</b> The Toas containing a yellow pigment as decoration that were examined, the number of unique sites on each toa studied, and the number of groups identified from spectral and statistical analysis. ....	179
<b>Table 6-5:</b> Preliminary statistical analysis on the yellow material used to decorate a selection of toas based on the normalised and derivatised average spectra per toa where statistically appropriate. ....	181
<b>Table 6-6:</b> Descriptive statistics on the yellow material used to decorate a selection of toas based on the normalised and derivatised average spectra per toa where statistically appropriate. ....	182
<b>Table 6-7:</b> The Toas containing a red pigment as decoration that were examined, the number of unique sites on each toa studied, and the number of groups identified from spectral and statistical analysis. ....	186
<b>Table 6-8:</b> Statistical analysis on the normalised, derivitised and then averaged spectra for the red areas of all toas studied. ....	190
<b>Table 6-9:</b> Descriptive statistics for the normalised, derivitised and then averaged spectra for the red areas of all toas studied. ....	191
<b>Table 9-1:</b> Weight loss of Hattrick goethite Y163 after heating at the shown temperatures for the shown times. ....	231
<b>Table 11-1:</b> Results of NAA on the NIST internal standards.....	252



# CHAPTER ONE: INTRODUCTION

Since prehistoric times, humans have left markings on their environments [1]. Primitive beings scratched markings into trees and the landscape using rocks and other early tools to mark pathways and areas of interest, such as a food or water sources. These markings became more prominent with the addition of colour, and with this came the development of paints and painted artworks [1, 2]. In indigenous Australian culture, ochre is significant and highly valued pigment that has been associated with dreamtime stories.

This thesis details the work undertaken towards and the results obtained from the development of a portable and non-destructive spectroscopic technique for the analysis of Australian Aboriginal ochre materials. This introductory chapter highlights briefly the use of all pigment globally throughout history before focusing on ochre and Australia. The chemical composition and properties of ochre are discussed. This chapter also presents reviews of current literature on the analysis of ochres in a variety of forms including raw pigment, rock art, ceramics and wall paintings, and explores the many methods commonly utilised for analysis.

### 1.1. Pigments

#### 1.1.1. Pigments and their use in artwork throughout history

Pigments form the basis of all paints and similar media, and have been used around the globe for millennia [3, 4]. The Oxford Dictionary defines a pigment as






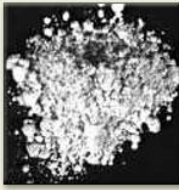

*'noun*


- *the natural colouring matter of animal or plant tissue*
- *a substance used for colouring or painting, especially a dry powder, which when mixed with oil, water, or another medium constitutes a paint or ink'*

In the context of artwork, a pigment is the substance, usually a powder, which, when combined with a binder in suspension, gives the paint, ink, plastic, fabric, cosmetics or similar medium, its colour [5]. Scientifically, colour results when the wavelength of light either transmitted or reflected by the material is changed as a result of selective absorption by the medium. Visible colour is a common property in many minerals, and those used in modern artwork are typically chosen for their colour, stability, their concentrations and their state at a variety of temperatures [1, 5, 6].



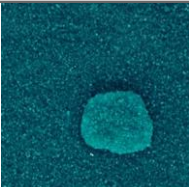





Pigments can be naturally derived from plants or animals (organic), salts or metal oxides (inorganic), or synthetically produced. Examples of some of the many naturally occurring and synthetic pigments, along with their colour and chemical formulae, are given in Table 1-1. Early pigments were typically ground clays and minerals, which were combined with a medium such as egg white, fat, saliva or water to form a paint like substance [4]. Modern pigments are most commonly synthetic and offer an increased colour palette and can be applied to a greater variety of mediums [1, 7]. Presented below is a brief introductory overview of common mineral pigments used throughout the ages. Organic pigments and dyes will be excluded from this discussion.

**Table 1-1:** Examples of many of the naturally occurring and synthetic pigments, their colours and their chemical compositions. The pigments presented here are listed based on their chronological order beginning with antiquity though the ages to modern times. This list is indicative and not exhaustive.









Pigment name	Image	Chemical Name / Composition	Chemical Formulae
Carbon Black		Amorphous carbon	C
Black Bone		10% carbon, 84% calcium phosphate and 6 % calcium carbonate	$\text{Ca}_3(\text{PO}_4)_2 + \text{CaCO}_3 + \text{C}$
Umber		Iron(III)-oxide, partly hydrated + manganese oxide + aluminium oxide	$\text{Fe}_2\text{O}_3 \cdot (n \text{ H}_2\text{O}) + \text{MnO}_2 \cdot (n \text{ H}_2\text{O}) + \text{Al}_2\text{O}_3$
Red Ochre		Anhydrous iron(III)-oxide	$\text{Fe}_2\text{O}_3$
Yellow Ochre		Iron oxyhydroxide, jarosite, natrojarosite	$\text{FeO}(\text{OH}), \text{KFe}_3(\text{SO}_4)_2(\text{OH})_6, \text{NaFe}_3(\text{SO}_4)_2(\text{OH})_6$
Lime White		Calcium carbonate + calcium hydroxide (bianco San Giovanni)	$\text{CaCO}_3 + \text{Ca}(\text{OH})_2$
Madder Lake		Alizarin (1,2-dihydroxyanthraquinone), Purpurin (1,2,4-trihydroxyanthraquinone)	$\text{C}_{14}\text{H}_8\text{O}_4, \text{C}_{14}\text{H}_8\text{O}_5$





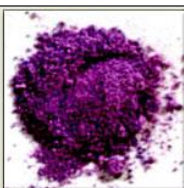


Pigment name	Image	Chemical Name / Composition	Chemical Formulae
<b>Carmine Lake</b>		Carminic acid (Cochineal), kermesic acid (Kermes)	$C_{22}H_{20}O_{13}$ , $C_{16}H_{10}O_8$
<b>Realgar</b>		Arsenic sulfide	$As_4S_4$
<b>Malachite</b>		Basic copper(II) carbonate	$2 CuCO_3 \cdot Cu(OH)_2$
<b>Orpiment</b>		Arsenic sulfide	$As_2S_3$
<b>Egyptian Blue</b>		Calcium copper silicate	$CaCuSi_4O_{10}$
<b>Indigo</b>		Indigotin (2,2'-Biindolinylyden-3,3'-dion)	$C_{16}H_{10}N_2O_2$
<b>Azurite</b>		Basic copper(II)-carbonate	$2 CuCO_3 \cdot Cu(OH)_2$
<b>Red Lead</b>		Lead(II,IV)-oxide	$Pb_3O_4$

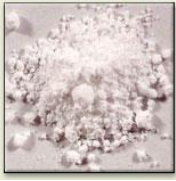


Pigment name	Image	Chemical Name / Composition	Chemical Formulae
Vermilion		Mercuric sulfide	HgS
Earth Green		Complex aluminosilicate minerals	$K[(Al,Fe^{III}), (Fe^{II},Mg)](AlSi_3, Si_4)O_{10}(OH)_2$
Verdigris		Basic copper acetate	$Cu(OH)_2 \cdot (CH_3COO)_2 \cdot 5 H_2O$
Lead White		Basic lead(II)-carbonate	$2 PbCO_3 \cdot Pb(OH)_2$
Ultramarine		A complex sulfur-containing sodium aluminum silicate	$Na_{8-10}Al_6Si_6O_{24}S_{2-4}$
Lead-Tin Yellow		Lead stannate (Type I), lead tin oxide silicate (Type II)	$Pb_2SnO_4$ (Type I), $Pb(Sn,Si)O_3$ (Type II)
Smalt		Potassium glass containing cobalt	$SiO_2(65\%) + K_2O(15\%) + Al_2O_3(5\%) + CoO(10\%)$
Indian Yellow		Magnesium euxanthate	$C_{19}H_{16}O_{11}Mg \cdot 5 H_2O$

CHAPTER ONE

Pigment name	Image	Chemical Name / Composition	Chemical Formulae
Copper Resinate		Copper resinate	$\text{Cu}(\text{C}_{19}\text{H}_{29}\text{COO})_2$
Naples Yellow		Lead(II)-antimonate	$\text{Pb}(\text{SbO}_3)_2$ or $\text{Pb}(\text{SbO}_4)_2$
Van Dyke Brown		Iron(III)-oxide, partly hydrated + manganese oxide partly hydrated + humic acids	$\text{Fe}_2\text{O}_3 \cdot (\text{H}_2\text{O}) + \text{MnO}_2 \cdot (n \text{H}_2\text{O}) + \text{humic acids}$
Prussian Blue		Iron(III)-hexacyanoferrate(II)	$\text{Fe}[\text{Fe}^{3+}\text{Fe}^{2+}(\text{CN})_6]_3$
Cobalt Green		Cobalt(II)-oxide-zinc(II)-oxide	$\text{CoO} \cdot \text{ZnO}$
Cobalt Blue		Cobalt(II) oxide-aluminum oxide	$\text{CoO} \cdot \text{Al}_2\text{O}_3$
Chrome Orange		Basic lead(II)-chromate	$\text{PbCrO}_4 \cdot \text{Pb}(\text{OH})_2$
Emerald Green		Copper(II)-acetoarsenite	$\text{Cu}(\text{CH}_3\text{COO})_2 \cdot 3 \text{Cu}(\text{AsO}_2)_2$

Pigment name	Image	Chemical Name / Composition	Chemical Formulae
Chrome Yellow		Lead(II)-chromate	$\text{PbCrO}_4$
Cadmium Yellow		Cadmium sulfide	$\text{CdS}$
Lemon Yellow		Barium chromate or strontium chromate or mixture of lead chromate + lead sulphate	$\text{BaCrO}_4$
Zinc White		Zinc(II)-oxide	$\text{ZnO}$
Cobalt Yellow		Potassium cobaltinitrite	$\text{K}_3[\text{Co}(\text{NO}_2)_6] \cdot \text{H}_2\text{O}$
Cobalt Violet		Cobalt(II)-phosphate or Cobalt(II)-arsenate	$\text{Co}_3(\text{PO}_4)_2$ or $\text{Co}_3(\text{AsO}_4)_2$
Cerulean Blue		Cobalt(II)-stannate	$\text{CoO} \cdot n \text{SnO}_2$
Cadmium Red		Cadmium orange/red: cadmium sulfide (CdS) + cadmium selenide (CdSe)	$\text{CdS} + \text{CdSe}$ (orange/red)

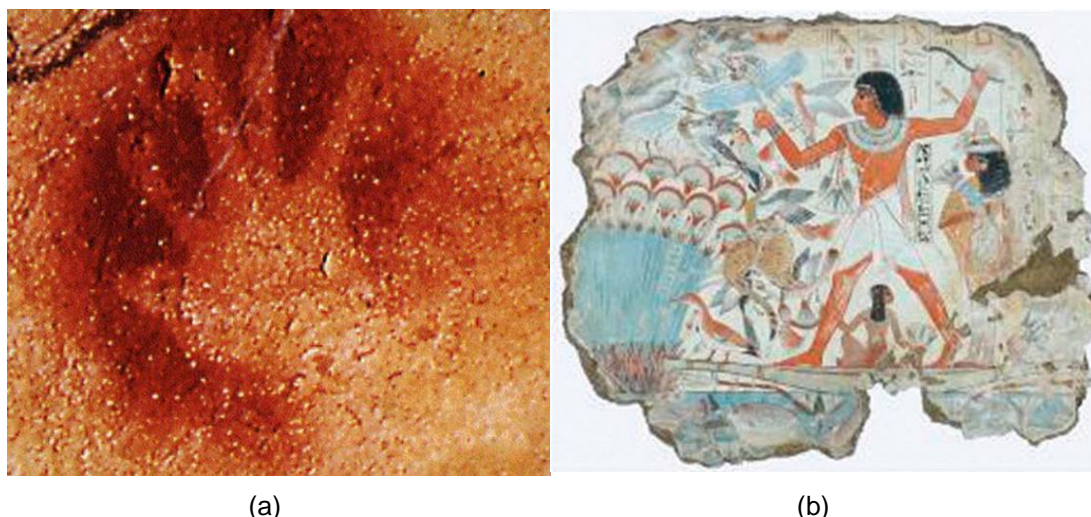
Pigment name	Image	Chemical Name / Composition	Chemical Formulae
Titanium White		Titanium dioxide	TiO <sub>2</sub>

Humans' use of paints and pigments has changed greatly throughout time. The earliest examples of artworks were completed in prehistoric times; a time where people were limited to materials that were readily available within a relatively short distance of their home, and to materials that required very little preparation for use. Consequently, pre-historic pigments were typically composed of earth and minerals, and are commonly known as 'earthy pigments.' Water was typically used for the binding medium, and early artworks were produced by paint application through using fingers. One of the oldest pigments known to man is iron-oxide based and known best as 'ochre'. It has been documented in a range of pre-historic objects and artworks including both prehistoric and Australian rock art, along with other iron-oxide based pigments including lime white, carbon and charcoal black. Pigments from prehistoric times were very limited in their colour range, and large ranges of today's colour spectrum (particularly greens and blues) were simply unavailable [1, 3, 4].

The Egyptians sought to change this colour limitation, and began the manufacture of pigments. From approximately 4000 BC they began producing new colours, and introduced new preparation methods that improved pigment stability, increased the colour strength and improved the purity of the pigments. The most notable development of pigments during this time was the discovery of Egyptian blue (calcium copper silicate, CaCuSi<sub>4</sub>O<sub>10</sub>), which was first produced approximately 3000 BC. Egyptian blue was synthesised by combining a calcium salt (carbonate, sulfate or hydroxide) with a copper based compound (oxide or malachite) and sand (quartz or silica), before heating the mixture to approximately 800°C for 10+ hours and grinding the product with sodium carbonate, potassium carbonate or borax. The resulting pigment is very stable, and examples of its use on wall paintings, as seen in Figure 1.1, and on artefacts are still available today [1, 8, 9].

The antiquity time period also saw the introduction of many other pigments and colours through the use of indigo, azurite (basic copper(II)-carbonate, 2CuCO<sub>3</sub>.Cu(OH)<sub>2</sub>), verdigris (basic copper acetate, Cu(OH)<sub>2</sub>.(CH<sub>3</sub>COO)<sub>2</sub>.5H<sub>2</sub>O), malachite (basic copper(II) carbonate, 2CuCO<sub>3</sub>.Cu(OH)<sub>2</sub>) and lead. Malachite is the oldest known green based pigment, and both it and azurite are seen in Egyptian tomb paintings and later in European paintings. Both are mineral based pigments and their colour is a result of copper carbonate [10-12].

In addition to the blues and greens, Egyptians also utilised yellows and reds. Sulphides and arsenic (arsenic sulphide, As<sub>2</sub>S<sub>3</sub>) were utilised as they were commonly found in volcanic and geothermal areas of Egypt. However, these pigments are chemically unstable and, when



**Figure 1-1:** (a) Example of an early painting utilizing ochre from a cave at Avignon, France [1]. (b) Example of the use of Egyptian blue in a wall painting from the antiquity time period.

exposed to light, the pigments fade with time. Jarosite (potassium ferric sulphate hydroxide,  $\text{KFe}_3(\text{SO}_4)_2(\text{OH})_6$ ) was also used for its pale yellow characteristics [1, 12].

The Egyptians were also responsible for the production of early dyes. They were the first to 'fix' colours by adding a liquid pigment to a transparent base or medium to form an insoluble pigment via a process known as lake making. This process was typically carried out on vegetable or plant based dyes [1].

The Egyptians were not the only civilisation interested in pigments, and developments were being made globally. The Greeks also feature strongly in pigment history and have been credited with the first production of white lead based pigments. Lead strips were stacked in porous jars and combined with vinegar before the heat required for the reaction was generated by encasing the jar in rotting animal faeces. The chemical structure of the white lead produced basic lead carbonate ( $2\text{Pb}(\text{CO}_3)_2 \cdot \text{Pb}(\text{OH})_2$ ), a stable pigment that, when combined with oil, was both fast drying and permanent. This formed the most readily available white pigment for all artists until the 19<sup>th</sup> century when its use was discontinued due to the discovery of its toxic nature [13-15].

In conjunction with white lead, the Greeks were influential in the development of red lead-based pigments. Red lead occurs naturally as a mineral known as minium (lead oxide,  $\text{Pb}_3\text{O}_4$ ), and can also be manufactured synthetically by heating litharge ( $\text{PbO}$ ). The use of red lead was common in the construction industry and continued until as recently as the 1990s [15-17].

Another exclusive pigment from this era is cinnabar (mercury sulfide,  $\text{HgS}$ ). Mined in Spain, this mineral based pigment was primarily utilised by Romans as a lipstick and it is seen in the statues and home textiles and artworks of the wealthiest citizens of Pompeii [18-20]. The Chinese were also amongst early contributors to this field, and utilised vermilion (mercuric sulfide,  $\text{HgS}$ ), a red pigment, centuries before the Romans utilised it. There are a number of





**Figure 1-2:** 'Assumption to Heaven' artwork from approximately 1518 showing the use of vermilion as the red based pigment.

alternate methods of production for this pigment, but it was typically produced using the minerals of mercury and sulfur, and synthetically produced vermilion was used in wall paintings as early as approximately 1518, as shown in Figure 1.2 [18].

Colours in the mediaeval era were characteristically bright and it was here, in the late 15<sup>th</sup> century, that the use of umbers is first noted. Umber (iron(III)-oxide, partly hydrated + manganese oxide + aluminium oxide,  $\text{Fe}_2\text{O}_3 \cdot n\text{H}_2\text{O} + \text{MnO}_2 \cdot (n\text{H}_2\text{O}) + \text{Al}_2\text{O}_3$ ) is a naturally occurring mineral based pigment found originally in Umbria, Italy [21]. The Italians also utilised other iron based pigments and ochres including raw sienna, raw umber and burnt sienna [1, 4].

The middle ages also saw the development of an alternative white pigment to the lead white (basic lead(II)-carbonate,  $2\text{PbCO}_3 \cdot \text{Pb}(\text{OH})_2$ ) previously found to be toxic. This discovery was made in the form of bone white, obtained by heating bones and grinding the ash. Alternatives including chalk, eggshells and oyster shells were also utilised, but use was limited as all these pigments lacked stability [11, 22, 23].

The colour red was obtained from a number of sources during the medieval and Renaissance periods. Orange lead and red lead (lead(II,IV)-oxide,  $\text{Pb}_3\text{O}_4$ ) were obtained by heating white lead (basic lead(II)-carbonate,  $2\text{PbCO}_3 \cdot \text{Pb}(\text{OH})_2$ ) or litharge ( $\text{PbO}$ ) in air, and were a cheaper alternative and more readily available than cinnabar [24, 25]. Biological sources of red pigments used throughout these times include cochineal, made from the insects known as kermes, and madder (alizarin (1,2-dihydroxyanthraquinone), purpurin (1,2,4-trihydroxyanthraquinone),  $\text{C}_{14}\text{H}_8\text{O}_4$ ,  $\text{C}_{14}\text{H}_8\text{O}_5$ ), which is derived from the roots of plants and contains the mineral alizarine [26-28].

Blue was also a developing colour of the middle ages, and in addition to the Egyptian blue and azurite previously discussed, a significant blue used during this time was ultramarine (a complex sulfur-containing sodium aluminum silicate,  $\text{Na}_{8-10}\text{Al}_6\text{Si}_6\text{O}_{24}\text{S}_{2-4}$ ). This pigment was produced by grinding the mineral lapis lazuli – a semi-precious rock given its colour from the presence of lazulite ( $(\text{Mg},\text{Fe}^{2+})\text{Al}_2(\text{PO}_4)_2(\text{OH})_2$ ). The use of ultramarine during the Renaissance signified purity, and the exclusivity of the pigment saw it used sparingly in paintings of religious importance [29-31].

A number of green pigments were also used during this period. Mineral based pigments were common and included malachite (basic copper(II) carbonate,  $2\text{CuCO}_3 \cdot \text{Cu}(\text{OH})_2$ ) and verdigris (basic Copper acetate,  $\text{Cu}(\text{OH})_2 \cdot (\text{CH}_3\text{COO})_2 \cdot 5 \text{H}_2\text{O}$ ) [17, 32-34].

In addition to the continuing use of ochre (iron oxyhydroxide,  $\text{FeO}(\text{OH})$ ) and orpiment (arsenic sulfide,  $\text{As}_2\text{S}_3$ ), Naples yellow (lead(II)-antimonate,  $\text{Pb}(\text{SbO}_3)_2$  or  $\text{Pb}(\text{SbO}_4)_2$ ) was used during this period as a yellow based pigment. Naples yellow is a lead based pigment comprised commonly of lead antimonate and bindheimite, and is formed via a heating process [17, 24, 35, 36]. The use of tin sulphide as a gold substitute was also explored during this era [1, 22].

A number of elements and minerals feature repeatedly in the early synthetic pigments. An example of this is cobalt, which when paired with minerals such as aluminium, phosphorous, tin or zinc, produced pigments of a variety of colours from blue to green and even violet [11, 24, 37-40]. Zinc has been heavily used in the production of white pigments [41], and cadmium is a key mineral to yellow and orange pigment development [24, 39, 42]. The colour of Indian yellow is attributed to organic magnesium obtained from the urine of cows fed an exclusive diet of mango leaves, and was banned in the early 20th century by the Hindus for religious reasons [1].

Naturally occurring emerald green (copper(II)-acetoarsenite,  $\text{Cu}(\text{CH}_3\text{COO})_2 \cdot 3 \text{Cu}(\text{AsO}_2)_2$ ) was first discovered in 1788 but wasn't successfully synthesised until 1914. Composed primarily of copper aceto-arsenite, synthetic emerald green was highly toxic and its use was discontinued in the 1960s [43-47].

Synthetic iron oxides were first manufactured in the 19<sup>th</sup> century. These are available today in a wide range of earthy colours from reds, yellows, browns, oranges and black, and are produced by heating an iron oxide. The final pigment colour is determined not only by its chemical composition but also the water content and by the process by which it was heated/treated. The manufacture of synthetic iron oxides was driven by a depletion in natural ochre supplies, and their use continues today [22, 48-51]. The study of these synthetic pigments could be useful for method development as their composition is well known and therefore the accuracy of the characterisation is immediately apparent.

CHAPTER ONE

**Table 1-2:** A summary of the use of various synthetic and natural pigments throughout time, where MEU represents minor early use and MLU represents minor late use.

	Pre-historic	Antiquity	Medieval	Renaissance and early modern	Industrial Revolution	Modern
<b>Carbon Black</b>	✓	✓	✓	✓	✓	✓
<b>Black Bone</b>	✓	✓	✓	✓	✓	✓
<b>Umber</b>	✓	✓	✓	✓	✓	✓
<b>Red Ochre</b>	✓	✓	✓	✓	✓	✓
<b>Yellow Ochre</b>	✓	✓	✓	✓	✓	✓
<b>Lime White</b>	✓	✓	✓	✓	✓	✓
<b>Madder Lake</b>	x	✓	✓	✓	✓	✓
<b>Carmine Lake</b>	x	✓	✓	✓	✓	✓
<b>Realgar</b>	x	✓	✓	✓	MEU	x
<b>Malachite</b>	x	✓	✓	MEU	x	x
<b>Orpiment</b>	x	✓	✓	✓	✓	x
<b>Egyptian Blue</b>	x	✓	x	x	x	x
<b>Indigo</b>	x	✓	✓	✓	✓	✓
<b>Azurite</b>	x	✓	✓	✓	MEU	x
<b>Red Lead</b>	x	✓	✓	✓	✓	x
<b>Vermilion</b>	x	✓	✓	✓	✓	x
<b>Earth Green</b>	x	✓	✓	✓	✓	✓
<b>Verdigris</b>	x	✓	✓	✓	MEU	x
<b>Lead White</b>	x	✓	✓	✓	✓	✓



	Pre-historic	Antiquity	Medieval	Renaissance and early modern	Industrial Revolution	Modern
<b>Ultramarine</b>	x	x	MLU	✓	✓	✓
<b>Lead-Tin Yellow</b>	x	x	MLU	✓	x	x
<b>Smalt</b>	x	x	MLU	✓	x	x
<b>Indian Yellow</b>	x	x	MLU	✓	✓	x
<b>Copper Resinate</b>	x	x	MLU	✓	x	x
<b>Naples Yellow</b>	x	x	x	✓	✓	✓
<b>Van Dyke Brown</b>	x	x	x	✓	✓	✓
<b>Prussian Blue</b>	x	x	x	x	✓	✓
<b>Cobalt Green</b>	x	x	x	x	✓	✓
<b>Cobalt Blue</b>	x	x	x	x	✓	✓
<b>Chrome Orange</b>	x	x	x	x	✓	✓
<b>Emerald Green</b>	x	x	x	x	✓	x
<b>Chrome Yellow</b>	x	x	x	x	✓	✓
<b>Cadmium Yellow</b>	x	x	x	x	✓	✓
<b>Lemon Yellow</b>	x	x	x	x	✓	✓
<b>Zinc White</b>	x	x	x	x	✓	✓
<b>Cobalt Yellow</b>	x	x	x	x	✓	✓
<b>Cobalt Violet</b>	x	x	x	x	✓	✓
<b>Cerulean Blue</b>	x	x	x	x	✓	✓
<b>Cadmium Red</b>	x	x	x	x	MLU	✓
<b>Titanium White</b>	x	x	x	x	MLU	✓

## 1.2. Ochre

### 1.2.1. The significance of ochre in Australian Aboriginal culture

As a result of their intense and varied colour, which ranges from yellow through to deep purple, ochre minerals were commonly used as early pigments and are regularly encountered in archaeology across the globe [52-55]. It is well documented in existing archaeological records that, since the earliest occupation of Australia, Australian Aboriginal groups have used ochres as pigments in their artworks [56-58]. Testament to the significance of ochre to Indigenous Australian Aboriginals' culture, the uses of the ochre have been shown to be for both ritual and aesthetic purposes for some 61000 years [56, 57, 59].

Whilst there are multiple known ochre deposits across Australia, not all deposits of ochre were held in the same regard amongst Indigenous Australians [60] and it is well documented that many Aboriginal groups travelled large distances, in the order of hundreds of kilometres, to obtain samples from specific ochre deposits [56]. It is known that many of the most desired ochres were collected from the Pukardu [60-62], Toolumbunner [56], and Wilgie Mia [60] mines.

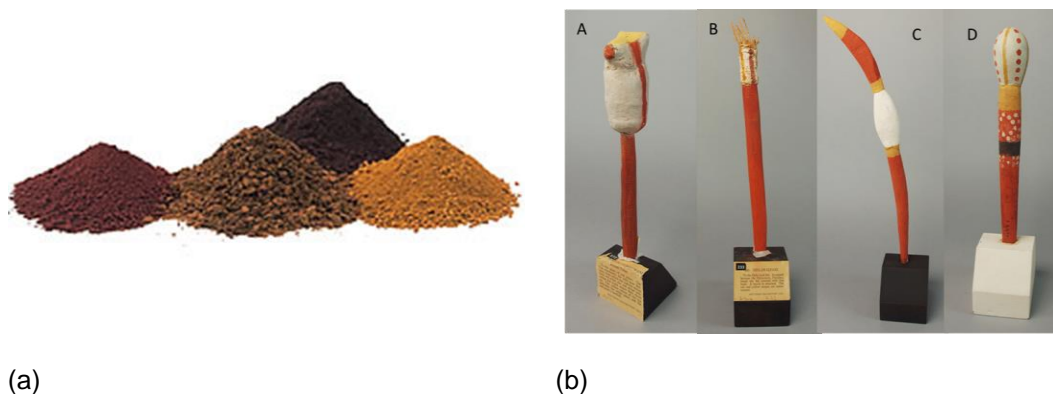
The role of ochre has been extensively studied, with both Sagona [56] and Jercher *et. al* [57] having studied deposits of red and yellow ochre in both pellet and ground form, located at the lowest levels of the Malakunanja rock shelter. Bowler *et al.* [59] have focused their investigations on the Lake Mungo skeleton coated in red pigment. These studies highlight not only the role that ochres play within Aboriginal Australian culture, but also its significance to Indigenous Australians' cultural beliefs, in particular Aboriginal Dreaming, where red ochre symbolises the blood of Dreaming Ancestors whom created and/or shaped landforms across the country [57].

A summary of the use of various synthetic and natural pigments throughout time is shown in Table 1-2.

The desired ochre deposits were highly regarded for both their specific properties and qualities, as well as for their cultural role. The significance of the various deposits is well illustrated by Sagona, where it is stated that

*'so treasured are some deposits of red ochre, and so perilous were certain ochre expeditions... that many Aboriginal people, such as the Dieri speakers of the Lake Eyre Districts, would hold a corroboree to commemorate the safe return of the party from the mines' [56].*

As well as the large distances travelled to reach an ochre deposit, often numerous other ochre deposits were passed on the expedition. Ochre was not collected from these deposits either because the site was not appropriate for the cultural rationale behind the expedition, or



**Figure 1-3:** (a) Ochre samples from Clearwell Caves, Gloucestershire, showing some of the numerous colours that ochres naturally exhibit [63], (b) photographic example of some of the toas contained by The South Australian Museum in the Reuther Collection (A) A6301 (B) A6308 (C) A6178 and (D) A6477.

because the ochre did not exhibit the desired physical properties, including, but not exclusive to, colour, texture, and composition [56].

### 1.2.2. The chemistry of ochre and their varied colours

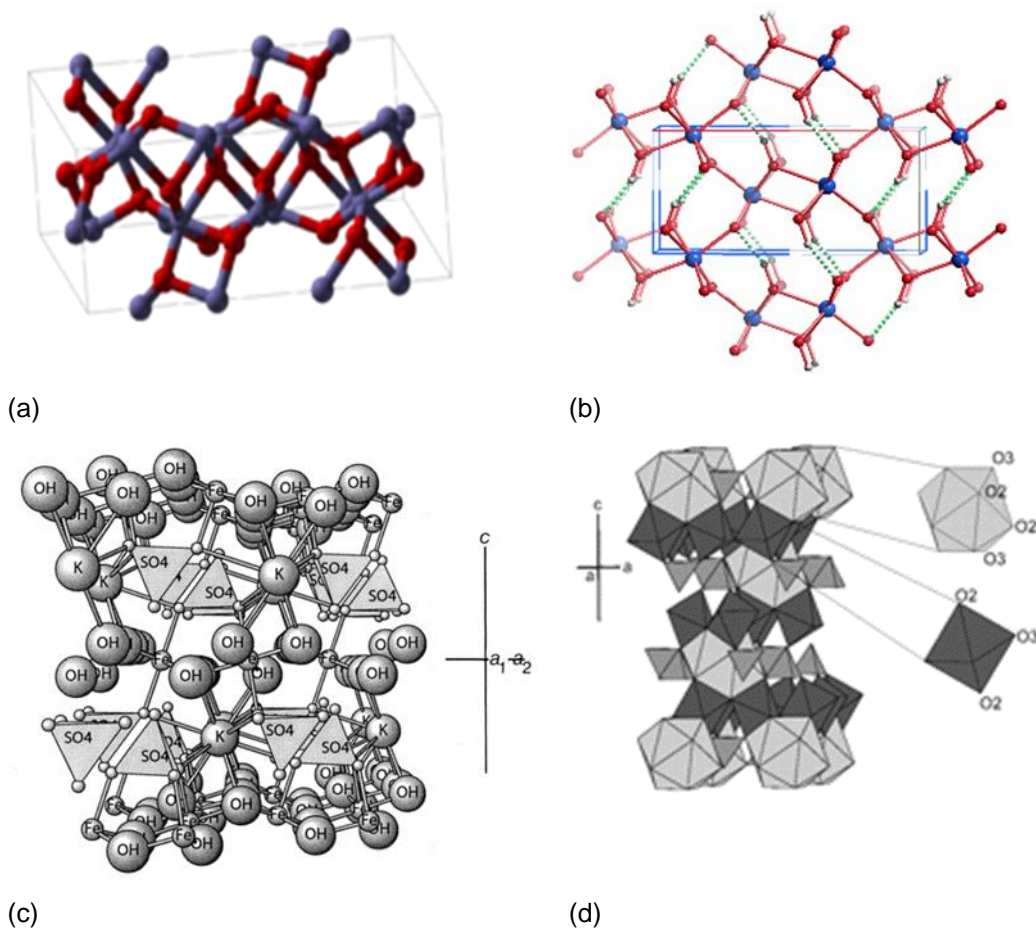
Australian Aboriginal groups have used a variety of geological substances as pigments, including both red and yellow ochres. Such materials are characteristically fine grained, soft and/or easily ground, and highly coloured, examples of which are shown in both their raw form and when applied to artefacts in Figure 1.3 [57].

Chemically, ochre is a complex, multiphase, inhomogeneous mixture, which contains either iron oxide or iron hydroxide as the chromophore (the component of the material responsible for the colour of the material) [52]. Ochres also typically contain a variety of accessory minerals, including (but not exclusive to) clay silicates, quartz, mica, gypsum, sulphates, carbonates, and other metal hydroxides/oxides [57, 64, 65].

### 1.2.3. Structure of ochre

Considering all the known factors contributing to the colour of ochres, it is accepted that the dominant factor is the chemical composition of the sample. Generally, red-coloured ochres contain haematite ( $\alpha\text{-Fe}_2\text{O}_3$ ) as the predominant pigment component, while yellow ochres typically contain goethite ( $\alpha\text{-FeOOH}$  or  $\text{Fe}_2\text{O}_3\cdot\text{H}_2\text{O}$ ) as the predominant pigment component [52, 66]. Alternatively, the characteristic colour of yellow ochre can also be a result of the dominant presence of minerals such as jarosite ( $\text{KFe}_3(\text{SO}_4)_2(\text{OH})_6$ ) and natrojarosite ( $\text{NaFe}_3(\text{SO}_4)_2(\text{OH})_6$ ) [57].

As well as the principle component contribution, the colour of ochre materials is often also influenced by the presence of one or more accessory minerals, including but not exclusive to clays, quartz, mica, gypsum, sulphates, carbonates, and other metal oxides/hydroxides.,



**Figure 1-4:** Chemical Structure of (a) Haematite  $\alpha\text{-Fe}_2\text{O}_3$ , (b) Goethite  $\alpha\text{-FeOOH}$ , (c) jarosite ( $\text{KFe}_3(\text{SO}_4)_2(\text{OH})_6$ ) and (d) natrojarosite ( $\text{NaFe}_3(\text{SO}_4)_2(\text{OH})_6$ ) where sodium polyhedra (A site) are light gray, iron octahedra are dark gray (B site) [67].

These accessory minerals are typically associated with the iron oxides [57, 64, 65], and influence the colour in combination with the particle size distribution and morphology.

Further to this, it has been shown that haematite is a dominant pigment, and as such, a small molar fraction of haematite will impart a red hue upon ochre, even in the presence of larger amounts of other pigmented minerals [64, 68]. This is reported by Mortimore *et al.* [64] where their analysis reveals significant variance in composition, as shown in Table 1-3, despite the naked untrained eye classifying samples A-C as red.

### 1.2.1. Factors that influence the colour of ochre

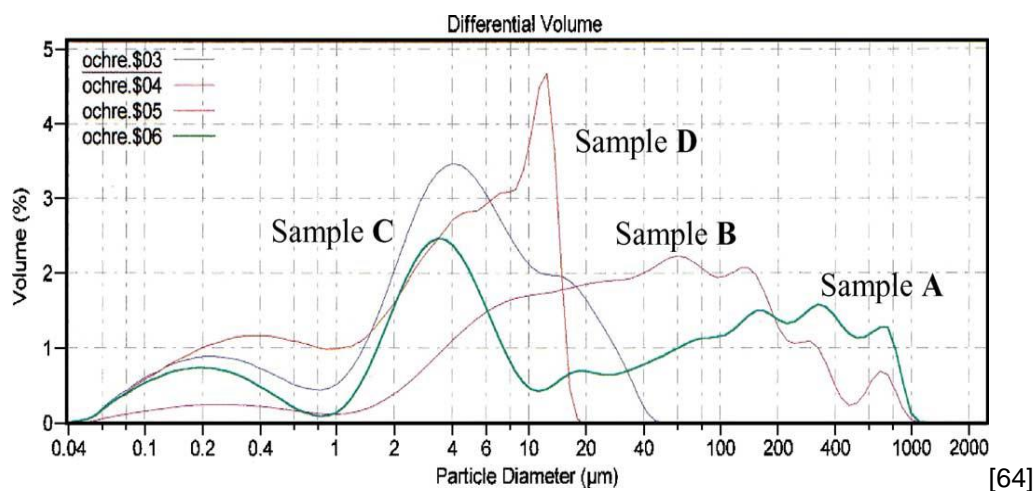
A number of factors are known to influence the colour of ochre. These include, but are not exclusive to, the chemical structure of the iron oxide chromophore, the type and quantity of accessory minerals associated with the ochre, the particle size, distribution, morphology and agglomeration, the extent of cation substitution, and whether the colour has been enhanced by heat or other treatment methods [52-55]. As a result of these factors, it is possible to have two samples of the same type of mineral with significant variations in their colour.

**Table 1-3:** Measured content of the major components of four tested ochre samples. Table reproduced from [64]

Haematite and goethite content of ochres A–D from Clearwell Caves, UK		
Sample	Haematite (%)	Goethite (%)
A	70 ± 4	2 ± 1
B	83 ± 5	4 ± 1
C	59 ± 4	20 ± 2
D	0	70 ± 5

Marshall *et al.*, in their investigation into a number of samples from Clearwell Caves, aimed to determine what role, if any, particle size has in determining the colour of ochres [52]. They combined X-ray diffraction (XRD) analysis with both infrared (IR) and inductively coupled plasma mass spectrometry (ICP-MS) and results indicate that whilst the dominant chromophore is a significant factor in the colour of the sample, particle size also plays a role. For example, when a purple ochre sample and red ochre sample are ground to the same particle size composition, significant spectral similarities are noticed [52].

Similarly, Mortimore *et al.* have also investigated the effect of varying particle sizes of ochre on the samples colour [64]. Their results for four ochre samples, previously discussed in Table 1-3, are shown in Figure 1-5 with their colours matched against the Munsell scale, as defined by Bikiaris [55], for defining soil colours and may be described as follows: A, red/brown (Munsell: 2.5R 3/4); B, mid-brown (Munsell: 10R 2.5/2); C, brown–orange (Munsell: 10R 3/4); D, orange–yellow (Munsell: 7.5YR 5/8).



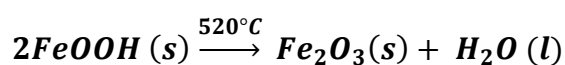
**Figure 1-5:** Particle diameter of four ochre samples of varied colours as presented by Mortimore *et al.*

When comparing the samples, the most significant variation is that of sample D where the majority of the sample lies within a much narrower particle diameter range than the other three samples, and the maximum particle diameter of any particle is fifty times smaller than any of the other three samples. This is significant as it is sample D that is yellow, whereas samples

A-C show a predominantly red colour. An interesting area of research would be to see if different particle sizes exhibited different colours. For example, in sample C if the 20+ micron particles were removed from it, would it become yellow? Alternatively, if the samples could be sieved into fractions, would these fractions exhibit different colours?

### 1.2.2. The dehydration of goethite to haematite

The percentage by weight of both the goethite and haematite components of ochres is of interest as it is known that goethite can be easily converted to haematite via a dehydration process at a temperature between 260 degrees and 550 degrees. These conditions were easily achievable for Indigenous Australians by heating the ochre - such as roasting at a camp fire – and the transition mechanism is shown by the equation below [69-71].



**Equation 1-1:** *The chemical equation for the conversion of goethite to haematite via dehydration.*

This suggests that the heat treatment of yellow ochre can result in the characteristic red colour associated with haematite, whilst still maintaining the predominant structure and majority composition of goethite. Furthermore, the chemical and phase compositions of the individual minerals are variable, through metal ion substitutions or structural phase transitions [57]. As a result it is possible to obtain a range of colours from the same type of mineral [68]. As a consequence of this, the composition of ochres that appear red can be distinctly varied, and this is significant given the cultural implications previously discussed.

### 1.3. Analysis of ochre

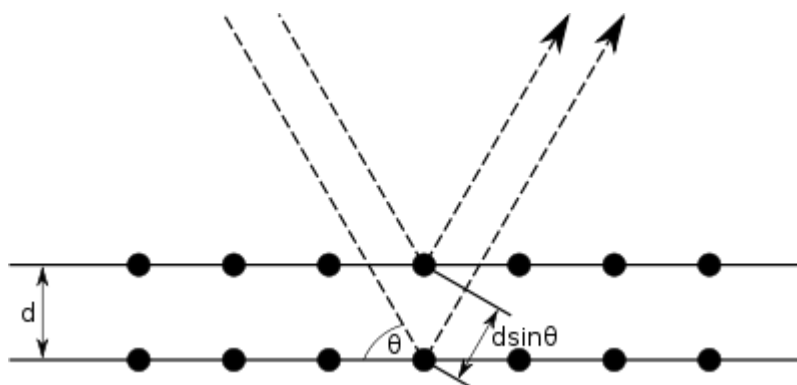
As a result of the multiple factors contributing to the distinctive colour of ochre materials, a number of studies have previously been completed in an attempt to characterise ochres. Interest in ochre is also in part due to their significance to Indigenous Australians and other groups throughout the world, combined with their multiple uses throughout history. Many of these studies have been conducted in an attempt to determine the nature of the pigments, as well as their composition and provenance, and these studies have often resulted in the development of new technology or methodology.

This section will now explore many of the studies currently available in the literature. A number of the commonly utilised techniques will be discussed in respect to both their technical aspects as well as their applications, advantages and limitations of their use.

### 1.3.1. Analysis of ochre utilising X-ray diffraction analysis and other X-ray based techniques

X-ray diffraction (XRD) is a well-established technique used to investigate the structure of crystalline materials, typically in a powdered or solid form. It is commonly used to study the atomic arrangement, crystal orientation, average grain size and crystal defects within a range of organic, inorganic and biological sample types including minerals, proteins, salts, metals and crystals [72-75].

There are a variety of similar methods based on X-ray crystallography, where generally a monochromatic beam of X-rays strikes the sample and a diffraction pattern is produced based on constructive interference and detected within the instrument [75-78]. When two X-ray beams of an identical wavelength interact with two atoms in separate planes of the same target, each beam of light travels a different distance depending on the atom with which the beam is interacting [76, 79, 80].



**Figure 1-6:** The pathways of two beams of X-rays demonstrating the different distances travelled based on atom interactions.

Here, the lower beam traverses an extra length of  $2d\sin\theta$ , with  $\theta$  representing the scattering angle. Constructive interference occurs when this length is equal to an integer multiple of the wavelength of the radiation. This leads to Bragg's law:

$$2d\sin\theta = n\lambda$$

**Equation 1-2:** Bragg's Law.

where  $n$  is an integer determined by the order given, and  $\lambda$  is the wavelength.

When conditions satisfy Bragg's Law, the interaction between the X-rays and the target produce diffraction beams scattered at specific angles determined by the lattice planes in the sample. The angles and intensities of the diffracted beams are specific to the lattice planes present and can be used to construct a three-dimensional picture of the electron density within the crystal, allowing for the determination of the periodic atomic arrangement [76, 79, 80]. Given that atomic arrangement differs for different crystalline structures, XRD essentially gives each individual sample a "fingerprint" diffraction pattern [78].

## CHAPTER ONE

When XRD analysis is used for mineral analysis (such as for ochre) two main data analysis procedures are undertaken; qualitative mineral identification and quantitative compositional analysis. Comparison of the XRD diffraction pattern to those patterns in the International Centre for Diffraction Data (ICDD) standards database allows for qualitative phase identification of many crystalline samples [81]. When combined with Rietveld analysis [82], quantitative information about the ratio of the different crystalline components within a mineral sample is able to be obtained. Whilst this can be informative, the absolute percentages of components within the mineral are unable to be determined as amorphous material cannot be detected using this technique and therefore a number of components may be unknowingly excluded [81, 83].

XRD has many advantages, including speed and accuracy of analysis, its non-destructive nature, and sample requirements including a small sample size and minimal to no sample preparation. It is a valuable tool in mineral identification but it is not without its limitations. With respect to ochre analysis, the major limitation is that it often lacks the ability to connect a sample of unknown origin with its provenance as its sensitivity levels are often too low and ochre samples from multiple regions will have significant similarities in their fingerprints.

There are many research groups currently utilising XRD for the analysis of ochre and related materials, on a variety of substrates [19, 57, 58, 65, 71, 84-97]. Other X-ray based techniques have also been applied to ochre. These include but are not exclusive to particle/proton-induced X-ray emission (PIXE) and energy dispersion X-ray analysis.

Shown below is a summary of some of the recent research currently available on ochre and related material utilising XRD and other X-ray based techniques.

It can be seen from this table that use of X-ray analytical techniques for the analysis of ochres is global, and sample types are varied. When considering ochre in its raw state (and synthetic standards created to mimic this), X-ray based techniques have been utilised by many groups with varying results, discussed below. Many of these research groups have previously been discussed, including Jercher *et al.* [57], Julia *et al.* [98], Mortimore *et al.* [64], O'Neil *et al.* [92] Clarke [61], Mazzocchin *et al.* [19], Elias *et al.* [66] and Calligaro *et al.* [99]

Mortimore *et al.* [64] have conducted numerous studies into the chemical nature of ochres utilising techniques including, but not exclusive to, Raman spectroscopy, scanning electron microscopy (with energy-dispersive X-rays (EDX) analysis), powder X-ray diffraction, diffuse reflection UV-vis spectroscopy and atomic absorption spectroscopy. Their results indicate that samples typically vary in not only the minerals present, but also in the ratio of the various elements present [64]. Creagh. *et al.* [86], Genestar *et al.* [100], Gil *et al.* [89] have also undertaken similar studies that establish that there is variation in the elemental composition of ochres.



**Table 1-4:** Summary of current research into the analysis of ochre utilizing X-ray based techniques [19, 57, 58, 65, 71, 84-97].

Author	Publication Year	Sample Location	Sample Type	Primary Analysis Method	Secondary Analysis Methods	Key Findings and Comments
<b>Beck L. <i>et al.</i></b>	2011	France	fragments from artwork and raw ochre	PIXE		PIXE shown to be successful at characterization
<b>Calza C. <i>et al.</i></b>	2010	Brazil	paintings	portable EDXRF		some pigments identified, including ochre
<b>Creagh D.C. <i>et al.</i></b>	2007	Australia	pigment material	synchrotron radiation X-ray Diffraction (SR-XRD)	PIXE	preliminary work, some composition identified
<b>David B <i>et al.</i></b>	1993	Northern Australia	raw ochre	proton induced X-ray emission (PIXE)		elemental 'fingerprint' identified for each sample
<b>David B <i>et al.</i></b>	1995	North Queensland	raw ochre	XRD	petrographic, SEM/EDXA, FTIR, PIXE/PIGME	mineralogical and elemental fingerprint defined
<b>Erlandson J.M <i>et al.</i></b>	1999	North America	raw ochre	PIXE	principal component analysis	minimal success at geological distinction

## CHAPTER ONE

<b>Author</b>	<b>Publication Year</b>	<b>Sample Location</b>	<b>Sample Type</b>	<b>Primary Analysis Method</b>	<b>Secondary Analysis Methods</b>	<b>Key Findings and Comments</b>
<b>Gil M. <i>et al.</i></b>	2007	Portugal	raw ochre	WDXRF	XRD, CIELAB, munsell colour	mineral compositions identified
<b>Jercher M <i>et al.</i></b>	1998	Australia	raw ochre	Rietveld XRD	XRF	partial provenance distinctions achieved
<b>Genestar Julia C <i>et al.</i></b>	2004	Spain	raw ochre, synthetic standards	XRD	thermal analysis (TG and DTG)	detection and quantification of the main component achieved
<b>Manasse A <i>et al.</i></b>	2006	Siena, Italy	raw and burnt sienna	XRD	SEM-EDS, TEM-EDA, thermal, TG/DTA and DRIFT	hematite pigment dominates colour
<b>Mazzocchin G.A. <i>et al.</i></b>	2003	Venezia, Italy	wall paintings	XRD	SEM, EDS microanalysis, FTIR, optical microscopy	successful identification of a number of pigments
<b>Ohkawa M <i>et al.</i></b>	2000	Japan	ore deposits	XRD	electron microprobe, IR	preliminary characterisation and distinction achieved
<b>O'Neill P.M. <i>et al.</i></b>	2004	Arnhem Land	raw materials	synchrotron radiation XRD		inter-site variation demonstrated

Author	Publication Year	Sample Location	Sample Type	Primary Analysis Method	Secondary Analysis Methods	Key Findings and Comments
<b>Ortega M. <i>et al.</i></b>	2001	Mexico	prehistoric pigments	energy dispersion X-ray analysis	electron microscopy (scanning, and high resolution transmission) and FTIR	techniques used in artworks linked to other cultures
<b>Popelka-Filcoff R.S. <i>et al.</i></b>	2007	Missouri	raw ochre (mines)	XRF	INAA	provenance based trends identified
<b>Prasad P.S.R. <i>et al.</i></b>	2006	India	natural samples from a banded iron formation, synthetic standards	XRD	differential scanning calorimetry (DSC) thermal analysis, FTIR	similar behaviours exhibited for the two naturally occurring and synthetic goethites
<b>Reiche I. <i>et al.</i></b>	2005	India	painting pigments	external beam PIXE	XRF, PIGE	typical pigment palette of the 17th - 19th century established
<b>Stievano L. <i>et al.</i></b>	2003	Italy	ceramics	Mössbauer spectroscopy		systematic study into Mössbauer spectroscopy and its applications in archaeology

<b>Author</b>	<b>Publication Year</b>	<b>Sample Location</b>	<b>Sample Type</b>	<b>Primary Analysis Method</b>	<b>Secondary Analysis Methods</b>	<b>Key Findings and Comments</b>
<b>Valadas S. <i>et al.</i></b>	2008	Portugal	mortars, mural paintings	XRD	TGA, SEM-EDX, optical microscopy, CHNS elemental analysis	pigments confirmed to be from local sources
<b>Weinstein-Evron M <i>et al.</i></b>	1994	Israel	ochre fragments, synthetic standards	XRD	Inductively Coupled Plasma-Atomic Emission Spectroscopy (ICP-AES)	possible sources found for the ochre in the rock art

Marshall *et al.* have utilised XRD in their investigation into a number of raw ochre samples from Clearwell Caves with their primary aim being to determine what role, if any, particle size has in determining the colour of ochres [52]. They have combined XRD analysis with both infrared spectroscopy and inductively coupled plasma mass spectrometry and results indicate that whilst the dominant chromophore is a significant factor in the colour of the sample, particle size also plays a role as when a purple ochre sample and red ochre sample are ground to the same particle size composition, significant spectral similarities are noticed [52].

Ohkawa *et al.* have also utilised XRD in combination with a number of other techniques including but not exclusive to infrared spectroscopy and electron-probe microanalysis in their work, in which they study the haematite components in pyrophyllite ore deposits in the Shobara district in southwestern Japan [65]. The results of this study indicate that these techniques have the ability to both identify haematite and to examine the relative contributions of impurities, including water, however no attempts are made to determine geographical provenance of unknown samples [65].

Recent work by Creagh *et al.* [86] is of interest because it focuses not only on the use of X-ray technology for the analysis of ochre, but more specifically if such analysis can be used to determine the provenance of the ochres being investigated. Here, synchrotron radiation was used to determine the phase composition of raw ochre, and comparisons are made to samples obtained from mines in central and Western Australia. Whilst results are not conclusive at this stage with results proving to be not precise enough to determine exact sample origin, the work shows promise in this expanding area.

### 1.3.2. Spectroscopic and spectrometric analysis of ochre

There are many analytical methods available today that employ spectroscopic and spectrometric based techniques. These include but are not exclusive to infrared spectroscopy, Raman spectroscopy, Mossbauer spectroscopy, spectro-photo-colourimetry, visible/electronic spectroscopy, laser induced breakdown spectroscopy, far-infrared spectroscopy (FIR), laser ablation inductively coupled plasma mass spectrometry (LA-ICP-MS) and diffuse-reflectance spectrophotometry.

A large number of research groups have utilised a number of these spectroscopy based techniques over the last decade. Those publications specifically relating to pigments and ochres are shown in Table 1-5. Infrared and Raman spectroscopy are the most commonly applied of these techniques and are reviewed below.

CHAPTER ONE

**Table 1-5:** Summary of current research into the analysis of ochre utilizing Raman and infrared spectroscopy based techniques [19, 52, 53, 55, 64, 66, 69, 70, 101-111]

Author	Publication Year	Sample Location	Sample Type	Primary Analysis Method	Secondary Analysis Methods	Key Findings/ Comments
Bikiaris D <i>et al.</i>	1999	Greece	raw and treated ochres, paintings	micro-Raman	micro-FTIR spectroscopy, SEM	minor basic differentiation achieved
Blanch A.J. <i>et al.</i>	2007	South Australia	raw ochre and synthetic standards	autocorrelation infrared spectroscopy		experimental parameters have little influence on aurocorrelation values
Castro K <i>et al.</i>	2004	Paris	lithographs, books	micro-Raman	FTIR spectroscopy	successful determination of some inorganic pigments
de Faria <i>et al.</i>	2002	Brazil	cave paintings	Raman	thermogravimetry, XRD, SEM	study aimed to differentiate natural hematite from heated goethite and observed the transformation when heated, but differentiation was unsuccessful
Dubiel S.M. <i>et al.</i>	2011	France	raw ochre	Mossbauer Spectroscopy		a* and b* colour curves

Author	Publication Year	Sample Location	Sample Type	Primary Analysis Method	Secondary Analysis Methods	Key Findings/ Comments
Edreira M.C. <i>et al.</i>	2001	Spain	roman wall paintings	visible/electronic spectroscopy - Otsuka MCPD 1100 UV	FTIR, EDS, XRD	no provenancing was able to be established, but suggestions made that ochre sources may be geochemically distinctive
Edreira M.C. <i>et al.</i>	2003	Spain	roman wall paintings	visible/electronic spectroscopy - Otsuka MCPD 1100 UV	EDS, FTIR, XRD, SEM	some sample distinctions made
Edwards H.G.M	2003	Rome	cave paintings and paint fragments	FT-Raman spectroscopy		some decorative pigments identified
Elias M <i>et al.</i>	2006	France	Industrial Ochres	spectro-photo-colourimetry	X-ray Diffraction, SEM, TEM	L*a*b colour scale and diffuse reflectance
Helwig K	1998		earth pigments, cultural artefacts	infrared spectroscopy	XRD, Mossbauer spectroscopy, TA, XRF	complete sample distinction based on infrared spectroscopy unsuccessful.
Lazic V. <i>et al.</i>	2003	Italy	Renaissance dishes	laser induced breakdown spectroscopy	laser induced fluorescence	demonstrated that techniques are non-

## CHAPTER ONE

Author	Publication Year	Sample Location	Sample Type	Primary Analysis Method	Secondary Analysis Methods	Key Findings/ Comments
						destructive and semi-quantitative
Marshall L-J <i>et al.</i>	2005	Gloucestershire, UK	raw ochre	IR spectroscopy	diffuse reflectance UV-Vis-NIR, XRD, ICP-AES, particle size analysis	the effect of particle size on colour composition demonstrated
Mazzeo R. <i>et al.</i>	2004	Nepal	pigments from a painted temple	micro-Raman	microscopy, SEM-EDX	preliminary identification of layers in the painting achieved, further investigation required
Mirti P <i>et al.</i>	2004	Southern Italy	pottery	portable spectrometry - Minolta CM-508i	sample preparation via heating	colour curves based on I*a*b and CIE
Mortimore J.L <i>et al.</i>	2004	Turkey and UK	raw ochre	IR spectroscopy	Raman, SEM, powder XRD, SEM (with EDX), Diffuse Reflectance UV-Vis, AAS	comparison of iron oxide content between the two locations

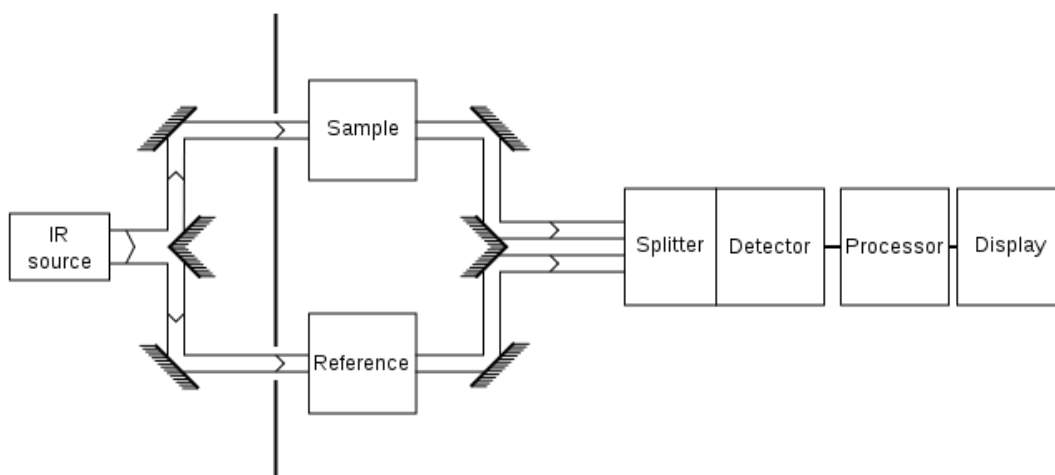


Author	Publication Year	Sample Location	Sample Type	Primary Analysis Method	Secondary Analysis Methods	Key Findings/ Comments
Perardi A. <i>et al.</i>	2000	Siena, Sardinia	iron nails, Renaissance paintings	micro-Raman		explores possible applications of micro-Raman
Ruan H.D. <i>et al.</i>	2002		synthetic alumina phases	far-infrared spectroscopy (FIR)	FT-Raman, mid-IR and near -IR	separation of some phases achieved
Ruan H.D. <i>et al.</i>	2002		synthetic goethite	FT-IR		study of goethite-hematite dehydration
Smith K. <i>et al.</i>	2005		synthetic paints	LA-ICP-MS		distinction between manufacturers possible (forgery detection preliminary work)
Wang J <i>et al.</i>	2005		synthetic iron oxide hematite	Diffuse-reflectance	SEM, Munsell colour notation, Raman	possible mechanisms for the optical properties proposed

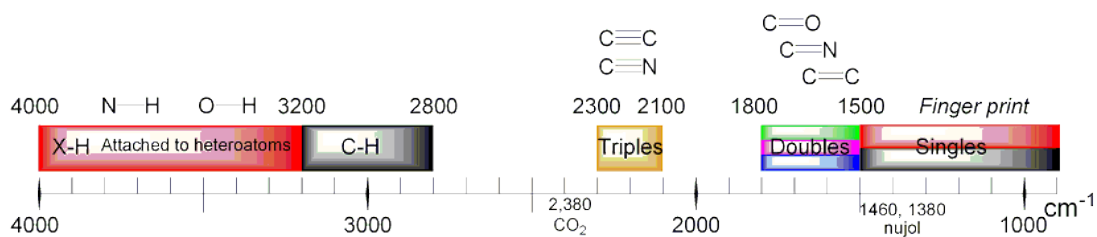
## 1.3.2.1. Infrared methods

A range of techniques are based on infrared spectroscopy where detection of molecular vibrations is exploited. These include near-, mid- and far-infrared spectroscopy, Fourier-transform infrared (FTIR) spectroscopy, and diffuse reflectance. Here substances emit or absorb infrared light in conjunction with vibrational-rotation movements, and most infrared spectroscopy techniques exploit the absorption and transmission of photons within the range of infrared light [112-114]. Infrared radiation can be further sub-classified into three groups; near-infrared spectroscopy that uses the region of  $14000\text{-}4000\text{cm}^{-1}$ , (this aligns with the upper limit of the visible spectrum), mid-infrared the region of  $4000\text{-}400\text{ cm}^{-1}$ , and far-infrared based in the region of  $400\text{-}10\text{ cm}^{-1}$ . IR spectroscopy techniques examine and analyse the constituent bonds present in the molecules based on the characteristic vibrations observed. Functional groups within a molecule can have one or multiple modes of stretching and bending oscillations. In order for a vibrational mode in a molecule to be able to be detected utilising infrared spectroscopy based techniques, the vibrational mode must also be associated with a change in dipole moment. The frequency at which a photon is absorbed is unique for each functional group present, and as a result, analysis results in a gain of information surrounding the sample composition and the functional groups present [114-116].

All IR instruments will contain a source (usually incandescent or quartz halogen based globe or a light-emitting diode), a Fourier transform interferometer or a dispersive element (typically a diffraction grating but also commonly a prism or similar) and a detector (with the type of detector varying primarily based on the wavelengths being investigated but including 2D arrays, electron multipliers and silicon based CCDs). The infrared spectrum of the molecule is recorded by passing the beam of infrared light through the sample. Absorption occurs when the frequency of the beam of light is equal to the vibrational frequency of the functional group, and detection and analysis of the transmitted light shows the relationship between the energy absorbed and the incident wavelength [114-118].



**Figure 1-7:** A simple schematic of a two-beam absorption infrared spectrometer.

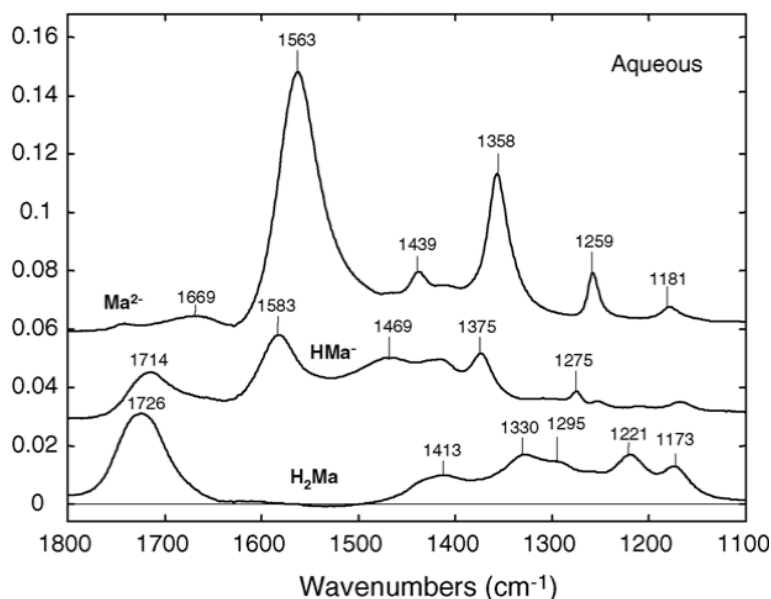


**Figure 1-8:** Infrared spectroscopy correlation table showing the bands over which peaks are present and the functional groups responsible within the structures studied.

A number of various types of data collection and analysis exist. For example, FTIR spectroscopy is based on a mathematical process of converting the raw data into the spectrum. Here, the infrared light passes through an interferometer separately to the sample, with a moving mirror used to alter the distribution of light passing through the interferometer. The raw data is then processed and the spectra collected. Alternatively, the scanning monochromator method (otherwise known as the dispersive method) relies on a single wavelength passing through the sample at a time. Whilst this is understandably more time consuming and less practical than the Fourier transfer method, both methods are common in modern laboratories [117, 119].

Allan *et al.* have utilised infrared spectroscopy in their studies into the mineralogy of 11 concretions from the Bronze Age settlement horizons at Brean Down near Weston-super-Mare, Somerset, UK [120]. The samples investigated have been found to contain impurities, varying between samples but including quartz, calcite and apatite. Their work also centres on the rapid identification of coprolitic material from archaeological sites utilising both infrared spectroscopy and scanning electron microscopy [120].

The work conducted by Hug *et al.* also centres on the use of Infrared Spectroscopy [121]. Their work primarily consisted of studies into the adsorption of oxalate, malonate and succinate on anatase, rutile and lepidocrocite utilising attenuated total reflectance Fourier-transform infrared spectroscopy (ATR-FTIR). Visibly different spectra were obtained for the same sample when comparing the aqueous species to the sample where the species is adsorbed to a surface. An example of this is shown in Figure 1-9 where the spectra of malonate adsorbed to anatase and rutile from aqueous malonate solutions (200-M,  $I = 0.01M$ ) at different pH values from 9.0 to 3.0, and of the aqueous malonate and malonic acid species (100 mM) are shown. Clearly evident from this image is the distinct differences in the spectra. The authors comment that the most noticeable difference is the absence of the C=O frequencies in adsorbed malonate. They also make mention that the COO vibration is shifted from  $1563\text{ cm}^{-1}$  when the sample is aqueous to  $1581\text{ cm}^{-1}$  and  $1583\text{ cm}^{-1}$  when the sample is adsorbed, and that this shift suggests a strong interaction is occurring. This study concluded that surface specific interactions could be used as a diagnostic tool for mineral oxides [121].



**Figure 1-9:** ATR-FTIR spectra showing the variations observed as a result of altering the pH of the aqueous malonate solutions [121].

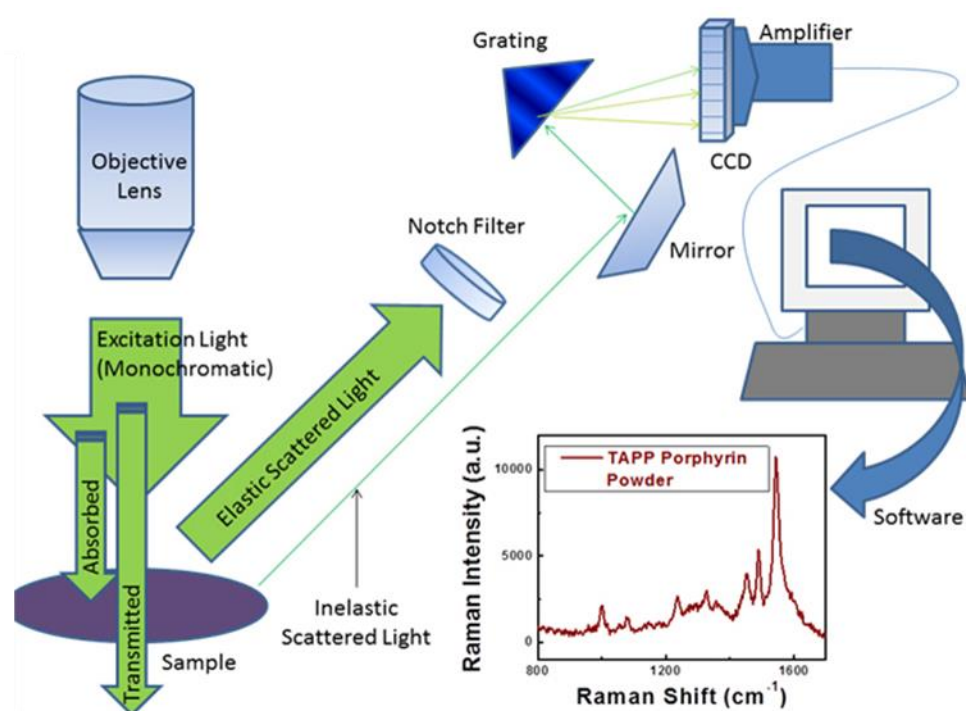
Recently, Blanch *et al.* have implemented the use of an autocorrelation infrared (ACIR) method of analysis to a number of synthetic and natural mineral samples and ochres [105]. Varying experimental factors including sample preparation, instrumental and data collection parameters, was shown to have little effect and the authors concluded that the ACIR technique is both reproducible and valuable for the analysis of synthetic iron oxides that show only slight variations in composition or structural states [105]. Whilst the use of autocorrelation analysis showed that the comparison of the autocorrelation values obtained from the infrared spectra across a large range of absorbance peaks was not an effective method for linking ochres to their source deposits, the use of infrared spectroscopy combined with alternate analysis methods cannot be discarded.

#### 1.3.2.2. Analysis of ochre utilising Raman based techniques

Raman spectroscopy is an analytical method based on the Raman Effect. It can be used not only for characterisation of materials, but also to determine the crystallographic orientation of a sample tissue [122, 123].

The Raman Effect is when a molecule is excited from its ground state to a virtual energy state by a photon. Relaxation of the molecule to a third state, typically a vibrational or rotational state, results in the emission of a photon. The new state of the molecule and the ground state have different energies, and this difference results in a shift in the photon's frequency, with the shift dependent on the exact difference in the energy states [124-127].

Raman spectroscopy is an analysis method based on this photon energy shift. The shift in photon energy is typically a result of the molecular vibrations caused by an interaction between the target and a monochromatic light source [129-131]. Observed modes are typically low-



**Figure 1-10:** Schematic diagram of Raman spectroscopy. Image from [128].

frequency and include vibrational and rotational modes, with scattering measured in the infrared or near-IR range [129].

In a typical experimental set up, the sample is illuminated by a laser beam. A lens collects the resulting light and a monochromator filters any light detected that might be a result of Rayleigh scattering, before the remaining light is passed to a detector [132, 133].

Many research groups around the globe are using Raman for a number of applications [19, 55, 69, 101-104]. Discussed below is a summary of some of the recent research currently available on ochre and related material utilising Raman.

Castro *et al.* utilised Raman Spectroscopy, specifically Fourier transform Raman spectroscopy, as a means to identify the pigments present in nineteenth-century artwork, in particular hand-painted lithographs [101]. Samples were placed in a planar kit for paper samples, and analysed with an approximated resolution of 0.5mm. This method eliminated the need for optical microscopy, and the non-destructive nature of FT-Raman allowed for complete restoration of the artworks. This work has the potential to not only date the art work, but also assists in the verification the authenticity of many of the paintings.

Edwards has applied the non-destructive technique of Raman spectroscopy to a number of samples including, but not exclusive to, prehistoric cave paintings (ca 3000 BC) from the Rio Grande region, paint fragments from recent excavations at King Herod's Palace, Jericho (ca 6 BC), medieval wall paintings from Winchester Cathedral and Sherborne Abbey, medieval wall paintings from the Convento de la Peregrina, (Sahagun, Spain) and from the church of

SS Cosmo y Damien, Basconillos del Tozo, (Burgos, Spain) as well as a polychrome medieval statue of Santa Anna from Silos, (Spain) and a biodeteriorated Renaissance frescoes from the Palazzo Farnese (Caprarola, Italy) [102]. His research has focused primarily on the establishment of a database concerning the microscopic components of the pigments as a result of various mixing and substrate treatment, as well as variations in the composition of the pigments. Edwards was also able to determine, via the use of known developmental timelines of various plasters, and utilising Raman spectroscopy as a means of comparison, the approximate age of a number of pieces of artwork. This is significant as it can be used to assist in the identification of forgeries and in determining possible origins of the artwork [102].

Raman spectroscopy has been further utilised by Mazzeo *et al.* [134]. Their work focused primarily on the characterisation of the composition of the pigments present in a number of paint samples collected from the south and east wall decorations of the 15th century Thubchen Lakhang monastery located in Lo Manthang, upper Mustang, Nepal. Initial analysis included the preparation of cross-sections of the samples followed by stratigraphical pigment composition analysis [134].

### 1.3.3. Trace element methods

A number of the techniques discussed previously rely on the elemental analysis of ochre for discrimination. These include NAA, XRD, laser ablation ICPMS, and XRF. Of these, NAA is the most commonly applied to ochre. NAA is a technique by which the properties of the atomic nucleus are utilised to determine the sample composition for more than 70 elements, approximately 30 of which are commonly present in soil and ochre [135]. When the sample is exposed to neutrons the elements present form radioactive isotopes. These isotopes and subsequent emissions and decay paths are unique for each element, and the spectra obtained from these emissions can then be used to determine elemental concentrations [136]. Advantages of NAA include sample preparation – samples are not contaminated, and because NAA is a nuclear technique the results are not affected by the state of the sample. NAA is also considered a non-destructive technique, although considerations do need to be made for the possible radioactivity remaining in the samples. NAA allows for the discrete sampling of elements, independent of the chemical form [135, 137].

The elemental composition of ochre is key to the understanding of inter-site and intra-site variation, and is a vital tool for the discrimination of ochre based on source. Table 1-6 highlights a number of published studies that utilise NAA, XRD, laser ablation ICPMS, and XRF with the primary aim of provenancing.

Work by Beck L. *et al.* [84] applied PIXE to discriminate between sources based on trace elemental composition, and comparisons are made to rock art in surrounding areas. Results indicate that that element ratios such as Mn/Fe and Zn/Fe demonstrate a clear discrimination between samples and work has expanded to include sampling of other potential source areas.

**Table 1-6:** Summary of current research into the analysis of ochre utilizing a number of techniques where trace element analysis is the primary aim [58, 84, 87-89, 91, 94, 138].

Author	Publication Year	Sample Location	Sample Type	Primary Analysis Method	Secondary Analysis Methods	Key Findings and Comments
Beck L. et al.	2011	France	fragments from artwork and raw ochre	PIXE		PIXE shown to be successful at characterization
David B et al.	1993	Northern Australia	raw ochre	PIXE		elemental 'fingerprint' identified for each sample
David B et al.	1995	North Queensland	raw ochre	XRD	petrographic, SEM/EDXA, FTIR, PIXE/PIGME	mineralogical and elemental fingerprint defined
Erlandson J.M et al.	1999	North America	raw ochre	PIXE	principal component analysis	minimal success at geological distinction
Gil M. et al.	2007	Portugal	raw ochre	WDXRF	XRD, CIELAB, Munsell colour	mineral compositions identified
MacDonald B.L. et al.	2008	British Columbia	raw ochre	INAA		chemical composition of ochres determined
MacDonald B.L. et al.	2011	British Columbia	raw ochre	NAA		chemical groups differentiated through elemental and statistical analysis
Popelka-Filcoff R.S. et al.	2011	Australia	raw ochre	NAA		comparison between relative comparator and K0-NAA
Popelka-Filcoff R.S. et al.	2012	Australia	raw ochre	NAA		elemental compositions identified

#### 1.3.4. Analysis of ochre utilising non-traditional or multidisciplinary based techniques

It is evident from many studies previously presented, that a single technique is often insufficient for precise and accurate studies into difficult sample media. Often one technique is the primary method used with complimentary minor techniques utilised, and other studies require a truly multidisciplinary approach. The latter will be discussed here, with relevant literature presented in Table 1-7.

Marshall *et al.* acknowledge that they are building on the work of Bikiaris *et al.* [55] who, have utilised a number of spectroscopic and microscopic techniques including but not exclusive to scanning electron microscopy (SEM), FTIR spectroscopy and Raman. Results of this work indicate that various minerals and synthetic additives can be identified and distinguished between in a number of mediums, and that there are multiple factors contributing to the dominant colour of ochres [55].

Whilst XRD is the most common technique utilised in the analysis of ochres, it is apparent that it is not the only method available. Laser ablation inductively coupled plasma mass spectrometry (LA-ICP-MS) is a growing area of research that allows for sensitive trace element analysis.

Watling *et al.* are currently utilising this method in their research into the authentication of works of art [139]. As previously discussed, ochres are a mixture of iron oxides (varying depending on the colour of the ochre but typically either goethite or haematite), and a combination of a number of impurities including but not exclusive to clay silicates, quartz, mica, gypsum, sulphates, carbonates, and other metal hydroxides/oxides. The work of Walting *et al.* exploits this variability in ochre composition and has involved attempts to provenance art work by comparison of the unique 'fingerprint' results of the elemental composition of the ochre composition of dyes in the art work to results of ochres from known locations [139].

An example of the 'fingerprint' analysis results are shown in Figure 1-11, where two ochre samples are compared and are visibly distinguishable.

Further work by Walting *et al.* has focused on the establishment of data bases based on the canvas type and manufacture process, any papers involved, as well as arson and various constituents of paints and the manufacturing process involved in further attempts to identify forgeries [139].

Clarke has also completed studies into the properties of ochres utilised as pigments [61]. Here, samples were collected from Western Australia of both white and red natural ochres that have been used in rock paintings and examined microscopically in order to determine the particle



**Table 1-7:** Summary of current research into the analysis of ochre utilizing multidisciplinary techniques [60, 61, 93, 97, 99, 140-145].

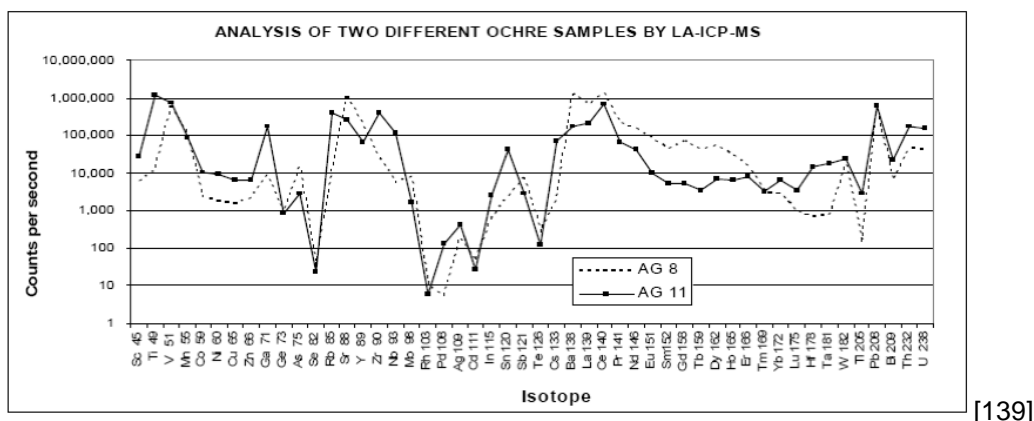
Author	Publication Year	Sample Location	Sample Type	Primary Analysis Method	Secondary Analysis Methods	Key Findings/ Comments
<b>Aquila E. et al.</b>	2011	Italy	painting wall fragments	multi-disciplinary	XRF, SEM-EDS, FT-IR	substrates and pigments identified using the multi-technique approach
<b>Brugger J. et al.</b>	2006	South Australia	raw ochre	electron micro-probe analysis		geographical chemical characteristics identified
<b>Calligaro T. et al.</b>	2003	France	museum arts	photo-detection	iron beam analysis, PIXE, PIGE	new trends in the use of photo-detectors in Art and Archaeology are presented
<b>Colombini M.P et al.</b>	2004	Greece	astragalos	multi-disciplinary	microscopy, environmental SEM, ESEM-EDX, FTIR, micro-ATR, HPLC, UV-fluorescence, GCMS	analysis showed that egg was used in sample preparation
<b>Clarke J</b>	1976	Western Australia	rock art pigments	multi-disciplinary	microscopic spectrographic analysis, particle size and shape, refractive index, XRD,	
<b>Frost R.L et al.</b>	2003	Flinders Rangers, South Australia	natural raw ochre	TGA	XRD, FTIR, DSC	phase changes observed when heating

Author	Publication Year	Sample Location	Sample Type	Primary Analysis Method	Secondary Analysis Methods	Key Findings/ Comments
<b>Goss C.J</b>	1987		synthetic goethite	TGA	XRD, transmission electron microscopy	study into the dehydration mechanism of goethite
<b>Green R.L et al.</b>	2007	Western Australia and Northern Territory	powdered raw ochre	LA-ICP-MS		some provenancing achieved via trace metal composition
<b>Iriarte E. et al.</b>	2009	Spain	cave paintings, raw ochre	multi-disciplinary	petrography, XRD, SEM-EDX, ICP-MS	successful identification and characterisation of different ochre types
<b>Montagner C. et al.</b>	2013	Lisbon	oil paintings, powdered ochres	multi-disciplinary	m-FTIR, m-EDXRF, XRD, raman	no single technique completely successful, but combined shows promise
<b>Mooney S.D. et al.</b>	2003	unknown sources	raw quarry ochre	magnetic parameters		able to distinguish between some samples, but more detail needed to confirm provenance of unknown ochres
<b>Ortega-aviles M et al.</b>	2001	Cacaxtla	painting fragments	multi-disciplinary	Electron microscopy, SEM, TEM, FTIR, XRD	pigment components identified, include hematite

---

<b>Author</b>	<b>Publication Year</b>	<b>Sample Location</b>	<b>Sample Type</b>	<b>Primary Analysis Method</b>	<b>Secondary Analysis Methods</b>	<b>Key Findings/ Comments</b>
<b>Smith M.A. <i>et al.</i></b>	1997	central Australia	fine-grained quartz from raw ochre	oxygen- isotope ratios		limited success in provenancing ochres
<b>Valdez B. <i>et al.</i></b>	2008	Mexico	rock paintings	multi- disciplinary	SEM, EDS, FTIR	physical and chemical characteristics determined

---



**Figure 1-11:** LA-ICP-MS spectra obtained for two ochre samples showing their variation. [139]

size and shape, utilising X-ray diffraction technology to determine the sample purity, and with electron probes. Studies focused on establishing a link between the ochres properties and their durability with the ultimate goal of preservation [61].

Colombini *et al.* utilised a number of techniques, both destructive and non-destructive, in order to investigate the origin of the pigment in a series of paintings in Greek caves [146]. These techniques included, but were not exclusive to, optical microscopy, environmental scanning electron microscopy coupled with X-ray microanalysis, FTIR spectroscopy with micro-attenuated total reflection, high performance liquid chromatography coupled with UV-fluorescence, and gas chromatography–mass spectrometry, and results indicate that the pigments used in the cave paintings studies included ground ochres [146].

Mazzocchin *et al.* have also utilised a number of techniques in an attempt to characterise a series of samples obtained from Roman wall paintings, focusing on colour preparation and application [19]. These techniques included but were not exclusive to optical microscopy, scanning electron microscopy equipped with an EDS microanalysis detector, X-ray powder diffraction and FTIR spectroscopy. Results of these studies indicated that the principal pigment components, such as cinnabar, haematite, red ochre, celadonite, cuprorivaite (Egyptian blue), yellow ochre, goethite and carbon, were often identifiable as a result of a combination of techniques, however no attempts were made to distinguish between samples of the same pigment component [19].

#### 1.4. Provenance of ochre

The provenancing of ochre continues to be the focus of a number of research groups across the globe. Work in this area is ever expanding due to the significant information that is able to be obtained both chemically and culturally from the successful provenancing of ochre material. Vital cultural information about trade routes and source desirability can be gained by examining the chemical composition of a wide range of ochre and considering the inter-site and intra-site elemental similarities and differences.

**Table 1-8:** Oxygen Isotope ratios in quartz in a number of ochre samples. The table is reproduced from reference [60]

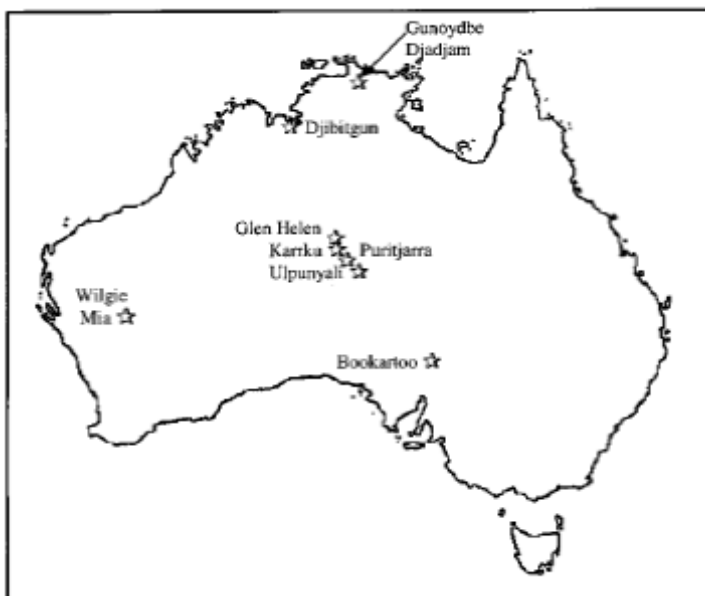
Sample	SiO <sub>2</sub> (%)	Number of analyses	Mean $\delta^{18}\text{O}\%$ (SMOW)	Range $\delta^{18}\text{O}\%$ (SMOW)
N5/24-6	54	3	11.8 ± 0.20	11.7 ± 12.1
Ulpunyali	43	3	11.7 ± 0.21	11.6 ± 12.0
Karrku	30	2	11.8 ± 0.22	11.7 ± 12.0
Paterson X	34	3	12.3 ± 0.15	12.1 ± 12.4
Bookartoo	20	2	13.8 ± 0.50	13.5 ± 14.2

Smith *et al.* [60] utilised oxygen isotope ratios in quartz as a means of establishing the provenance of origin in a series of archaeological ochre samples. Whilst the method of stable oxygen isotope ratios is well established, Smith *et al.* were the first to apply this technique to Australian ochres. Their results indicate that, if used in conjunction with other techniques, the ratio of stable oxygen isotopes can be used to distinguish between ochres of distinctly different geographical origin. However, the technique was not specific enough as to distinguish between ochres from the same region, such as the Karrku and Ulpunyali mines, which geographically are separated by approximately 150km [60].

Shown below in Table 1-8 are the results obtained by Smith *et al.* for the oxygen-isotope ratios of the quartz component of natural ochre samples. This demonstrates that samples taken from ochre deposits within close geological proximity are unable to be distinguished between using the oxygen-isotope ratios in quartz as a stand-alone technique. Significant however, is the variation, even when considering error, between the unknown sample (N5/24-6), Paterson X, and particularly Bookartoo. The authors say that, “on the basis of these results sample N5/24-6 is unlikely to have come from Bookartoo, or from the same source as Patterson X” [60].

Elias *et al.* [66], though their analysis of a series of both ancient and modern ochres, have attempted to determine the geological origin of the samples. Utilising a series of techniques, including diffuse reflectance spectrophotometry, X-ray diffraction, scanning electron microscopy, transmission electron microscopy and laser diffraction particle size analysis, they have demonstrated that, in combination, these techniques have the ability to, for a given sample, give an indication as to its geographical origin [66]. However, they were unable to distinguish between known ochre sites and mines within the same geographical region [66]. This was also the case for Genestar Juliá and Pons Bonafé where, utilising thermal analysis techniques based on the differential separation of ochres, general geographical origin was able to be determined, but with sensitivity that would not allow for specific site determination [98].

Similar results were obtained from Mooney *et al.* where, by utilising the samples specific magnetic properties such as the isothermal resonance and magnetic susceptibility, they were able to distinguish between multiple ochre samples of known geographical origin [145]. These



**Figure 1-12:** Location of ochre sources utilised by Mooney *et al.* [144]

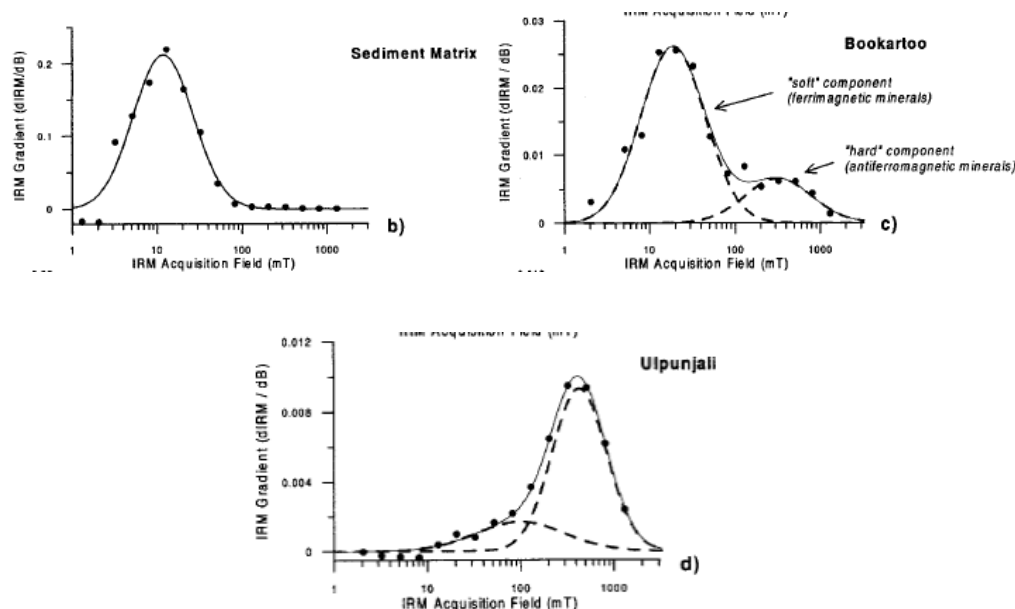
geographical origins varied significantly with samples being taken from a number of known Australian ochre sites (shown below), including but not exclusive to Ulpunyali, Bookartoo (also known as Pukartu), Karrku, Djibitgun, Puritjarra, Paterson X, Wilgi Mia and Glen Helen [145].

Results of this analysis indicate that there are significant variations between the magnetic susceptibility of the samples tested. For example, shown below are the results of preliminary analysis on ochres from significantly different geographical providences, and evident is the variation in their IRM acquisitions [144].

However, this level of variation is not always apparent and whilst the techniques that Mooney *et al.* utilised were largely non-destructive, they required a large sample volume, and in general the sensitivity was low such that the methods utilised could not determine the geographical location of unknown samples [145].

David *et al.* have also performed analysis on Australian ochres. They focused primarily on red ochres and utilised PIXE (particle induced X-ray emission), whereby a large number of elements can be determined both qualitatively and quantitatively. Their research was largely exploratory but showed that this technique is capable of creating a characteristic fingerprint of an ochre sample, which can then be compared to that of a known origin. However, results indicate that the sensitivity is low such that differentiation between sources of close geological location is not always possible [87].

The PIXE technique is also utilised by Erlandson *et al.* where, in their study of eight red ochre samples from North America, it is reported that the technique showed unique characterisation of the samples with significant variation within the elemental composition to distinguish between samples. This is evident in **Table 1-9** which gives a summary of their results.



**Figure 1-13:** IRM acquisitions of various ochre samples from significantly different geographical provenance. [144]

**Table 1-9:** Summary of the elemental composition of eight red ochre samples from Western North America [88].

Common Geochemical Constituents in Eight Red Ochre Sources from Western North America.

Locality	Elemental Composition										
	Al	Ca	Cr	Fe	K	Mn	Ni	Si	Sr	Ti	Zn
Gold Harbor (GH)	11.84	0.80	109	11.25	1.89	1300	130	20.69	60	11110	554
	±0.79	±0.06	±25	±0.74	±0.13	±90	±13	±1.36	±18	±740	±40
Red Rock (RR)	2.68	1.43	853	64.03	0.31	9400	207	29.44	—	5500	674
	±0.01	±0.01	±88	±0.64	±0.01	±158	±47	±0.29	—	±200	±45
Sulphur Bank (SB)	0.66	0.04	379	24.78	1.33	50	15	25.83	286	8360	—
	±0.11	±0.01	±44	±1.63	±0.09	±24	±8	±1.71	±38	±570	—
Tajiguas (TJ)	3.22	2.55	119	11.67	0.85	3143	632	33.19	309	2498	122
	±2.41	±0.17	±31	±0.77	±0.06	±210	±46	±2.18	±39	±195	±13
Minam Grade (MG)	12.43	1.38	—	13.86	0.28	2500	19	23.22	127	21040	171
	±0.84	±0.09	—	±0.91	±0.2	±170	±7	±1.53	±23	±1390	±15
China Creek (CC)	19.39	1.12	883	33.45	1.98	853	172	37.04	447	65650	334
	±0.19	±0.04	±98	±0.33	±0.05	±99	±42	±0.37	±153	±696	±39
Blue Mtns (BM)	11.23	1.36	16	4.48	2.03	727	12	31.20	250	5540	82
	±0.76	±0.09	±10	±0.29	±0.14	±50	±3	±2.06	±23	±370	±7
Sunrise Mine (SM)	14.36	0.30	—	19.13	6.00	314	430	17.24	968	252	2350
	±0.96	±0.03	—	±1.26	±0.40	±37	±35	±1.14	±94	±72	±161

Note: Al, Ca, Fe, K, and Si concentrations reported as percentages; Cr, Mn, Ni, Sr, Ti, Zn as parts per million (ppm). The reported uncertainties are the statistical uncertainty in a single measurement. Empty cells indicate that an element was not detected at observable limits.

Erlandson *et al.* also reported that there is significant enough variation to assist in the identification of the source, suggesting that if this technique were combined with others, the determination of geographical origin may be possible [88].

Recently, Reiche *et al.* have applied the PIXE technique to a number of archaeological artefacts, in particular Mughal paintings [96]. Results show that the principal components of the various pigments, including ochres, were able to be identified, with mole fractions determined in a number of cases where multiple components were present [96].

Calligaro *et al.* utilise a number of non-destructive photo detector-based techniques in their studies of various pieces of art works and archaeological finds. Their work aims to answer three fundamental questions: what is the material (i.e. identification), where did it come from (provenance determination) and has it been modified in any way (either chemically or naturally through aging) [99]? Techniques used include but are not exclusive to photography under various wavelengths and sources including direct and grazing light, ultraviolet and infrared radiations, radiography, electron emission radiography,  $\beta$ -radiography, infrared reflectography, XRD, energy-dispersive X-ray spectroscopy analysis conducted by means of scanning electron microscopy (SEM-EDX), inductively coupled plasma atomic emission spectroscopy (ICP-AES), Ion beam analysis, PIXE, Rutherford backscattering spectrometry (RBS) and nuclear reaction analysis (NRA), which is often further classified into a subcategory known as particle-induced  $\gamma$ -ray emission (PIGE) [99]. This combination of techniques, many of which are common to ochre and art work analysis, is utilised in their work as a means of authenticating art work through both their ability to age the piece, as well as the location of hidden signatures. Their results also indicate the ability to identify principal components of dyes, including haematite and goethite, and also suggest that chemical information and fine structure details may also be able to be determined [99].

### 1.5. Project scope

Whilst a number of methods have been established for the analysis of ochre, the majority of these require the use of laboratory based instrumentation and are not readily transferred to the field. Furthermore, this analysis is often destructive, or requires that samples be removed from culturally significant objects, and requires significant sample preparation.

This project aims to develop methodology that is suitable for the non-destructive analysis of ochre samples from within the field, and eventually provenancing. Several phases to this study were identified:

- Initially a reference set of synthetic and natural ochres were characterised using the traditional laboratory based methods of XRD, Raman and IR spectrometry and thermal analysis and NAA.
- Subsequently, these ochres were used in the development of a portable colorimetric method using a hand held spectrometer known commercially as the i1Pro. The suitability of this instrument for use on these materials was established by determining the error in parameters such as reproducibility and accuracy.
- The effect of factors such as the substrate and various application methods were explored to determine if the methodology established was suitable for application to artworks and artefacts.
- A number of models for the prediction of the goethite/haematite sample composition based on colour and the methodology established were explored.



- The i1Pro and established methodology was applied to a large number of well provenanced Australian ochres in a study into the inter-site and intra-site variation.
- A case study was completed into the application of the i1Pro to a series of toas (Aboriginal artefacts) in an attempt to identify the source of the ochre material used in the decoration of the objects.



**CHAPTER TWO:  
THE ANALYSIS OF  
OCHRE UTILISING  
TRADITIONAL  
METHODS**

## CHAPTER TWO

Literature has shown that a number of methods are commonly utilised in the characterisation of ochre materials. This chapter will explore many of these techniques, including X-Ray diffraction, infrared, neutron activation analysis and Raman, by applying them to the characterisation of synthetic haematite and goethite standards, and a series of raw ochre samples obtained from the South Australian Museum mining collection.

The primary aim of this analysis is to determine the sample as a means of provenancing. Focus will also be on the establishment of a preliminary database and the establishment of a set of well characterised samples that can be used for method development. This chapter also introduces the use of thermal gravimetric analysis as a means of ochre characterisation based on the weight loss observed from the goethite to haematite transition, as previously detailed.

### **2.1. Experimental methods**

#### **2.1.1. X-Ray diffraction**

X-ray diffraction spectroscopy was performed at the Science Centre in the Adelaide Museum, located in Adelaide – South Australia. Room temperature XRD was performed on ground samples approximately 0.0025 grams in weight, adhered to Mylar film with acetone following the addition of approximately 10% silicon powder as a phase standard with an exposure time varying from 60 to 1000 minutes. Powder X-ray diffraction patterns were collected on a Huber Guinier Imaging Plate G670 with  $\text{CoK}\alpha_1$  radiation ( $\lambda=1.78892 \text{ \AA}$ ) generated at 35 kV and 34 mA, and processed using Jade software. Quantitative phase analyses were performed using the Rietveld method with the aid of a computer program called Rietica for Windows (v1.7.7).

The silicon powder was added as it is used as an internal phase standard during the Rietveld quantitative phase analysis (RQPA), by which the percentage of silicon calculated can be compared to the known amount present, confirming the accuracy of the analysis. Silicon is not a naturally accruing substance and would not be present in the samples if it were not for the known addition.

#### **2.1.2. Raman spectroscopy**

Raman spectroscopy was performed at the Ian Wark Institute, located on the Mawson Lakes campus of the University of South Australia. The instrument is a Renishaw Ramascope System 1000, which is comprised of a single spectrograph fitted with holographic notch filters and a Peltier cooled CCD detector. The spectrograph is coupled to a Leica DMLM microscope and the spectrometer has a maximum lateral resolution of  $2\mu\text{m}$  and depth resolution of  $2\mu\text{m}$ .

Spectra were then acquired using both a 523nm and later a 785nm laser in attempt to minimise any fluorescence interferences. Initial acquisitions were acquired across a  $4000\text{-}250\text{cm}^{-1}$  range for 30 seconds to confirm the presence of signal and eliminate areas of the spectra with no data of interest, before multiple detailed scans were performed across a  $2000\text{-}250\text{cm}^{-1}$

range for 60 seconds each and the spectra signals combined to reduce the final signal to noise ratio. Each disk was scanned at a minimum of three locations and two disks were made from each ochre sample to ensure that the data obtained was reproducible.

### 2.1.3. Thermal gravimetric analysis

Thermal gravimetric analysis (TGA) was performed at Flinders University utilising the Auto TGA 2950HR version 6.1A. Samples were in the powdered form, having previously been ground if required. All samples were in the region of 3-5mg, with the weight of the pan automatically subtracted. Samples were run under air with a flow rate of 50mls/min and heated to between 600 and 1000°C at a rate of 10°C per minute using the equilibrate method.

### 2.1.4. Infrared

Spectra were obtained using a Nicolet Nexus 870 (Thermo Electron Corporation) research grade FTIR spectrometer, with the aid of OMNIC software. Spectra were collected across a region of 0-700 wavenumbers ( $\text{cm}^{-1}$ ), although data collected below  $200\text{cm}^{-1}$  proved to be inaccurate. Each spectra is comprised on 128 scans at a frequency spacing of  $0.482\text{cm}^{-1}$ .

### 2.1.5. Neutron activation analysis

Full details of the standard operating procedure for neutron activation analysis ( $k_0$ -NAA) at the Australian Nuclear Science and Technology Organisation (ANSTO) is presented for publication by Bennett *et al* [147]. Consequently, only details specific to these experiments are given here.

Quality control data was obtained using a number of different references, including SMELS1-3, SRM 1633b, SRM 679, SRN 278 and SRM 688, and results of this quality control analysis are presented in Appendix C.

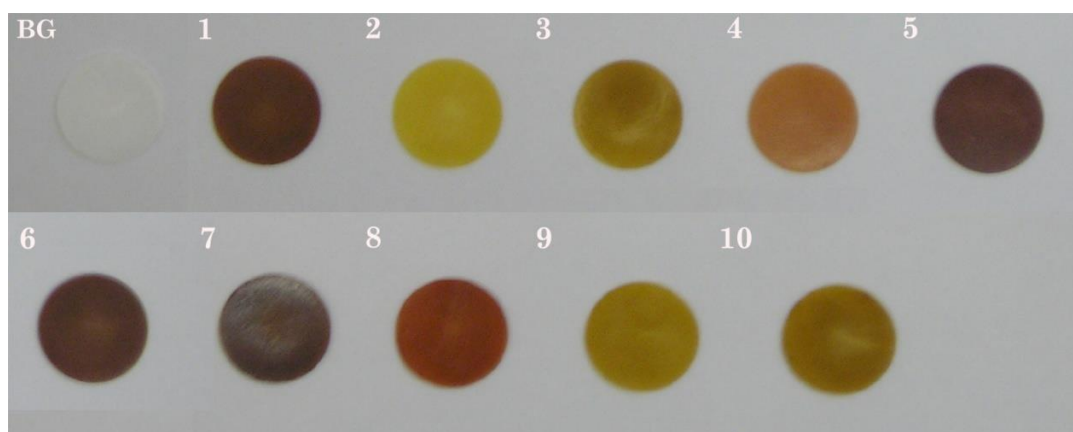
## 2.2. Sample Selection

### 2.2.1. Natural ochres

Preliminary investigations will focus on ten samples collected from mining sites across Australia currently held by the South Australian Museum. These samples were selected based on their visually distinct and varying colours, density and particle size, as well as their availability and their pre-approval for use with the ethics board. These samples are listed in Table 2-1, their locations given in Figure 2-2 and shown in Figure 2-1, where they have been pressed into pellets for analysis.

**Table 2-1:** A description of the ten Australian mining samples used in this study, their corresponding image number and map location.

Ochre Number	Image Number	Map Location	Description
1150	1	A	Mt. Sienna, Birdwood (red)
3742	2	B	Moorilyanna Stn, Musgrave Ranges
3696	3	A	Mt. Sienna, Birdwood (yellow)
1137	4	C	Williamstown
1139	5	D	Middleback Ranges
1293	6	E	Pernatty Lagoon, via Woocalba
1323	7	F	50km West of Oodnadatta
1337	8	G	Virginia Mine, Wadnaminga
1286	9	H	Peterborough (District Council)
1285	10	I	Copper King Mine, Beltana



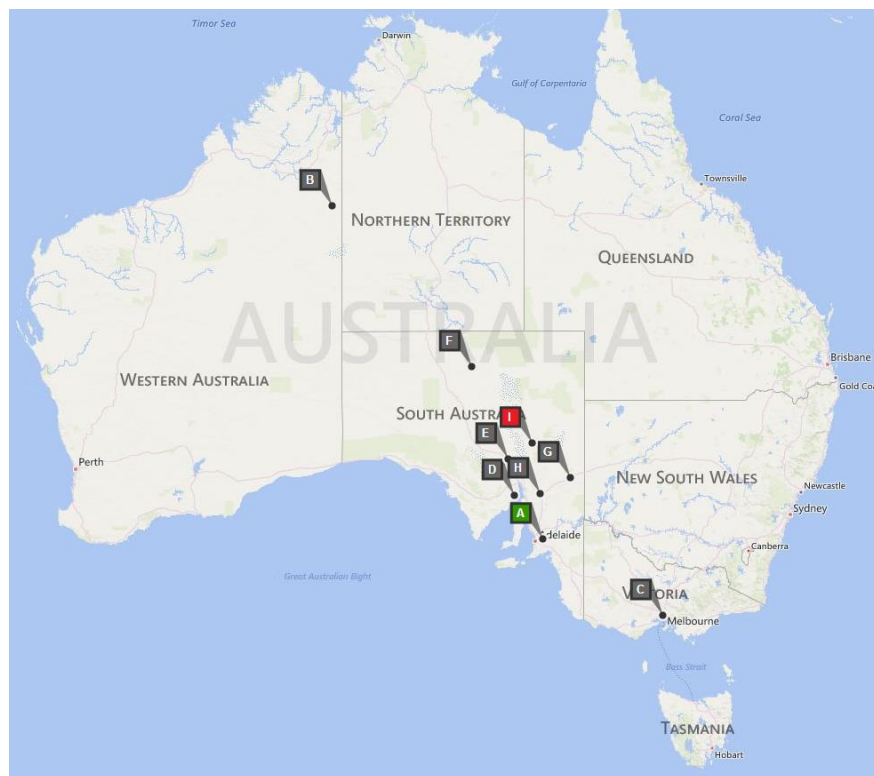
**Figure 2-1:** Photograph of selected mining samples pressed prior to analysis showing the distinct differences in colour.

### 2.2.1. Standards and reference materials

Pure goethite and haematite standards used in this thesis were used as received from Sigma Aldrich. Goethite powder has a batch number of 71063 and a CAS # 20344-49-4. Goethite's chemical formula is given as  $\text{FeO}(\text{OH})$  with approximately 35% Fe w/w. Haematite powder has a batch number of 310050 and is quoted as being >99%  $\text{Fe}_2\text{O}_3$  (Iron (II) Hydroxide) with a particle size <5 $\mu\text{M}$ .

### 2.2.2. Sample selection based on techniques

XRD analysis was performed on all ten mining samples as well as the two pure haematite and goethite standards. Raman analysis was performed on all ten mine samples as well as the two pure haematite and goethite standards and a 50:50 mixture of the standards. TGA analysis was performed on the two pure haematite and goethite standards and all mining samples that



**Figure 2-2:** Map of Australia showing the locations of the mining samples (see Table 2-1 for key).

results of XRD analysis confirmed the presence of goethite –ochres 1285, 1286, 3696 and 3742. IR and NAA analysis was performed on all ten mining samples.

## 2.3. Sample preparation

### 2.3.1. X-Ray diffraction

XRD samples of approximately 0.0025 grams in weight were ground following the addition of approximately 10% silicon powder as a phase standard. This ground samples was adhered to Mylar film with acetone.

### 2.3.2. Raman spectroscopy

Raman spectroscopy sample preparation involved the grinding of small quantities (approximately 1 gram) of samples with a mortar and pestle for three minutes. The powdered samples were then pressed into disks 1cm in diameter under 20-25 tonnes of pressure for approximately 30 minutes. The creation of these disks was necessary to ensure a smooth and uniform surface.

### 2.3.3. Thermal gravimetric analysis

Thermal gravimetric analysis was completed on samples in the powdered form, having previously been ground if required. All samples were in the region of 3-5mg.

### 2.3.4. Infrared

Infrared analysis sample preparation involved approximately 50mg of sample being ground for three minutes. 1mg of the ground sample was then combined with 200mg of pre-ground caesium iodide (CsI) before the mixture was ground for a further 3 minutes. The ground mixture was then pressed under 10 tonnes of force for ten minutes, resulting in a disk approximately 1cm in diameter.

### 2.3.5. Neutron activation analysis

Neutron activation analysis sample preparation was completed at ANSTO. Two sub-samples were taken from each ochre sample, with one used for short irradiation and the other for long irradiation. Each sub-sample was approximately 60mg in weight and was contained in a high-purity polyethylene capsule. The short irradiations were performed at a neutron flux of  $\sim 1.561013 \text{ cm}^{-2} \text{ s}^{-1}$  for approximately 60 seconds. Following this, gamma-ray spectra were collected for 180s and 720s after decay times of  $\sim 4\text{min.}$  and  $\sim 18\text{min.}$  respectively. Long irradiations completed at a neutron flux of  $\sim 461012 \text{ cm}^{-2} \text{ s}^{-1}$  for a period of 12 hours before gamma-ray spectra were collected for 30 min and 4 h after 4 days and 15 days, respectively. Results of this analysis present the concentration of fifty trace elements.

## 2.4. Results and discussion

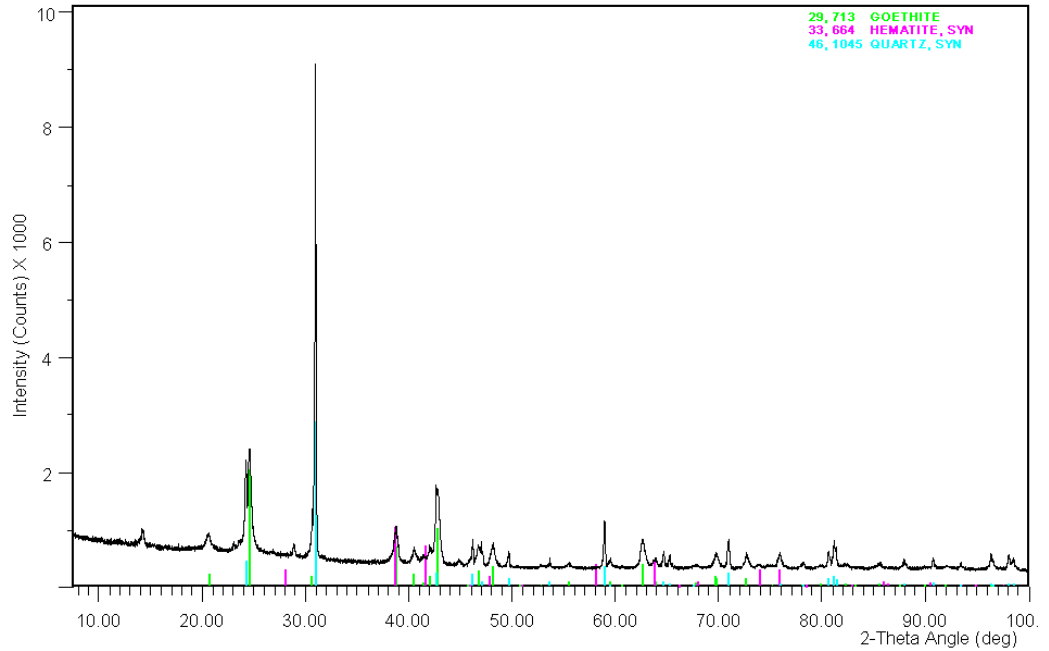
### 2.4.1. X-Ray diffraction

Ochre 1286, 1285, 3696 and 3742 are all yellow in colour. Consequently, these samples were expected to contain the yellow pigments goethite, jarosite or natrojarosite and minor components. Given their colour it is expected that there would be very low or no detectable levels of haematite. This is because haematite causes the ochre to appear red in colour and is known to be the dominant pigment. Analysis showed that all the yellow ochres studied contained goethite as the chromophore. Exemplar XRD spectra obtained for ochre 1286 is shown in Figure 2-3.

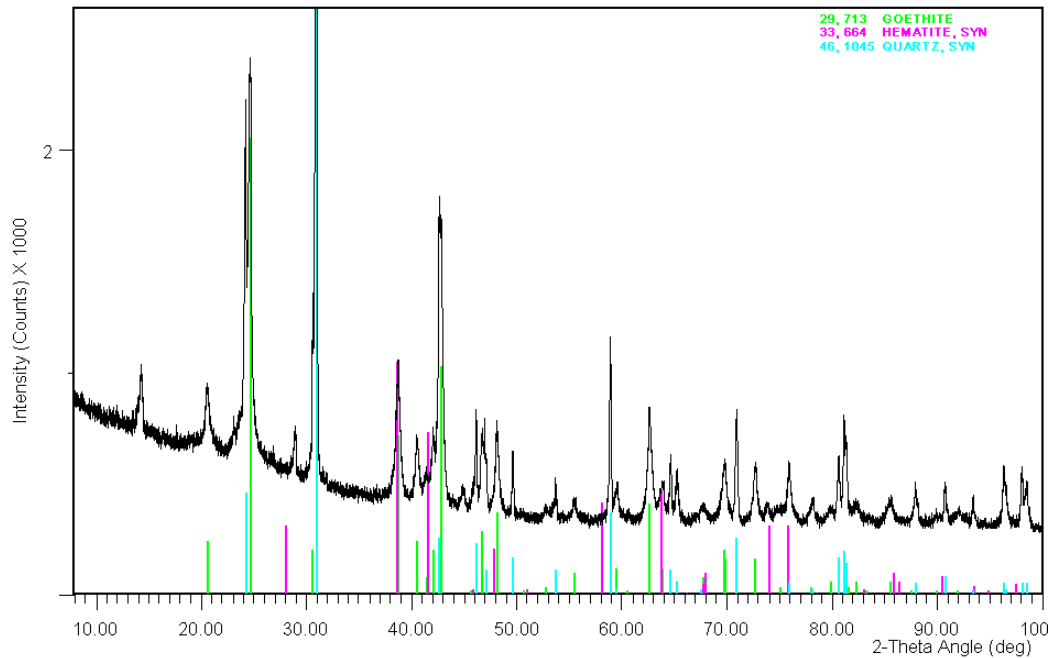
It can be seen that a number of peaks are present in the XRD spectra of ochre 1286, and the overlay shows where the expected location of these peaks would be if they can be attributed to the components haematite (shown in purple) and goethite (shown in green), the two primary ochre components, as well as quartz (shown in blue). The presence of quartz is not uncommon or unexpected and is a result of the soil medium of the sample.

Close examination of this spectrum, with the overlay ICDD patterns of haematite, goethite and quartz, shows the dominant quartz peak at theta-angle 31deg, making the details quite difficult to example and a reduction of the intensity scale and thus impact of this peak is necessary. Shown in *Figure 2-4* is the same scan with an altered intensity scale.



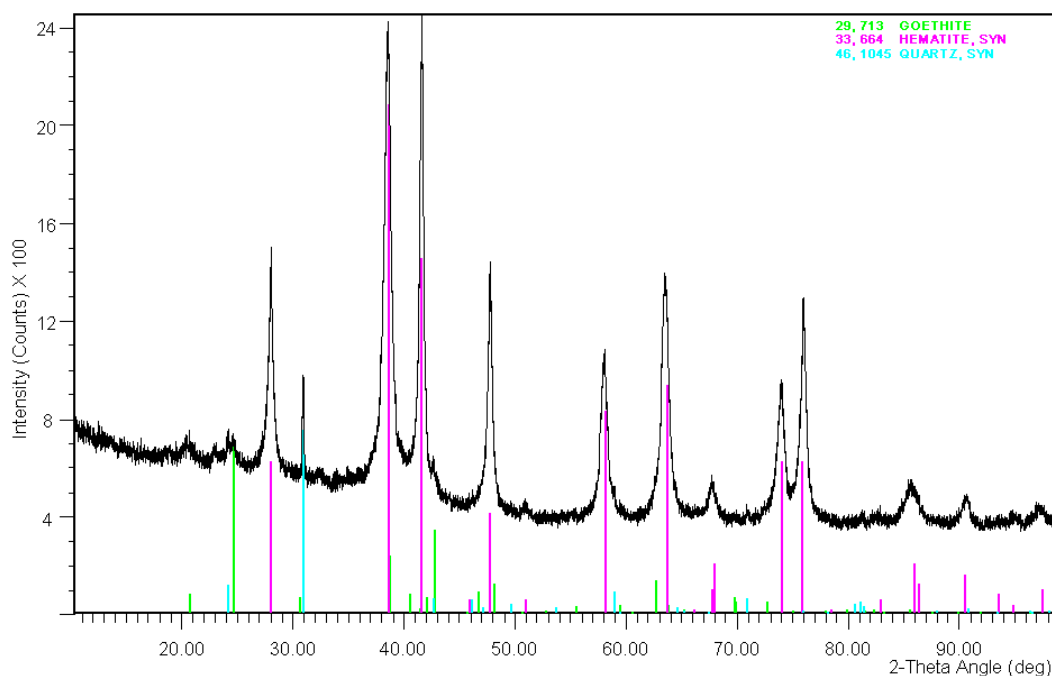


**Figure 2-3:** XRD Analysis of Ochre 1286 with overlay ICDD Patterns.



**Figure 2-4:** XRD Analysis of Ochre 1286 at low intensities with overlay ICDD Patterns.

It can be seen in this case, particularly at 2-theta angle approximately 42° and 58°, that where the haematite ICDD spectra is overlaid, that there are no peaks present. At alternate sites, such as 2-theta angle approximately 74° and 76° there appears to be peaks corresponding to the hematite ICSS spectra. However, these peaks and the haematite ICDD spectra vary significantly in their intensity ratios. As the number of possible sources for each peak is large, this variation in intensity combined with the absence of some peaks suggests that the sample may not contain any haematite. This is consistent with what was expected as ochre number



**Figure 2-5:** XRD Analysis of Ochre 1323 with overlay ICDD Patterns.

1286 appears yellow in colour, and as haematite is a dominant pigment, if it was present in concentrations above approximately 4% the colour of the ochre would reflect this.

As well as the previously identified goethite and quartz, ochre 1286 contained additional peaks that are not accounted for by the known components. These are most noticeable at low 2-theta angles, with the most dominant being present at approximately 15°. A search of the ICDD database was unable to successfully identify this component, and consultation with experts in the area suggest that it is most likely due to clay components present in the soil and the ochre.

Results of the remaining yellow ochres are similar to the results shown above. Some minor variation occurs in the intensity of peaks and the location of the peaks unable to be identified with ochre 3742 having an additional peak at a 2-theta angle of approximately 15° and ochre 3696 at 12°, and some samples show a small concentration of haematite is present. The spectra obtained for these ochres can be seen in Appendix C, with the results tabulated and discussed later in this section.

XRD analysis was then performed on the ochre samples 1150, 1137, 1139, 1293, 1323 and 1337, all of which appear red in colour and suspected of containing haematite as the dominant chromophore. Shown in Figure 2-5 is an example of such analysis in the spectra obtained from the red coloured ochre number 1323.

Closer examination of ochre 1323 confirms the presence of all three suspected components. It also shows that all major peaks can be attributed to one of the three components, suggesting that no other components are present. A reduction in scale is not required for ochre 1323 as the intensity of the peak at 31° is low, suggesting low concentrations of quartz are present in this sample.

**Table 2-2:** Results of XRD analysis showing identified sample components.

Ochre Number	Colour	Hematite	Goethite	Quartz	Other
1. (1150)	Red	Yes		Yes	
2. (3742)	Yellow		Yes	Yes	
3. (3696)	Yellow		Yes	Yes	
4. (1137)	Red	Yes	Yes	Yes	Yes
5. (1139)	Red	Yes			Yes
6. (1293)	Red	Yes	Yes	Yes	
7. (1323)	Red	Yes	Yes	Yes	
8. (1337)	Red	Yes		Yes	Yes
9. (1286)	Yellow		Yes	Yes	Yes
10. (1285b)	Yellow		Yes	Yes	

Studies were also conducted on the remaining red ochre samples with similar and varied results. Some samples showed the additional presence of peaks unable to be attributed to any specific mineral in the data base. Many of these peaks are at low theta angles, for example ochre 1139 has a series of additional peaks in the region of 2-theta angles 11-15°, ochre 1337 at angles of 15° and 46°, and ochre 1137 at 10°, 15°, 24°, 26° and 33°-38°. In addition to this, only two of the red ochre samples studied, ochre 1139 and ochre 1337, show no detectable levels of goethite. The spectra obtained for these ochres can be seen in Appendix C, and the results presented in Table 2-2, where the visible colour and the identified components are indicated. Whilst the XRD identified quartz, hematite and goethite, simply identifying these components is insufficient for discriminating the sources. Consequently, Rietica software was used to analyse the XRD powder diffraction patterns previously shown. This software allows the ratios between the successfully identified components to be calculated, resulting in quantitative phase analysis.

As the method used to calculate these values is largely interpretive, a blind study was conducted to ensure accuracy. A sample was prepared by a member of staff at Flinders University by combining the two ochre standards and a silicon standard before being analysed utilizing the same methods as the mining samples were analysed with. The results were calculated and presented before being compared to the actual composition, and the results of this are shown in

Table 2-3.

It can be seen from these that the results obtained agree within acceptable experimental error, confirming that, where samples are suitable, this is an acceptable method of ochre analysis. The variation seen for the haematite and silicon phases is significantly larger than that

observed for goethite. This may be a result of an inhomogeneous sample. Phase analysis of the ochre samples is shown in Table 2-4. In this instance, the peaks attributed to clay silicates

**Table 2-3:** Results of quantitative phase analysis using Rietveld refinement on a sample of known composition.

	Goethite	Haematite	Silicon Standard
<b>Calculated %</b>	46.40	47.01	6.59
<b>Error (<math>\pm</math>)</b>	1.03	0.59	0.31
<b>Actual %</b>	45.71	45.50	8.79
<b>Variation</b>	0.69	1.51	-2.2

**Table 2-4:** Results of XRD analysis showing calculated sample compositions, expressed as a %weight. X suggests that analysis was unsuccessful.

Ochre Number	Colour	Hematite	Goethite	Quartz	Other
<b>1. (1150)</b>	Red	41.40	0.00	58.60	
<b>2. (3742)</b>	Yellow	X	X	X	
<b>3. (3696)</b>	Yellow	X	X	X	Yes
<b>4. (1137)</b>	Red	X	X	X	Yes
<b>5. (1139)</b>	Red	X	X	X	Yes
<b>6. (1293)</b>	Red	X	X	X	
<b>7. (1323)</b>	Red	93.66	3.89	2.45	
<b>8. (1337)</b>	Red	X	X	X	Yes
<b>9. (1286)</b>	Yellow	0.00	51.66	48.34	Yes
<b>10. (1285b)</b>	Yellow	X	X	X	

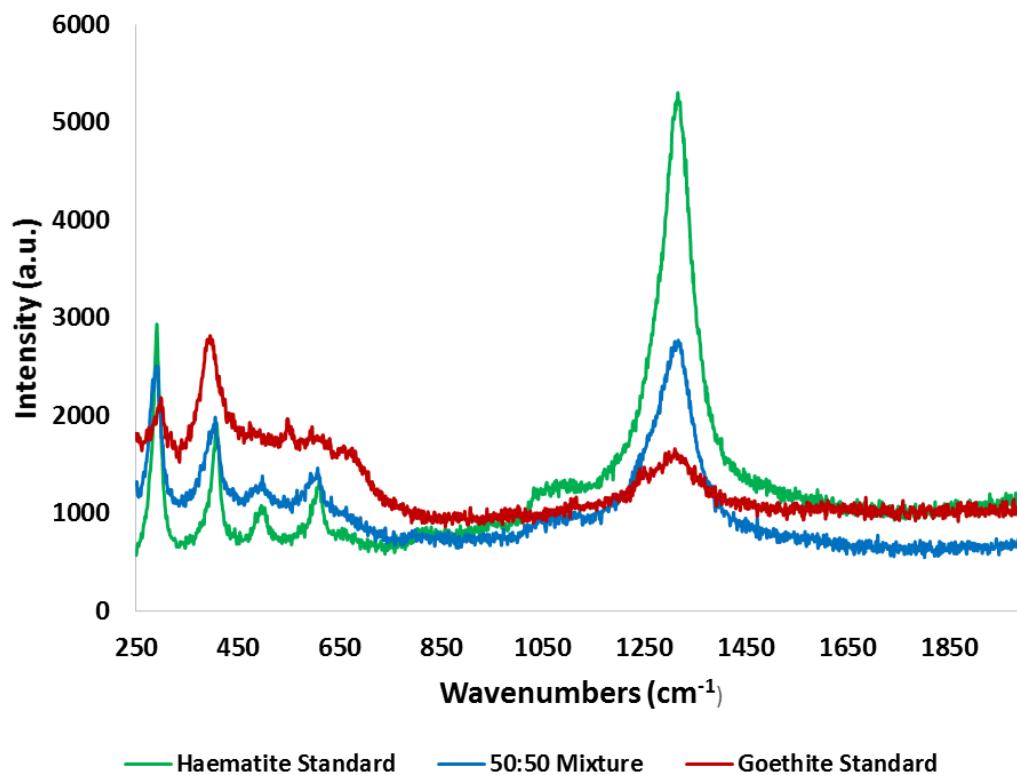
will be excluded, as their exact nature is unknown. The sample was assumed to be composed of only a combination of the haematite, goethite and quartz.

Quantitative phase analysis was unsuccessful for many of the ochre samples attempted. In many cases, the spectra had such a large background component that the noise made it difficult to accurately fit the calculation data. In these cases, whilst ratios were calculated, the associated error is too large for them to have statistical meaning. For others, not enough components were identifiable. This suggests that this method is likely to be unsuitable for the provenancing of ochre. However, it can be seen that, for those samples where analysis was successful, significant variation between the samples in terms of composition exists, and this is positive for the use of XRD as a method of distinguishing between samples.

## 2.4.2. Raman spectroscopy

### 2.4.2.1. Analysis of the standards

In order to establish that Raman spectroscopy was able to analyse ochre material and differentiate between samples, initial analysis was completed on both the pure standards and an equal standard mixture. Results of this analysis are shown in Figure 2-6.

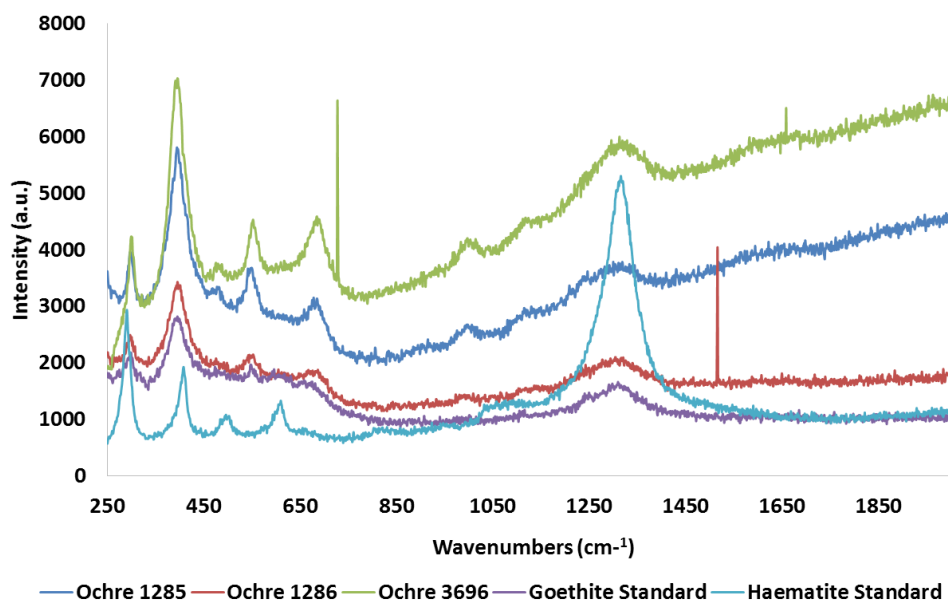


**Figure 2-6:** Spectra obtained for the Raman analysis of the ochre standards.

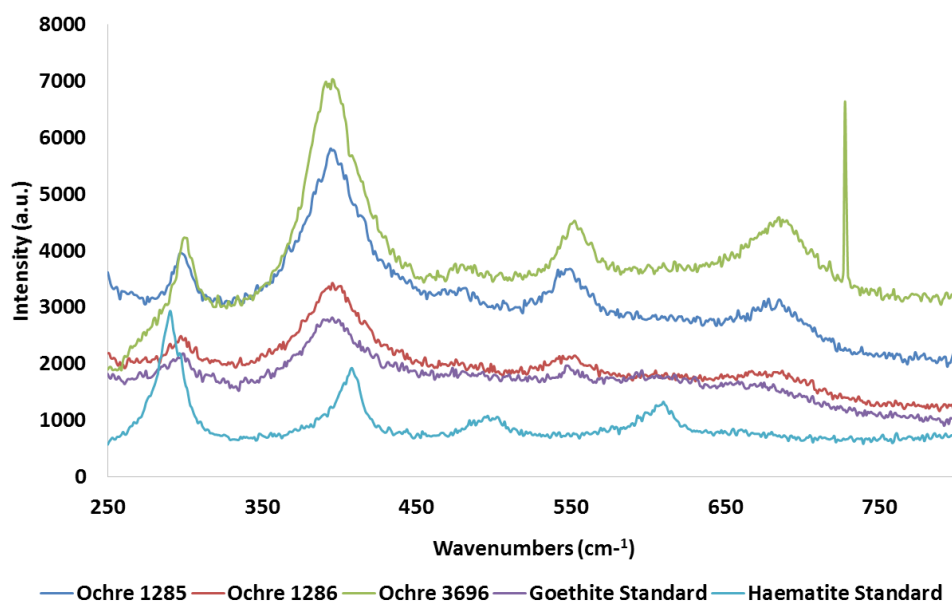
When analysing this data, a few areas of interest are obvious. Of note is that large peak present at approximately 1300 wave numbers. Whilst this peak dominates the haematite standard with an intensity of approximately 5200a.u. it is present at a significantly lesser extent in the goethite standard (intensity approximately 1500a.u.), and shows a mid-range intensity of approximately 2800a.u. for the mixed standard. This suggests that this peak may be able to act as an indicator of the concentration of haematite present. However, due to the nature of the experiment and inherent concerns surrounding background effects and noise, the accuracy of this technique for a quantitative analysis is questionable. The three samples also show similar trends of varying intensities in the lower region of the spectrum (800–250 wavenumbers).

### 2.4.2.2. Analysis of the mining samples

Analysis of the ten mining samples was subsequently completed. Results obtained from the yellow ochres, along with both pure standards, are shown in Figure 2-7. Of most significance is that the only sample shown in Figure 2-7 containing the large peak at approximately 1300



**Figure 2-7:** Spectra obtained for the Raman analysis of the visually yellow ochre samples.



**Figure 2-8:** Spectra obtained for the Raman Analysis of the visually yellow Ochre samples at low wavenumbers.

wave numbers is that of the haematite (red coloured) standard, shown here in light blue. As it is known that a small amount of haematite causes a colour change this confirms the results of the XRD and suggests that these ochres do not contain haematite. Whilst this is significant, red and yellow can easily be distinguished by the naked eye and thus is of little quantitative value.

When comparing the spectra obtained for the Ochre samples 1285, 1286 and 3696, it is easily noticeable that the background varies greatly. This is as a result of background fluorescence, most likely due to quartz in the samples. It is also important to note here that the Raman

spectra for ochre sample 3742, is not shown, as no peaks were distinguishable above the background fluorescence. A number of efforts were made to reduce the fluorescence, including the use of a number of different lasers at both 523nm and later a 785nm, however the problem persisted. This undermines the effectiveness of this technique and its application to natural ochres. The most subtle yet significant differences between the spectra are seen at the low wave numbers, and this area of the spectra is shown in Figure 2-8.

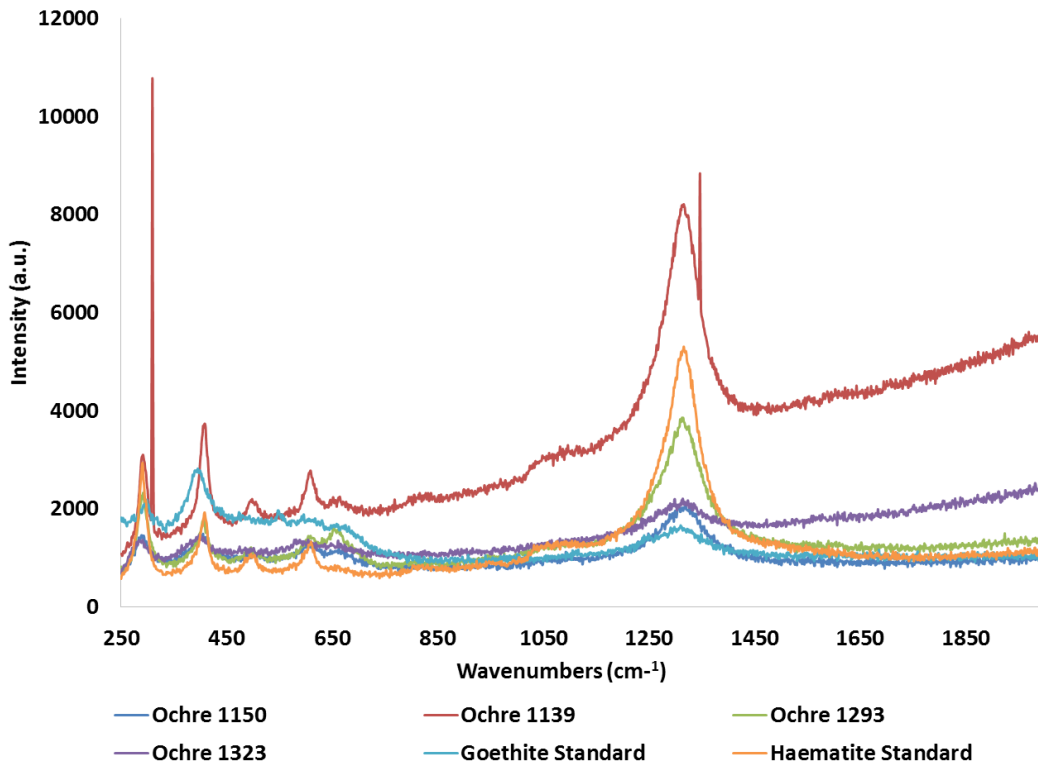
Aside from the obvious differences in the spectra obtained from the haematite standard, the spectra obtained for the samples visually appearing yellow in colour, including the goethite standard, appear to vary predominantly in intensity only, and not in peak location. There appears to be a small, broadly shaped and low intensity additional peak present at approximately 460 wavenumbers in ochre 3696 and 1285 that is not present in ochre 1286 or the goethite standard. However, as this peak is only present slightly above the background it is difficult to hypothesise its realness.

Analysis of those samples appearing visually red in colour, along with both pure standards, are shown in Figure 2-9. Here, the peak in the region of 1300 wavenumbers was the dominant peak and showed the greatest variation in intensity. Of note is that the peak appears much smaller and smoother in the Goethite standard (visually coloured yellow), and in ochre sample 1323, than in all the other samples. As this peak is known to be from the haematite component, this shows that although ochre 1323 appears to be red in colour, it is likely to be composed of a mixture of haematite and goethite, and this was confirmed in the analysis previously performed utilising XRD.

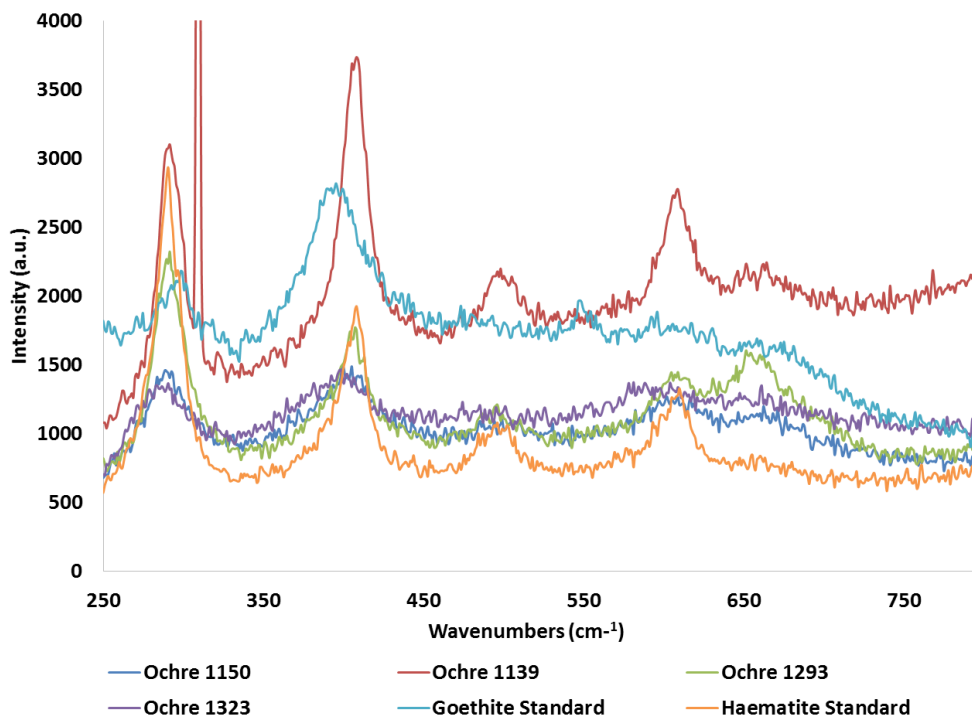
The intensity of this peak may be a valuable way of quantifying the haematite component, however, the error in this is statistically large based on background interferences. As a result, the measurement is of little value as this information can be more accurately obtained via other methods, such as the previously detailed XRD.

Aside from the obvious differences in the spectra obtained from the goethite standard, the spectra obtained for the samples visually appearing red in colour, including the haematite standard, appear to vary predominantly in intensity only and not in peak location. Ochre 1293 appears to have an additional peak in the region of 650 wavenumbers that, if present, is not observable above background noise in the remaining samples. A peak present at approximately 500 wavenumbers is most dominant in ochre 1130 and the haematite standard, and the same samples show significant differences to the remaining ochres in both peak intensity and peak width for a peak present at approximately 400 wavenumbers.

As with the yellow ochres, the most significant differences between the spectra of the red ochres are seen at the low wavenumbers. This region of the spectra is shown in Figure 2-10.



**Figure 2-9:** Spectra obtained for the Raman analysis of the visually red ochre samples.



**Figure 2-10:** Spectra obtained for the Raman analysis of the visually red ochre samples at low wavenumbers.

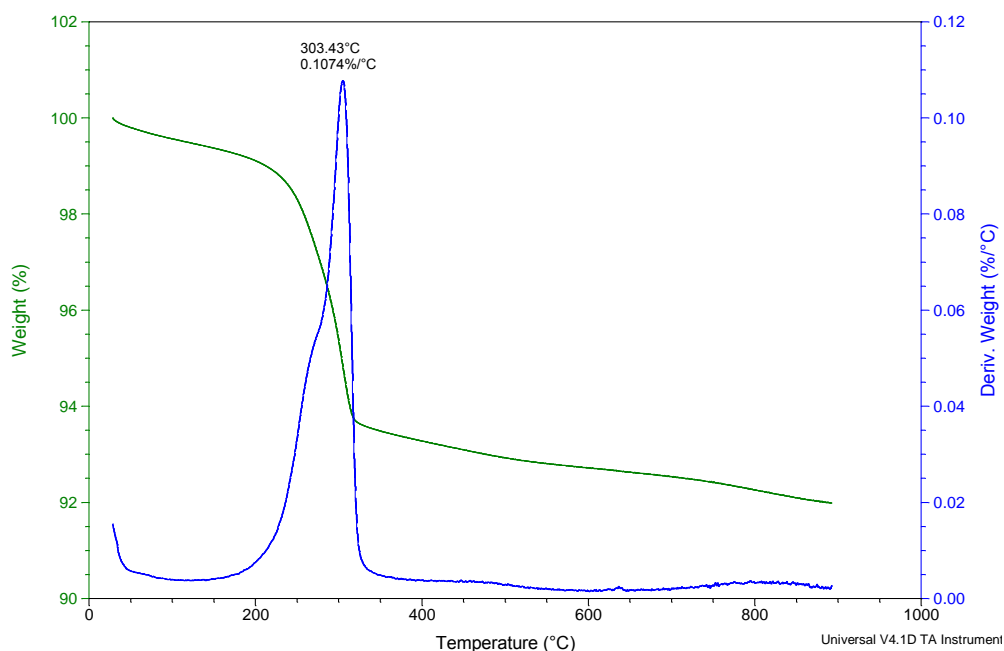


### 2.4.3. Thermal gravimetric analysis

#### 2.4.3.1. Analysis of the standards

##### 2.4.3.1.1. Goethite

It is known that goethite can be easily converted to haematite via a dehydration process at a temperature between 260°C and 550°C [69-71]. This suggests that the heat treatment of yellow ochre can result in the characteristic red colour associated with haematite, whilst still maintaining the predominant structure and majority composition of goethite.



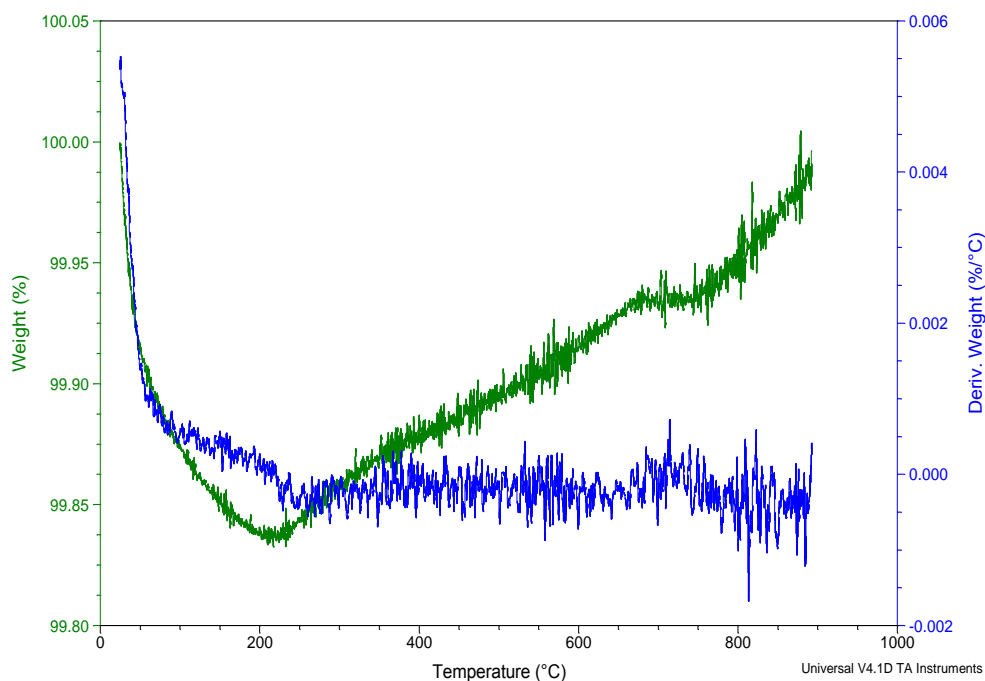
**Figure 2-11:** TGA weight loss spectra (shown in green) and derivative (shown in blue) of goethite to a maximum of 900°C, showing a transformation temperature of 303.43°C.

Thermal gravimetric analysis was completed on the goethite standard to confirm the temperature at which the transition to haematite occurs. Results of this are shown in Figure 2-11.

TGA analysis shows a sharp and significant mass loss peak representing the transformation temperature of 303.43°C. To confirm this temperature and the reproducibility of this measurement, this was repeated, giving alternate temperatures of 301.11°C, 300.37°C, 301.11°C, 299.63°C, 304.66°C, 298.15°C, and 301.85°C. Combined with the original reading, this gives an average temperature of 301.29°C with a standard deviation of  $\pm 2.06^\circ\text{C}$ .

##### 2.4.3.1.2. Haematite

As the mass loss seen is from the conversion of goethite to haematite, it is not anticipated the TGA of haematite will yield any changes. However, to confirm that the synthetic haematite standard is pure the haematite standard was run under the same conditions as the goethite



**Figure 2-12:** TGA weight loss spectra (shown in green) and derivative (shown in blue) of haematite to a maximum of 900°C, showing no significant weight loss.

standard was with the results shown in Figure 2-12. Results of this confirm that no significant weight loss results from the heating of haematite, with weight variations of less than 0.5% observed. This small weight loss is likely to be a loss of moisture, possibly from the crucible.

#### 2.4.3.2. Analysis of mining samples

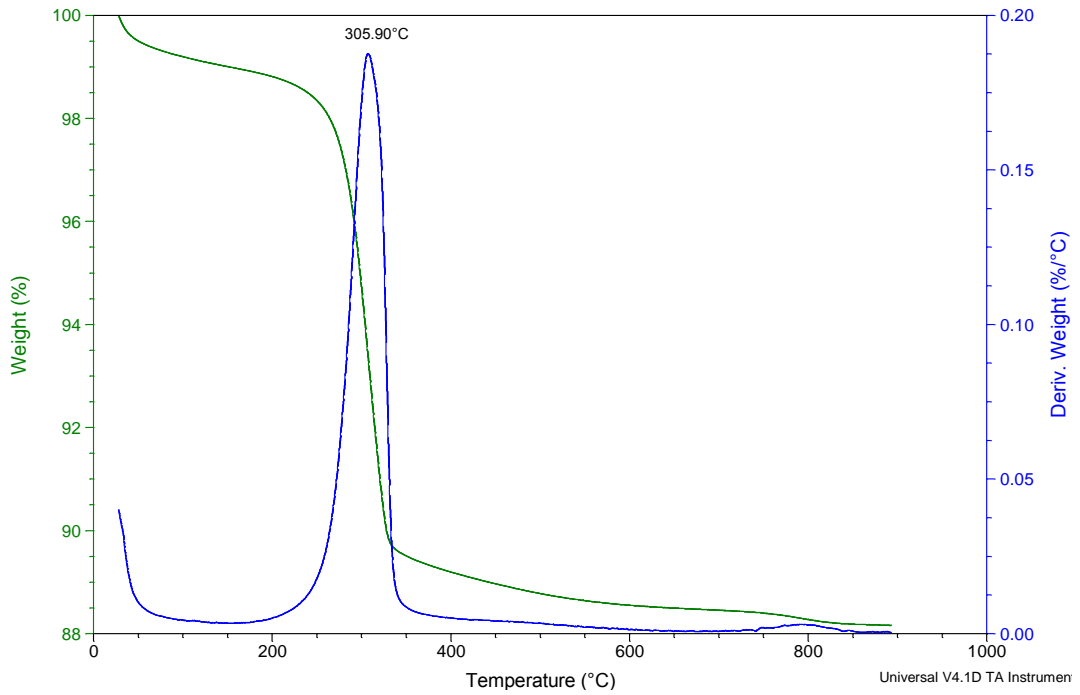
As previous studies confirmed no effect from TGA heating on haematite samples, only those mining samples having previously been confirmed to contain goethite were analysed using this method, with results shown in Figure 2-13, Figure 2-14, Figure 2-15 and Figure 2-16.

Initially apparent is the presence of the mass loss peak at approximately 300°C due to the conversion of goethite to haematite. Whilst the exact temperature of conversion varies slightly, this peak is present in all samples, as expected.

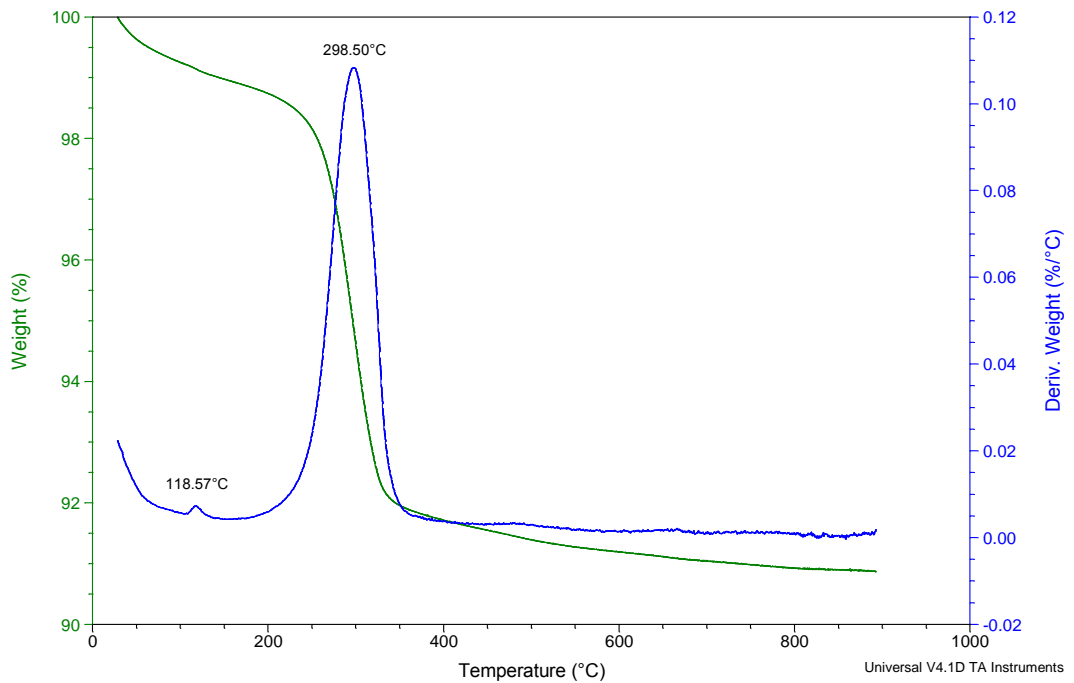
Also present in the results obtained for ochre's 3696 and 1286 is a small peak at approximately 115°C, most likely due to the loss of water present in small quantities in these samples.

Ochres 3742 and 1286 also show an additional weight loss peak in the region of 505°C, possibly due to organic components present within the samples, showing significantly varying intensities.

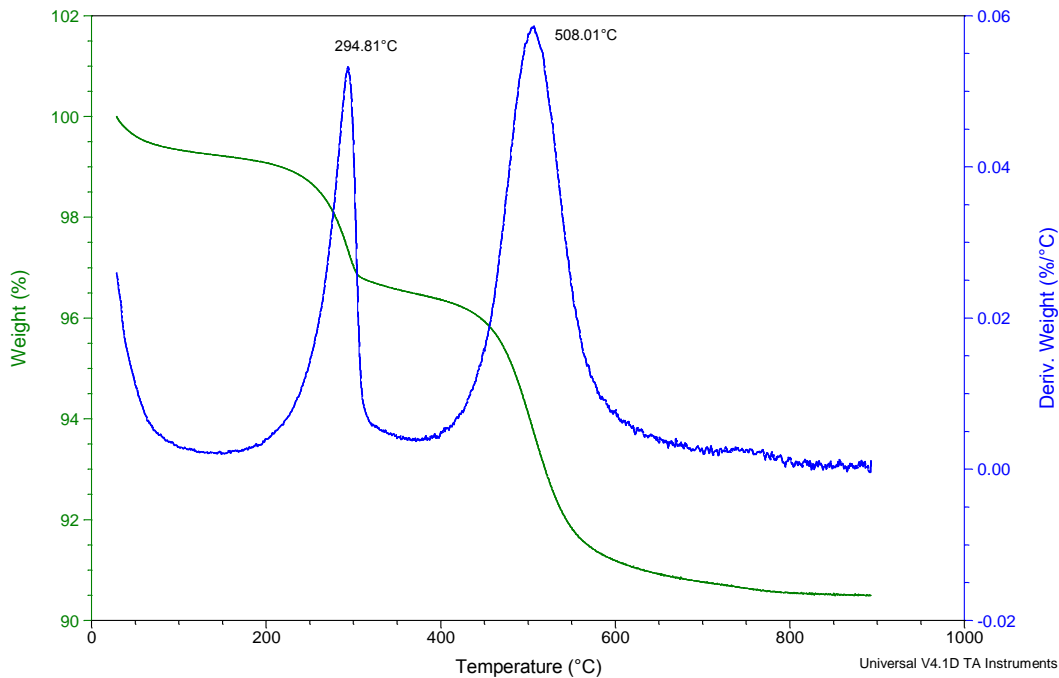
All four natural ochre samples exhibit a weight loss percentage in the region of 10%. This is confirmed in the literature as being related to aluminium substitution, and the results obtained are in the anticipated region [140]. Further analysis of this data shows that, whilst all samples exhibit a similar total weight loss, the cause of this weight loss is not always the same. Ochre 1286 and 3696 show a small dehydration peak at approximately 115°C and this weight loss is



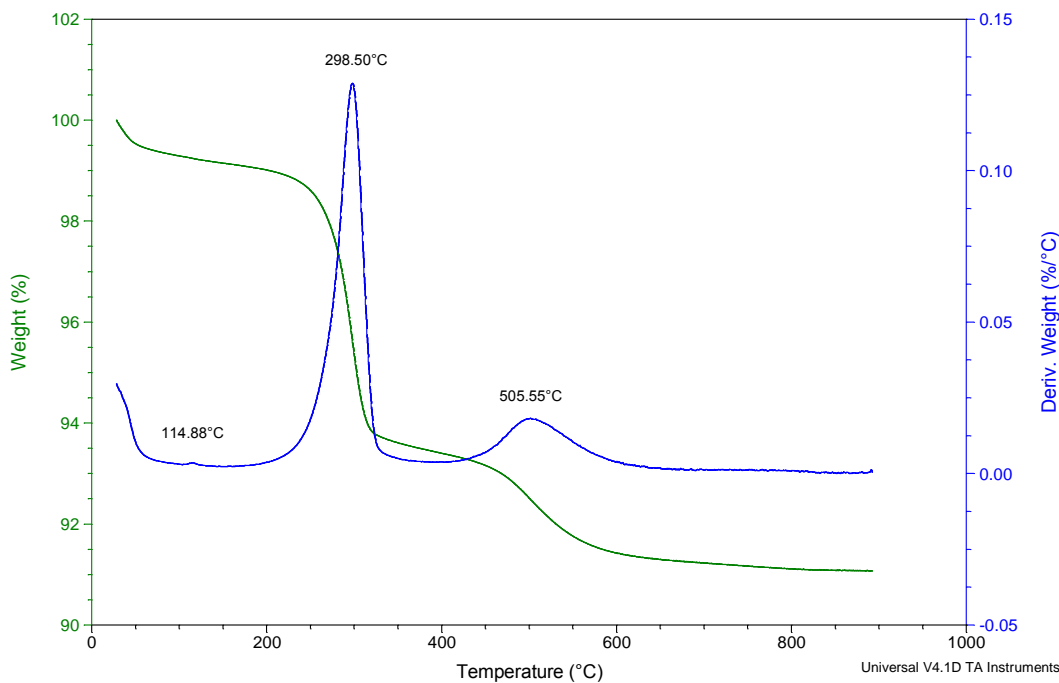
**Figure 2-13:** TGA weight loss spectra (shown in green) and derivative (shown in blue) of ochre 1285 to a maximum of 900°C, showing a transformation temperature of 305.90°C.



**Figure 2-14:** TGA weight loss spectra (shown in green) and derivative (shown in blue) of ochre 3696 to a maximum of 900°C, showing a transformation temperature of 298.50°C, and a secondary weight loss peak at 118.57°C.



**Figure 2-15:** TGA weight loss spectra (shown in green) and derivative (shown in blue) of ochre 3742 to a maximum of 900°C, showing a transformation temperature of 294.81°C, and a secondary weight loss peak at 508.01°C.



**Figure 2-16:** TGA weight loss spectra (shown in green) and derivative (shown in blue) of ochre 1286 to a maximum of 900°C, showing a transformation temperature of 298.50°C, a secondary weight loss peak at 505.55°C, and a small secondary peak at 114.88°C.

due to the loss of water. The weight loss due to the organics at approximately 505°C also varies with this causing approximately 2% with ochre 1286 and 5% with ochre 3742. The weight loss due to the goethite-haematite transition also varies and is attributed to approximately 5% in ochre 1286, 3% in ochre 3742, 7.5% in ochre 3696 and 10% in ochre 1285.

From a provenancing perspective, the four TGA spectra are remarkably different and can be very easily visually separated without the need of statistical analysis. Whilst this is of value, with such a small sample field it is difficult to draw conclusions about the viability of this technique for differentiation between samples at this stage.

#### 2.4.4. Infrared

Far IR analysis was performed on the ten mining samples utilised in previous studies, with the spectra obtained shown in Figure 2-17.

Common trends, such as the peaks seen at approximately 480 wavenumbers and again at approximately 520 wavenumbers are clearly observed and basic grouping of the ochres is achieved. However, many minor details in the spectra are lost and no significant trend exists to the extent required for characterisation and provenancing. In an attempt to gain more useable data, autocorrelation IR was applied to this data by Blanch *et al.* [105] Results of this analysis are shown in Table 2-5.

**Table 2-5:** Results of autocorrelation analysis on various mining samples.

Ochre Number	Colour	$\Delta\text{corr (cm}^{-1}\text{) Smoothed}$	$\Delta\text{corr (cm}^{-1}\text{) Unsmoothed}$
1150	Red	68.64	68.68
3742	Yellow	38.89	38.9
3696	Yellow	75.15	74.69
1137	Red	43.37	43.19
1139	Red	45.86	45.95
1293	Red	102.91	102.58
1323	Red	81.28	81.49
1337	Red	51.49	51.73
1286	Yellow	73.21	72.88
1285	Yellow	65.45	65.7

Results of this analysis show a large range of values were obtained. Based on the observations of the original spectra and the variations seen there, this is not an unexpected result. It is observed that IR spectra that appear similar in characteristics, such as ochre 3696 and ochre 1286, also show similar autocorrelation values. Whilst this is promising, similar

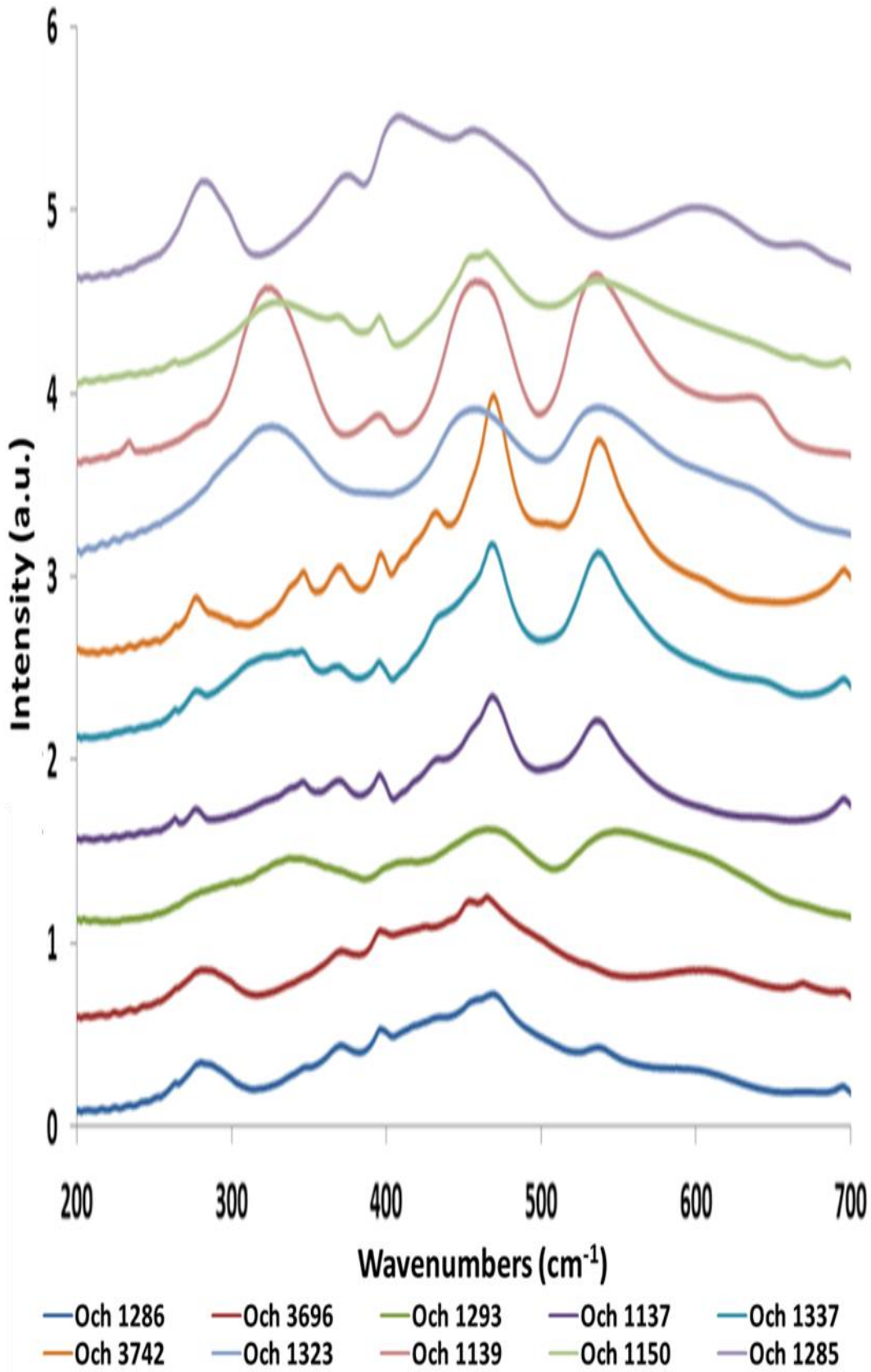


Figure 2-17: Results of near-IR analysis for the ten raw ochre mining samples.

results are also seen from IR spectra not exhibiting the same spectral similarities, such as 1137 and 1139, and 1150 and 1286. These results suggest that this method of analysis is not able to accurately distinguish between samples based on their colour and composition, and as a result would not be suitable for the provenancing aims of this project.

#### 2.4.5. Neutron activation analysis

Results of the neutron activation analysis (NAA) undertaken at ANSTO for the ten mining samples is shown in Table 2-6 and Table 2-7. All quantities are displayed in units of mg/kg. Uncertainties (unc.) represent one standard deviation and include random and systematic uncertainties. Indicative detection limits (LD) are shown for all elements, whether or not a concentration was determined. Data is reported as supplied by ANSTO.

It is clear from these results that some elements play a more critical role in the distinction between ochres than others. Table 2-8 shows only the elements detected in at least one ochre sample, with the limits of detection and uncertainties not shown, but equal to those in the previous tables.

From this it can be seen that some elements are seen above the detection limits in only one ochre. For example selenium (Se) in ochre 1137, strontium (Sr) ochre 1167, molybdenum (Mo) in ochre 1139, and rhenium (Re) in ochre 1323. For the samples selected, these are obviously distinctive characteristics, and could be useful in the source attribution (provenance) of unknown materials.

There are also a number of elements that are only observed above the detection limits in some of the ochres including Mg, K, Ca, Ti, Cu, Ga, Rb, Zr, In, Sb, I, Cs, Ba, Pr, Nd, Gd, Ho, Hf, Ta, W, Au and Th. Trends observed in a combination of these could also prove valuable for provenancing.

Also of interest, however, are the elements observed above the detection limits in all ochres sampled. Great importance is placed on those elements where the quantities detected vary greatly between ochres. These include elements Na, Al, Cl, Sc, V, Cr, Mn, Fe, Co, Zn, As, Br, La, Ce, Sm, Eu, Tb, Dy, Yb and U. Those elements detected in quantities below 100mg/kg are shown in Figure 2-18. Here it is apparent that, not only do the quantities at which the elements were detected vary greatly, but so does the relationship between the elements detected.

A number of elements were also observed above the detection limits in all ochres in much higher concentrations. Those detections in quantities not exceeding 1000mg/kg are shown in Figure 2-19 and Figure 2-20. Those detections in quantities not exceeding 60000mg/kg are shown in Figure 2-21 and Figure 2-22.

CHAPTER TWO

**Table 2-6:** NAA data obtained for ochres 1323, 1337, 3742, 1293 and 1139 for all elements investigated. Data is reported as supplied by ANSTO.

Ochre	1323			1337			3742			1293			1139		
	mg/kg	Conc.	Unc.	LD	Conc.	Unc.	LD	Conc.	Unc.	LD	Conc.	Unc.	LD	Conc.	Unc.
<b>Na</b>	5031	223.1	0	1447	68.81	0	2078	85.36	1.053	30080	1154	0	2254	96.36	0.5893
<b>Mg</b>	5636	490.1	1147	1073	152.1	548.1	1783	136.6	426.4			5489	999	128.3	474.2
<b>Al</b>	6538	230.3	12.06	87720	3075	60.19	98490	3470	65.03	7481	271.1	89.43	16780	589	15.78
<b>S</b>			48710			37850			27770						50250
<b>Cl</b>	3608	151.6	96.04	1430	59.11	37.42	1894	92.89	31.57	51430	1828	257.4	3352	123.9	37.29
<b>Ar</b>			14.31			8.675			6.973			50.92			1.204
<b>K</b>			1433	1606	340.3	1236	9789	594.2	1173			5814			1272
<b>Ca</b>	3496	564.5	944.7			340	456.7	107.5	246.9			4418			490.7
<b>Sc</b>	3.064	0.1094	0.01017	27.33	0.9629	0.01009	12.63	0.4443	0.01276	8.716	0.3072	0.008552	6.509	0.2318	0.01057
<b>Ti</b>	545.3	102.8	397.3	6793	269.8	515.5	8174	306.4	295.2			3157			548.2
<b>V</b>	23.28	1.022	1.119	320.5	11.41	1.632	710.7	25.03	1.745	129.1	5.432	6.094	167.4	5.979	1.381
<b>Cr</b>	7.03	0.9372	3.529	174.7	7.185	3.652	188.2	6.809	4.158	34.56	1.455	3.06	88.54	3.235	3.705
<b>Mn</b>	2627	92.14	2.168	294	10.35	0.863	46.22	1.689	0.6783	11570	405.6	3.465	785.2	27.65	0.7308
<b>Fe</b>	564400	19760	173.3	214800	7541	180.5	177200	6228	210.6	509900	17860	149.1	638500	22380	182.7
<b>Co</b>	17.88	0.636	0.1169	4.929	0.1836	0.1528	0.9795	0.0664	0.1891	22.18	0.7821	0.1188	6.231	0.2282	0.1362
<b>Ni</b>			16650			7611			5628			23410			5849
<b>Cu</b>			71.99			51.99			29.75			119.6			43.29



THE ANALYSIS OF OCHRE UTILISING TRADITIONAL METHODS

Ochre	1323		1337			3742			1293			1139			
<b>Zn</b>	46.3	4.895	5.75	103	5.772	5.715	17.54	4.053	7.217	357	13.33	4.832	94.37	8.243	6.018
<b>Ga</b>			118.5			34.38	35.44	8.191	0			110.1			41.39
<b>Ge</b>			1597			2779			1537			28260			2618
<b>As</b>	3.658	0.4624	1.665	39.73	1.468	1.255	26.67	1.021	1.153	119	4.284	2.447	10.92	0.4794	1.004
<b>Se</b>			2.684			1.883			3.925			2.705			2.349
<b>Br</b>	3.615	0.3808	1.742	4.765	0.2772	1.346	2.289	0.2505	1.32	10	0.5791	2.514	13.64	0.5181	1.135
<b>Rb</b>	69.63	9.436	20.48			16.36	78.96	13.65	24.29			27.75	41.49	9.858	20.85
<b>Sr</b>			255.7			267.6	167	37.25	144			216.3			269.1
<b>Y</b>			49210			15170			8405			69850			14350
<b>Zr</b>			351.6	330.7	82.68	7.144	521.5	59.55	7.293			214.5			187.6
<b>Nb</b>			3497			2608			2087			13380			2063
<b>Mo</b>			3.084			8.064			2.085			19.64	19.16	2.228	2.571
<b>Ru</b>			0.8912			1.644			3.018			2.064			2.543
<b>Rh</b>			23.04			93.22			52.16			323.6			30.46
<b>Pd</b>			325.7			436.5			286.9			113400			368.7
<b>Ag</b>			0.7088			3.326			3.687			2.566			3.34
<b>Cd</b>			17.04			12.16			11.76			26.93			9.683
<b>In</b>			0.3629	0.1665	0.04142	0.07112	0.2698	0.02515	0.03923	0.7747	0.1403	0.5453			0.1258
<b>Sn</b>			428			457.2			520.8			366.2			440.8
<b>Sb</b>			0.1395			0.1509	0.349	0.07398	0.3008	0.9587	0.2036	0.09487	4.807	0.1809	0.2588
<b>Te</b>			14.33			3.785			9.561			15.42			0.3381
<b>I</b>	41.11	6.675	25.69			9.727	8.015	1.367	5.154			125.4	26.54	2.369	8.355

CHAPTER TWO

Ochre	1323		1337			3742			1293			1139			
<b>Cs</b>			0.5501	0.8964	0.1533	0.5993	4.321	0.2031	0.6554			0.4707		0.5905	
<b>Ba</b>			174.8	224.2	34.13	176.2	270.8	28.41	0.4237	8407	365	1.152		122.4	
<b>La</b>	11.02	0.4008	0.0721	5.196	0.1937	0.06377	34.06	1.198	0.11	7.083	0.273	0.1153	15.17	0.575	0.08395
<b>Ce</b>	18.88	0.9273	0.281	36.75	1.404	0.1845	53.65	2.06	0.1883	23.3	1.051	0.5123	25.59	1.281	0.1728
<b>Pr</b>			31.34			17.4			15.87			75.9		15.52	
<b>Nd</b>	11.25	2.112	0.2413			4.393	38.23	2.796	0.1636	24.94	2	0.4396	24.99	3.417	0.2171
<b>Sm</b>	2.639	0.0951	0.058	1.338	0.04868	0.03717	6.197	0.2209	0.03867	3.995	0.1433	0.08886	6.844	0.2453	0.03009
<b>Eu</b>	0.7378	0.02723	0.03348	0.3436	0.01454	0.04246	0.9821	0.03613	0.05261	0.7434	0.02704	0.03588	2.04	0.07224	0.04541
<b>Gd</b>			5.286			5.246			6.628	7.147	1.476	4.439	6.617	1.38	5.501
<b>Tb</b>	0.3903	0.06033	0.1911	0.3766	0.02324	0.1991	0.5691	0.02893	0.2328	0.6612	0.03879	0.1651	0.6064	0.05105	0.204
<b>Dy</b>	3.31	0.3267	1.076	4.287	0.7011	0.6387	4.069	0.1819	0.3781	5.15	0.6334	2.425	4.085	0.1914	0.4941
<b>Ho</b>			0.6091			0.534	1.04	0.1934	0.7533			0.7949	3.208	0.1916	0.5994
<b>Er</b>			301.4			99.39			54.25			310.3		91.44	
<b>Tm</b>			0.4677			0.6423			0.8632			0.5522		0.3396	
<b>Yb</b>	1.66	0.08418	0.3876	1.724	0.1018	0.2746	2.601	0.1064	0.2525	1.383	0.08692	0.4104	1.833	0.1078	0.2193
<b>Lu</b>			67.21			22.54			13.38			88.42		19.62	
<b>Hf</b>	0.401	0.07884	0.2493	5.895	0.2247	0.2511	9.479	0.3791	0.3119	1.215	0.08822	0.2112		0.2699	
<b>Ta</b>			0.3629	0.8881	0.07909	0.187	1.602	0.08573	0.2364			0.3063		0.3808	
<b>W</b>			3.413			2.552			2.508			5.154		2.166	

THE ANALYSIS OF OCHRE UTILISING TRADITIONAL METHODS

Ochre	1323		1337			3742			1293			1139		
<b>Re</b>	66.51	7.223	0.175			0.1154			0.1179			0.2754		0.08907
<b>Os</b>			0.5594			0.5642			0.7078			0.4748		0.5553
<b>Ir</b>			4.631			5.494			1.125			13.23		0.9498
<b>Pt</b>			7.753			5.221			5.258			12.31		3.908
<b>Au</b>			0.01442			0.01031			0.009551			0.02285		0.006653
<b>Hg</b>			0.3962			0.5478			1.205			0.8524		1.043
<b>Th</b>	0.6525	0.09321	0.3595	20.43	0.7244	0.3731	37.96	1.339	0.432	3.077	0.1343	0.3092		0.2834
<b>U</b>	2.966	0.3503	1.597	2.623	0.2381	1.036	4.528	0.2746	1.103	4.745	0.6322	2.406	26.02	0.9484
														0.8377

CHAPTER TWO

**Table 2-7:** NAA data obtained for ochres 1137, 1150, 1286, 3696 and 1285 for all elements investigated. Data is reported as supplied by ANSTO.

Ochre	1137			1150			1286			3696			1285		
	mg/kg	Conc.	Unc.	LD	Conc.	Unc.	LD	Conc.	Unc.	LD	Conc.	Unc.	LD	Conc.	Unc.
<b>Na</b>	645	26.6	0	377.1	20.34	0	1111	46.91	0	1748	69.9	0	1188	47.23	0
<b>Mg</b>	2177	111.2	243	6578	286	324.6	2754	411.4	674	7714	297.1	348.2	1414	139.5	233.5
<b>Al</b>	84240	2952	56.35	13470	473	15.47	30020	1053	24.71	9106	321	11.21	6508	238.9	17.08
<b>S</b>			16750			30510			94460			32260			6324
<b>Cl</b>	149.9	8.225	14.22	192	13.93	20.37	1532	58.2	44.4	2185	78.84	26.72	1395	50.88	18.79
<b>Ar</b>			6.374			3.91			1.651			2.913			3.892
<b>K</b>	15990	1059	206.2	1020	74.71	214.2	490.3	65.99	233	560.6	104.7	393			467.1
<b>Ca</b>	451.3	74.63	141.4	597.1	95.08	209.7	1245	164.2	399.4	1184	114.8	278.4	351.8	75.06	143.8
<b>Sc</b>	23	0.81	0.01063	11.42	0.4022	0.009805	14.06	0.4969	0.01043	18.98	0.6701	0.0136	42.48	1.488	0.02373
<b>Ti</b>	6974	254.7	169.9	2269	140.8	272	1759	130.2	563.6	783.2	77.57	285.5			146.9
<b>V</b>	247.2	8.787	1.006	430.9	15.23	1.294	111.3	4.485	2.044	367.7	12.92	0.5499	657.8	23.23	0.793
<b>Cr</b>	144.7	5.174	2.838	391.3	13.99	2.63	55.97	2.124	2.805	547.7	19.66	3.708	920.2	32.63	6.512
<b>Mn</b>	79.08	2.793	0.3973	431.8	15.13	0.5248	1487	52.16	1.01	638.4	22.36	0.5537	151.8	5.334	0.3766
<b>Fe</b>	73680	2584	163.4	402700	14110	144.6	299500	10480	158.1	476100	16690	201.6	558000	19560	360
<b>Co</b>	5.081	0.1932	0.1742	94.39	3.407	0.1588	13.98	0.4999	0.1682	194.8	6.868	0.2205	152.9	5.92	0.3889
<b>Ni</b>			3726			3631			7632			4627			2237
<b>Cu</b>	298.5	28.05	5.251	203.2	28.23	6.689	348	51.86	6.38	120.5	29.49	9.897	232.9	24.85	12.66

THE ANALYSIS OF OCHRE UTILISING TRADITIONAL METHODS

Ochre	1137			1150			1286			3696			1285		
<b>Zn</b>	148.8	6.532	6.487	105.2	5.741	5.974	56.77	4.718	6.349	53.83	6.123	8.232	57.67	9.105	14.2
<b>Ga</b>	22.66	2.305	0			29.35			57.64			33.72			10.86
<b>Ge</b>			906.9			1744			4016			2140			926.7
<b>As</b>	99.08	3.486	0.491	111.9	3.941	0.638	86.39	3.048	0.5636	48.79	1.754	0.9215	43.86	1.594	1.142
<b>Se</b>	9.297	2.011	2.403			2.227			3.267			4.155			5.266
<b>Br</b>	1.813	0.1549	0.752	1.32	0.2408	0.9331	4.809	0.2225	0.8364	4.528	0.2798	1.347	5.753	0.3213	1.646
<b>Rb</b>	82.4	4.914	14.23	93.01	6.325	12.34			18.63			26.51			42.55
<b>Sr</b>			99.29			187.7			244.8			229.2			104
<b>Y</b>			4985			9564			22470			11690			5111
<b>Zr</b>	287.9	74.3	6.946			250.8			222.6			411.4			701.3
<b>Nb</b>			1146			1391			2936			1711			1137
<b>Mo</b>			0.5622			12.26			2.367			3.641			21.67
<b>Ru</b>			2.14			1.892			1.679			2.684			4.841
<b>Rh</b>			30.37			33.18			61.71			17.45			30.4
<b>Pd</b>			62.04			92.08			72.1			134			159.2
<b>Ag</b>			3.457			2.972			3.359			4.22			6.896
<b>Cd</b>			11.89			15.64			13.34			20.95			25.45
<b>In</b>	0.132 3	0.01411	0.02217	0.1491	0.01879	0.0419	0.1751	0.03625	0.09685	0.1693	0.01987	0.04998	0.1032	0.01768	0.02335

CHAPTER TWO

Ochre	1137			1150			1286			3696			1285		
<b>Sn</b>	262.7			239.6			255.7			335.6			289.8		
<b>Sb</b>	1.096	0.07526	0.1886	1.281	0.1087	0.378	1.28	0.099	0.3287	0.9388	0.1608	0.1398	2.142	0.1877	0.6617
<b>Te</b>	6.173			5.606			5.428			6.879			9.59		
<b>I</b>	2.521			14.94	1.573	5.716	16.65			7.892	1.594	6.231	15.75	1.073	3.352
<b>Cs</b>	1.861	0.1453	0.6366	0.542			0.6143			0.7703			1.301		
<b>Ba</b>	330.2	15.64	0.4036	57.34			89.51			108.1			48.03		
<b>La</b>	18.71	0.6603	0.09779	59.28	2.078	0.09154	7.666	0.2787	0.1268	49.34	1.742	0.2121	118.4	4.155	0.1429
<b>Ce</b>	43.34	1.712	0.1793	130.4	4.813	0.2569	19.49	0.7755	0.2127	117.9	4.409	0.3262	276	11.52	0.3132
<b>Pr</b>	8.121			13.37	2.126	7.763	8.65			12.75			29.62	4.18	15.16
<b>Nd</b>	19.14	1.219	0.1555	42.68	1.866	0.2212	14.89	1.174	0.1862	71.44	3.453	0.2866	114.1	4.774	0.2706
<b>Sm</b>	5.18	0.2276	0.03451	9.787	0.3501	0.05032	4.211	0.1496	0.03885	13.35	0.4698	0.07103	18.81	0.662	0.08293
<b>Eu</b>	0.772 4	0.02859	0.04838	3.613	0.1282	0.0455	0.9366	0.03472	0.04782	3.632	0.1284	0.06306	4.675	0.4039	0.1065
<b>Gd</b>	5.948			8.579	0.848	5.459	5.824			36.58	3.72	7.57	13.04		
<b>Tb</b>	0.747 4	0.03307	0.1925	1.301	0.0561	0.1713	0.7377	0.04049	0.1857	1.664	0.07522	0.2409	0.84	0.08612	0.4055
<b>Dy</b>	3.743	0.1473	0.2084	8.684	0.3235	0.3527	5.649	0.2675	0.6772	11.05	0.4025	0.3761	2.198	0.09649	0.1975
<b>Ho</b>	0.699 7	0.0992	0.3802	1.702	0.1551	0.5605	1.464	0.1232	0.432	2.68	0.2195	0.7696	0.9164		
<b>Er</b>	33.03			61.63			142			72.9			34.12		

THE ANALYSIS OF OCHRE UTILISING TRADITIONAL METHODS

Ochre	1137		1150			1286			3696			1285			
<b>Tm</b>			0.7171			0.6721			0.6748			1.017			0.8186
<b>Yb</b>	2.025	0.08422	0.3403	3.656	0.1344	0.3103	3.88	0.1433	0.3473	4.384	0.1642	0.4499	1.15	0.1747	0.7187
<b>Lu</b>			3.052			13.47			28.61			15.89			7.506
<b>Hf</b>	5.294	0.2173	0.2284	3.547	0.1439	0.2148	3.443	0.1334	0.2258	1.878	0.09678	0.2933	0.9375	0.1262	0.5351
<b>Ta</b>	1.18	0.08257	0.2031	0.426	0.1029	0.1873	0.6748	0.2566	0.1983			0.5018			0.8122
<b>W</b>	11.29	0.43	0.9204	5.983	0.2891	1.184	1.506	0.1803	1.036	3.082	0.3729	1.68	14.32	0.61	2.082
<b>Re</b>			0.1221			0.1165			0.06129			0.2166			0.3656
<b>Os</b>			0.3572			0.3285			0.3496			0.4593			0.8798
<b>Ir</b>			3.226			0.4578			0.3835			0.6092			0.7736
<b>Pt</b>			6.293			9.23			6.958			12.38			15.16
<b>Au</b>	0.036 55	0.002816	0.01076	0.026	0.003642	0.01385			0.01171	0.7165	0.03828	0.01915	3.357	5.113	0.0218
<b>Hg</b>			1.079			0.8259			0.9034			1.168			2.065
<b>Th</b>	33.68	1.188	0.2852	3.631	0.1442	0.2589	8.157	0.2974	0.2842	1.353	0.1046	0.3672	4.512	0.2319	0.6607
<b>U</b>	4.023	0.2558	1.097	3.765	0.3858	1.569	6.328	0.3566	1.222	10.53	0.6027	2.201	5.878	0.5505	1.979

CHAPTER TWO

**Table 2-8:** NAA results for all ochres, showing only the elements detected.

Ochre	1323	1337	3742	1293	1139	1137	1150	1286	3696	1285
<b>Na</b>	5031	1447	2078	30080	2254	645	377.1	1111	1748	1188
<b>Mg</b>	5636	1073	1783		999	2177	6578	2754	7714	1414
<b>Al</b>	6538	87720	98490	7481	16780	84240	13470	30020	9106	6508
<b>Cl</b>	3608	1430	1894	51430	3352	149.9	192	1532	2185	1395
<b>K</b>		1606	9789			15990	1020	490.3	560.6	
<b>Ca</b>	3496		456.7			451.3	597.1	1245	1184	351.8
<b>Sc</b>	3.064	27.33	12.63	8.716	6.509	23	11.42	14.06	18.98	42.48
<b>Ti</b>	545.3	6793	8174			6974	2269	1759	783.2	
<b>V</b>	23.28	320.5	710.7	129.1	167.4	247.2	430.9	111.3	367.7	657.8
<b>Cr</b>	7.03	174.7	188.2	34.56	88.54	144.7	391.3	55.97	547.7	920.2
<b>Mn</b>	2627	294	46.22	11570	785.2	79.08	431.8	1487	638.4	151.8
<b>Fe</b>	564400	214800	177200	509900	638500	73680	402700	299500	476100	558000
<b>Co</b>	17.88	4.929	0.9795	22.18	6.231	5.081	94.39	13.98	194.8	152.9
<b>Cu</b>						298.5	203.2	348	120.5	232.9
<b>Zn</b>	46.3	103	17.54	357	94.37	148.8	105.2	56.77	53.83	57.67



THE ANALYSIS OF OCHRE UTILISING TRADITIONAL METHODS

Ochre	1323	1337	3742	1293	1139	1137	1150	1286	3696	1285
Ga			35.44			22.66				
As	3.658	39.73	26.67	119	10.92	99.08	111.9	86.39	48.79	43.86
Se						9.297				
Br	3.615	4.765	2.289	10	13.64	1.813	1.32	4.809	4.528	5.753
Rb	69.63		78.96		41.49	82.4	93.01			
Sr			167							
Zr		330.7	521.5			287.9				
Mo					19.16					
In		0.1665	0.2698	0.7747		0.1323	0.1491	0.1751	0.1693	0.1032
Sb			0.349	0.9587	4.807	1.096	1.281	1.28	0.9388	2.142
I	41.11		8.015		26.54		14.94		7.892	15.75
Cs		0.8964	4.321			1.861				
Ba		224.2	270.8	8407		330.2				
La	11.02	5.196	34.06	7.083	15.17	18.71	59.28	7.666	49.34	118.4
Ce	18.88	36.75	53.65	23.3	25.59	43.34	130.4	19.49	117.9	276
Pr							13.37			29.62

CHAPTER TWO

<b>Ochre</b>	<b>1323</b>	<b>1337</b>	<b>3742</b>	<b>1293</b>	<b>1139</b>	<b>1137</b>	<b>1150</b>	<b>1286</b>	<b>3696</b>	<b>1285</b>
<b>Nd</b>	11.25		38.23	24.94	24.99	19.14	42.68	14.89	71.44	114.1
<b>Sm</b>	2.639	1.338	6.197	3.995	6.844	5.18	9.787	4.211	13.35	18.81
<b>Eu</b>	0.7378	0.3436	0.9821	0.7434	2.04	0.7724	3.613	0.9366	3.632	4.675
<b>Gd</b>				7.147	6.617		8.579		36.58	
<b>Tb</b>	0.3903	0.3766	0.5691	0.6612	0.6064	0.7474	1.301	0.7377	1.664	0.84
<b>Dy</b>	3.31	4.287	4.069	5.15	4.085	3.743	8.684	5.649	11.05	2.198
<b>Ho</b>			1.04		3.208	0.6997	1.702	1.464	2.68	
<b>Yb</b>	1.66	1.724	2.601	1.383	1.833	2.025	3.656	3.88	4.384	1.15
<b>Hf</b>	0.401	5.895	9.479	1.215		5.294	3.547	3.443	1.878	0.9375
<b>Ta</b>		0.8881	1.602			1.18	0.426	0.6748		
<b>W</b>						11.29	5.983	1.506	3.082	14.32
<b>Re</b>	66.51									
<b>Au</b>						0.03655	0.026		0.7165	3.357
<b>Th</b>	0.6525	20.43	37.96	3.077		33.68	3.631	8.157	1.353	4.512
<b>U</b>	2.966	2.623	4.528	4.745	26.02	4.023	3.765	6.328	10.53	5.878

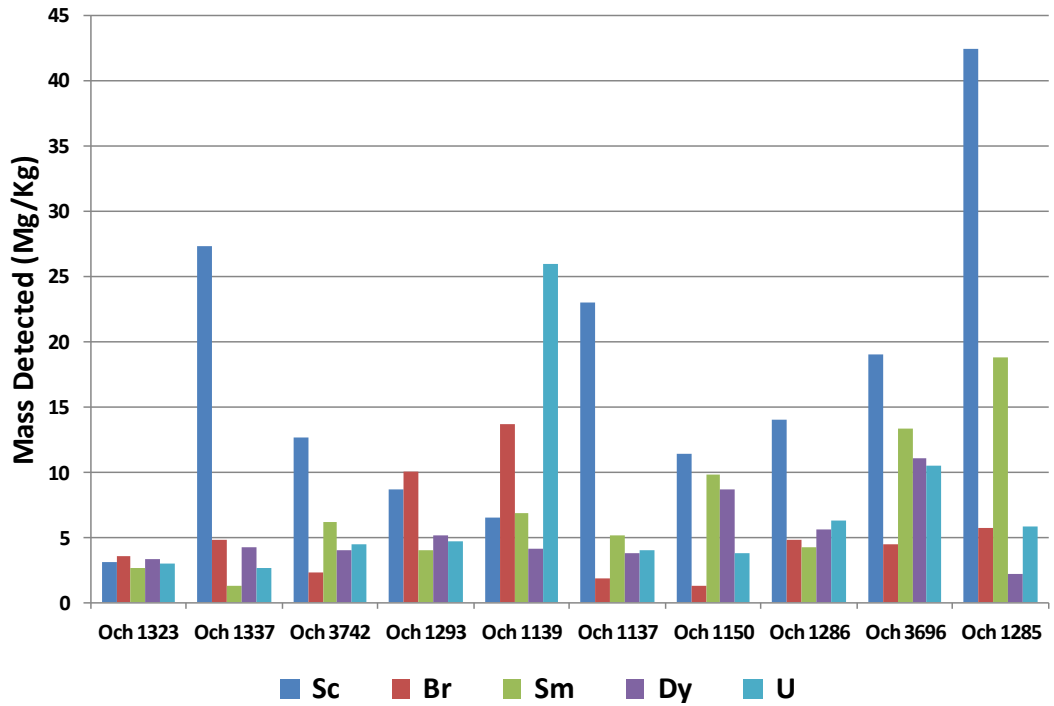


Figure 2-18: NAA results for elements detected in all ochre samples at concentrations not exceeding 100mg/kg.

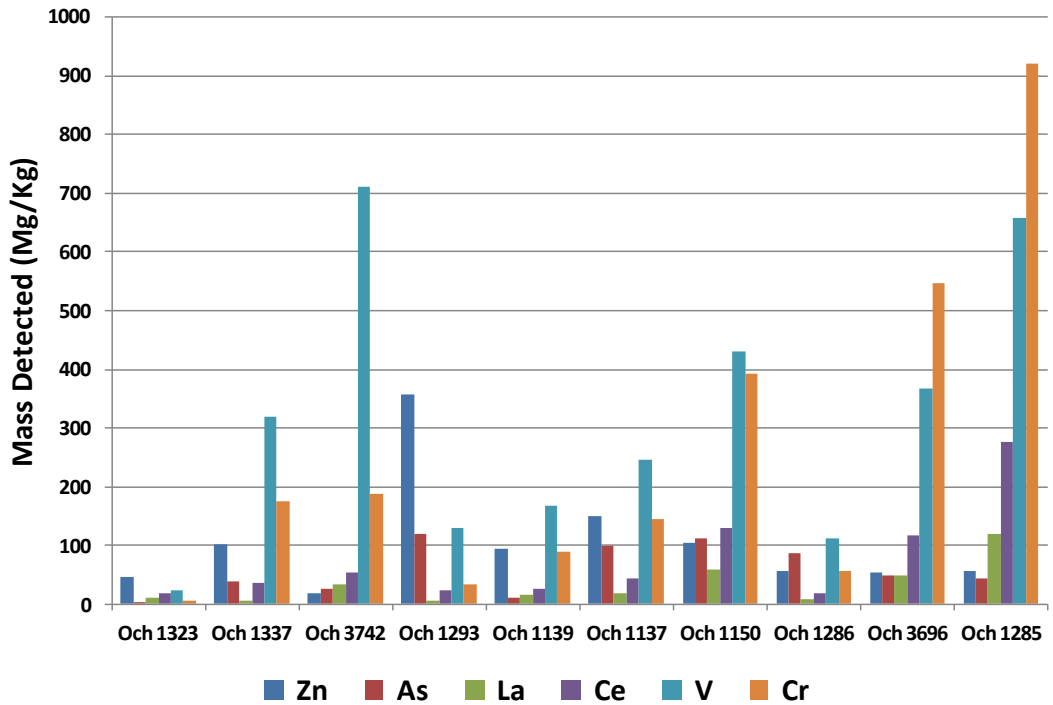


Figure 2-19: NAA results for elements detected in all ochre samples at concentrations greater than 50mg/kg in at least one sample, but not exceeding 1000mg/kg.

CHAPTER TWO

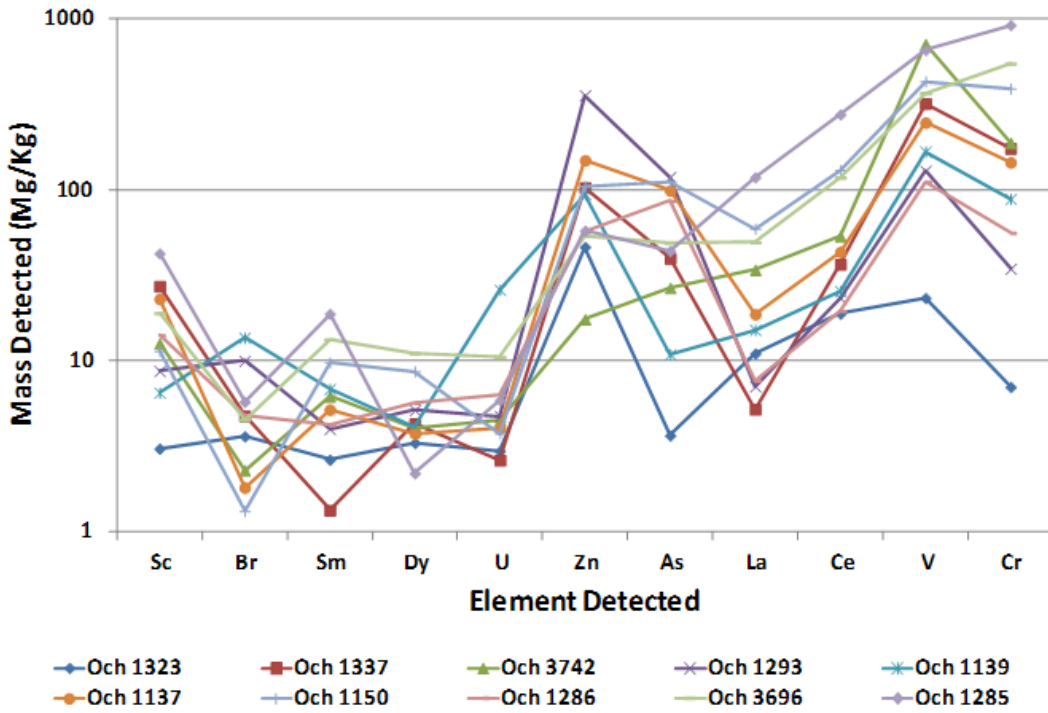


Figure 2-20: NAA results of all elements detected in all ochre samples at concentrations not exceeding 1000mg/kg.

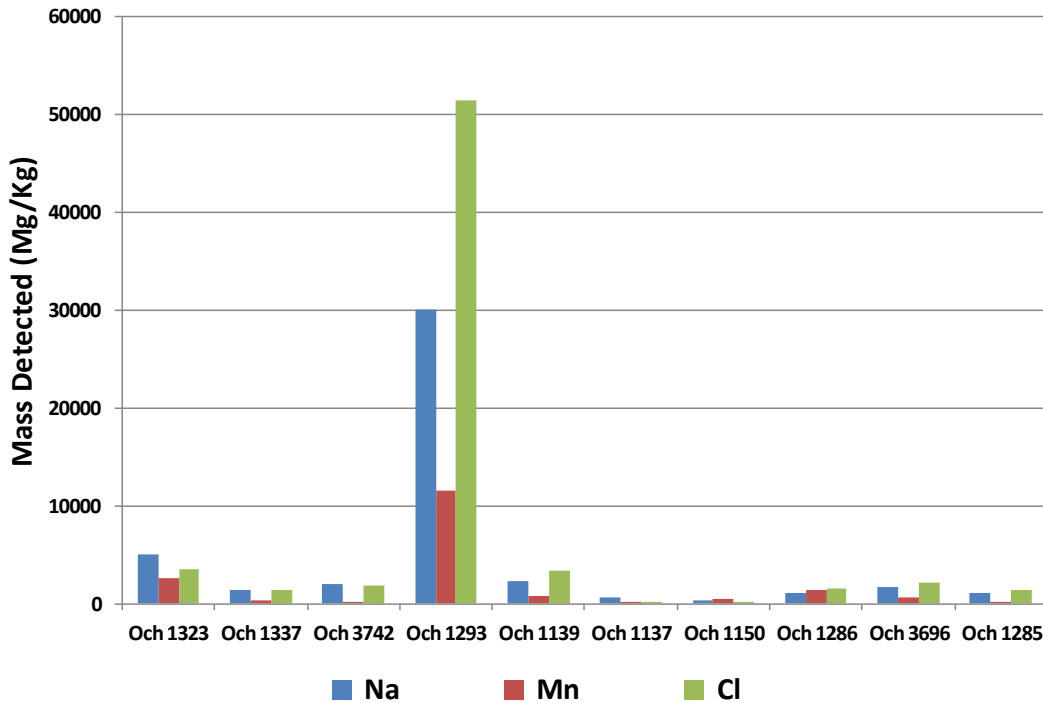
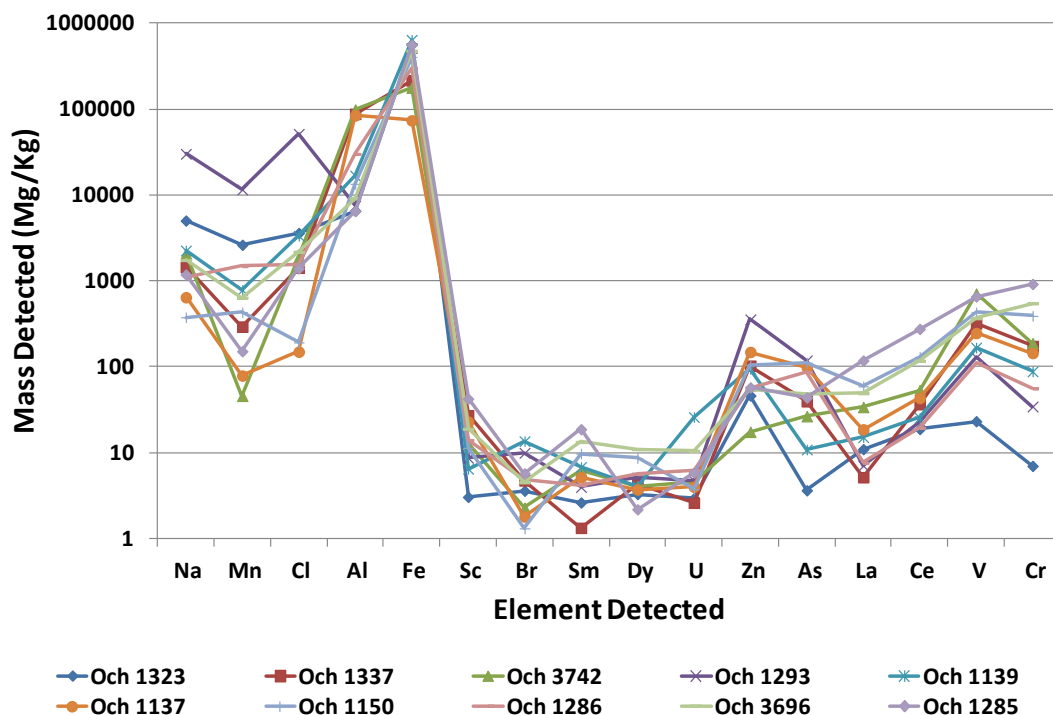


Figure 2-21: NAA results for elements detected in all ochre samples at concentrations not exceeding 60000mg/kg.



**Figure 2-22:** NAA results for elements detected in all ochre samples at concentrations not exceeding 60000mg/kg.

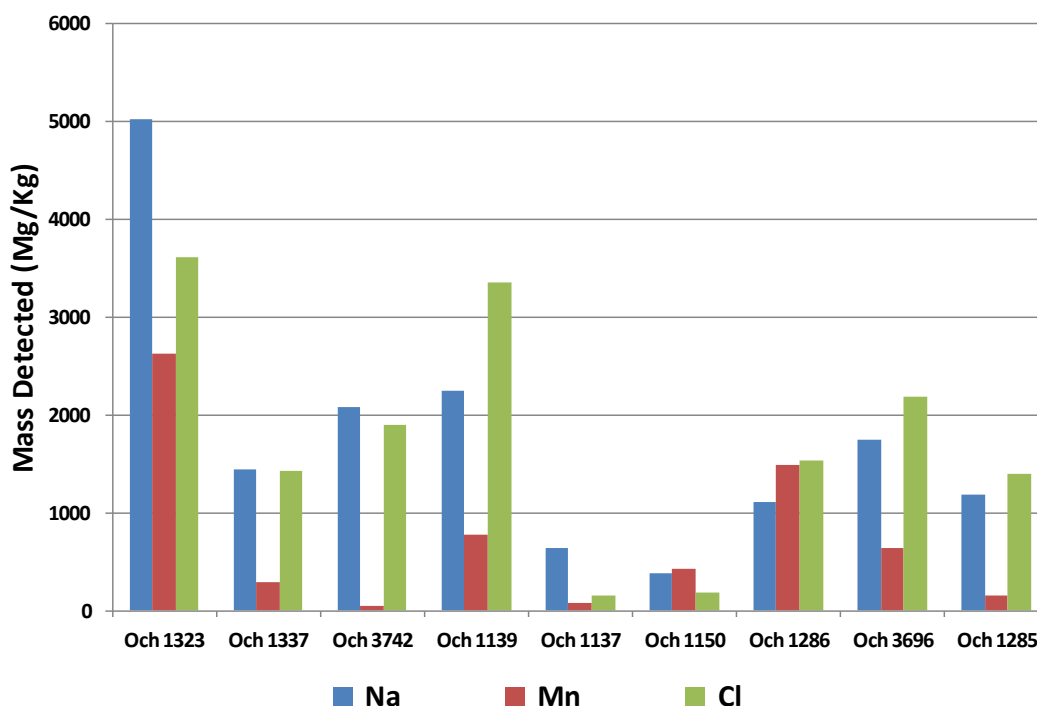
Here it can be seen that even greater variation in the individual concentrations of elements is observed. This is most apparent with ochre 1293 and these elements with concentrations up to but not exceeding 60000mg/kg, where all elements observed are approximately 10x higher concentration than other ochres. This gives an overall concentration of Na (commonly known to be a component of NaCl, otherwise known as typical table salt) in the region of 3%. This is potentially diagnostic, and reflective of the locality of ochre 1293, obtained from the salt lake regions in South Australia. The variation between the remaining ochres is best illustrated by removing ochre 1293 from the plot, and this is presented in Figure 2-23.

From this it can clearly be seen that the results of NAA are able to successfully characterise and distinguish between the ten mining samples studied. Not only are the concentrations of the studied elements different, but there is also significant variation in the ratios between these elements. This allows for easy comparison of unknowns and possible successful identification.

## 2.5. Conclusions

This chapter initially aimed to verify the purity of the synthetic standards of haematite and goethite purchased for use within this study. This was achieved via analysis with TGA and Raman spectroscopy.

This chapter then verified that a number of raw samples present in the mining collection of The South Australian Museum were in fact ochres. It was confirmed that their primary chromophores are goethite and haematite and that a number of samples contain quartz and



**Figure 2-23:** NAA results for elements detected in all ochre samples at concentrations not exceeding 60000mg/kg, with ochre 1293 omitted for scaling reasons.

clay silicates. This was necessary to ensure that all samples were ochre and that one or more, for example, were not simply soil. This allowed for comparisons to be made between the ochre samples. This was achieved by exploring a number of the commonly utilised methods for the analysis of ochre. Whilst analysis utilising these methods was successful, individually they are not without limitations.

X-ray diffraction analysis was successfully able to identify a number of components present in the ochre. However, detailed analysis proved difficult and there was not enough distinction between samples to successfully use this method for complete characterization to a level that would allow for the identification of unknown samples. Raman analysis was successfully completed on all samples and was able to identify a number of peaks that may be of interest in the characterization of ochre. The influence of quartz and the subsequent fluorescence peak proved problematic. Thermal gravimetric analysis relies on the transition of goethite to haematite and was successfully applied to all ochres appearing yellow in colour. Characteristic differences were present in all the spectra, however analysis is destructive and not enough samples were present here to establish the range of possible spectra obtainable across Australian ochres. Samples were then analysed using infrared analysis and autocorrelation analysis was applied. Results suggest that this method of analysis is not able to accurately distinguish between samples based on their colour and composition. Neutron activation analysis was able to successfully characterize and distinguish between the ten mining samples studied based on elemental composition and elemental analysis was achieved. Whilst much of the NAA data was of good quality and able to distinguish well between samples, it has a

number of limitations that reduce its promise to applications in this area. These are of specific concern when considering the analysis of artefacts as a large amount of sample is required, the technique is destructive and sample preparation is often difficult. XRD, IR and Raman did not have as many limitations as a result of the sample type and preparation, as often the sample was powdered and untreated and these techniques are non-destructive. However, they still require the sample in a specific form and these methods could not easily be applied to artefacts.

Combining the results of many of the techniques studied gives a good overall picture of the sample material. Many of the techniques are successfully able to distinguish between samples, and thus would be ideal for the establishment of a data base and the provenancing of unknowns. However, limitations include that they are destructive in nature, expensive and limited in availability, or require samples in a specific state and thus would not be able to be applied to artefacts. Almost all of these techniques are laboratory based and do not offer a portable alternative, and as a result would not be able to be applied to cave art works and other location based sites. Specifically, a portable and non-destructive instrument that can be used to distinguish between and link samples based on their provenance is required.





**CHAPTER THREE:  
A PRELIMINARY  
STUDY INTO THE  
SUITABILITY OF  
PORTABLE  
COLORIMETRY FOR  
THE ANALYSIS OF  
OCHRE MATERIALS**

Chapter two explored the use of many of the techniques traditionally utilised in the characterisation of ochre materials, and identified many of the associated limitations. The most significant of these included the sample preparation methods required, their often destructive nature, and the inability to perform on-site analysis due to the lack of portability of instruments. The need for a method that eliminated many of these limitations is clear.

An instrument that overcomes these limitations is the handheld EFI ES-1000, also known as the X-rite i1Pro. This instrument is a portable, handheld spectroscopic device typically used in the printing industry, and is utilised in the collection reflectance spectra in the UV/visible region. This chapter applies this handheld instrument to a number of synthetic and natural ochre based materials. This chapter contains method developed as it examines a number of variable parameters to determine if the instrument is accurate in the analysis of the ochre materials utilised previously, and if so, what parameters are optimal.

### 3.1. Background instrumental information

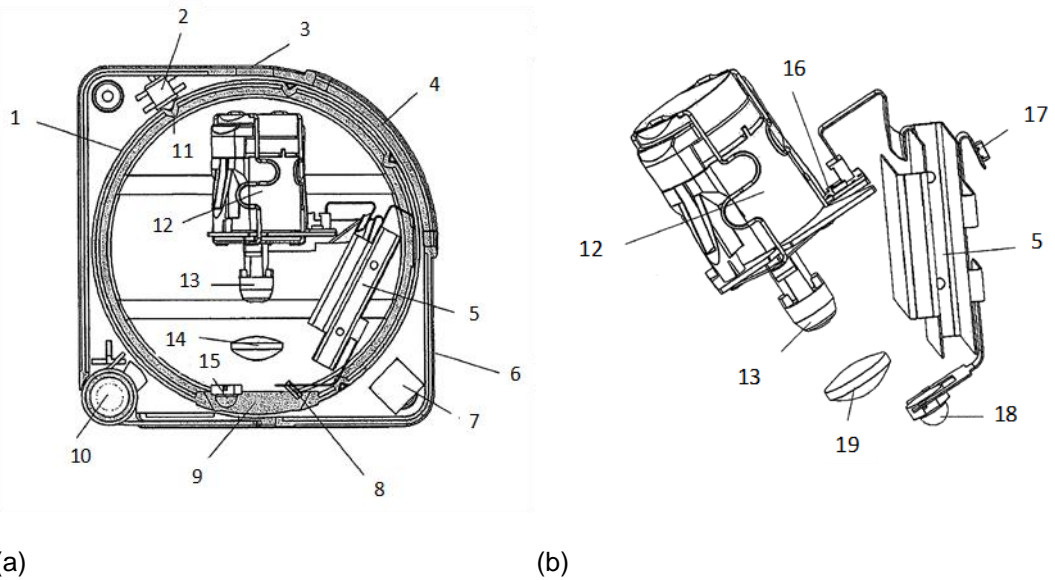
The EFI ES-1000 is a handheld device developed for colour analysis and calibration in the printing industry and shown in Figure 3-1. Due to a change in ownership, this instrument is now manufactured by x-rite and referred to as an i1-Pro system. Both instruments are internally identical and have been used in this study.



**Figure 3-1:** *The EFI ES-1000 hand-held spectrophotometer.*

The instrument patented (US 7671991 B2), and includes a housing in which an optoelectronic measurement unit is located which receives measurement light originating from a measurement object, converts it into corresponding electrical measurement signals and processes these measurement signals into preferably digital measurement data characterising the color of the object [148].

The instrument has a gas-filled tungsten type-A light source, combined with an LED array, with a UV-filter, and a holographic diffraction grating analyser with 128 pixel diode array detector. The measurement geometry is from 45°/0° from a dual channel, and spectral data is collected over the range of 380-730nm with 10nm steps in reflectance mode. The illumination diameter is 7mm with a measurement aperture of 4-4.5mm diameter. Output is in the forms of XYZ,



**Figure 3-2:** (a) Diagram showing a cross section of the internal schematics of the *i1 pro* instrument, with only the functionally essential elements shown, and (b) an oblique view of the opto-electronic measurement arrangement of the handheld colour measurement device.

CIE,  $L^*a^*b^*$  and spectra, with a total measurement time in the region of 2.5 seconds per sample. The instruments operating temperature is within the range of 5°C to 40°C, provided the humidity is less than 85% [149, 150].

The schematics of the instrument are shown in Figure 3-2 (a) where only the operationally required components are shown, and (b) shows an oblique view of the opto-electronic measurement arrangement.

These components are:

1 and 6 - Two device blocks which can be moved, relative to one another, into different, defined positions.

2 – Cam that the first housing block engages under spring bias. The cam can thereby also function at the same time as position sensor and can deliver a corresponding position signal to the control electronic which can then be used for the adjustment of the measurement sequences or evaluation of the measurement data required for the respective application function.

3 - An ambient light measurement window.

4 - A projector measurement window for the measurement on projector surfaces, which are illuminated, for example, by an electronic projector (beamer).

5 - Processing control electronics.

7 - White reference standard.

8 – Additional optical sensor.

9 - A sufficiently large opening through which the measurement light from the measurement object enters into the interior of the second device block and through which also the illumination light of the light source passes.

10 – Release button.

11 – Cutouts at the outer circumference of the second housing block into which a cam in the first housing block engages under spring bias.

12 – Spectrometer with associated electronics for the light converters and a processing and control electronic, which is built on a flexible and, for reasons of space savings, folded circuit board.

13 – Pickup head.

14 – Input lens.

15 – Light source for remission measurements on measurement objects which themselves do not illuminate.

16 – Electronic for the light converters.

17 – A USB-interface through which the power supply is also carried out.

18 – A white light emitting diode for remission measurements on measurement objects which themselves do not illuminate.

19 – An input lens.

The design of the tertiary moulded external housing and calibration base, as shown in Figure 3-1, is described in and covered under US Patent number D523766 [151]. It has a height of 67mm, width of 66mm, a length of 151mm, and weights 185g when completely assembled [149, 150]. This small size is essential for this project, where portability is key to the aim of on-site field investigations.

The instrument connects to any laptop or desktop based PC via a USB connection. It operates under ColorPort 1.0.1 software, which, combined with the instrument, has inbuilt calibration capabilities. Raw data is available in either the .CSV or .TXT format.

## **3.2. Experimental methods**

### **3.2.1. Samples**

The goethite and haematite standards discussed previously were used in these studies. A series of samples of known composition varying by approximately 5% were prepared, and are detailed in Table 3-1.

**Table 3-1:** Series of standard goethite and haematite samples varying in composition by approximately 5%.

Sample Number	Goethite %	Haematite %
1.00	0.00	100.00
2.00	4.94	95.06
3.00	10.28	89.72
4.00	15.31	84.69
5.00	20.74	79.26
6.00	25.12	74.88
7.00	28.48	71.52
8.00	35.00	65.00
9.00	40.16	59.84
10.00	45.38	54.62
11.00	50.32	49.68
12.00	54.95	45.05
13.00	60.24	39.76
14.00	64.61	35.39
15.00	69.84	30.16
16.00	75.20	24.80
17.00	79.95	20.05
18.00	84.38	15.62
19.00	90.03	9.97
20.00	95.07	4.93
21.00	100.00	0.00

### 3.2.2. Experimental techniques

Sample application methods and substrates vary greatly through this and subsequent chapters as the instruments capabilities are explored. It is therefore difficult to give a single experimental method. However, some typical parameters are used.

Approximately 10-15mg of sample was rubbed onto to a single piece of Fuji Xerox 80g/m<sup>2</sup> white laserprint paper and (using gloved hands) to form a circle approximately 2.5cm in diameter. Typically 3-5 sites on the resulting circle were selected as sample sites, and the instrument was placed over the sample site. Multiple measurements (typically 5 but up to 100 depending on the experiment) were taken from the site without moving the instrument. The area of the instrument in contact with the sample was then cleaned, before this process is repeated with the next sample site.

### 3.2.3. Data analysis methods

Raw data was converted to excel format, where each sample site is firstly considered. The spectral data from each site was collated using MS excel. Statistical analysis was completed to determine the standard deviation for each data point on the spectra, before a Q-test was applied to determine any outliers. Once statistically acceptable, the data for each data point was averaged. This process is repeated considering each site per sample, resulting in a single averaged spectrum per sample. This data was then analysed statistically, with the standard deviation calculated using [152]

$$SD = \sqrt{\frac{\sum(x-\bar{x})^2}{n-1}} \quad \text{Equation 3-1}$$

where  $\bar{x}$  is the arithmetic mean and n is the number of samples.

#### 3.2.3.1. Derivative analysis

It is documented that derivative spectroscopy can improve quantitative and qualitative analysis by applying the first- or higher order derivatives of the original spectrum. Here, first order derivatives are applied to the spectra. This is calculated by considering the rate of change of the absorbance with respect to the rate of change in the wavelength, and is expressed mathematically as

$$\frac{dA}{d\lambda} = f'(\lambda) \quad \text{Equation 3-2}$$

where  $A$  represents absorbance, and  $\lambda$  the wavelength.

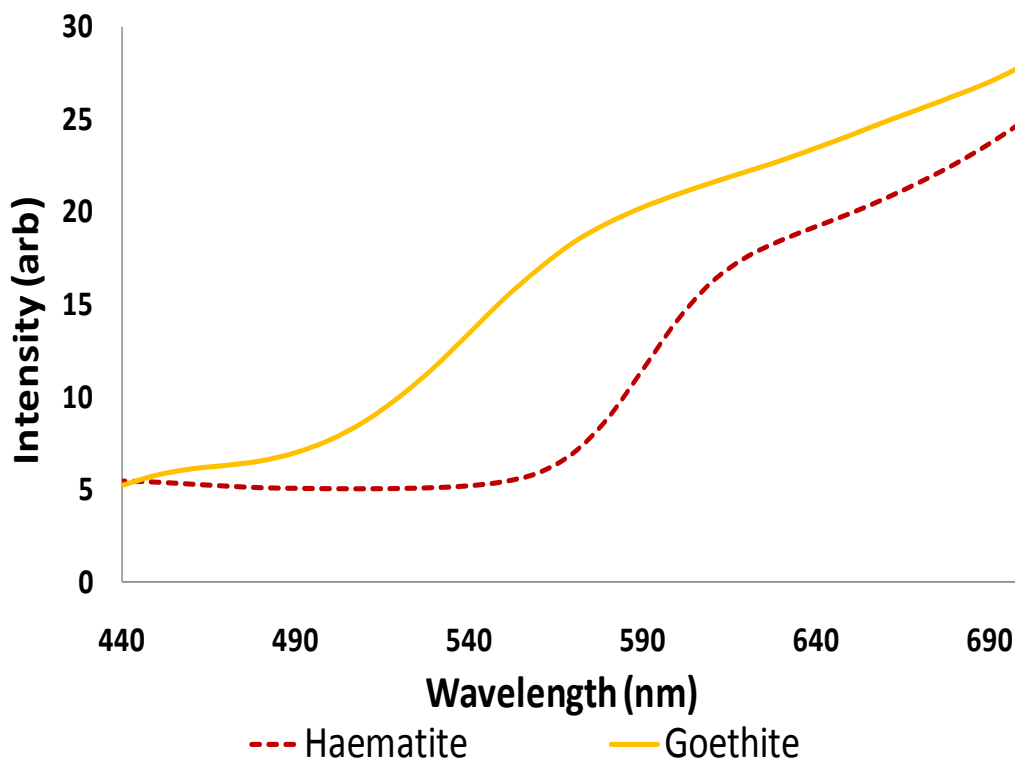
## 3.3. Results and discussion

### 3.3.1. Application of the i1Pro to synthetic ochre standards

In order to demonstrate that the X-Rite i1 Pro system was capable of distinguishing between hematite and goethite, reflectance measurements were taken from goethite and hematite (used as received from Sigma Aldrich) rubbed onto white photocopier paper as described earlier. As can be seen in Figure 3-3, the reflectance spectra from the goethite sample was observed to exhibit a two stage increase in intensity, beginning at approximately 450nm, with the greatest change seen in the region of 520-570nm. In contrast, haematite shows very little reflectance in the region of 520-570nm, instead showing an increase in reflectance over the region of 570-630nm. This variation is consistent with the reflectivity and colour of the standards, with goethite appearing yellow-brown in colour, and haematite a rich, deep red.

### 3.3.2. Determining the reproducibility of results

The manufactures of this instrument report the reproducibility of measurements to be x,y:  $\pm 0.002$  [149]. In order to ascertain the reproducibility of the i1pro with hematite and goethite, replicate measurements were performed and statistical analysis of the resulting intensity at each wavelength undertaken.



**Figure 3-3** : Reflectance Spectra obtained for goethite (yellow) and haematite (red) standards utilising the i1Pro system.

### 3.3.2.1. Repeatability of measurements from single point on standard

#### 3.3.2.1.1. Goethite standard

Two hundred measurements were taken from a single point on a goethite standard sample of approximately 0.01 grams in size rubbed into a single piece of Fuji Xerox 80g/m<sup>2</sup> white laserprint paper to form a circle approximately 2.5cm in diameter. The results of this are shown in Table 3-2.

As shown, at low wavelengths (400-430nm) the resulting standard error was greater than that reported by the manufacturer ( $\pm 0.002$ ). This was particularly so at 400nm which had a standard error of  $\pm 0.07$  and a relative standard deviation of greater than 14% for goethite. It is important to note here that the instrument is not being used for the purpose for which it was manufactured. This additional variation may be a result of a number of factors, including natural variations of colour within the sample, and surface roughness and background effects. Furthermore, the measured reflectance of the sample was low at these wavelengths, thus compounding the error. Excluding the region of 400-430nm, on average the error in the measurement across all the wavelengths was  $\pm 0.002$  for goethite, within the manufacturers specifications. For this study we aimed for a standard deviation of less than 1% across replicate measurements. Results shown indicate that low wavelengths (less than 440nm) must therefore be excluded, and that the deviation obtained by this study across the remainder of wavelengths of less than half of one percent is experimentally acceptable.

**Table 3-2:** Results obtained for two hundred measurements of standard Goethite utilising the EFI ES-1000.

Wavelength (nm)	Average Intensity (arb)	% Deviation	Standard Error
400	6.599	14.387	0.07
410	4.957	6.889	0.02
420	4.863	2.785	0.010
430	5.473	0.981	0.004
440	6.241	0.518	0.002
450	6.915	0.345	0.002
460	7.310	0.281	0.001
470	7.542	0.282	0.002
480	7.831	0.293	0.002
490	8.357	0.251	0.001
500	9.174	0.194	0.001
510	10.341	0.188	0.001
520	11.897	0.231	0.002
530	13.733	0.223	0.002
540	15.824	0.213	0.002
550	17.905	0.181	0.002
560	19.694	0.133	0.002
570	21.241	0.083	0.001
580	22.375	0.077	0.001
590	23.270	0.078	0.001
600	23.984	0.095	0.002
610	24.638	0.105	0.002
620	25.255	0.094	0.002
630	25.858	0.094	0.002
640	26.559	0.056	0.001
650	27.247	0.047	0.0009
660	27.989	0.038	0.0008
670	28.698	0.040	0.0008
680	29.419	0.037	0.0008
690	30.156	0.049	0.001
700	31.080	0.039	0.0009



#### 3.3.2.1.2. **Haematite (iron (III) oxide) standard**

Whilst studies have proven the i1Pro to give reliable and reproducible results on the goethite standard, yellow in colour, Ochre exists in a variety of colours, and thus the reproducibility studies were repeated for the red iron (III) oxide (haematite). As for the goethite, two hundred measurements were taken from a single point on a haematite standard sample of approximately 0.1g in mass rubbed into a single piece of Fuji Xerox 80g/m<sup>2</sup> white laserprint paper to form a circle approximately 2.5cm in diameter. The results of this are presented in Table 3-3. The results of this mirrored those of the goethite with poor relative standard deviations and higher than expected standard errors of the mean at wavelengths below 440nm. Thus all further analysis focussed only on data from 440nm to 700nm.

#### 3.3.2.1. **Repeatability of sample application**

The sample application method used for determining the reproducibility of the reflectance comprised rubbing a small mass of ochre onto paper. There was some question as to whether this was an appropriate method of subsampling and collecting data. Consequently, five goethite standard samples of approximately 0.1g in mass were rubbed into a single piece of Fuji Xerox 80g/m<sup>2</sup> white laserprint paper to form a circle approximately 2.5cm in diameter. Each individual sample was then measured twenty times to reduce any errors. The results of this are presented in Figure 3-4. Similarly, this was repeated with five hematite standard samples of approximately 0.1g in mass were rubbed into a single piece of Fuji Xerox 80g/m<sup>2</sup> white laserprint paper to form a circle approximately 2.5cm in diameter. The results for hematite are presented in Figure 3-5.

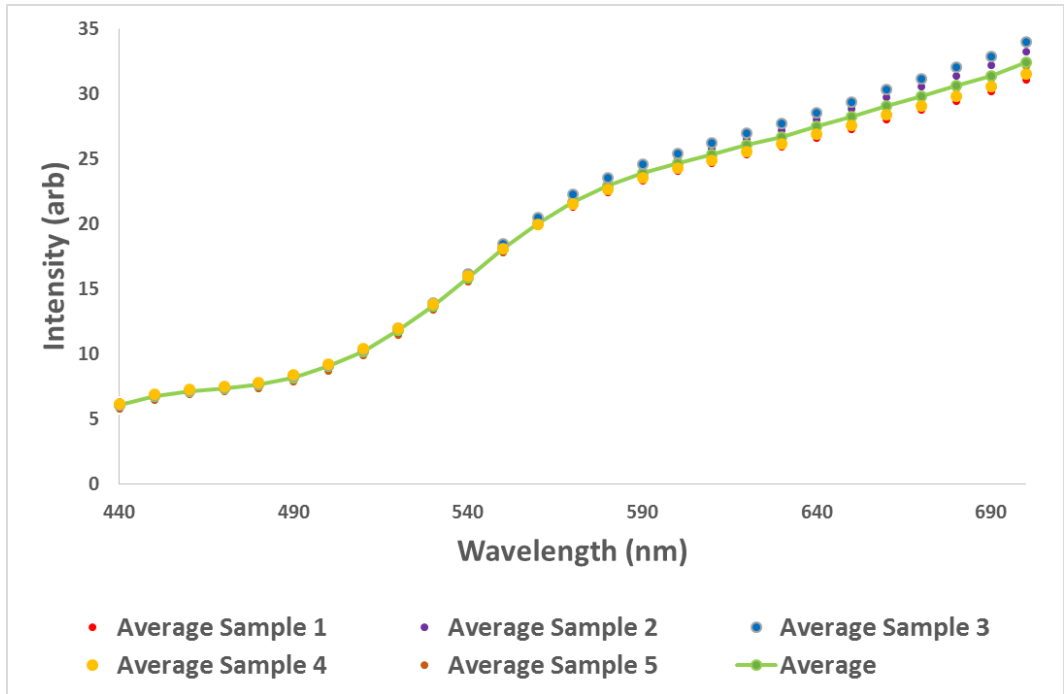
It can be seen that whilst the trends appear to be very similar, the raw values for goethite do in fact show some variation, particularly apparent at the higher wavelengths (above 570nm). It is likely that this variance may be due to small variations in the mass of sample applied to the paper. The spectra of hematite, however was much more reproducible, with very little variation across all wavelengths.

#### 3.3.2.1. **Derivative analysis**

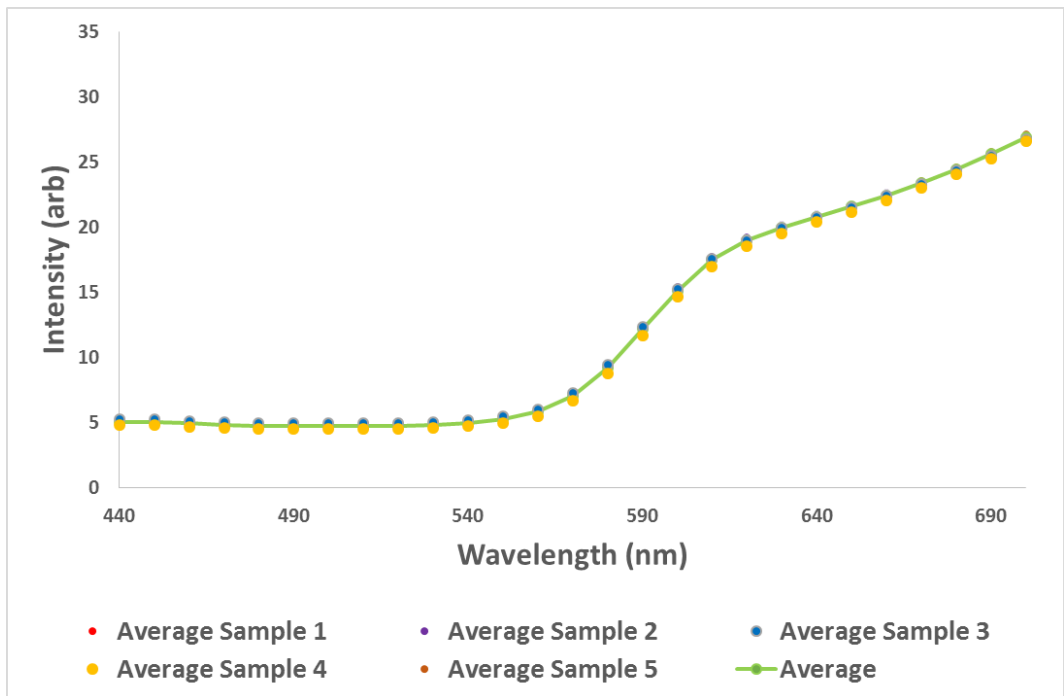
It is documented that derivative spectroscopy can improve quantitative and qualitative analysis by applying the first- or higher order derivatives of the original spectrum. In particular it enhances spectral features where the samples have very similar absorption values, and suppresses broad background absorbance. As a result, derivate calculations are vital for discriminating key areas in the reflectance spectrum [153-155]. This is highlighted in Figure 3-6

**Table 3-3:** Results obtained for two hundred measurements of standard haematite utilising the EFI ES-1000.

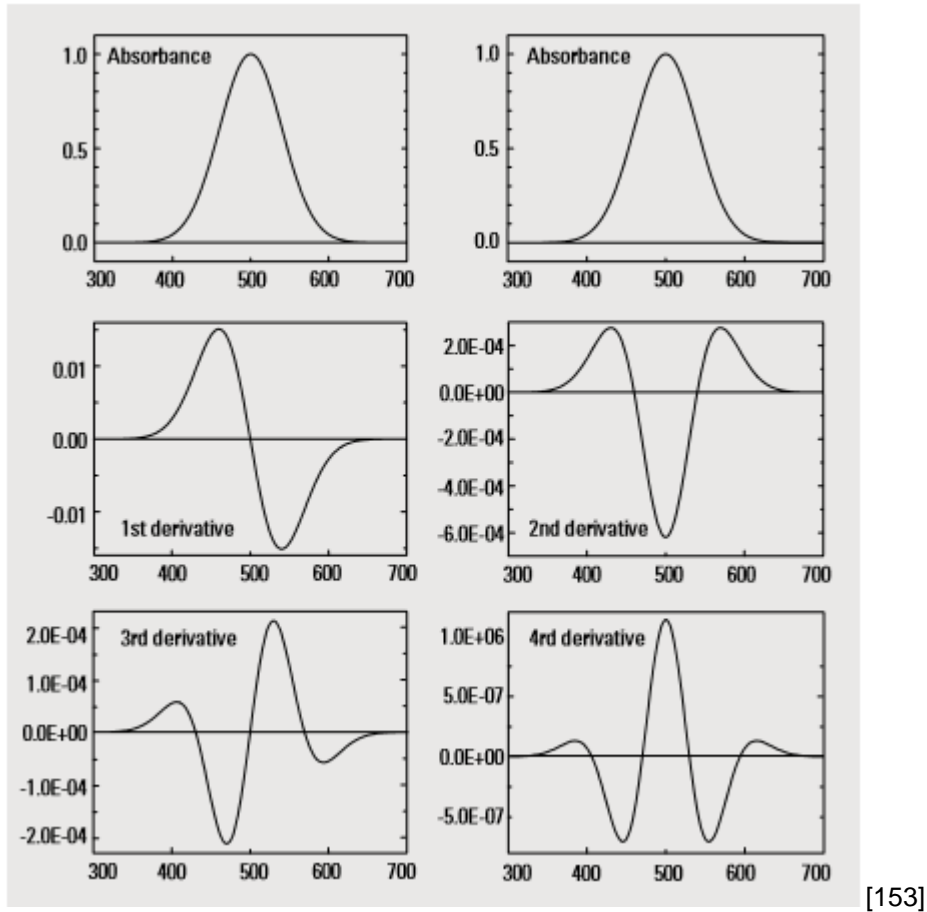
Wavelength (nm)	Average Intensity (arb)	% Deviation	Standard Error
400	5.929	18.025	0.08
410	5.015	6.876	0.02
420	4.901	2.756	0.010
430	5.015	0.843	0.003
440	5.075	0.466	0.002
450	5.020	0.366	0.001
460	4.930	0.319	0.001
470	4.830	0.309	0.001
480	4.751	0.255	0.0009
490	4.729	0.220	0.0007
500	4.727	0.185	0.0006
510	4.732	0.170	0.0006
520	4.765	0.191	0.0006
530	4.824	0.167	0.0006
540	4.958	0.152	0.0005
550	5.235	0.133	0.0005
560	5.816	0.125	0.0005
570	7.057	0.157	0.0008
580	9.224	0.213	0.001
590	12.170	0.232	0.002
600	15.174	0.209	0.002
610	17.519	0.153	0.002
620	19.034	0.112	0.002
630	20.038	0.084	0.001
640	20.872	0.064	0.0009
650	21.654	0.052	0.0008
660	22.530	0.049	0.0008
670	23.493	0.047	0.0008
680	24.544	0.046	0.0008
690	25.722	0.050	0.0009
700	27.041	0.046	0.0009



**Figure 3-4:** Average Spectra obtained for five separate Goethite Standard samples, each measured twenty times, with the average spectra shown in green.



**Figure 3-5:** Average Spectra obtained for five separate haematite standard samples, each measured twenty times, with the average spectra shown in green.



**Figure 3-6:** Absorbance and derivative spectra of a Gaussian band highlighting the effect of first and higher order derivative calculations on the spectra.

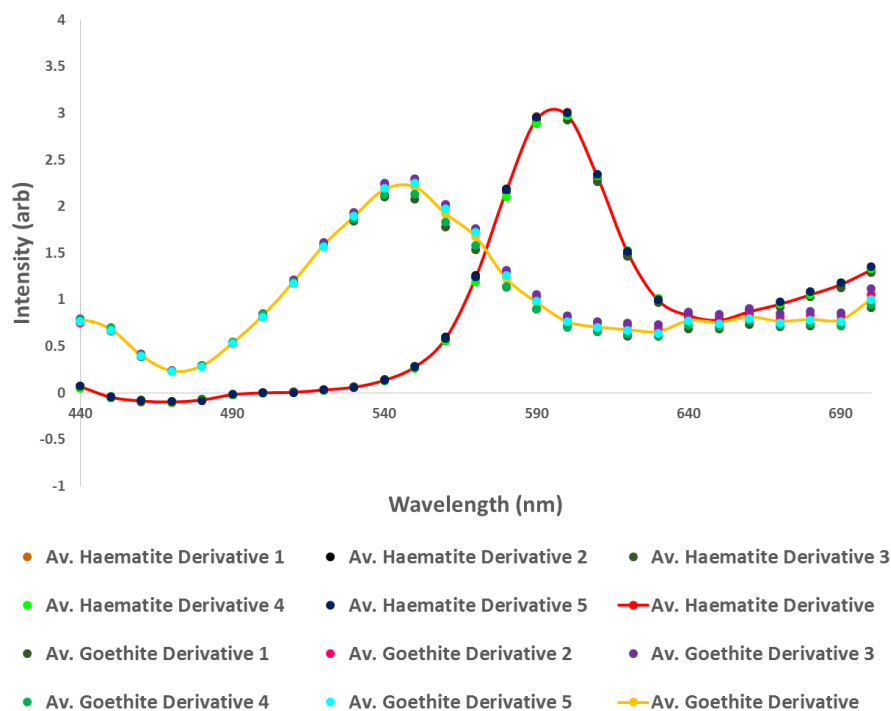
The derivative spectra for the goethite and hematite samples described above were calculated, and results of this are shown in Figure 3-7.

Importantly, whilst the reflectance spectra is similar for the hematite and goethite, the derivative spectra emphasises the differences between the two samples. The goethite spectra show a peak maxima at approximately 540nm, compared to the 590nm maxima observed for haematite. In addition to this, the goethite peak is much broader than that of haematite, and shows a lower intensity of the peak maxima.

It can be seen when comparing Figure 3-7 to Figure 3-4 and Figure 3-5 that the variation shown between the derivatives is less than that shown between the average spectra, especially at higher wavelengths.

### 3.3.1. Detecting colour variations

Whilst reproducibility is extremely important, for the i1Pro to have viable applications to ochre and similar materials, it must be able to accurately distinguish between different coloured materials, as well as confirm the similarities in colour of materials from the same source. In order to confirm the instruments ability to accurately complete this task, a study was



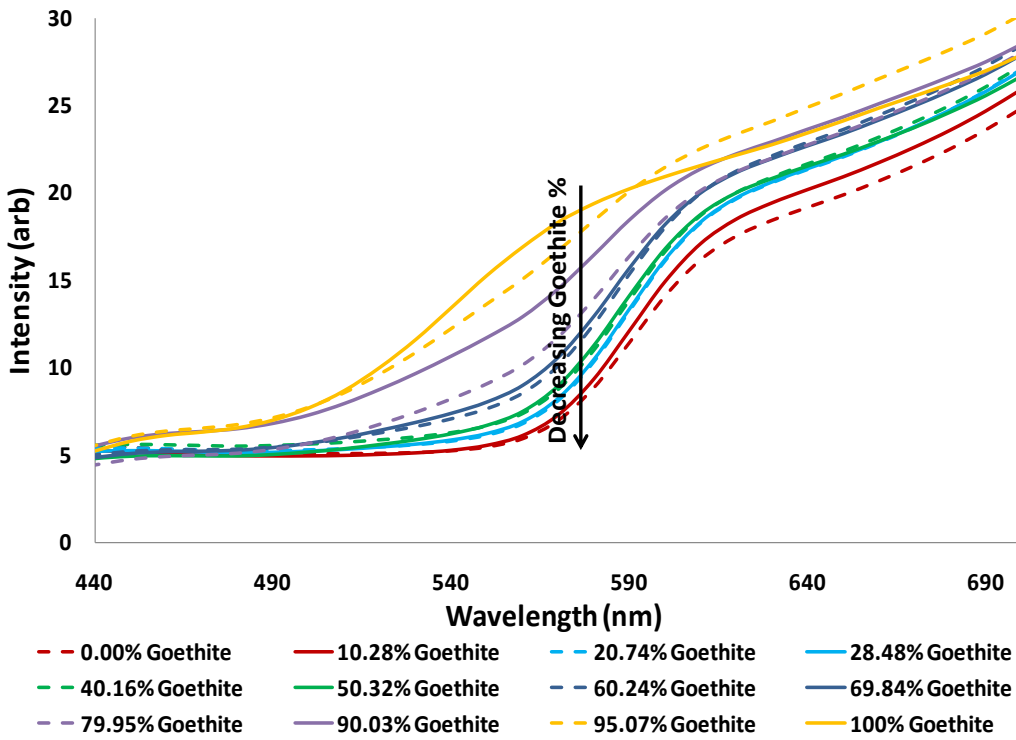
**Figure 3-7:** Derivatives of the average spectra obtained for five separate goethite and five separate haematite Standard samples, each measured twenty times, with the overall average goethite spectra shown in yellow and haematite spectra in red.

undertaken using standards of known composition ranging from pure goethite, hematite/goethite mixtures, to pure haematite

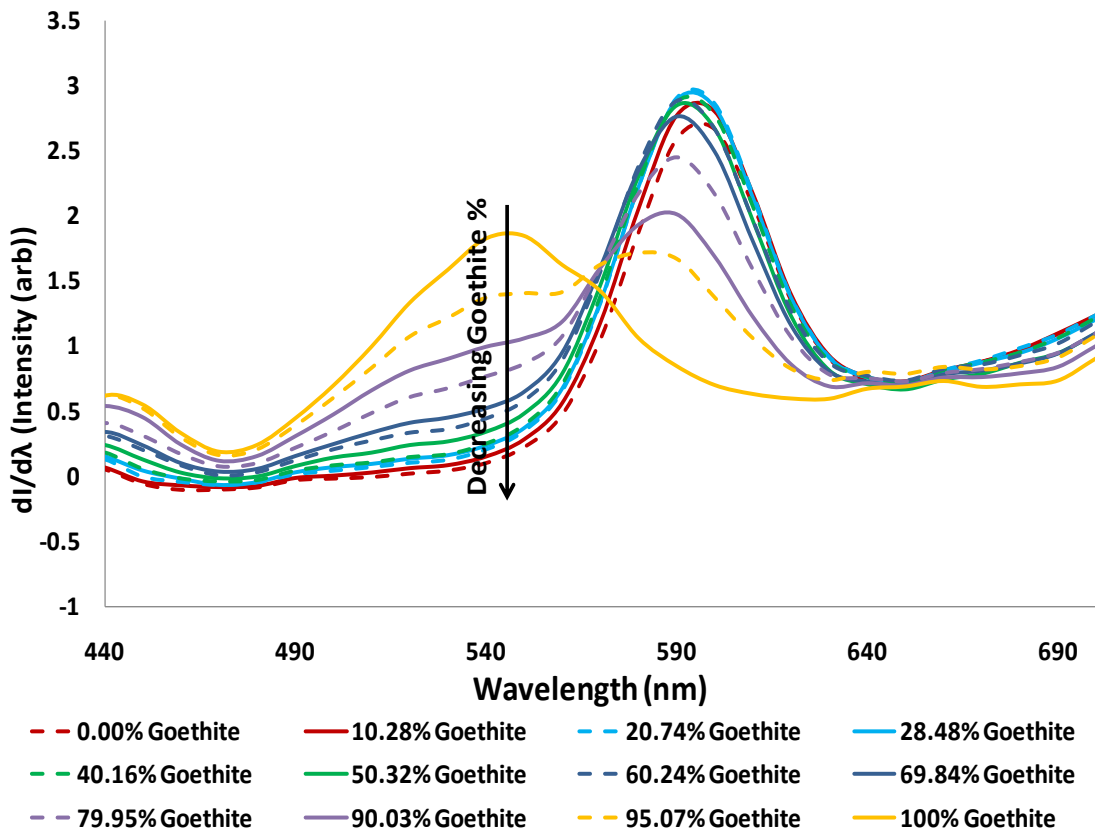
Experimentally, twenty one separate standard samples of various compositions were prepared (as per Table 3-1) and approximately 0.1g in mass were rubbed into a single piece of Fuji Xerox 80g/m<sup>2</sup> white laserprint paper to form a circle approximately 2.5cm in diameter. Each individual sample was then measured ten times and the spectra averaged to reduce any errors. Results of this are shown in Figure 3-8. Please note alternate spectra have been removed at goethite percentages less than 90% to increase the ease of interpretation.

When examining the spectra, a general trend becomes immediately apparent, especially in the region of 500-600nm, where increasing goethite concentration appears to see a shift in the peak towards lower wavelengths, as well as an increased intensity. What is also apparent is that, although the variation in composition is approximately equal at five percent per sample, the separation and trend in peak shift between the samples is not, with the higher the concentration of haematite present in the sample, the more similar the spectra appear. The uneven distribution of the spectra across the range of goethite and haematite compositions is significant as it confirms what was previously discussed with the XRD Reitfeld data, that a small percentage of haematite has a large influence over the colour of the ochre.

In order to enhance differences between the samples, the derivative spectra were calculated. Results of this are shown in Figure 3-9. Results of this show a more exaggerated trend with a dominant shift in peak position from approximately 540nm to 590nm with increasing haematite



**Figure 3-8:** Average spectra obtained for varying goethite and haematite composition samples utilising the EFI ES-1000.



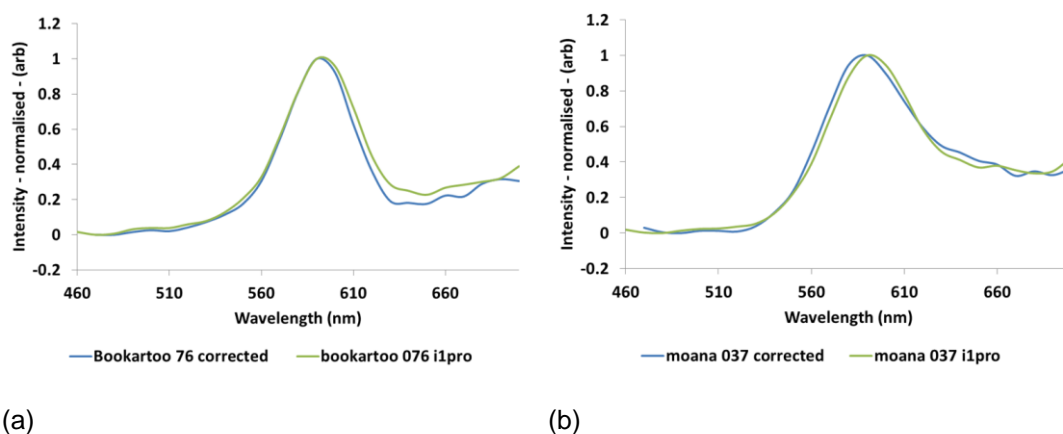
**Figure 3-9:** First derivatives of the average spectra obtained for varying goethite and haematite composition samples utilising the EFI ES-1000.

composition. Also of significance is the increasing intensity in the peak at approximately 590nm with increasing haematite concentration, and a subsequent decrease in intensity of the peak at approximately 530nm.

### 3.3.2. Comparison of the i1Pro to bench top grade instrumentation

It has been demonstrated that the i1Pro is capable reproducibly measuring the colour of synthetic ochre samples. It is now desirable to determine if the measurements obtained from the portable i1Pro system are comparable to those obtained from a traditional laboratory based instrument.

A number of ochre samples from two South Australian sites known to be used by Indigenous Australians being Bookartoo and Moana were chosen for analysis. A total of eight samples were measured, with similar results. Two typical samples are presented here, and the remaining data is available in Appendix C. The samples presented here both appeared red in colour. Sample preparation and analysis techniques were completed using the methods previously described. Samples were measured (with one sample from each site shown for comparison) using the Perkin-Elmer Lambda 950 UV-VIS-NIR utilising the methods previously described, and data obtained over the region of 470-700nm is compared to the i1Pro data obtained from the same samples. Results of this are shown in Figure 3-10. It can be seen here that the data obtained for both instruments observes the same trend and the peak maxima is located at the same wavelength. Given the different technology in both instruments, and considering factors such as portability and cost, the results shown here demonstrate that the i1Pro is capable of these types of measurements. The small differences observed are likely due to the capabilities of the lamps being used, especially greater than 650nm where the i1Pro instrument is reaching maximum capabilities.



**Figure 3-10:** Comparison of the derivatives of the spectra obtained for (a) Bookartoo ochre 076 and (b) Moana ochre 037 utilising both the i1Pro system (shown in green) and the Perkin-Elmer Lambda 950 (shown in blue).

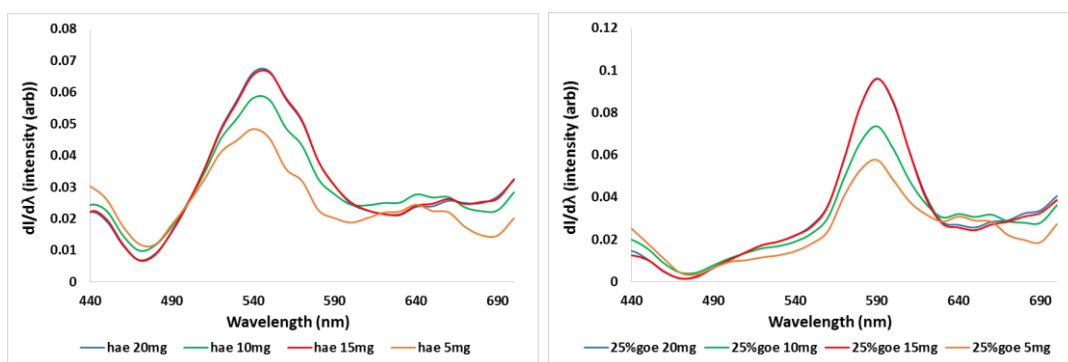
### 3.3.3. Investigating the effect of varying sample thickness

Ochre is often applied to artefacts at a variety of thicknesses, and these thicknesses can change with wear and tear over time. In order for the X-Rite i1 Pro colour recognition technique to be applicable to real samples, investigations into the instruments ability to distinguish between sources not only slightly varying in colour, but also varying significantly in sample thickness and coverage, are necessary.

Experimentally, the same twenty one separate goethite and haematite standard samples of various compositions that were previously successfully separated were again examined. Samples were applied to a single piece of Fuji Xerox 80g/m<sup>2</sup> white laserprint paper as previously described to form a circle approximately 2.5cm in diameter. Samples of 20mg, 15mg, 10mg and 5mg were studied. Each individual sample was then measured at three separate locations with each location measured five separate times to reduce any errors.

The spectra obtained covered a region of 400-700nm, and demands for increased accuracy see the derivatives of the spectra with only the region of 440-700nm used for statistical analysis. The raw data was taken (not the derivatives), an outlier test was performed and the remaining data, typically fifteen spectra, were averaged and normalised and derivatised for comparison.

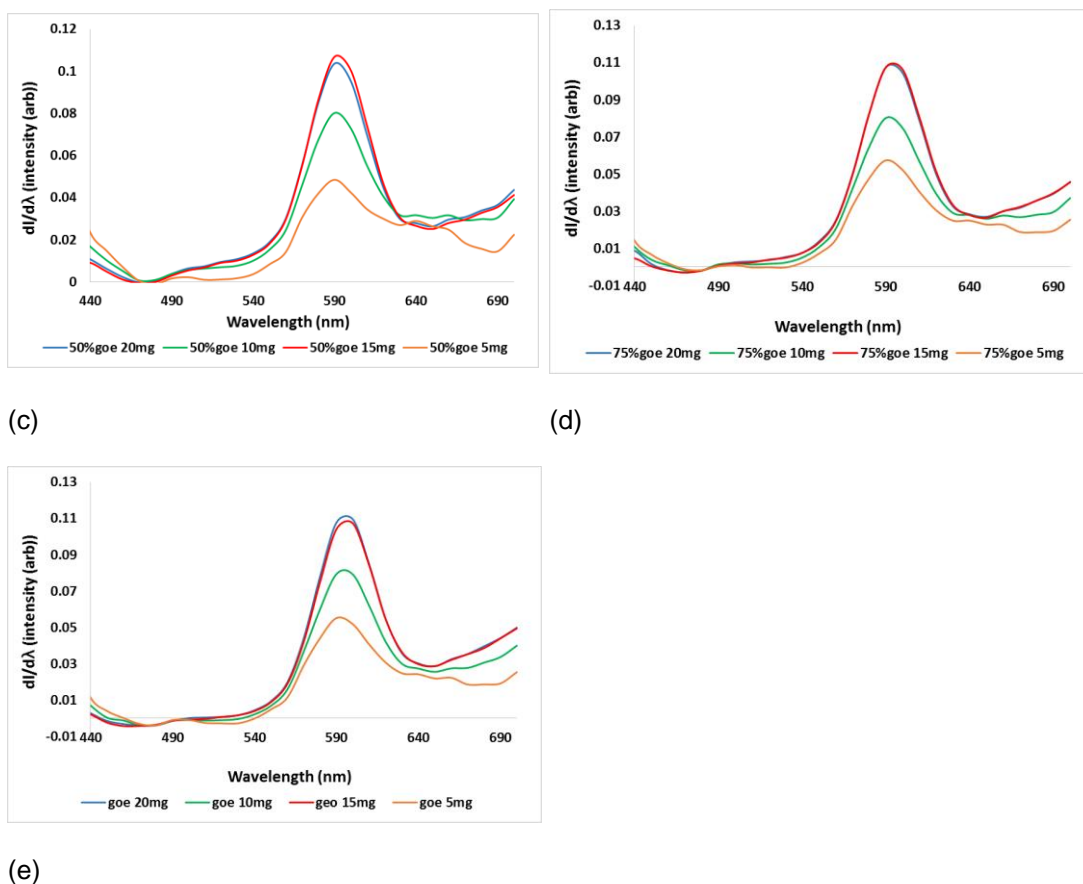
Analysis is completed for all 21 standard goethite/haematite standard sample compositions utilised previously, however only some data will be presented. The additional data not presented here is available in Appendix 11. Shown in Figure 3-11 is The i1Pro results obtained for the (a) haematite standard, (b) standard containing a 25/75% w/w mixture of goethite and haematite, (c) a 50/50% w/w mixture of goethite and haematite, (d) a 75/25% w/w mixture of goethite and haematite and (e) the goethite standard at four various thicknesses with 20mg shown in blue, 15mg in red, 10mg in green and 5mg in orange. For all compositions, the 20mg and 15mg samples show good agreement in both spectra intensity and trend. The 10mg and 5mg samples vary significantly from both the thicker samples and from each other in intensity and demonstrate a lower reflectance. Some minor variations are also observed in trend at higher wavelengths.



(a)

(b)





**Figure 3-11:** The *i1Pro* results obtained for the (a) haematite standard, (b) standard containing a 25/75% w/w mixture of goethite and haematite, (c) a 50/50% w/w mixture of goethite and haematite, (d) a 75/25% w/w mixture of goethite and haematite and (e) the goethite standard at four various thicknesses with 20mg shown in blue, 15mg in red, 10mg in green and 5mg in orange.

Results have demonstrated that there is little to no difference in the normalized spectra obtained for samples above 15mg in thickness. Contrary to this, variation in intensity is apparent at lower sample thicknesses. This suggests that the *i1-Pro* instrumentation would be suitably acceptable to analyse and compare samples of varying thicknesses provided the minimum thickness requirements are met.

### 3.3.4. Investigating the effect of varying sample application methods

So far, all sample preparation has involved manually smearing the powdered raw sample onto the surface of paper. Whilst this is quick and technically non-destructive, the sample is not then easily reusable for other analysis methods and this sample method may not be applicable to culturally significant ochres, especially those already applied to artefacts. Therefore, an investigation was carried out into the effect of the sample preparation method, and if the instrument is still able to distinguish between samples when it is applied to alternative substrates.

## CHAPTER THREE

It is known that Australian Aboriginals often applied ochre to artefacts and artworks, as well as themselves, in the form of a paste [61, 156]. The composition of this paste varies greatly, and often contains oils, insects and plant sap. It is therefore likely that, should this data analysis method be applied to artefacts, that the ochre on these artefacts was prepared as a paste using a number of mediums. In order to investigate what, if any, effect the use of different mediums has on the i1Pro results, the effect of different binders is now investigated.

The same twenty one standard samples as studied previously were again used for this study, with samples varying based on the haematite:goethite ratio. Samples were prepared by adding approximately 0.025g of ochre based material to approximately 1mL of binder. An artist's paint brush was then used to apply a portion of the paste to the Fuji Xerox 80g/m<sup>2</sup> white laserprint paper, covering an area approximately 1.5cm<sup>2</sup>, before being allowed to dry for 24 hours before colour measurements were taken.

As has become practice, each sample was analysed in three different areas, with each area scanned five times giving a total of fifteen spectra per sample. These spectra were then averaged before the derivative taken. Statistical analysis was then completed using MiniTab (Version 15.1.30.0), using the parameters previously established.

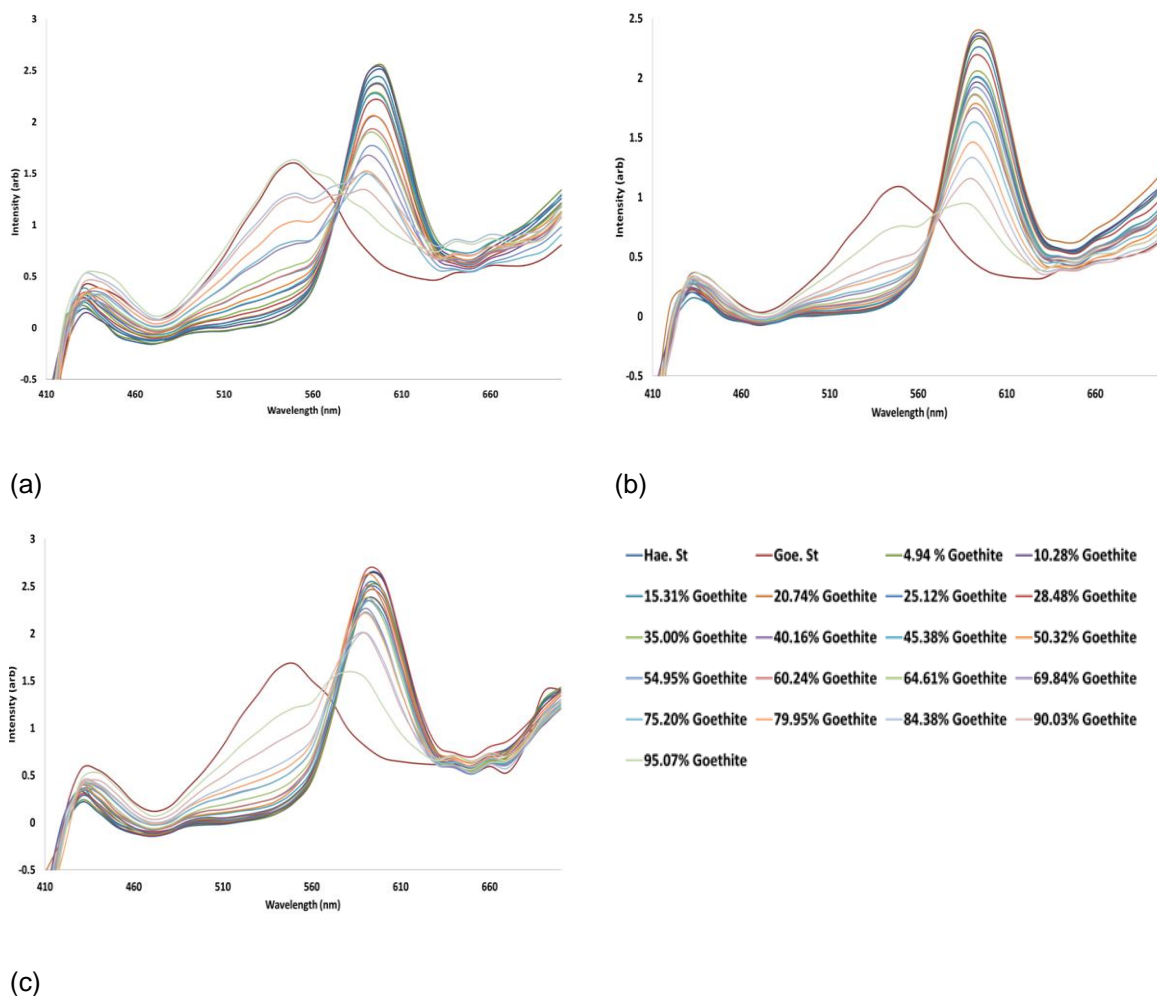
Three binders were initially chosen in water, emu oil, and the sap of orchids. Water was chosen as a binder material to be studied as it is readily available and is therefore likely to have been used by many Aboriginal Australians. It is also clean, non-toxic, and is unlikely to have any lasting effects on the colour of ochre as it completely evaporates in a short period of time at room temperature.

Studies then focused on the creation of a paste using emu oil. The emu oil used in this study was obtained from Talyata Emu Farm [157]. This emu oil was purchased and used by a previous member of the research group, Alisa Blee, for her study on the identification of possible binders on a series of stone knives, with the results of her study published in 2010 [158].

It is important to note here that when the instrument was applied to the sample, even after a period greater than one month, it was clear that the sample was not completely dry, and the instrument removed sample from the paper with contact. This means that this method would prove problematic if applied to artefacts as it would no longer be considered non-destructive. It also significantly increases the risk of cross contamination, and removes the possibility of future retesting. However, as these samples were only standards, experimentation continued.

A paste was then formed with the sap of orchids. The orchid plants used in this study were donated by the South Australian Museum. Orchids were chosen as it is known to have been available and used by Indigenous Australians, and is therefore a likely source of sap that may be encountered in artworks. The stems of the plant were crushed and the sap collected. Despite having a large number of stems available, very little sap was obtained, resulting in a change to application method.

## A PRELIMINARY STUDY INTO THE SUITABILITY OF PORTABLE COLORIMITRY



**Figure 3-12:** Derivatives of the spectra obtained for samples of various goethite/haematite composition when applied to paper as (a) a water based paste, (b) an emu oil based paste, and (c) an orchid sap based paste.

Such little sap was collected that a paste could not be created with each of the twenty one standard ochre samples, and instead the samples were applied to Fuji Xerox 80g/m<sup>2</sup> white laserprint paper such that the ochre material covered an area approximately 1.5cm<sup>2</sup>, before the sap was painted over the material. This ensured the maximum number of samples could be prepared, as no sap was lost during the mixing with the ochre material. Once the sap was applied, a visible change in colour was observed, with the ochres appearing darker than previously. Results of this is shown in Figure 3-12 with the water paste shown in (a), emu oil in (b) and orchid sap in (c).

It can be seen that for each of the paste types the same general trend is observed as sample composition moved from high goethite to high haematite. Some variation does exist, particularly for the orchid sap where the separation in the region of 590nm is not as great and the peak shift appears more exaggerated. Similarly, the high goethite concentration samples for the emu oil paste show reduced separation in the region of 530nm. Having said that, statistical separation was achievable for each paste type and the i1Pro has been shown to be

suitable for distinguishing between samples of this nature based on composition. Studies now shift to determine if this classification of samples is also possible when comparing binder types.

### 3.3.5. Comparison between ochre made with various pastes

It is common that very little is known about specific Aboriginal artefacts, including the binder types used in the application of ochre and related materials. In most instances it is the ochre material and not the binder that is of interest, therefore it is hoped that the binder has no influence on the colour and therefore, even when the binder type is not known, does not need to be considered. In order to investigate this, the derivatives of the average spectra obtained for the three binders studied are considered and compared. Shown in Figure 3-13 is the normalised derivatives of the spectra obtained for samples of (a) haematite standard, (b) 25/75 goethite/haematite (w/w%) sample, (c) 50/50 goethite/haematite (w/w%) sample, (d) 75/25 goethite/haematite (w/w%) sample and (e) goethite standard when applied to paper as a water based paste (shown in blue), an emu oil based paste (shown in black), and an orchid sap based paste (shown in purple).

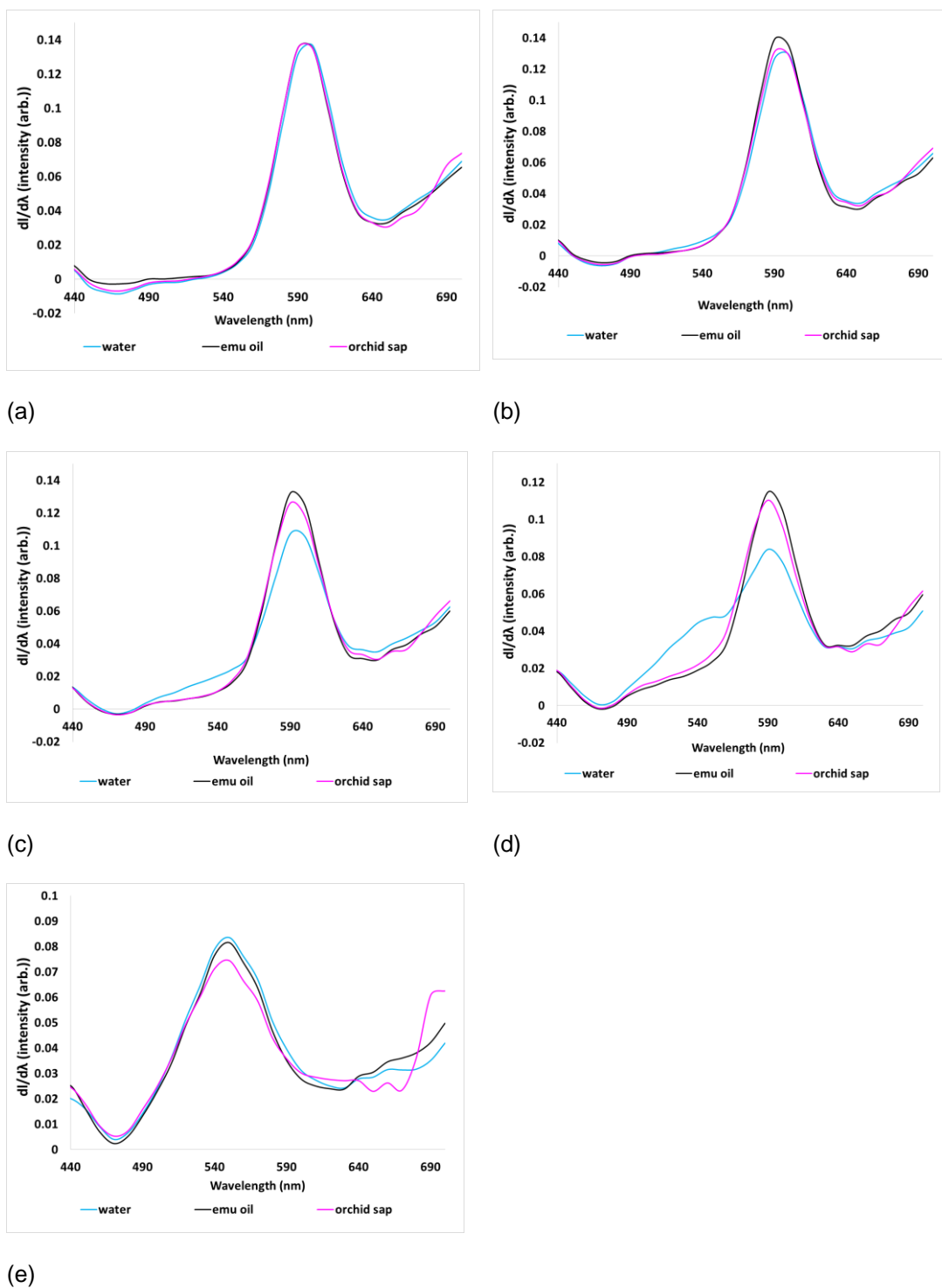
When examining Figure 3-13 it is apparent that the haematite standard and for sample compositions with low goethite (25% w/w), reproducibility and agreement between the spectra is good. As the goethite composition increases (to 50% and 75% w/w) the variation between the water based paste and the emu oil and sap based paint become more obvious. Whilst the emu oil and the orchid sap pastes display similar spectral characteristics, the intensity of the maxima for the water based paint at 590nm is lower and the peak at 530nm that is typically observed is suppressed in the emu oil and orchid sap spectra. As the peak at 530nm is due to reflectance in the yellow region, this suggests that the emu oil and orchid sap are making the samples appear darker and more red/brown in colour, thus affecting their reflectance. The pure goethite sample shows better agreement between the samples, with the water based paint now having the highest intensity at the maxima.

#### 3.3.1. Use of i1Pro and derivative spectra to determine the composition of hematite/goethite mixtures

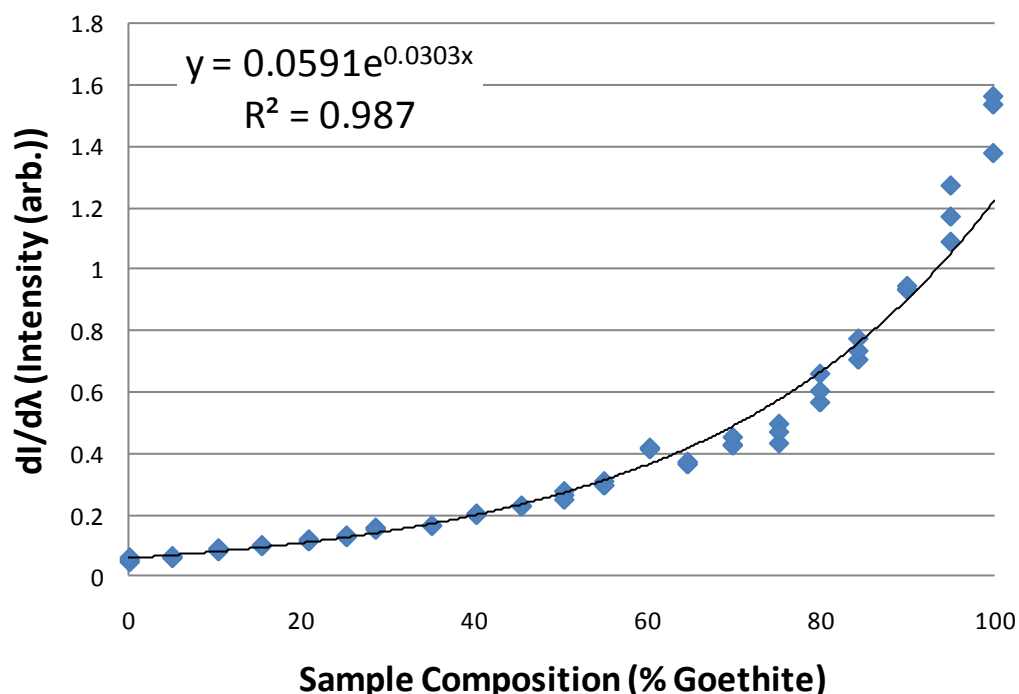
##### 3.3.1.1. Single wavelength calibration

It has previously been shown that the variation between the spectra of samples of known composition shows a predictable and reproducible pattern. This variation is at its maximum in two regions; at approximately 530nm, where intensity increases with increasing goethite concentration, and at approximately 590nm, where intensity decreases with increasing goethite concentration. However, the peak at approximately 590nm also shows a shift in its maxima towards a lower wavelength with increasing goethite concentration. For this reason, 530nm was used for the development of a single wavelength calibration. Figure 3-14 shows the derivative at 530nm versus concentration of goethite (%w/w) within the goethite hematite mixtures outlined in Table 3-1. As shown, the increase in intensity is non-linear, following an

## A PRELIMINARY STUDY INTO THE SUITABILITY OF PORTABLE COLORIMITRY



**Figure 3-13:** Derivatives of the normalised spectra obtained for samples of (a) haematite standard, (b) 25/75 goethite/haematite (w/w%) sample, (c) 50/50 goethite/haematite (w/w%) sample, (d) 75/25 goethite/haematite (w/w%) sample and (e) goethite standard when applied to paper as a water based paste (shown in blue), an emu oil based paste (shown in black), and an orchid sap based paste (shown in purple).



**Figure 3-14:** The intensity of the derivate of the spectra at 530nm for each sample site with respect to sample composition.

exponential function. At high goethite concentrations (>70% by mass) there is more variability, whereas below this level there is greater reproducibility of the samples and very good agreement of the standards with the trend line. This suggests that the model would be more accurate for samples containing a low % goethite (<60% by mass), however this is also the region where the smallest change in the derivative intensity is observed.

In order to test the quantitative accuracy of this model, a series of ten “blind” samples were prepared by Ms Caroline Watson. These were applied to paper in the same manner as previously reported. Each sample was measured at a minimum of three sites, with each site measured a minimum of five times. The derivatives were calculated and the calibration model applied to predict the concentration of the unknowns. Results are shown in Table 3-4. As can be seen, the determined concentrations and the actual concentrations show good agreement, with the maximum variation being less than 2% and, in most cases, less than 1%. This agrees with the good reproducibility shown previously in this chapter and confirms that the X-Rite i1Pro has an accuracy and reproducibility within a range that makes it an acceptable system to be applied to Aboriginal ochre and materials. However variability at higher goethite composition is of concern. In addition to this, the model accuracy has been shown to be greatest at low goethite composition (less than 60% by mass), but it is also in this region that the smallest change is observed in the derivative intensity. As this is not ideal, two other models that have been utilised in the literature will also be applied.

**Table 3-4:** Results of analysis of samples of undisclosed composition, with comparison to known composition, using the 530nm prediction model, with values expressed as the percentage of goethite in each sample.

Unknown	Goethite %	Concentrations		
	Calculated	Std Dev	Actual	Variation
1	89.69	0.63	90.21	-0.52
2	4.05	0.24	4.76	-0.71
3	68.88	0.16	69.61	-0.73
4	40.66	0.68	40.77	-0.11
5	29.62	0.41	28.55	1.07
6	94.80	0.36	95.14	-0.34
7	89.22	0.43	88.07	1.15
8	64.90	0.22	66.79	-1.89
9	53.70	0.36	55.64	-1.94
10	18.90	0.10	17.24	1.66

### 3.3.1.2. A model based on $\Delta E$

As well as the spectroscopic results, the X-Rite i1 Pro system also gives L\*a\*b values for each site measured. These values represent colour spaces. L denotes lightness and ranges from 0 – 100, with 0 being the lack of light, or black, and 100 being diffused brightness, or white. a denotes the red – green scale, with negative numbers being dominated by red/magenta, and positive numbers by green. Similarly, b denotes the samples position between yellow and blue, with negative numbers being dominated by blue and positive numbers yellow. The numbers given by L\*a\*b therefore represent a three-dimensional model and space.

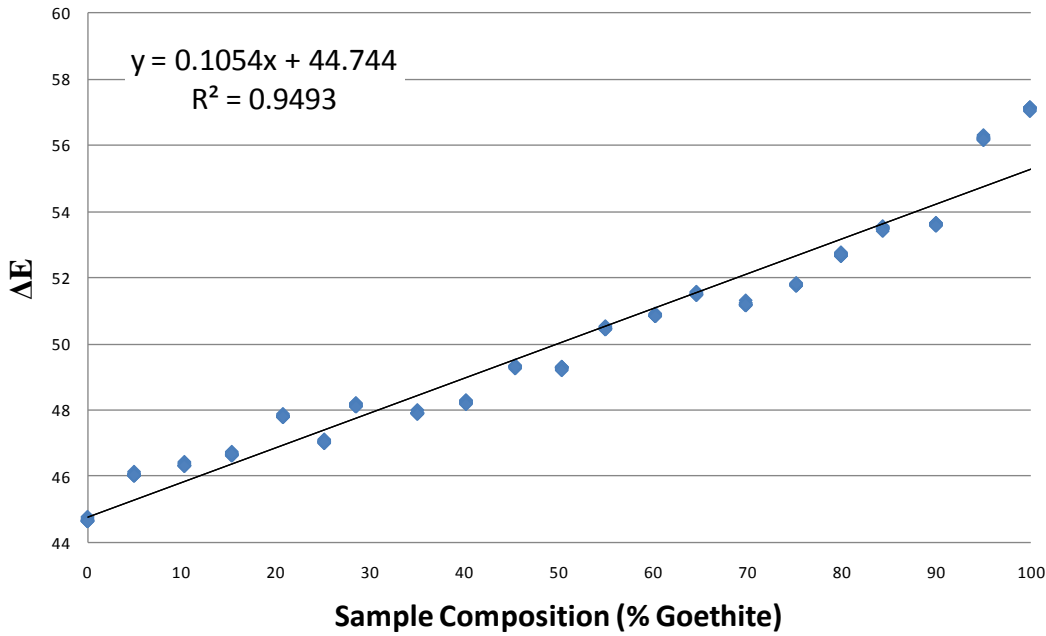
A number of different calculations and models are available based on these values, and recent work by Casadio focuses on  $\Delta E$ , or the distance between two points in this three dimensional space [159].  $\Delta E$  is calculated by the following equation:

$$\Delta E = \sqrt{(L_1 - L_2)^2 + (a_1 - a_2)^2 + (b_1 - b_2)^2} \quad \text{Equation 3-3}$$

For the purpose of this model,  $\Delta E$  will be calculated as the distance from the origin, where  $L_1=0$ ,  $a_1=0$  and  $b_1=0$ . Therefore, the equation simplifies to:

$$\Delta E = \sqrt{L^2 + a^2 + b^2} \quad \text{Equation 3-4}$$

This equation was applied to the data obtained from the standards previously measured for the establishment of the single wavelength analysis model. A Q-test was applied to remove any outliers, before the three average  $\Delta E$  values per composition were plotted, as shown in Figure 3-15. It can be seen that, where the  $\Delta E$  value for each sample site with respect to



**Figure 3-15:** The  $\Delta E$  value for each sample site with respect to sample composition.

**Table 3-5:** Results of analysis of samples of undisclosed composition, with comparison to known composition, using the  $\Delta E$  prediction model, with values expressed as the percentage of goethite in each sample.

Unknown	Goethite %	Concentrations		
	Calculated	Std Dev	Actual	Variation
1	106.13	2.70	90.21	15.92
2	107.07	0.36	4.76	102.31
3	16.94	2.76	69.61	-52.67
4	18.00	1.34	40.77	-22.77
5	74.52	1.41	28.55	45.97
6	68.63	2.38	95.14	-26.51
7	45.88	0.60	88.07	-42.19
8	46.76	1.49	66.79	-20.03
9	37.75	1.49	55.64	-17.89
10	34.75	0.68	17.24	17.51

sample composition is shown, that the trend obtained is approximately linear, with a reasonable  $R^2$  value of 0.9493. The greatest variation from linearity is seen at the highest goethite compositions.

The  $\Delta E$  values were then calculated for each measured spectra of each sample of undisclosed composition, before a Q-test was applied to remove any outliers, the remaining values



averaged, and the standard deviation calculated. The calculated values were then compared to the known concentrations, and tabulated in Table 3-5.

It can be seen here that the  $\Delta E$  model of prediction is significantly less accurate than the previously described 530nm model. No composition was predicted within the experimentally acceptable 3% variation, with some predictions varying by greater than 30%. This shows that the  $\Delta E$  model of prediction is not acceptable for ochre materials on paper.

3.3.1.3. **Multiple linear regression analysis**

The final model to be investigated is multiple linear regression (MLR) analysis. This is a statistical method of analysis that investigates and models the relationship between two or more explanatory variables by fitting a linear equation to the observed data. The value of each independent variable is associated with a value for the corresponding dependant variable, and the population regression line describes how the mean response changed with the explanatory variables. Here again the intensity of the derivatives of the standards spectra were considered. Using The Unscrambler X (version 10.0.1), these values were analysed using MLR with a 95% confidence level. Results of this are shown in Figure 3-16. It can be seen that the MLR analysis model is verified. The data presents with both slope and R2 values being close to the desired value of 1 and the offset (intercept) close to the desired value of 0. In addition, no outliers were detected by Unscrambler.

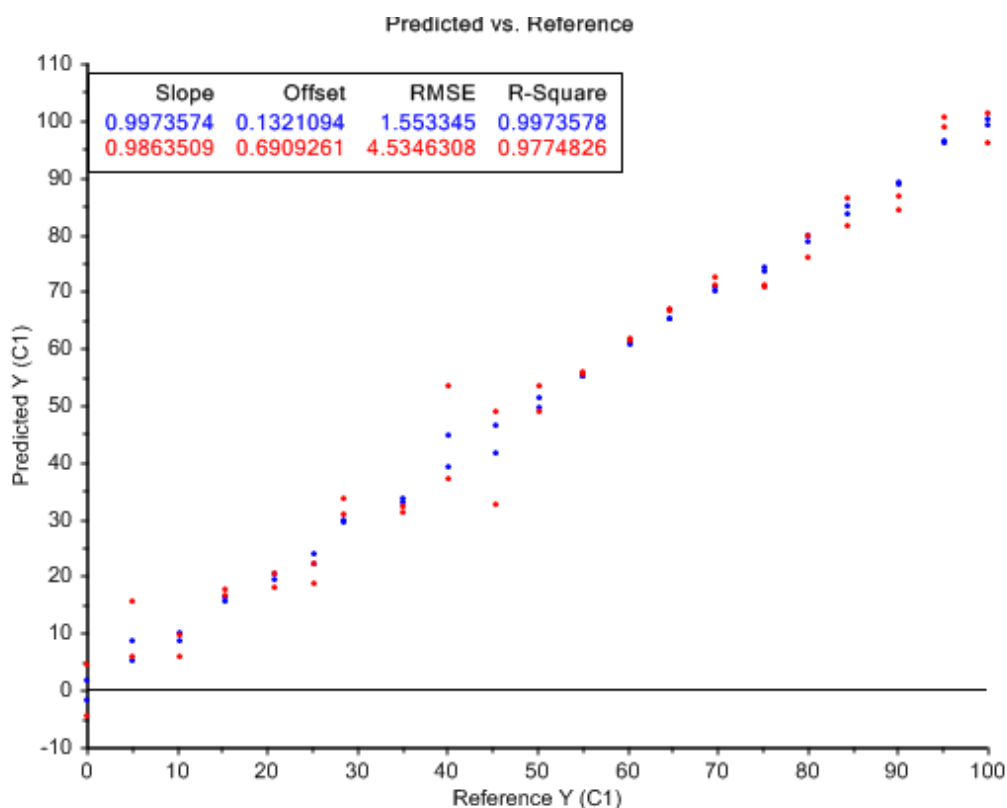


Figure 3-16: Predicted Vs Reference data from the multiple linear regression model.

**Table 3-6:** Results of analysis of samples of undisclosed composition, with comparison to known composition, with values expressed as the percentage of goethite in each sample.

Unknown	Goethite %		Concentrations	
	Calculated	Std Dev	Actual	Variation
1	90.27	4.74	90.21	0.06
2	4.92	3.30	4.76	0.16
3	69.69	5.20	69.61	0.08
4	40.74	4.75	40.77	-0.03
5	29.21	5.56	28.55	0.66
6	95.98	3.76	95.14	0.84
7	88.67	3.17	88.07	0.6
8	66.03	2.94	66.79	-0.76
9	55.48	2.72	55.64	-0.16
10	18.34	1.37	17.24	1.1

This function was applied to the unknown samples and the calculated concentrations compared to the actual concentrations (expressed as a goethite %) are shown above (Table 3-6).

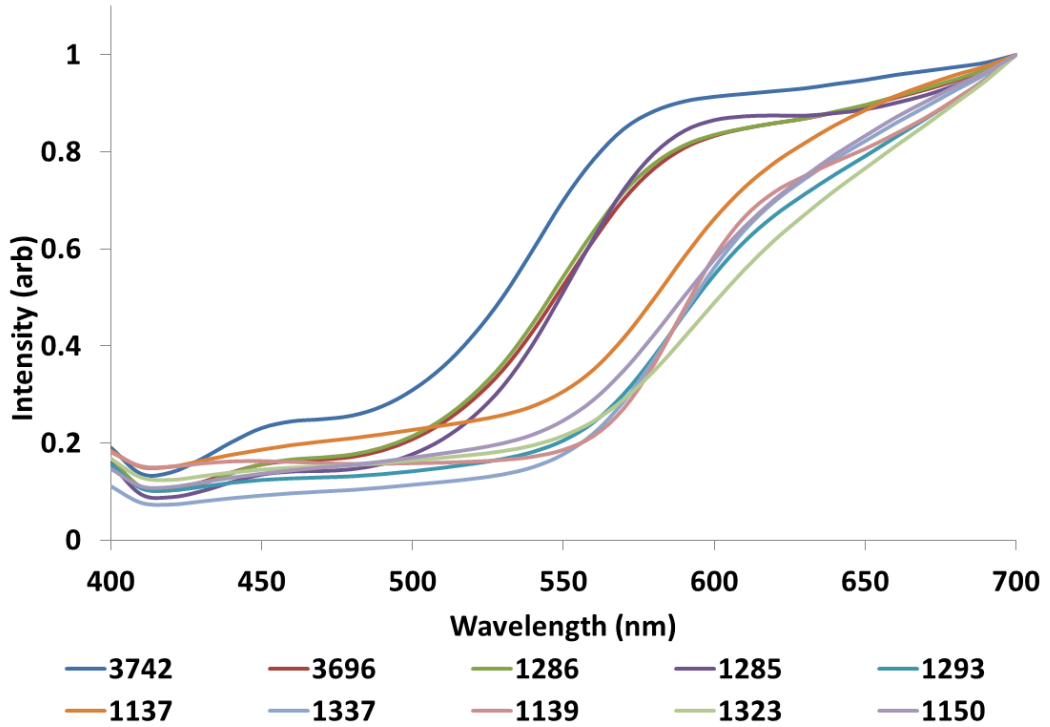
Comparisons between the calculated value where the composition was undisclosed, and the known concentrations show good agreement, with the maximum variation being less than 2%. The analysis was completed in triplicate, and variation between the samples was, in most cases, less than 1%. When compared to the previous two models, this model resulted with the greatest accuracy.

### 3.3.2. Application of the i1Pro to 'real' samples

Now that it has been established that the i1Pro is reproducible when applied to synthetic standards, the i1Pro was applied to the ten mining samples studied in previous chapters in order to investigate if any of the components found in natural samples effect the instruments performance.

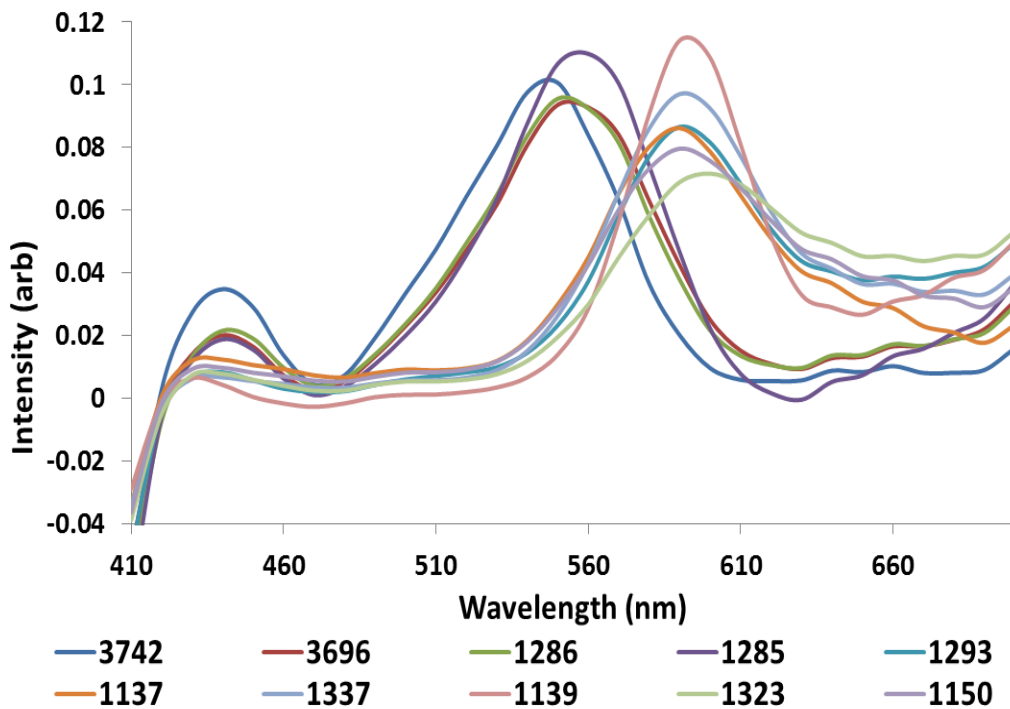
#### 3.3.2.1. Application of the i1pro to natural ochre samples

The i1Pro was then applied to the ten ochre samples obtained from the Museum of South Australia's mining collection that were previously studied, as detailed in Table 2-1. Samples were prepared in the same manner as detailed previously, and each sample measured at three spots five consecutive times, giving fifteen spectra per sample. The results obtained allow for the fifteen spectra obtained for each sample to be normalised and averaged so that a single data set is presented for comparison.



**Figure 3-17:** Results obtained for the ten mining samples utilizing the i1Pro.

It is immediately apparent that the distinction exists between the four yellow coloured ochres and the six red coloured ochres tested, in the same way the distinction exists between the synthetic standards. In order to accentuate these differences and investigate further, the derivatives of the normalised spectra are taken and presented in Figure 3-18.



**Figure 3-18:** Derivatives of the results obtained for the ten mining samples utilizing the i1Pro.

Immediately apparent here is the similarities in the spectra obtained for ochres 3696 and 1286. This is of interest as these two samples obtained similar results when utilising some of the traditional methods of analysis, in particular IR and auto-correlation methods. The remaining spectra are both visually and statistically different, thus confirming that the i1Pro is a valuable instrument in the measurement of ochre based on colour, and further investigation into the viability of the instrument follow.

### **3.4. Conclusions**

The X-Rite i1 Pro instrument and analysis system have proven to be very accurate when applied to ochre materials across a large variety of sample thicknesses, binder materials, and substrates. The instrument produces spectra across a range of 400-700nm, although reproducibility studies showed it to be inaccurate below 430nm. Studies also showed that the derivatives of the spectra obtained gave more accurate statistical analysis results as this removed any accumulation effects.

Whilst reproducibility studies showed the accuracy of the system to be an order of magnitude higher than the manufactures reported measurements to be  $x,y: \pm 0.002$ , this is attributed to the samples being studied being of a different nature and composition to what the manufactures intended [149]. This is likely due to natural colour variation within the samples, and the variation obtained for both goethite and haematite is significantly lower than a number of other analytical methods commonly used.

The X-Rite i1 Pro system was then shown to be capable of distinguishing between twenty one samples, each varying in goethite and haematite composition by approximately five percent. Statistical analysis showed complete and accurate separation, with clusters formed based on sample composition.

The X-Rite i1 Pro system was then compared to a traditional, lab based UV-vis instruments and the data obtained for both instruments observes the same trend and the peak maxima in located at the same wavelength.

**CHAPTER FOUR:  
APPLICATION OF  
THE I1-PRO AND  
PREDICTION MODELS  
TO A VARIETY OF  
SUBSTRATES**

Previous work has demonstrated the i1 Pro's ability to distinguish between a number of samples of various compositions of goethite and haematite accurately across a large variety of sample thicknesses, binder materials, and substrates. Statistical analysis showed complete and accurate separation, with clusters formed based on sample composition.

Comparisons to traditional, lab based instruments demonstrated that no precision was lost with the new method, with trends and peak maxima observed to be the same for both instruments. This is significant as it allows for the advantages of the portable spectrometer to be utilised in the field.

In order for this technology to have applications to artefacts and existing raw samples, the system must be optimized to ensure that the reproducibility seen in previous studies exists under varying sample conditions. As the i1pro is based on reflectance, it is possible that factors such as surface colour, roughness and texture may also impact the spectral data obtained. This chapter aims to investigate the effect that the substrate to which the sample is applied may have on the reproducibility of results obtained and on the accuracy of the models used previously to determine the sample composition.

### **4.1. Experimental Methods**

#### **4.1.1. Samples**

The goethite and haematite standards discussed previously were used in these studies. A series of samples of known composition varying by approximately 5% were prepared, and are detailed in Table 4-1 **Table 3-1**.

#### **4.1.1. Experimental techniques**

Sample application methods and substrates vary greatly through this and subsequent chapters as the instruments capabilities are explored. It is therefore difficult to give a single experimental method. However, some typical parameters are used.

Approximately 10-15mg of sample was rubbed onto to a single piece of Fuji Xerox 80g/m<sup>2</sup> white laserprint paper and (using gloved hands) to form a circle approximately 2.5cm in diameter. Typically 3-5 sites on the resulting circle were selected as sample sites, and the instrument was placed over the sample site. Multiple measurements (typically 5 but up to 100 depending on the experiment) were taken from the site without moving the instrument. The area of the instrument in contact with the sample was then cleaned, before this process is repeated with the next sample site.

#### **4.1.2. Data analysis methods**

Raw data was converted to excel format, where each sample site is firstly considered. The spectral data from each site was collated using MS excel. Statistical analysis was completed to determine the standard deviation for each data point on the spectra, before a Q-test was

**Table 4-1:** Series of standard goethite and haematite samples varying in composition by approximately 5%.

Sample Number	Goethite %	Haematite %
1.00	0.00	100.00
2.00	4.94	95.06
3.00	10.28	89.72
4.00	15.31	84.69
5.00	20.74	79.26
6.00	25.12	74.88
7.00	28.48	71.52
8.00	35.00	65.00
9.00	40.16	59.84
10.00	45.38	54.62
11.00	50.32	49.68
12.00	54.95	45.05
13.00	60.24	39.76
14.00	64.61	35.39
15.00	69.84	30.16
16.00	75.20	24.80
17.00	79.95	20.05
18.00	84.38	15.62
19.00	90.03	9.97
20.00	95.07	4.93
21.00	100.00	0.00

applied to determine any outliers. Once statistically acceptable, the data for each data point was averaged. This process is repeated considering each site per sample, resulting in a single averaged spectrum per sample. This data was then analysed statistically, with the standard deviation calculated using [152]

$$SD = \sqrt{\frac{\sum(x-\bar{x})^2}{n-1}}$$

**Equation 4-1**

where  $\bar{x}$  is the arithmetic mean and n is the number of samples.

#### 4.1.2.1. Derivative analysis

It is documented that derivative spectroscopy can improve quantitative and qualitative analysis by applying the first- or higher order derivatives of the original spectrum. Here, first order derivatives are applied to the spectra. This is calculated by considering the rate of change of the absorbance with respect to the rate of change in the wavelength, and is expressed mathematically as

$$\frac{dA}{d\lambda} = f'(\lambda) \quad \text{Equation 4-2}$$

where  $A$  represents absorbance, and  $\lambda$  the wavelength.

## 4.2. Determining the instrument accuracy with application to varying substrates

As well as binder types (which have been discussed previously in Section 3.3.3), Australian Aboriginal artefacts also vary greatly in the substrates to which the ochre material is applied. As well as using their own bodies as canvases, artefacts exist on stones (both within caves and as individual items), on various woods and barks, and on modern papers and on canvas, with wood and stone being the most common [56, 62]. It is therefore likely that, should this data analysis method be applied to artefacts, the ochre on these artefacts will be on a variety of surfaces. The effect of different substrates is now investigated in order to determine if the instrument is accurate on individual surfaces, which would allow for 'unknowns' to be prepared in a similar method for analysis.

Unless otherwise described, experiments to follow in this section were completed on the same twenty one standard samples as studied previously, with samples varying based on the haematite:goethite ratio. Samples were prepared by adding approximately 0.025g of ochre based material to approximately 1mL of demineralised water. An artist's paint brush was then used to apply a portion of the paste to the substrate being studied, covering an area approximately 1.5cm<sup>2</sup>, before being allowed to dry for 24 hours prior to testing.

Studies will focus on two substrate types – wood and stone – with a number of sub-classifications considered. Wood was chosen as it is naturally available and it is known to have been used by Australian Aboriginals in artwork. The wood samples used in this case are approximately 1m in length, 40mm in width, and with a depth between 8 and 16mm. All wood samples were purchased from Bunnings Warehouse.

Stone was chosen as the next substrate to study as it is naturally available and it is known to have been used by Australian Aboriginals in artwork. The stone samples were generously donated by Allstone Pty Ltd [160]. A number of natural and artificial stones in a variety of colours and sizes were donated, but studies will focus on natural sandstone, natural slate, synthetic sandstone, and a synthetic paver with a purple/red undertone.

The synthetic sandstone used in this study is a light brown in colour. There are a few areas of pattern feature, primarily lines of orange colour, but overall the colour is fairly uniform. The sample is also quite dense, with the water from the paste taking approximately thirty minutes to be completely absorbed. This allowed for the particles of goethite/haematite to settle on the surface, resulting in an even distribution of sample.

The natural slate used in this study is a light grey colour. There are a few areas where the grey colour varies in darkness, and some white specks of colour are visible in some regions, but

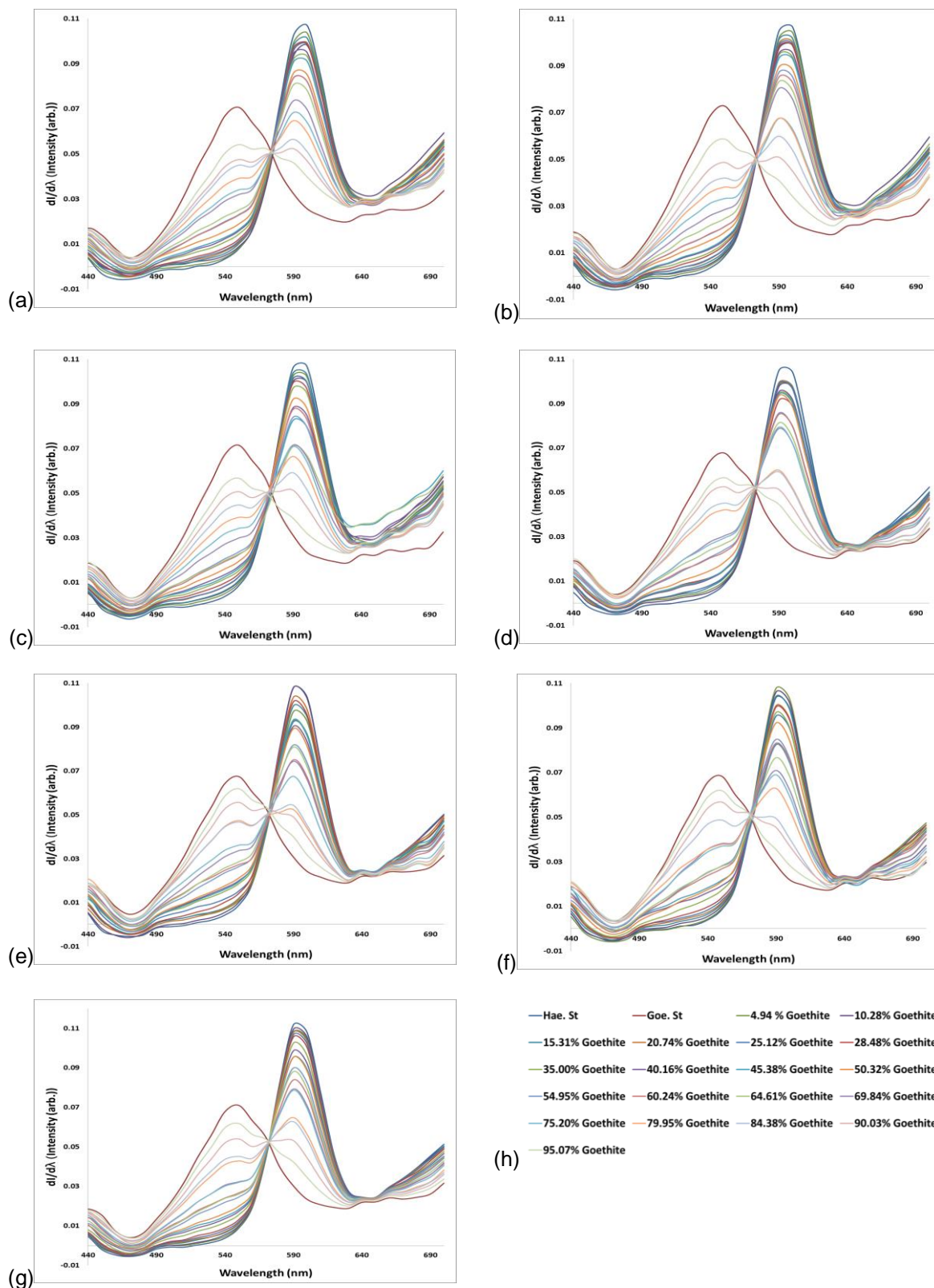


overall the colour is relatively uniform. The sample is also quite dense, with the water from the paste taking approximately thirty minutes to be completely absorbed. This allowed for the particles of goethite/haematite to settle on the surface, resulting in an even distribution of sample.

The synthetic pavers obtained are dense and have a smooth surface to touch. They are comprised of small particles, similar to sand or grains of sugar, and the variation of colour in these individual samples is large with colour ranging from white to grey and black, and also the spectrum of reds, purples and browns. However, the small size of the particles and the even distribution of the particles in the samples results in a relatively uniform surface colour. Whilst the surface of the pavers is smooth, it also proved to be extremely hydrophobic, with the water/paste forming a bubble on the surface. The edges of this bubble did not want to maintain contact with the paver, thus making even spreading of the paste difficult. This resulted in an increased volume of sample being required to achieve an area of coverage on the paver large enough for examination. The hydrophobicity of the surface also resulted in the water taking a large amount of time (in excess of six hours) to be absorbed into the stone, and it is possible that a large percentage of this water was lost to the atmosphere rather than being absorbed into the stone. The additional sample volume required, together with the lengthy drying time, allowed for the sample to disperse equally and form a very uniform and thick coverage of the surface, which should be ideal for this study, but may make comparison between stone types difficult, as previous studies have shown that sample thickness can adversely affect the effectiveness of statistical analysis.

Results of the analysis on wood and stone are presented in Figure 4-1, which shows the normalised derivatives of the spectra obtained for samples of various goethite/haematite compositions when applied as a water based paste to (a) pine, (b) Australian oak, (c) natural jarrah, (d) natural sandstone, (e) synthetic sandstone, (f) natural slate, (g) synthetic pavers. When examining Figure 4-1 it is apparent that the goethite/haematite samples exhibit a similar trend when applied to the various surfaces. A decreasing goethite concentration corresponds to a drop in intensity in the region of 530nm and an increase in intensity at 590nm. Many substrates, and in particular the pine, oak and jarrah, exhibit an approximately equal transition between samples. These three wooden samples also show a decreased intensity at wavenumbers greater than 630nm for the goethite standard.

The stone based substrates show a slightly more uneven distribution. There are a number of possibilities for this incomplete separation, and a number of factors to be considered. For example, the natural sandstone sample (for which this variation is most obvious) obtained and used in this study is light cream in colour with patterns of various shades of orange and yellow, typically linear, running through the stone. This results in some variation in the stones colour- so whilst overall the stone is uniform, over a small area it shows natural variation and this may be contributing to the incomplete separation. The natural sandstone is also very porous, and the water from the paste was absorbed immediately following its application. This has resulted



**Figure 4-1:** Derivatives of the spectra obtained for samples of various goethite/haematite compositions when applied as a water based paste to (a) pine, (b) Australian oak, (c) natural jarrah, (d) natural sandstone, (e) synthetic sandstone, (f) natural slate and (g) synthetic pavers. The legend for these figures is presented in (h)..

in a slightly irregular distribution of sample. This uneven distribution, when combined with the irregular background, creates significant variation within each standard sample. This natural variation has resulted in significant variation and less reproducibility within the measurements obtained for each individual standard. Whilst the instrument accuracy was maintained, with each of the five measurements taken at each sample site showing little to no variation, the variation of the measurements taken at different sites of the same sample is large. This has not been seen previously.

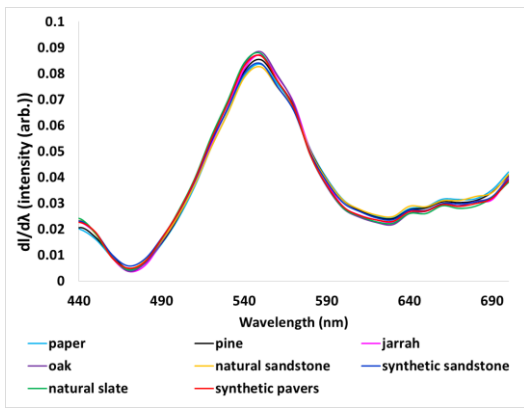
The variety of stone found in Australia is too large to test every ochre on every substrate type, and thus the question of comparison between substrate samples is raised. Shown in Figure 4-2 are the normalised and derivitised i1Pro reflectance spectra obtained for a water based paste when applied to paper (bright blue), pine (black), jarrah (pink), oak (purple), natural sandstone (yellow), synthetic sandstone (deep blue), natural slate (green) and synthetic pavers (red) for the (a) goethite standard, (b) 25/75 goethite/haematite (w/w%) sample, (c) 50/50 goethite/haematite (w/w%) sample, (d) 75/25 goethite/haematite (w/w%) sample and (e) haematite standard. The additional sample compositions are available in appendices C. With the exception of the 75/25 goethite/haematite (w/w%) sample, all samples show good agreement between spectra, suggesting that the sample substrate has little effect on the reflectance spectra.

### **4.3. Application of the composition prediction models to unknowns on alternate surfaces**

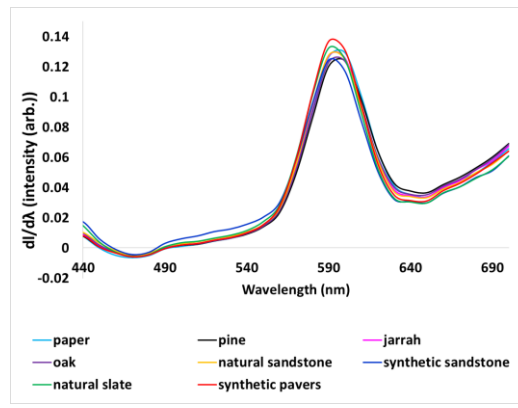
It has been demonstrated previously (Section 3.3.8) that an accurate model for sample composition can be established and applied using both the single wavelength calibration and the multiple linear regression analysis models for the goethite/haematite standards when applied to paper. Whilst the accuracy of these prediction models to ochre materials on paper is promising, the majority of ancient artefacts' and objects are not paper based. As the long term goal of this project is applications to such artefacts' and objects, the effectiveness of the model on these surfaces is of significance.

In order to investigate this, the series of ten samples of known but undisclosed concentrations were then prepared by Ms Caroline L Watson, a research student in the Popelka-Filcoff laboratory were applied to alternate wood (pine, Australian oak and jarrah) and stone (slate, synthetic sandstone, and red paver) surfaces. The same thirty measurements were taken per sample as the standards, with each individual derivative spectra then analysed using the model created.

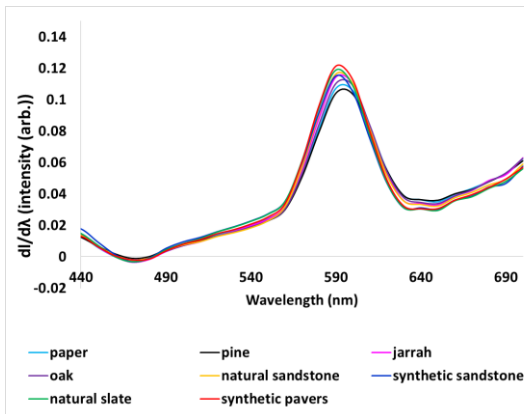
CHAPTER FOUR



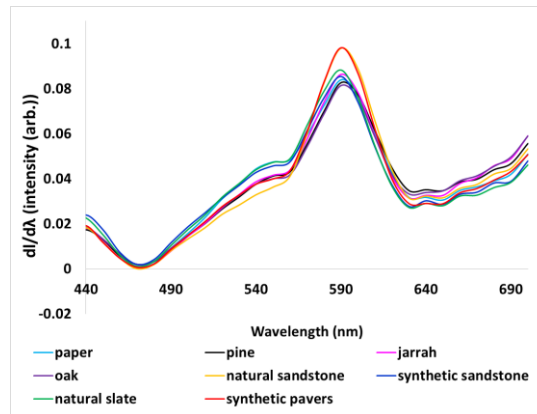
(a)



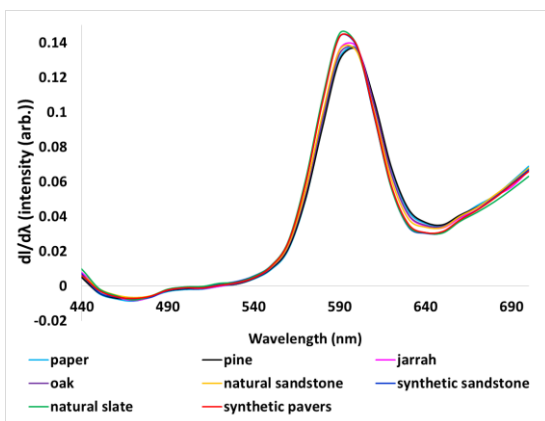
(b)



(c)



(d)



(e)

**Figure 4-2:** Normalised and derivitised *i1Pro* reflectance spectra obtained for a water based paste when applied to paper (bright blue), pine (black), jarrah (pink), oak (purple), natural sandstone (yellow), synthetic sandstone (deep blue), natural slate (green) and synthetic pavers (red) for the (a) goethite standard, (b) 25/75 goethite/haematite (w/w%) sample, (c) 50/50 goethite/haematite (w/w%) sample, (d) 75/25 goethite/haematite (w/w%) sample and (e) haematite standard.

## 4.3.1. Single wavelength calibration

The calculated concentrations compared to the actual concentrations (expressed as a goethite%) for the single wavelength calibration model are shown in Table 4-2. A Q-test was applied to remove any outliers (95% confidence), before the standard deviation was calculated.

**Table 4-2:** Results of analysis of samples of undisclosed composition, with comparison to known composition, with values expressed as the percentage of goethite in each sample, with samples applied to wood and stone surfaces, using the 530nm prediction model.

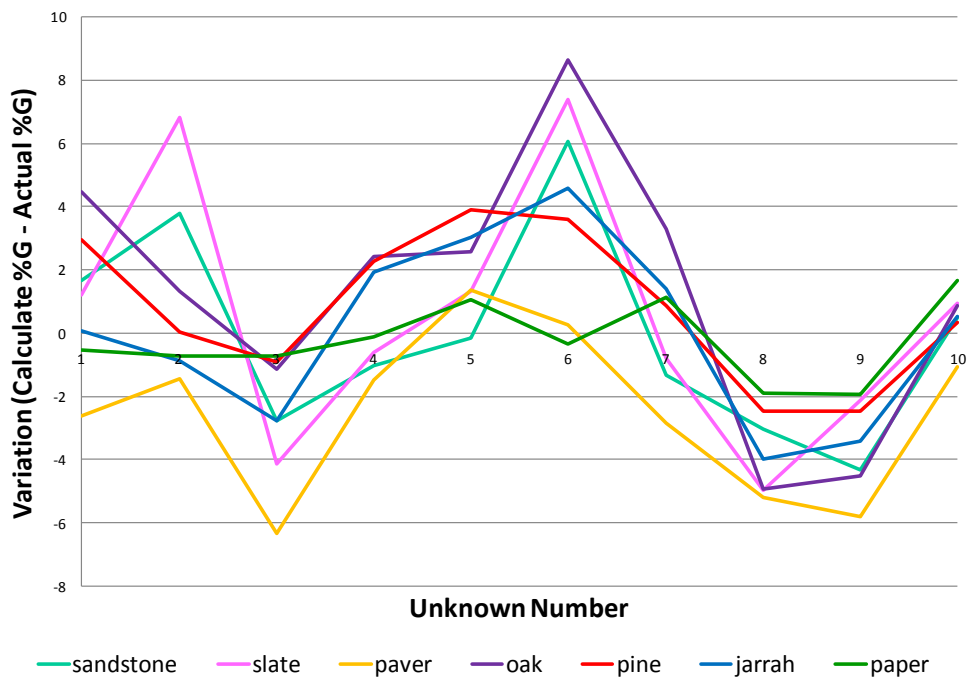
	Substrate	Actual Goethite %	530nm Predicted Goethite %	Standard Deviation	Variation in Goethite %
<b>Unknown 1</b>	Paper	90.21	89.69	0.63	-0.52
	Pine	90.21	93.16	0.67	2.95
	Oak	90.21	94.69	0.43	4.48
	Jarrah	90.21	90.27	0.44	0.06
	Slate	90.21	91.42	0.27	1.21
	Sandstone	90.21	91.87	0.42	1.66
	Paver	90.21	87.60	0.38	-2.61
<b>Unknown 2</b>	Paper	4.76	4.05	0.24	-0.71
	Pine	4.76	4.81	2.06	0.05
	Oak	4.76	6.09	2.20	1.33
	Jarrah	4.76	3.90	3.00	-0.86
	Slate	4.76	11.59	5.10	6.83
	Sandstone	4.76	8.57	1.71	3.81
	Paver	4.76	3.31	1.77	-1.45
<b>Unknown 3</b>	Paper	69.61	68.88	0.16	-0.73
	Pine	69.61	68.71	0.96	-0.90
	Oak	69.61	68.47	0.68	-1.14
	Jarrah	69.61	66.84	0.49	-2.77
	Slate	69.61	65.45	0.66	-4.16
	Sandstone	69.61	66.85	0.74	-2.76
	Paver	69.61	63.26	0.66	-6.35
<b>Unknown 4</b>	Paper	40.77	40.66	0.68	-0.11
	Pine	40.77	43.05	1.31	2.28
	Oak	40.77	43.20	1.62	2.43
	Jarrah	40.77	42.71	1.26	1.94
	Slate	40.77	40.17	2.06	-0.60

	Substrate	Actual Goethite %	530nm Predicted Goethite %	Standard Deviation	Variation in Goethite %
	Sandstone	40.77	39.74	1.84	-1.03
	Paver	40.77	39.27	1.18	-1.50
<b>Unknown 5</b>	Paper	28.55	29.62	0.41	1.07
	Pine	28.55	32.45	1.31	3.90
	Oak	28.55	31.11	1.20	2.56
	Jarrah	28.55	31.57	1.25	3.02
	Slate	28.55	29.86	1.32	1.31
	Sandstone	28.55	28.41	1.13	-0.14
	Paver	28.55	29.90	2.22	1.35
<b>Unknown 6</b>	Paper	95.14	94.80	0.36	-0.34
	Pine	95.14	98.76	0.28	3.62
	Oak	95.14	103.78	0.47	8.64
	Jarrah	95.14	99.74	0.91	4.60
	Slate	95.14	102.53	0.38	7.39
	Sandstone	95.14	101.21	0.92	6.07
	Paver	95.14	95.41	0.71	0.27
<b>Unknown 7</b>	Paper	88.07	89.22	0.43	1.15
	Pine	88.07	88.94	0.41	0.87
	Oak	88.07	91.37	0.40	3.30
	Jarrah	88.07	89.46	0.55	1.39
	Slate	88.07	87.28	1.03	-0.79
	Sandstone	88.07	86.73	0.94	-1.34
	Paver	88.07	85.23	1.30	-2.84
<b>Unknown 8</b>	Paper	66.79	64.90	0.22	-1.89
	Pine	66.79	64.33	1.21	-2.46
	Oak	66.79	61.85	0.65	-4.94
	Jarrah	66.79	62.79	0.57	-4.00
	Slate	66.79	61.82	0.90	-4.97
	Sandstone	66.79	63.74	0.44	-3.05
	Paver	66.79	61.60	0.67	-5.19
<b>Unknown 9</b>	Paper	55.64	53.70	0.36	-1.94
	Pine	55.64	53.16	0.89	-2.48
	Oak	55.64	51.12	0.77	-4.52
	Jarrah	55.64	52.23	0.92	-3.41
	Slate	55.64	53.51	0.78	-2.13
	Sandstone	55.64	51.31	0.69	-4.33

	Substrate	Actual Goethite %	530nm Predicted Goethite %	Standard Deviation	Variation in Goethite %
<b>Unknown 10</b>	Paver	55.64	49.83	0.81	-5.81
	Paper	17.24	18.90	0.10	1.66
	Pine	17.24	17.59	2.91	0.35
	Oak	17.24	18.12	3.95	0.88
	Jarrah	17.24	17.78	3.32	0.54
	Slate	17.24	18.17	1.83	0.93
	Sandstone	17.24	17.72	2.16	0.48
	Paver	17.24	16.16	1.64	-1.08

Graphically, the above table is represented in Figure 4-3 where the variation between the calculated goethite composition and the actual goethite composition is shown, with series representing each sample substrate across the ten compositions.

It can be here that the accuracy of the 530nm predictor model is varied. On paper, shown in green, the variation is no more than 2% for any composition, well within the experimentally acceptable parameters. Unfortunately, this is the only substrate to display this accuracy across all unknown compositions. The model produces an accuracy within 4% when applied to pine, and the greatest variance seen is 8.64% for sample 6 on oak.



**Figure 4-3:** Variation between the actual %goethite and the calculate %goethite for the samples of undisclosed composition using the 530nm prediction model.

However, of most interest is the trends seen in predicting the composition of specific unknowns across all surfaces. For example, the predicted goethite concentration for unknowns 8 and 9 is always lower than the actual composition, for all surfaces studied, and there is generally good agreement in the accuracy for both samples for each surface. The prediction for unknown 3 is also always lower than the actual composition, whilst unknowns 2, 5 and 6 are generally higher.

Whilst this model appears to be accurate at predictions on paper, it is scientifically very simple, and investigations continue in attempt to establish a more statistically acceptable method that is accurate across all substrates.

#### 4.3.2. Multiple linear regression analysis

The calculated concentrations compared to the actual concentrations (expressed as a goethite%) for the multiple linear regression analysis model are shown in Table 4-3. A Q-test was applied to remove any outliers (95% confidence), before the standard deviation was calculated.

**Table 4-3:** Results of analysis of samples of undisclosed composition, with comparison to known composition, with values expressed as the percentage of goethite in each sample, with samples applied to wood and stone surfaces.

	Substrate	Actual Goethite %	MLR Predicted Goethite %	Standard Deviation	Variation in Goethite %
<b>Unknown 1</b>	Paper	90.21	90.27	4.74	0.06
	Pine	90.21	90.33	4.46	0.12
	Oak	90.21	90.15	2.80	-0.06
	Jarraah	90.21	90.40	4.23	0.19
	Slate	90.21	91.20	4.89	0.99
	Sandstone	90.21	90.19	3.49	-0.02
	Paver	90.21	89.91	3.08	-0.30
<b>Unknown 2</b>	Paper	4.76	4.92	3.30	0.16
	Pine	4.76	4.73	3.11	-0.03
	Oak	4.76	5.19	1.30	0.43
	Jarraah	4.76	5.32	5.32	0.56
	Slate	4.76	25.46	6.30	20.70
	Sandstone	4.76	23.28	3.45	18.52
	Paver	4.76	24.14	5.20	19.38



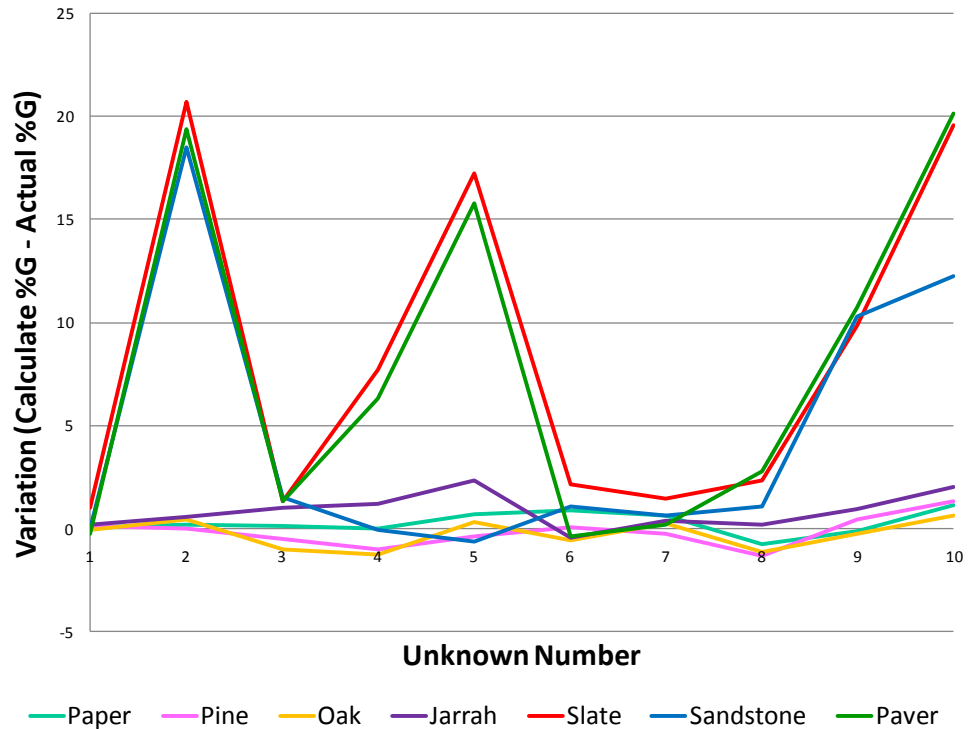
## APPLICATION OF THE I1-PRO AND PREDICTION MODELS

	Substrate	Actual Goethite %	MLR Predicted Goethite %	Standard Deviation	Variation in Goethite %
<b>Unknown 3</b>	Paper	69.61	69.69	5.20	0.08
	Pine	69.61	69.09	6.72	-0.52
	Oak	69.61	68.57	2.34	-1.04
	Jarrah	69.61	70.59	5.52	0.98
	Slate	69.61	70.90	4.34	1.29
	Sandstone	69.61	71.13	2.53	1.52
	Paver	69.61	70.93	4.24	1.32
	<b>Unknown 4</b>	Paper	40.77	40.74	4.75
Pine		40.77	39.73	7.14	-1.04
Oak		40.77	39.49	3.54	-1.28
Jarrah		40.77	41.97	3.64	1.20
Slate		40.77	48.45	5.77	7.68
Sandstone		40.77	40.69	7.87	-0.08
Paver		40.77	47.10	5.74	6.33
<b>Unknown 5</b>		Paper	28.55	29.21	5.56
	Pine	28.55	28.14	3.85	-0.41
	Oak	28.55	28.85	4.11	0.30
	Jarrah	28.55	30.89	6.58	2.34
	Slate	28.55	45.77	5.24	17.22
	Sandstone	28.55	27.92	6.32	-0.63
	Paver	28.55	44.36	7.49	15.81
	<b>Unknown 6</b>	Paper	95.14	95.98	3.76
Pine		95.14	95.20	2.88	0.06
Oak		95.14	94.53	3.48	-0.61
Jarrah		95.14	94.71	3.65	-0.43
Slate		95.14	97.29	2.87	2.15
Sandstone		95.14	96.20	3.32	1.06
Paver		95.14	94.71	2.68	-0.43
<b>Unknown 7</b>		Paper	88.07	88.67	3.17
	Pine	88.07	87.80	7.05	-0.27
	Oak	88.07	88.30	3.07	0.23

	Substrate	Actual Goethite %	MLR Predicted Goethite %	Standard Deviation	Variation in Goethite %
	Jarrah	88.07	88.46	5.79	0.39
	Slate	88.07	89.50	3.29	1.43
	Sandstone	88.07	88.66	5.36	0.59
	Paver	88.07	88.25	5.78	0.18
<b>Unknown 8</b>	Paper	66.79	66.03	2.94	-0.76
	Pine	66.79	65.46	3.89	-1.33
	Oak	66.79	65.66	3.87	-1.13
	Jarrah	66.79	66.97	5.33	0.18
	Slate	66.79	69.14	3.94	2.35
	Sandstone	66.79	67.84	7.18	1.05
	Paver	66.79	69.53	4.06	2.74
<b>Unknown 9</b>	Paper	55.64	55.48	2.72	-0.16
	Pine	55.64	56.06	4.81	0.42
	Oak	55.64	55.38	4.34	-0.26
	Jarrah	55.64	56.56	5.35	0.92
	Slate	55.64	65.46	5.89	9.82
	Sandstone	55.64	65.92	5.13	10.28
	Paver	55.64	66.34	5.21	10.70
<b>Unknown 10</b>	Paper	17.24	18.34	1.37	1.10
	Pine	17.24	18.57	3.05	1.33
	Oak	17.24	17.88	6.14	0.64
	Jarrah	17.24	19.22	7.17	1.98
	Slate	17.24	36.81	7.06	19.57
	Sandstone	17.24	29.48	6.79	12.24
	Paver	17.24	37.42	9.21	20.18

Graphically, the above table is represented in Figure 4-4, where the variation between the calculated goethite composition and the actual goethite composition is shown. Each series represents each sample substrate across the ten compositions.

Comparisons between the calculated value where the composition was undisclosed, and the known concentrations show good agreement for all compositions on all three wood surfaces,



**Figure 4-4:** Variation between the actual %goethite and the calculate %goethite for the samples of undisclosed composition using the MLR model on paper.

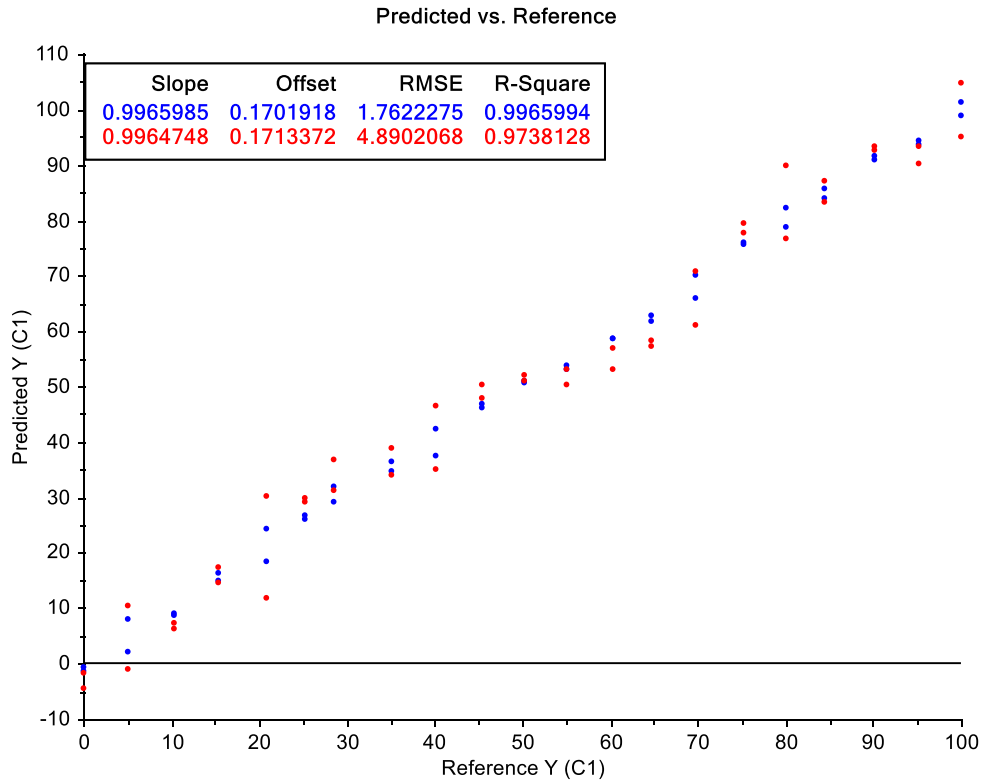
and for high goethite compositions on stone surfaces, with the majority of results showing a variation of less than 2%, and the maximum variation being less than 3%.

For stone surfaces with low goethite composition samples the variation is significantly larger, and outside acceptable limits. Whilst the model does not appear to be a good fit at low goethite compositions on stone, significant here is that, when comparing the results obtained for these samples the variation between results is less than 2%. The exception to this is unknown 10 on sandstone. This demonstrates that the error is systematic and within the model/substrate. It is proposed that this error is due to background effects as a result of surface roughness, resulting in uneven and incomplete sample coverage.

In order to investigate this, a Multiple Linear Regression (MLR) Model was constructed based on the data obtained from the standards on the slate surface and utilising the sample preparation method described previously. Data was then analysed using The Unscrambler X (version 10.0.1) and MLR with a 95% confidence level. Results of this are shown in Figure 4-5.

It can be seen here that the MLR analysis model is verified. The data presents with both slope and  $R^2$  values being close to the desired value of 1, and no outliers were detected by Unscrambler.

This model was then applied to the series of ten samples of known but undisclosed concentrations on the three stone surfaces, with the calculated concentrations compared to the actual concentrations (expressed as goethite%). A Q-test was applied to remove any



**Figure 4-5:** Predicted Vs Reference data from the Multiple Linear Regression model on Slate.

outliers (95% confidence), before the standard deviation was calculated. Results of this analysis are shown in Table 4-4.

**Table 4-4:** Results of analysis of samples of undisclosed composition, with comparison to known composition, with values expressed as the percentage of goethite in each sample, with samples applied stone surfaces, calculated utilising a MLR model created on slate.

	Substrate	Actual Goethite %	MLR Predicted Goethite %	Standard Deviation	Variation in Goethite %
<b>Unknown 1</b>	Slate	90.21	84.94	3.94	-5.27
	Paver	90.21	86.75	3.74	-3.46
	Sandstone	90.21	87.19	5.44	-3.02
<b>Unknown 2</b>	Slate	4.76	48.24	5.49	43.48
	Paver	4.76	51.41	8.67	46.65
	Sandstone	4.76	47.82	6.12	43.06
<b>Unknown 3</b>	Slate	69.61	59.02	4.78	-10.59
	Paver	69.61	60.88	4.51	-8.73
	Sandstone	69.61	67.95	2.96	-1.66

	Substrate	Actual Goethite %	MLR Predicted Goethite %	Standard Deviation	Variation in Goethite %
<b>Unknown 4</b>	Slate	40.77	47.09	3.69	6.32
	Paver	40.77	40.60	6.65	-0.17
	Sandstone	40.77	65.41	7.16	24.64
<b>Unknown 5</b>	Slate	28.55	43.75	4.32	15.20
	Paver	28.55	43.34	9.47	14.79
	Sandstone	28.55	62.88	5.01	34.33
<b>Unknown 6</b>	Slate	95.14	94.05	8.89	-1.09
	Paver	95.14	92.14	3.75	-3.00
	Sandstone	95.14	92.94	5.84	-2.20
<b>Unknown 7</b>	Slate	88.07	89.89	9.64	1.82
	Paver	88.07	89.91	7.29	1.84
	Sandstone	88.07	85.53	9.22	-2.54
<b>Unknown 8</b>	Slate	66.79	64.54	4.40	-2.25
	Paver	66.79	68.27	4.82	1.48
	Sandstone	66.79	84.80	5.41	18.01
<b>Unknown 9</b>	Slate	55.64	65.61	7.56	9.97
	Paver	55.64	73.04	4.26	17.40
	Sandstone	55.64	71.87	1.62	16.23
<b>Unknown 10</b>	Slate	17.24	49.03	10.02	31.79
	Paver	17.24	48.88	6.19	31.64
	Sandstone	17.24	57.00	7.01	39.76

It can be seen that the use of the second model, created on Slate, did not improve the accuracy of prediction of samples on unknown composition on various stone surfaces. Whilst predictions remained accurate on some samples, namely 6, 7 and 8, agreement between the three substrates decreased. This confirms that whilst the model created on paper showed accurate predictions on paper and wood, it is not suitable for all substrates. Specifically, it is unsuitable for application to stone when the sample contains a high percentage composition of haematite.

#### 4.4. Conclusions

The effect of different substrates (including various woods and stones) on the i1Pros ability to distinguish between samples was studied. Results of this showed that, for each individual

## CHAPTER FOUR

substrate, the samples were able to be distinguished between based on their goethite/haematite composition. Comparisons were then made between substrate types and the majority of sample compositions showed that the effect of the substrate was negligible.

This chapter then applied a number of models previously established to the samples on various substrates. The first of these models was based on the analysis of a single wave length, 530nms. This model was found to be the most accurate with an error of less than 2% on all ten samples analysed when applied to paper. The error was significantly larger and up to 8% when samples were applied to alternate substrates, thus limiting its application to artefacts.

The final model to be investigated is Multiple Linear Regression (MLR) Analysis. When the samples were applied to paper variation between the samples was, in most cases, less than 1%, with the maximum variation being less than 2%. Analysis was then performed on alternate substrates and results show good agreement for all compositions on all three wood surfaces, and for high goethite compositions on stone surfaces, with the majority of results showing a variation of less than 2%, and the maximum variation being less than 3%. For stone surfaces with low goethite composition the variation is significantly larger, and outside acceptable limits. In order to investigate this, a second MLR model was created using results obtained from a slate substrate, however this did not improve the accuracy of sample composition predictions.

CHAPTER FIVE:  
A STUDY INTO THE  
INTER-SITE AND  
INTRA-SITE  
VARIATION AT A  
NUMBER OF  
CULTURALLY  
SIGNIFICANT  
AUSTRALIAN SITES

Previous chapters have worked to confirm the suitability of the i1 Pro for application to ochre materials under a range of conditions including a large variety of sample thicknesses, binder materials, and substrates including various woods and stones. Statistical analysis showed complete and accurate separation, with clusters formed based on sample composition.

Investigations then centred on predictions, and if the i1 Pro was able to accurately predict the composition of undisclosed samples based on a number of models. A model based on a single wavelength – at 530nm – was found to be most accurate, with results obtained within 2% of the actual sample composition on paper.

However, in order for the i1 Pro method of colour analysis to be of most benefit, artefacts containing ochre of unknown origin would ideally be able to be easily linked with their most likely sources based purely on colour. For this to be possible, the level of intra-site variation would need to be small and inter-site variation large enough to be statistically significant. This chapter explores the level of inter- and intra-site variation across a number of well-known ochre sites with significance to Indigenous Australians.

### 5.1. Sample sites

The sites chosen for this study are Wilgie Mia, Bookartoo and Moana. These sites were selected because a number of samples are present in the collections available of well provenanced ochre with quantities large enough to explore both colour and trace element studies.

Bookartoo is also known as Parachilna – being the nearest town, is a site in South Australia. Bookartoo is now contained within the northern corner of the the Flinders Ranges National Park in the Heysen Range, approximately 400kms north of South Australia's capital city - Adelaide. The area derives its name from the Aboriginal *patajilnda*, meaning "place of peppermint gum trees", with the spelling difference due to an early translation error.

Bookartoo ochre was well value by Australian Aboriginals and was traded extensively in the late nineteenth century both within South Australia and beyond, travelling as far as 450kms north to Boulia, east to the Darling River and west to Oodnadatta. The mine itself is relatively small, covering approximately 80m<sup>2</sup>, and little is known about the mines as all had collapsed by approximately 1880 and prior to any recent investigations.

Wilgie Mia is a very well-known ochre site. It is located in the Weld Range in Western Australia, near the small town of Cue and approximately 620kms north-east of the capital city Perth. Excavations have occurred for at least 40000 years and are still ongoing today, making it one of the world oldest currently running mines.

It was documented in the mid 1950's [161] that this quarry provided the majority of red ochre utilised by Aboriginal Australians in the entire western region on Australia. The same reports suggests that as early as the late 1930's red ochre from this mine was being utilised as far north as Carnarvon (approximately 450kms north-west) and as far south as Kellerberrin



(525kms south). Ochre from this site was identified as far east as Wiluna (300kms north east) in the 1970s [61], making ochre from this mine one of the most travelled and sought after in Australia at the time.

Moana is a coastal suburb located approximately 40kms south of Adelaide – the capital city of South Australia. Just south of Moana, between Moana and a neighbouring beach is Ochre Point and Ochre Cove, where the Kurna people mined ochre ranging in colour from white to reds and yellows. The red/brown sandhills are still present today.

Shown below is the location of all three sites within Australia. Bookartoo is labelled as site 1, Wilgie Mia as site 2 and Moana as site 3.



**Figure 5-1:** Map of Australia showing the location of the three sites used in this study. Bookartoo is labelled as site 1, Wilgie Mia as site 2 and Moana as site 3.

## 5.2. Sample preparation

All available samples of certain origin for the selected areas were utilised in this study. From each available sample, three subsamples were taken. The samples varied in a number of ways including the volume of sample available – ranging from the milligrams to the tens of grams, the texture – ranging from finely ground powder to small stones to clay like material to large stones and often a combination of these was present in each sample, and the colour – ranging from yellow to orange to brown-red to true red. The samples utilised are detailed in the table below, where raw stones samples are described based on their sizes with samples less than 2cm in diameter are considered very small, between 2-5cm in diameter small, 6-9cm in diameter medium, 10-15cm in diameter large, and greater than 16cm in diameter extra-large.

## CHAPTER FIVE

Samples were prepared in the same manner as previous studies, being ground to a fine even powder before being approximately 10mg was applied to Fuji Xerox laser print paper covering an area of approximately 3cm<sup>2</sup> in a circular motion. i1pro analysis was then performed in quintuplicate for each subsample before the data was analysed.

**Table 5-1:** Table showing the ochre samples utilised in this study, including their database number, site location, a description of their colour and the corresponding L/A/B colour space values. A description of the sample type is also given where raw stones samples are described based on their sizes with samples less than 2cm in diameter are considered very small, between 2-5cm in diameter small, 6-9cm in diameter medium, 10-15cm in diameter large, and greater than 16cm in diameter extra-large.

Ochre Number	Site Location	Sample Colour	L/A/B Colour space			Comments
002	Moana	Brown/Red	68.70	20.97	22.39	Very small stones
019	Moana	Red	63.37	31.20	29.22	Small fragments, grind easily
020	Moana	Orange	82.25	20.64	30.83	Small stones
036	Moana	Orange	81.72	24.07	33.81	Small fragments, power easily
037	Moana	Red	62.54	30.82	25.35	A mixture of different samples, from power through to small stones
062	Wilgie Mia	Red	42.00	22.32	12.97	A mixture of powder and very small stones
063	Wilgie Mia	Red	41.88	27.98	19.82	A mixture of powder and very small stones
064	Wilgie Mia	Red	42.80	22.10	12.16	Small stones, difficult to grind
065	Wilgie Mia	Yellow	69.13	20.20	42.37	Small stones
066	Wilgie Mia	Red	44.14	27.62	20.57	Small stones, difficult to grind
067	Wilgie Mia	Red	44.08	29.91	24.29	Finely powdered with very small fragments
075	Bookartoo	Red	47.41	25.77	21.18	Single small-medium stone
076	Bookartoo	Red	48.78	19.32	12.32	Four small stones
077	Bookartoo	Red	47.41	25.77	21.18	Multiple small-medium stones

A STUDY INTO INTER-SITE AND INTRA-SITE VARIATION

Ochre Number	Site Location	Sample Colour	L/A/B Colour space			Comments
078	Bookartoo	Red	53.34	29.56	23.86	One medium-large stone and many small pieces
079	Bookartoo	Red	53.24	30.94	24.82	Three small-medium stones and a small amount of powder
101	Moana	Red and Yellow	(b - red) 58.39 35.40 32.49 (c - yellow) 89.67 7.66 38.84			Multiple samples of both red and yellow colour. Some powdered, some small stones
117	Wilgie Mia	Red	43.88	27.85	18.97	Multiple samples including two large and approximately eight medium stones, a number of smaller stones and power
118	Wilgie Mia	Red	42.09	32.76	24.41	A number of samples ranging from powder to small stones
119	Wilgie Mia	Red	41.05	24.64	16.29	A number of samples ranging from powder to small stones
141	Moana	Red	60.76	31.60	30.12	Two medium stones, easy to grind
142	Moana	Red	56.51	31.48	28.41	Two medium stones, easy to grind
190	Moana	Red	56.22	40.87	39.22	Two medium stones
192	Moana	Red	58.62	39.40	40.72	Single medium-large stone
203	Moana	Red	59.18	38.36	37.16	Single small stone
204	Moana	Red	59.13	35.38	37.28	Single large stone
254	Moana	Red	53.28	39.10	39.36	Multiple (approximately six – eight) small stones
257	Wilgie Mia	Red	41.74	32.97	23.59	Multiple very small – small stones

## CHAPTER FIVE

Ochre Number	Site Location	Sample Colour	L/A/B Colour space			Comments
258	Wilgie Mia	Yellow	76.10	13.49	45.74	Single small and single medium stones and powdered sample
260	Wilgie Mia	Red	41.41	32.90	23.94	Single very small stone and a small amount of powdered sample
263	Bookartoo	Red	46.97	23.63	18.48	Multiple very small stones, a single small stone and powdered sample
264	Wilgie Mia	Orange	59.95	22.05	28.42	Multiple very small stones, a single small stone and powdered sample
274	Bookartoo	Red	48.81	19.46	12.55	Three very small to small samples
275	Moana	Red	44.77	33.77	29.48	Large amount of sample ranging from powder to medium stones
276	Moana	Red	53.63	34.70	29.62	Three small to medium stones and powdered sample
277	Wilgie Mia	Red	41.37	32.58	23.31	Very small stones and powder
281	Moana	Brown/Red	66.18	21.24	22.37	Lots of subsamples, and containing power and/or very small stones
283	Moana	Yellow	83.01	16.36	53.68	Powder and very small stones. The sample feels different to others – almost damp and clay like
284	Moana	Yellow	85.73	13.05	48.30	Powder and very small stones. The sample feels different to others

A STUDY INTO INTER-SITE AND INTRA-SITE VARIATION

Ochre Number	Site Location	Sample Colour	L/A/B Colour space			Comments
						– almost damp and clay like
285	Moana	Yellow	84.66	14.61	51.33	Powder and very small stones. The sample feels different to others – almost damp and clay like
286	Moana	Yellow	83.32	15.98	54.31	Powder and very small stones. The sample feels different to others – almost damp and clay like
287	Moana	Yellow	77.99	17.11	50.95	Powder, very small stones and a single small stone. The sample feels different to others – almost damp and clay like
292	Moana	Brown/Red	69.58	22.62	26.55	Multiple small fragments
293	Moana	Brown/Red	69.70	23.39	27.83	Multiple small fragments
294	Moana	Brown/Red	73.34	22.12	26.37	Multiple small fragments
296	Moana	Yellow	88.67	10.32	37.13	Multiple small fragments
298	Moana	Brown/Red	76.07	18.17	18.13	Single small to medium stone. Multiple very small stones.
302	Bookartoo	Yellow	74.78	14.22	31.21	Multiple very small to small stones. Some course powder
303	Bookartoo	Orange	68.44	19.15	25.34	Multiple very small to small stones. Some course powder
304	Bookartoo	Orange	58.44	24.02	24.41	Multiple very small to small stones. Some course powder

Ochre Number	Site Location	Sample Colour	L/A/B Colour space			Comments
305	Bookartoo	Orange	56.57	24.51	24.08	Multiple very small to small stones. Some coarse powder
306	Bookartoo	Orange	57.77	23.16	34.94	Multiple very small to small stones. Some fine powder
307	Bookartoo	Orange	63.09	20.27	24.81	Multiple very small to small stones. Some coarse powder
308	Bookartoo	Orange	61.03	21.34	29.58	Multiple very small to small stones. Some coarse powder
309	Bookartoo	Yellow	71.80	14.21	34.97	Small to very small fragments
368	Moana	Red	55.63	36.82	32.19	Single extra-large stone. Feels sandy on the outside. Very easy to grind in some areas.

Visually, the samples for Bookartoo appear to be significantly different, ranging on colour from pale yellow to bright red to deep red and everything in between. Texturally, the samples were similar following grinding, but some required more grinding than others to become powdered.

Visually, the samples from Wilgie Mia appear more consistent than those from Bookartoo. However, texturally, two distinct groups were present. Some ochre samples were already finely powdered and very easy to work with (ochre 117-119 in particular), whilst others required much more grinding (such as ochre 062-064). Ochre 066 was noticeably different to the others, containing much larger 'impurities' of stone etc., and was difficult to grind to a consistent power. Also of note is that there appeared to be two qualities of ochre present, with some ochre appearing more damp and clay-like than others.

### 5.3. Colour analysis results

Colour analysis was performed utilising the X-rite i1Pro. Each sample has three subsamples, as previously described, and each subsample was measured five times, giving a total of fifteen measurements per sample. The raw spectra were normalized and the first order derivatives taken. A Q-test was performed and any outliers removed before initially averaging the results of each subsample, followed by an overall average per sample if appropriate.

The reflectance spectra of fifty seven ochres from Moana (28 ochres), Wilgie Mia (14 ochres) and Bookartoo (15 ochres) were collected. Samples from each site exhibited red, orange, brown and yellow hues and are described in Table 5-1.

Statistical analysis was performed using The Unscrambler version X 10.0.1. The data utilised is the raw i1Pro data, which is then normalized and the first order derivative taken. A Q-test is then applied and any outliers removed before all subsamples are averaged to give a single data set per ochre. Statistical studies will focus on the use of principle component analysis (PCA) where a mean uncentred singular value decomposition algorithm was used. A random cross validation or leverage method was utilised incorporating twelve segments with seven component outputs requested. Variables were evenly weighted.

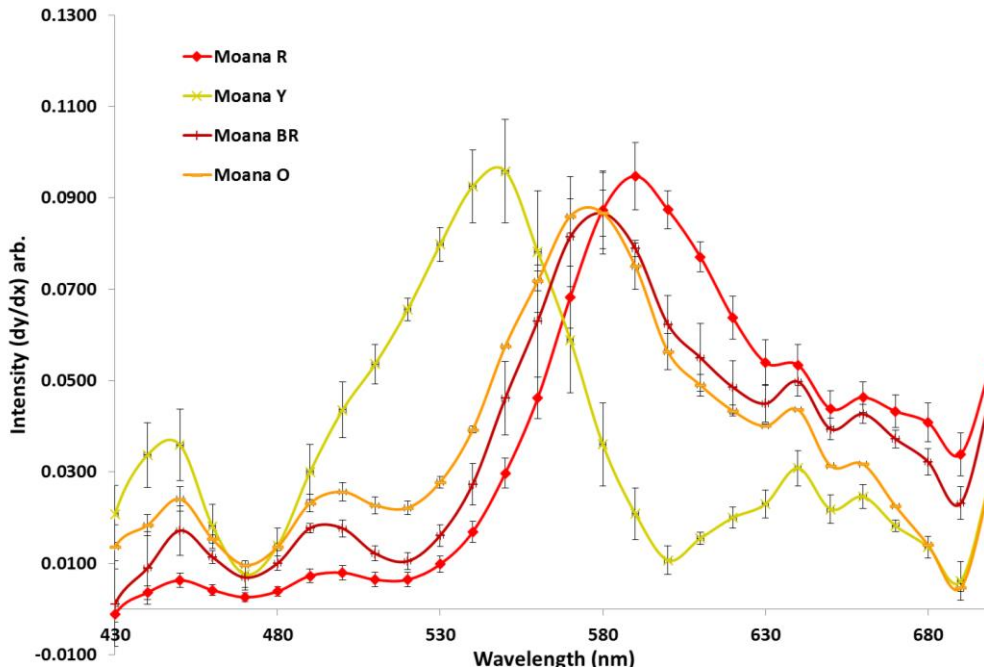
### 5.3.1. Moana

The Moana data was examined. The red coloured ochre was further subdivided into two groups – Red (R.) and Brown/Red (BR), as visually two distinct variations are present. Analysis initially focused on all wavelengths from 430-700nm, with 410nm and 420nm removed due to early studies showing their lack of accurate reproducibility. Figure 5-2 shows the spectra from samples from Moana. The spectra shown is an average of all spectra for each classified colour. Here, red is representative of 13 samples, brown/red of 6 samples, orange of 2 samples and yellow of 7 samples. The error bars represent a single standard deviation of the average spectra and do not take into account any instrumental errors, which are minor in comparison.

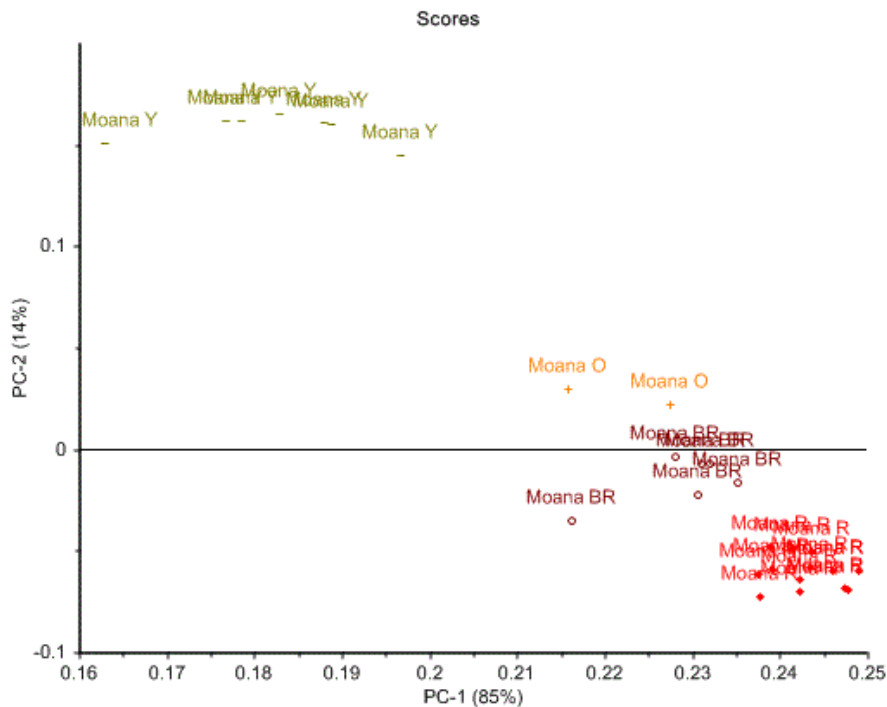
As expected, the spectra showed significant differences for the different coloured samples. Visually and statistically, all four sub classifications are easily distinguishable.

The yellow ochre displays the most visually different spectra, with a much lower peak maxima at approximately 540nm. Even considering the error range, this spectra is statistically different to the other three at almost every wavenumber, only exhibiting some similarities to the orange spectra at the extreme high and low wavelengths.

The spectra of the orange ochres is, in many ways, similar to that of the brown/red ochres. They both exhibit a peak maxima at approximately 570nm, and show a very similar trend line across the spectra with varying intensities. Where the orange and red/brown spectra are indistinguishable within error at their maxima, they exhibit very different ratios when comparing other wavelengths, for example, wavelengths 520/650. The orange ochres also exhibit similarities to the red ochres spectrally, especially at high wavenumbers. Statistical analysis was then applied to the spectral data, as described previously, where here the spectra from each subsample were averaged, giving a single data set per ochre number. The results of statistical analysis are shown in Figure 5-3 using principal component 1 and 2, where 99% of the variance is described.



**Figure 5-2:** The normalised and derivative spectra for each colour classification for all Moana samples. The error bars represent a single standard deviation of the average spectra.



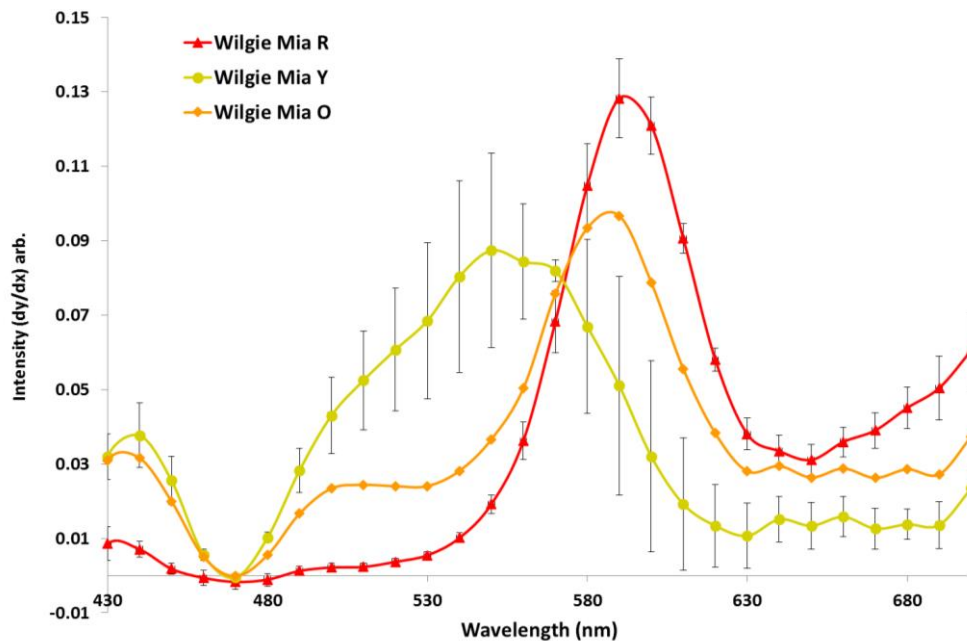
**Figure 5-3:** Results of principle component analysis for PC1 vs PC2 performed on all Moana samples.

Here it can be seen that the grouping of samples into the four predetermined subsets is apparent with good accuracy. It shows that the yellow ochres spectra are significantly different to the orange, brown/red and red, and this is reflected in the spectra previously discussed.



### 5.3.2. Wilgie Mia

The Wilgie Mia data was examined. Analysis initially focused on all wavelengths from 430-700nm, with 410 and 420nm removed due to early studies showing their lack of accurate reproducibility. Figure 5-4 shows the spectra from samples from Wilgie Mia. The spectra shown is an average of all spectra for each classified colour. Here, red is representative of 11 samples, orange of a single sample and yellow of 2 samples. The error bars represent a single standard deviation of the average spectra and do not take into account any instrumental errors, which are minor in comparison. As orange is represented by a single sample, statistical analysis was not able to be completed and as a result no error bars are present.



**Figure 5-4:** The normalised and derivative spectra for each colour classification for all Wilgie Mia samples. The error bars represent a single standard deviation of the average spectra.

The first observation from this data is that the error bars on the yellow spectra are significantly larger than any seen previously. As the yellow is representative of an average of only two samples, this suggests that the two samples are significantly different.

It can again be seen that, at the majority of wavelengths, all three classified colours are visually distinguishable within error. There is a shift in peak maxima from yellow at 550nm, orange at 580nm and red and 590nm. There is also a significant shift in the intensity of the maxima when comparing red to the remaining colours. The greatest similarities in the three spectra exist in the lower regions, most noticeably at wavelength 470nm, where the three samples are indistinguishable within error.

Statistical analysis was applied to the spectral data in the manner previously described. The spectra from each subsample were averaged, giving a single data set per ochre number.



**Figure 5-5:** Results of principle component analysis for PC1 vs PC2 performed on all Wilgie Mia samples.

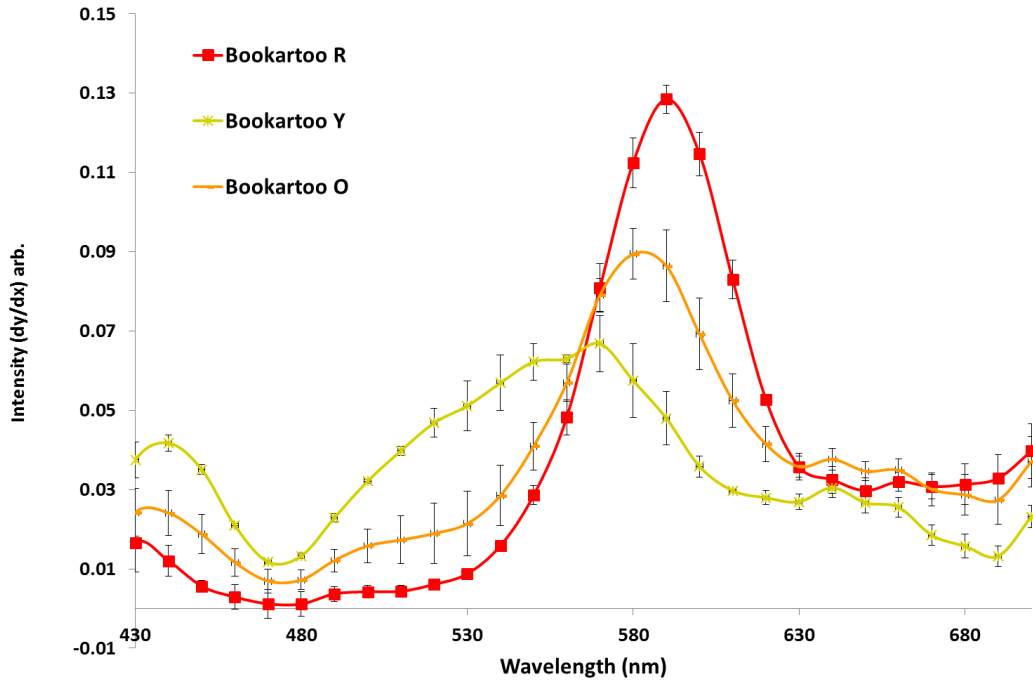
The results of statistical analysis are shown below using principal component 1 and 2, where 99% of the variance is described.

Of note in the PCA analysis is that the two yellow samples show no grouping and are separated as distinctly different. This reflects the error bars seen in the spectral study, and suggests the need for further sample analysis before conclusions can be drawn. As a single orange sample is all that was available for this study, it is difficult to comment on the analysis of it, suffice to say that it falls in the expected area between the yellow and red samples on the PCA analysis. The eleven red samples represented show good statistical grouping.

### 5.3.3. Bookartoo

The Bookartoo data was examined. Analysis initially focused on all wavelengths from 430-700nm, with 410 and 420nm removed due to early studies showing their lack of accurate reproducibility. Figure 5-6 shows the spectra from samples from Bookartoo. The spectra shown is an average of all spectra for each classified colour. Here, red is representative of 7 samples, orange of 2 samples and yellow of 6 samples. The error bars represent a single standard deviation of the average spectra and do not take into account any instrumental errors, which are minor in comparison.

It can be seen that, at the majority of wavelengths, all three classified colours are visually distinguishable within error. There is a shift in peak maxima from yellow at 570nm, orange at 580nm and red and 590nm. There is also a significant shift in the intensity of the maxima, with



**Figure 5-6:** The normalised and derivative spectra for each colour classification for all Bookartoo samples. The error bars represent a single standard deviation of the average spectra.

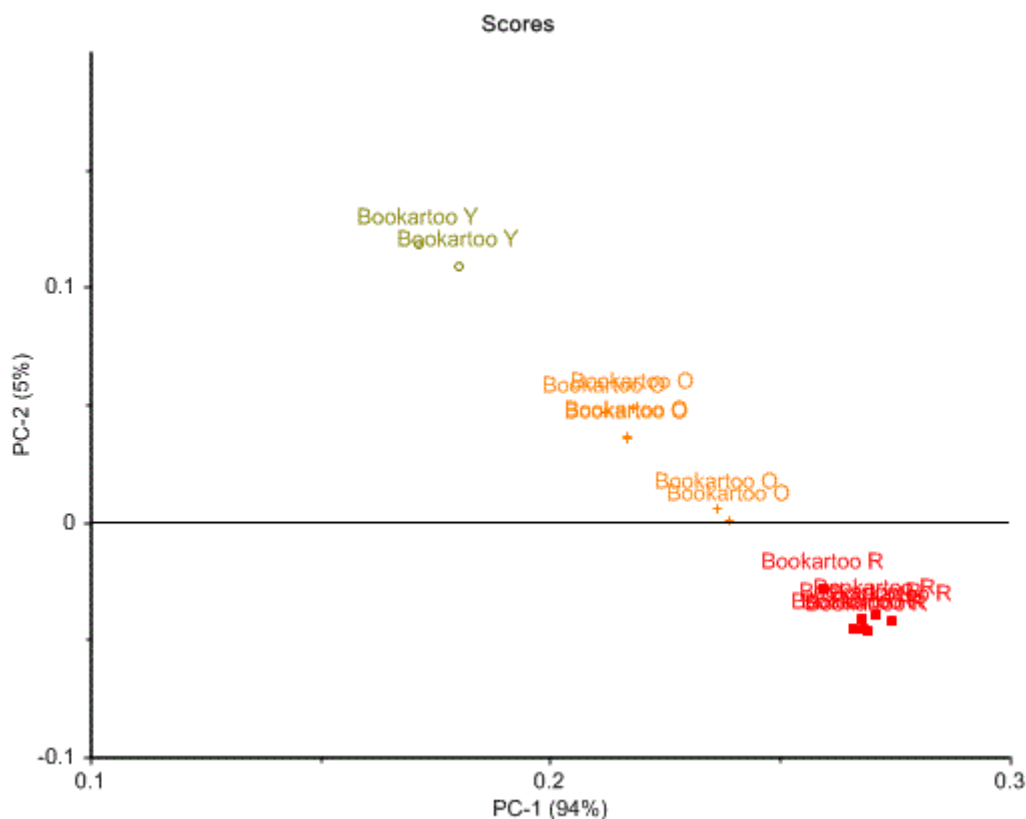
yellow much lower than orange and red higher again. The greatest similarities in the three spectra exist in the region of 630-680nm, where often two spectra are indistinguishable within error.

Statistical analysis was applied to the spectral data using the parameters previously details. The spectra from each subsample were averaged, giving a single data set per ochre number. The results of statistical analysis are shown in Figure 5-7 using principal component 1 and 2, where 99% of the variance is described.

The grouping of ochre based on their colour is clear here, with all three colours distinctly different from each other. The ochre labelled orange appears to have two subsets, one slightly redder in tone than the other, and this would aid in explaining the large error bars on the orange spectra seen previously as it suggests that significant variation within the samples exists. PCA analysis also shows that the yellow is more similar to the other classifications than was seen with the Moana samples, and this is again reflected in the spectra.

### 5.3.1. Comparison between all sites

Whilst all sites showed that the samples of various colours were easily distinguishable, this was entirely expected, and the focus now shifts to if samples of seemingly similar colour from alternate sites can be statistically separated with accuracy.

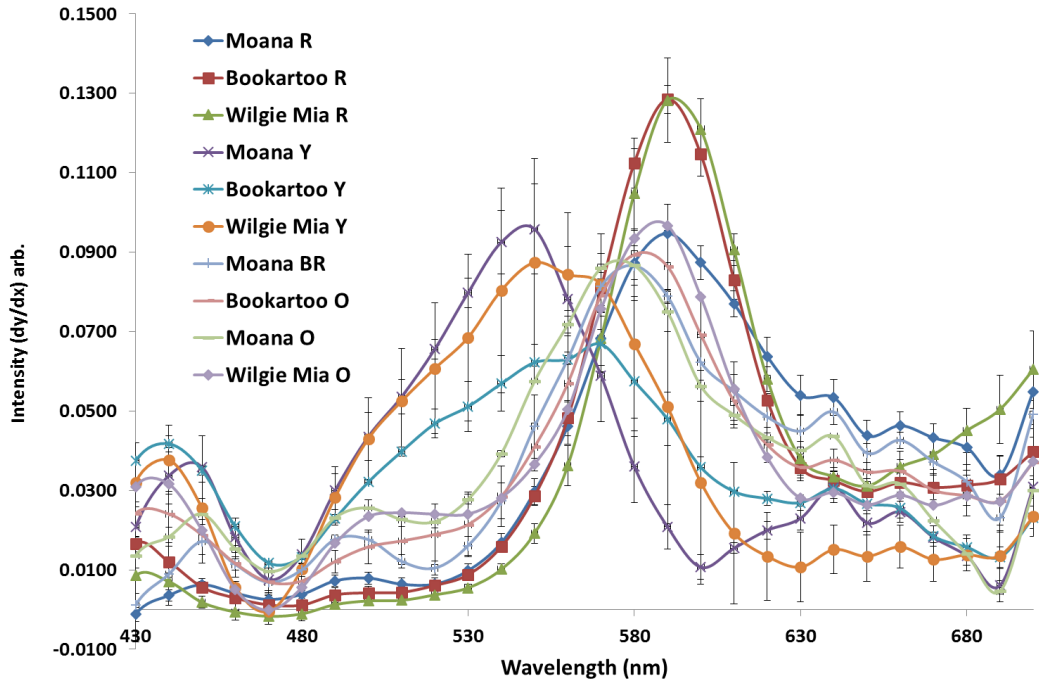


**Figure 5-7:** Results of principle component analysis for PC1 vs PC2 performed on all Bookartoo samples.

#### 5.3.1.1. All Data

Shown below is the overlaid data of all the data presented previously, representing the average of each colour classified for each site. The error bars represent a single standard deviation of the average spectra and do not take into account any instrumental errors, which are minor in comparison. As Wilgie Mia orange is represented by a single sample, statistical analysis was not able to be completed and as a result no error bars are present.

Visually, the three yellow samples appear different both to each other and to the other colours. Whilst some wavelengths are indistinguishable within error, the overall trends are quite different, including different peak's maxima. There appears to be much more overlap with the orange spectra with a number of similarities present. The peak maxima appear to be the same, as do the general trends of the spectra, with some noticeable variation in intensities. The Moana red and Moana brown/red samples exhibit many similarities to the orange samples from all three sites. The red samples from Bookartoo and Wilgie Mia, whilst similar to each other, are significantly different to all other spectra, most noticeably at their maxima with a much larger intensity recorded.

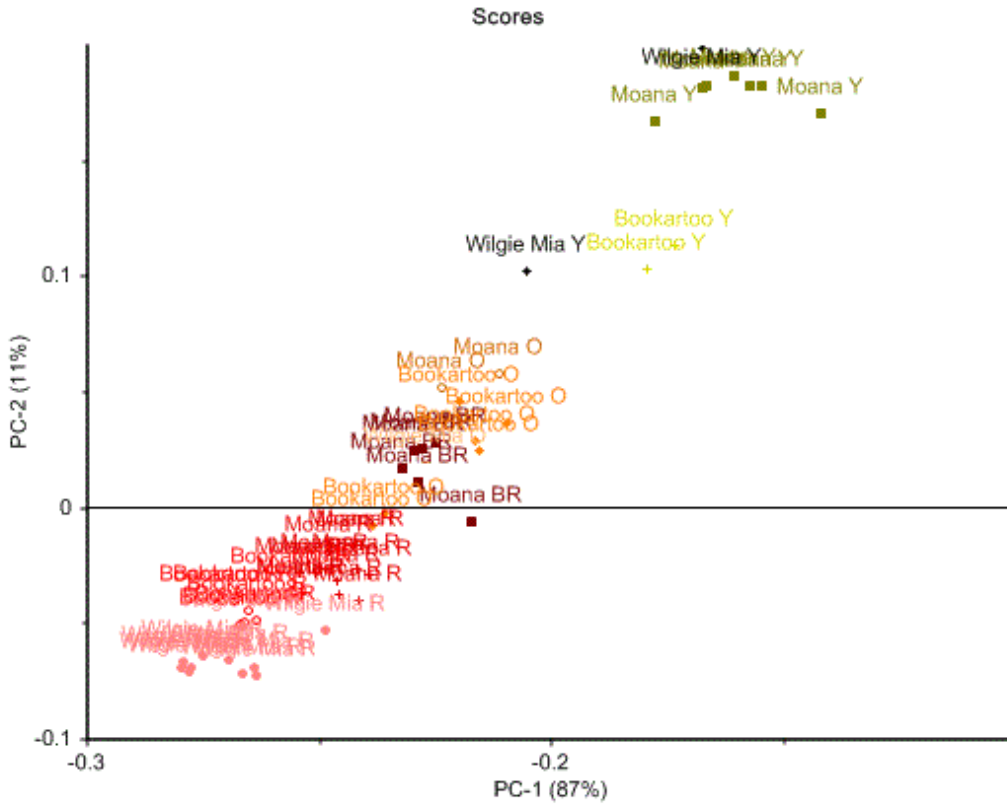


**Figure 5-8:** The normalised and derivative spectra for each colour classification for all Wilgie Mia, Bookartoo and Moana samples. The error bars represent a single standard deviation of the average spectra.

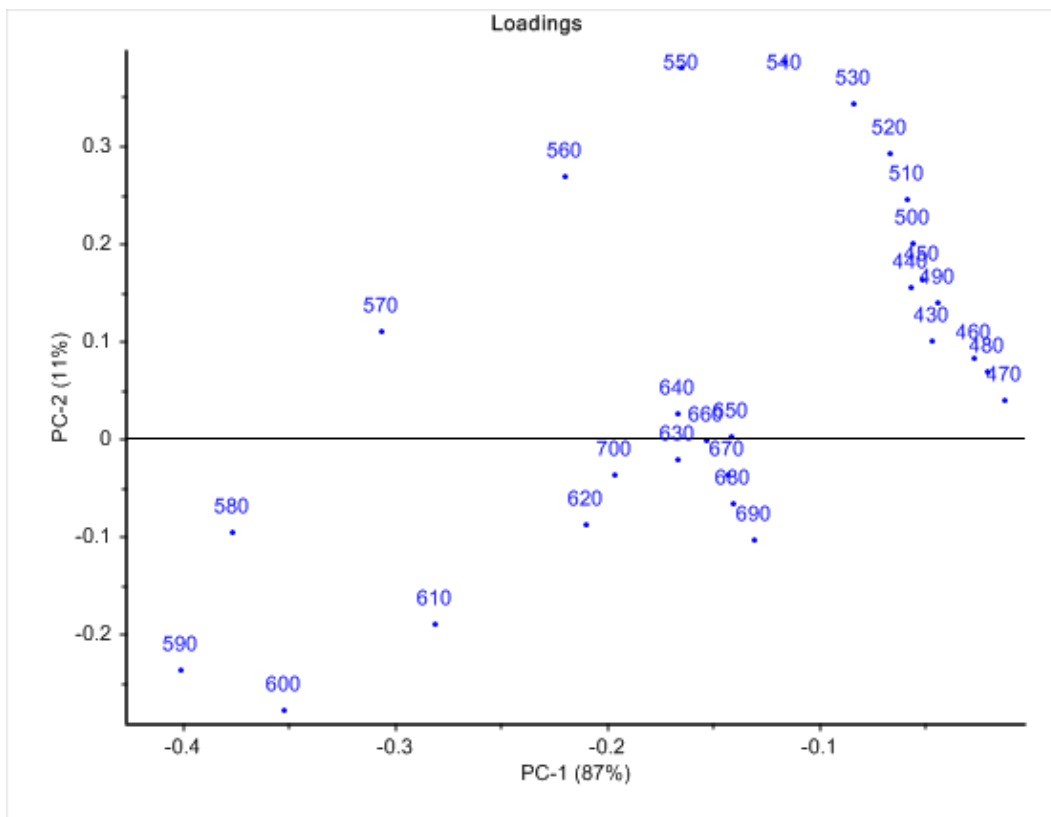
Statistical analysis was applied to the spectral data utilising PCA with the parameters previously described. The spectra from each subsample were averaged, giving a single data set per ochre number. Analysis initially focused on all wavelengths from 430-700nm, with 410 and 420nm removed due to early studies showing their lack of accurate reproducibility. The results of this are shown below using principal component 1 and 2, where 98% of the variance is described.

Evident in Figure 5-9, discrimination exists along both the x and y axis on the basis of colour from red to yellow, with red being more negative along both the PC1 and PC2 axis. This is consistent with the loadings plot shown in Figure 5-10, with wavelengths 590 and 600nm having the greatest influence of the most negative quadrant (lower left), and wavelengths 520-540nm the most influence on the upper right. Overlap exists between all red ochres with no clearly defined clusters. The orange ochres display similar overlap, and the Moana Red/Brown ochre also clusters in this region. Yellow ochre appears distinctly different from the others and clusters in the upper right quadrant. Consequently, discrimination using PC1 and PC2 is unsuitable for provenancing of unknown ochres thought to be from these regions.

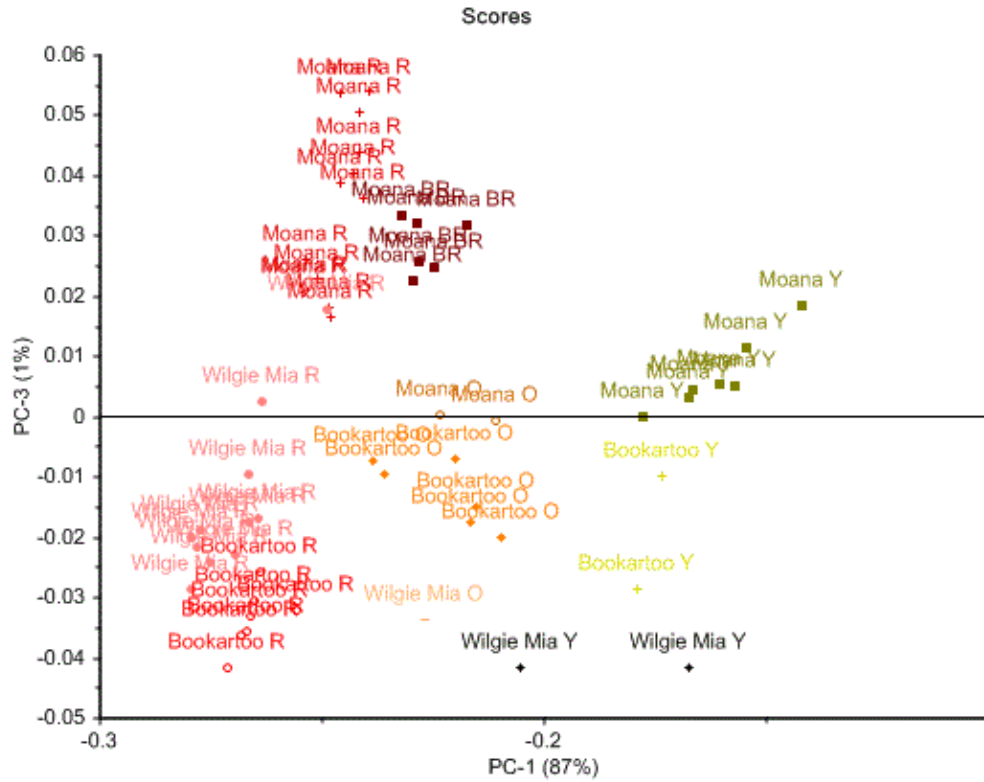
Changing the principle components examined from PC1 vs PC2 to PC1 vs PC3 (Figure 5-11) reduces the amount of variance described from 98% to 88%, but changed the trending directions to ensure more accurate grouping based on location.



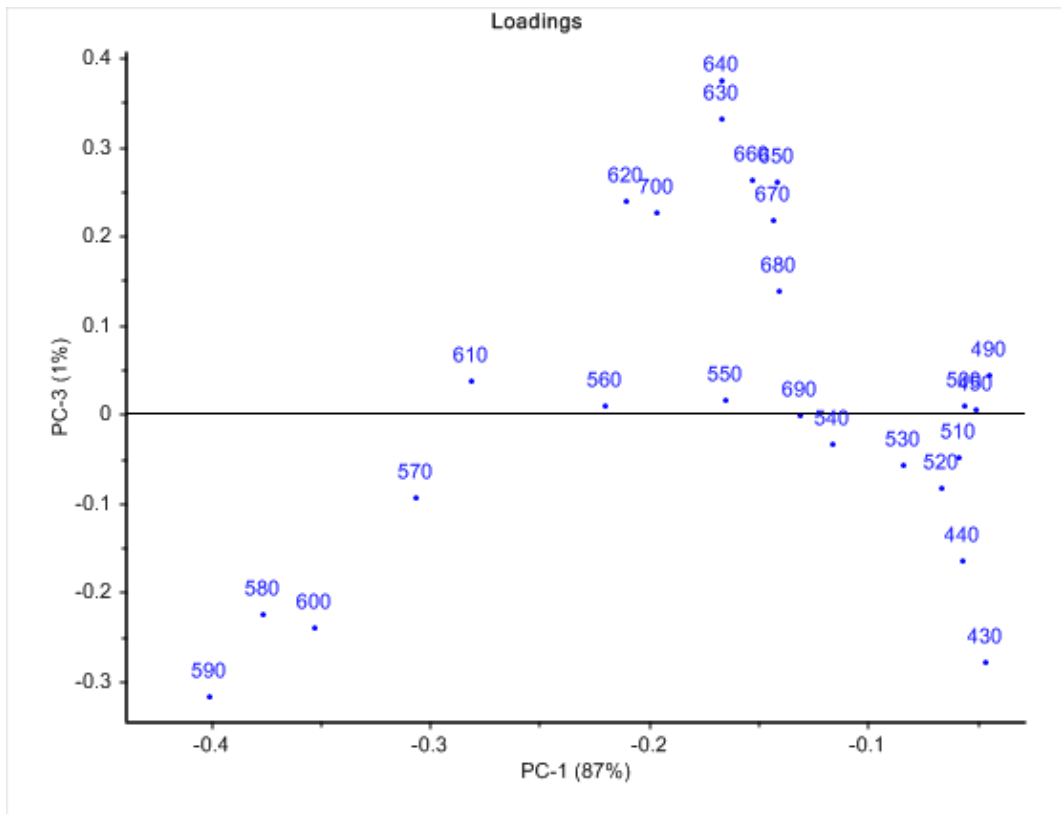
**Figure 5-9:** Results of principle component analysis for PC1 vs PC2 performed on all Wilgie Mia, Bookartoo and Moana samples.



**Figure 5-10:** Loadings plot corresponding to the principal component analysis results presented in Figure 5-9.



**Figure 5-11:** Results of principle component analysis for PC1 vs PC3 performed on all Wilgie Mia, Bookartoo and Moana samples.



**Figure 5-12:** Loadings plot corresponding to the principal component analysis results presented in Figure 5-11.

As with Figure 5-9, in Figure 5-11 separation based on colour is apparent in PC1, but location has a stronger influence on PC3. Moana exhibits positive values for PC3 and all samples appear in the upper half. Similarly, Bookartoo and Wilgie Mia are in the negative region of PC3 and the majority of samples appear in the lower half of the graph.

Moana Red, classified into red and brown/red, shown good grouping in the positive PC3 scale. The brown/red ochre shows a shift along PC1, allowing for distinction, but this variance is not reflected in the PC3 scale. Visual analysis shows that two further sub-groups appear to exist within the Moana Red ochre, separated by the PC3 scale.

When examining the lower half of the figure with respect to PC3, Bookartoo is less negative than Wilgie Mia for yellow and orange coloured ochres, but this trend is reversed when comparing the red ochre samples. The loadings plot, shown in Figure 5-12, suggests that it is predominantly wavelengths 520-580nm influencing this trend. Wilgie Mia red and Bookartoo red are not completely distinguishable here, which is not entirely unexpected given the similarities in the spectra, but general grouping is apparent.

Whilst Figure 5-9 and Figure 5-11 demonstrate good clustering of ochres based on colour, this is able to be achieved by eye. The influence of the additional orange and yellow ochre data may be contributing to the overlap in the red ochre clusters. Consequently, it was decided to focus solely on the red ochres.

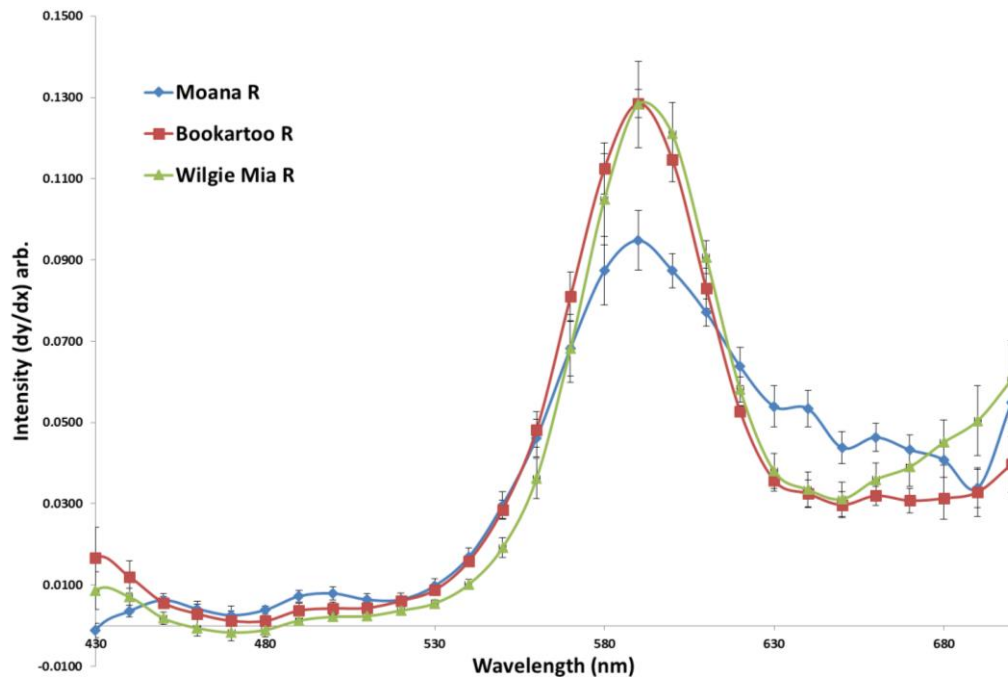
### 5.3.1.2. Red ochre

The data obtained for the ochre classified red in colour from all three sites was studied for comparison. As with previous studies, data from 430-700nm was evaluated. Figure 5-13 presents the average of the derivative spectra for the three sites studied. Here, Bookartoo is represented by 7 samples, Wilgie Mia by 11 and Moana by 13. The error bars represent a single standard deviation.

It is immediately apparent that the spectra obtained for Moana red ochre is visually different to those obtained for Bookartoo and Wilgie Mia. Whilst they all share the same peak maxima, at 590nm, Moana exhibits a much lower intensity, approximately 30% less than the other spectra. The Moana spectra also exhibits a significantly different trend in the higher wavelengths – it is a much broader peak about its maxima and does not reach such a dramatic minima in the region of 630nm, instead steadily declining to a minima at 690nm before rising sharply at 700nm.

The spectra obtained for Bookartoo and Wilgie Mia are visually very similar. They exhibit both the same peak maxima and peak intensity, as well as the same general trend. At the majority of wavelengths they are indistinguishable within error. Some subtle variations do exist however, and there are a number of wavelengths at which the two spectra are uniquely distinguishable, including 540-550nm, and 670-700nm. In addition to this, when considering the ratio of the data at a number of wavelengths, even wavelengths at which the spectra are indistinguishable within error, very different values are achieved. For example, the ratio



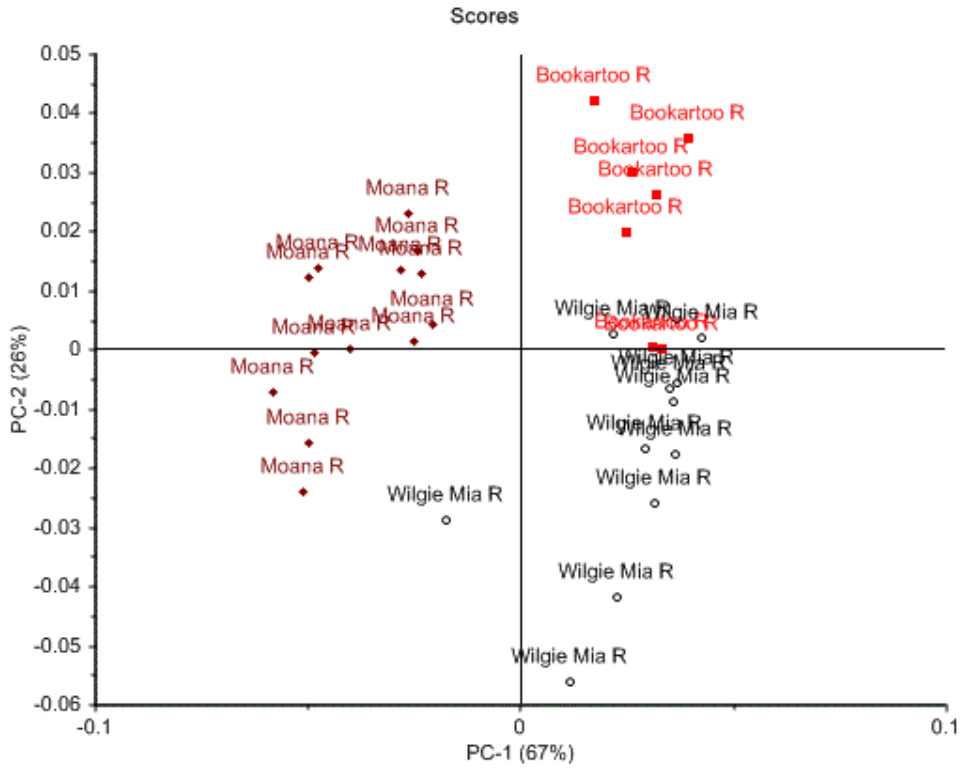


**Figure 5-13:** The normalised and derivative spectra for the ochres classified red in colour for Wilgie Mia (shown in green), Bookartoo (shown in red) and Moana (shown in red) samples. The error bars represent a single standard deviation of the average spectra.

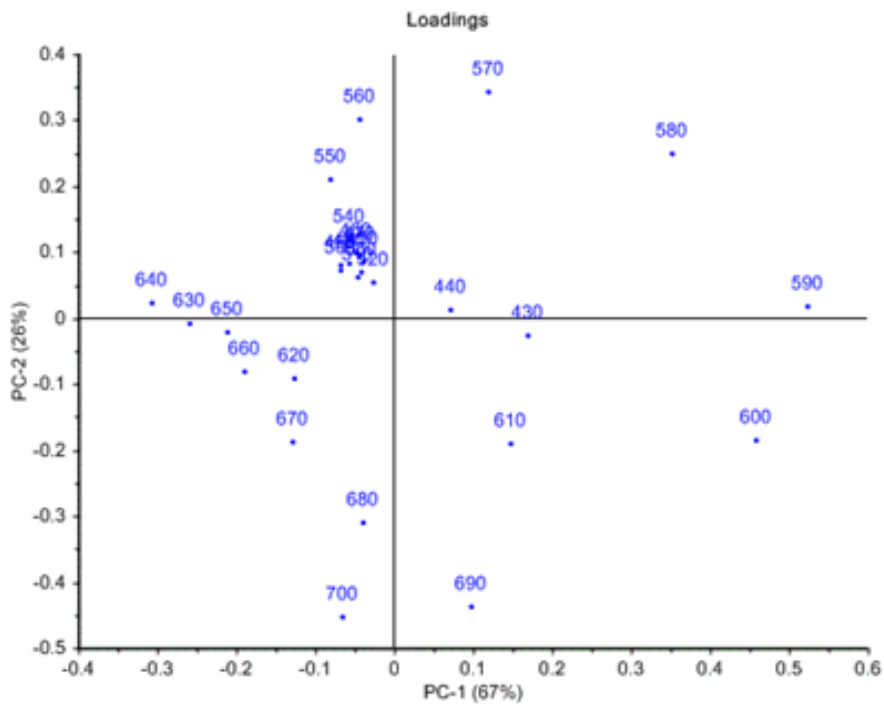
between wavelengths 610/570nm gives a value of 1.329 for Wilgie Mia and 1.026 for Bookartoo – distinctly different values considering the similarities in the spectra. This is again seen when considering wavelengths 680/550nm where values of 1.097 and 2.347 are achieved for Bookartoo and Wilgie Mia respectively.

PCA was applied to the average derivative spectra from each ochre utilizing the parameters previously discussed. Figure 5-14 shows PC1 vs PC2, where 93% of the variance is described.

It can be seen from these images that grouping based on site is reasonably successful. The results of the PC1 scale here exhibit similar trends to the results previously seen along the PC3 scale for all data (Figure 5-11). PC1 demonstrates negative values for Moana, and positive for Wilgie Mia and Bookartoo, with the exception of one Wilgie Mia sample which is slightly negative along the PC1 scale. As expected based on spectral observations, Moana is distinctly different to Bookartoo and Wilgie Mia, and is easily separated and clustered. There is some overlap between Wilgie Mia and Bookartoo, but given the similarities observed previously in the spectra, this is also to be expected, and the basic clustering exhibited here is promising. The PC2 scale shows discrimination between Wilgie Mia and Bookartoo, with Wilgie Mia appearing in the negative region and Bookartoo in the positive. Overall, this gives general groupings of Bookartoo in the upper right quadrant, Wilgie Mia in the lower right quadrant, and Moana in the two left quadrants.



**Figure 5-14:** Results of PCA for PC1 vs PC2 performed on all Wilgie Mia (shown in black), Bookartoo (shown in bright red) and Moana (shown in dark red) samples classified to be red in colour.



**Figure 5-15:** Loadings plot corresponding to the PCA data shown in Figure 5-14.

Shown in Figure 5-15 is the loading graph from the PCA shown in Figure 5-14. This graph highlights that 590nm and 640nm have a large impact on principal component one, as these are the most positive and negative values along this axis. This shows that the intensity of the maxima (at 590nm) strongly influences PC1. This is reflected in the spectra (shown in Figure 5-13) with Moana having a much lower intensity at this wavelength, resulting in the negative PC1 value. At 640nm, Moana has a much greater intensity than Wilgie Mia and Bookartoo, again separating the localities. These wavelengths have little to no impact on principal component two, staying relatively in the plane. Principal component two is here most influenced by wavelengths 560, 570, 690 and 700nm. This is reflected in Figure 5-13 where little change in intensity is seen in the spectra in these regions, however Wilgie Mia and Bookartoo are statistically different in these regions. For predictive purposes, the ratios of the intensity at these wavelengths may be of statistical value.

Of note in the loadings graph shown is that a number of the wavelengths described and utilised in ratio calculations have the opposite influence on principle component two. This is significant as this is the component that best separates Bookartoo and Wilgie Mia, suggesting that the ratio calculations are demonstrating the most significant variations in the spectra. This was further explored by calculating the ratios between the derivate spectral intensity at the wavelengths highlighted for each ochre sample. These results were then averaged based on location, with the results shown in Figure 5-16, where the error bars represent a standard deviation.

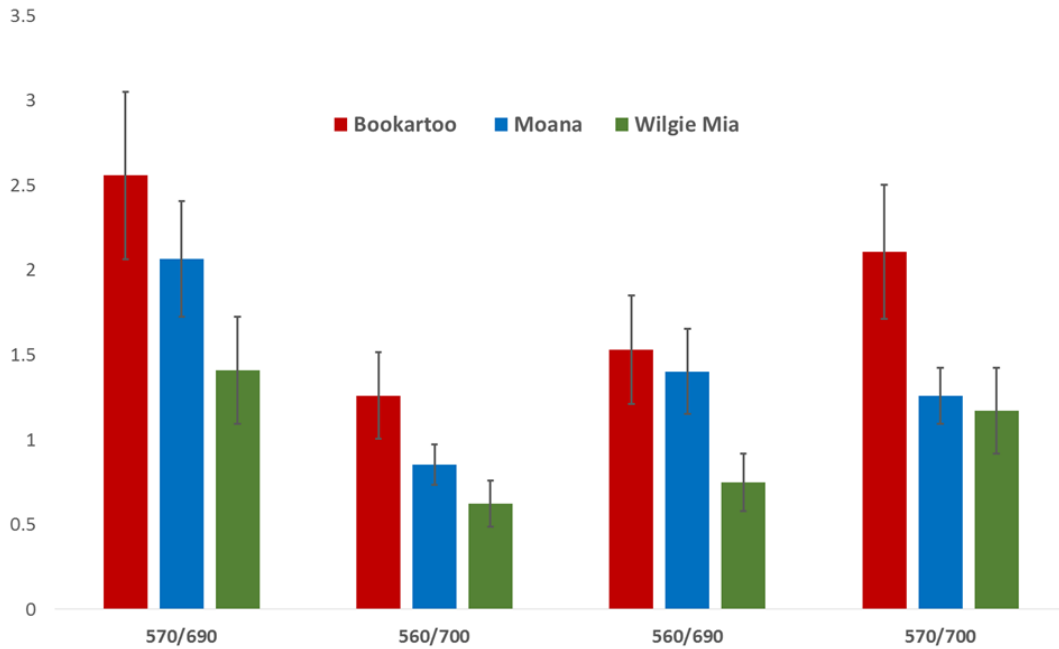
When examining this figure it is apparent that some ratios give a better distinction between individual locations than others. The 570/700nm ratio clearly separates Bookartoo from Wilgie Mia and Moana, however the latter two are indistinguishable within error. The same can be said for the 560/690nm ratio except here it is Wilgie Mia that is unique whilst Moana and Wilgie Mia remain statistically grouped within error. Using a combination of these ratios would therefore allow for complete separation and identification.

If the preference was to use a single ratio only, then 570/690nm and 560/700nm provide better alternatives, with 560/700nm being the most accurate. Here, there is a slight overlap with error bars between Moana and Wilgie Mia, with Bookartoo being distinctly different. When comparing this to the 570/700nm ratio the distinction between Bookartoo and the remaining sites is not as good, however the variation between Moana and Wilgie Mia is greater.

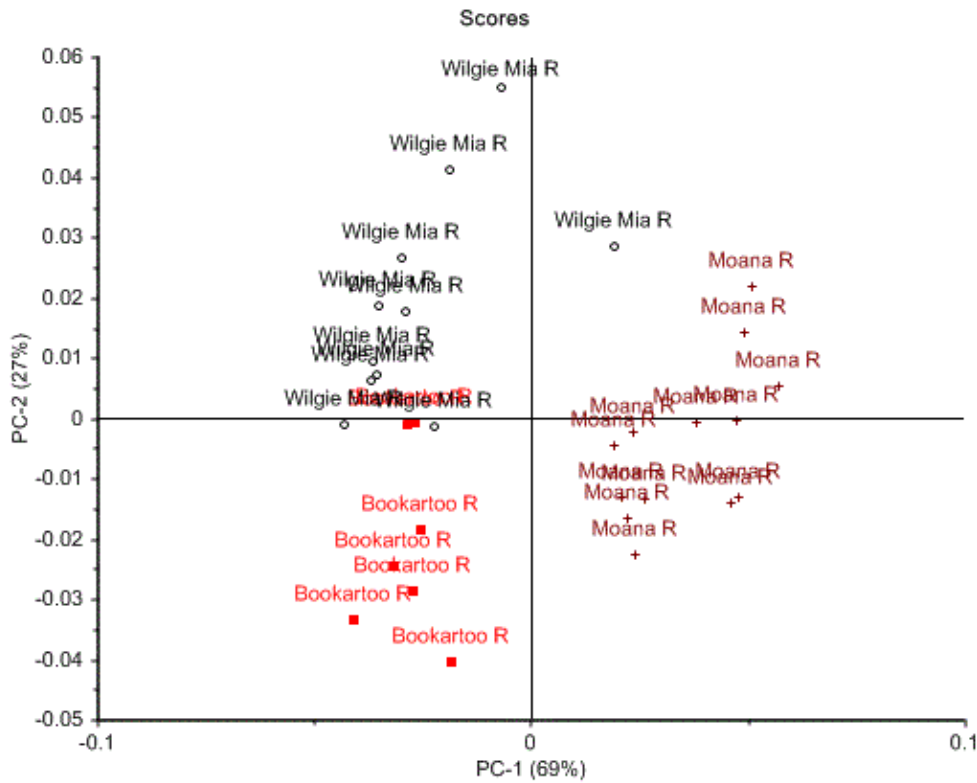
Noticeable in the loadings graph (shown previously in Figure 5-15) is that many wavelengths have little to no impact on the principle component analysis. In order to confirm this and in an attempt to improve grouping, the analysis was repeated only investigating wavelengths 530-700nm.

It can be seen from these results that, whilst the directional impact changes and visually the quadrants in which the spectra clustered in altered, the dominating wavelengths are not changed by the removal of the additional wavelengths and the accuracy of the clustering is not improved.

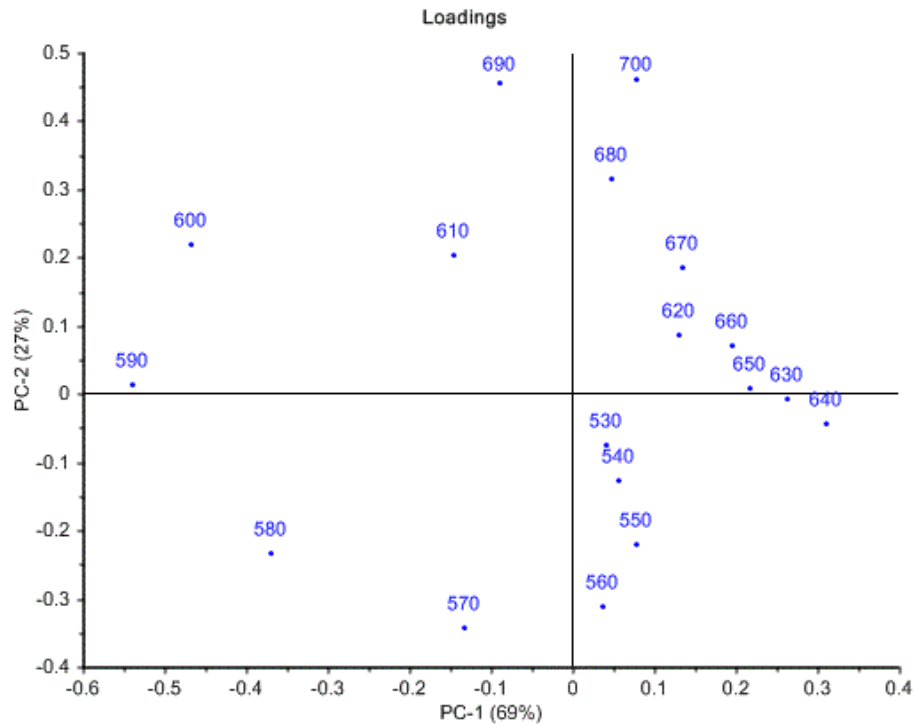
CHAPTER FIVE



**Figure 5-16:** Ratio calculations for derivative spectral intensity for Bookartoo (shown in red), Moana (shown in blue) and Wilgie Mia (shown in green). The error bars represent a standard deviation.



**Figure 5-17:** Results of principle component analysis for PC1 vs PC2 performed on all Wilgie Mia (shown in black), Bookartoo (shown in bright red) and Moana (shown in dark red) samples classified to be red in colour using only wavelengths 530-700nm.



**Figure 5-18:** Loadings plot corresponding to the PCA data shown in Figure 5-17.

### 5.3.2. Conclusions

The i1pro instrument has been successfully applied to fifty seven ochres from Moana (28 ochres), Wilgie Mia (14 ochres) and Bookartoo (15 ochres). Samples from each site exhibited red, orange, brown and yellow hues. Spectral analysis was combined with statistical analysis utilising principal component analysis and demonstrated that the i1Pro successfully examined the ochres from each individual site and distinguished between the ochre based on colour.

Analysis then progressed to comparisons between sites and, despite many spectral similarities, PCA yielded promising results. Clusters were successfully formed based on colour, with clear distinctions made between yellow, orange and red independent of the source.

When comparing ochres of the same colour from various sites, yellow and orange samples were able to be distinctly separated based on location. However, only a small number of samples were present for some colour/location combinations, and statistical analysis is difficult on low sample numbers. Red ochre was studied in the greatest depth due to its cultural significance as well as the large number of samples available. Both spectrally and with PCA, the red ochre from Moana was shown to be significantly different to the red ochre from Bookartoo and Wilgie Mia, and was easily distinguishable. The red ochre from Bookartoo and Wilgie Mia exhibited a number of similarities, making complete separation difficult. However, a number of subtle differences in the spectra exist, and PCA highlighted these and as a result was able to achieve approximate but incomplete separation, with some overlap present between the two clusters.

Given the nature of the instrument and the limitations of traditional methods that the I1Pro is able to overcome, these results are very promising. They suggest the possibility of a fast, transportable, affordable and non-destructive screening method that may be able to preliminarily identify ochre and, with statistical accuracy, exclude sites as possible sources of a material.

#### 5.4. Neutron activation analysis

In order to investigate this further, Neutron Activation Analysis (NAA) was performed on a number of the samples tested from Wilgie Mia, Moana and Bookartoo, and the results compiled and analysed. Analysis was performed on 61 samples, some of which are duplicated of the same ochre numbers. Of these, 13 were from Bookartoo, 20 from Wilgie Mia and 28 from Moana. The ochre numbers sampled are shown in Table 5-2. The raw data obtained from the NAA is given in Appendix C, and descriptive statistics of all the data obtained are shown in Table 5-3.

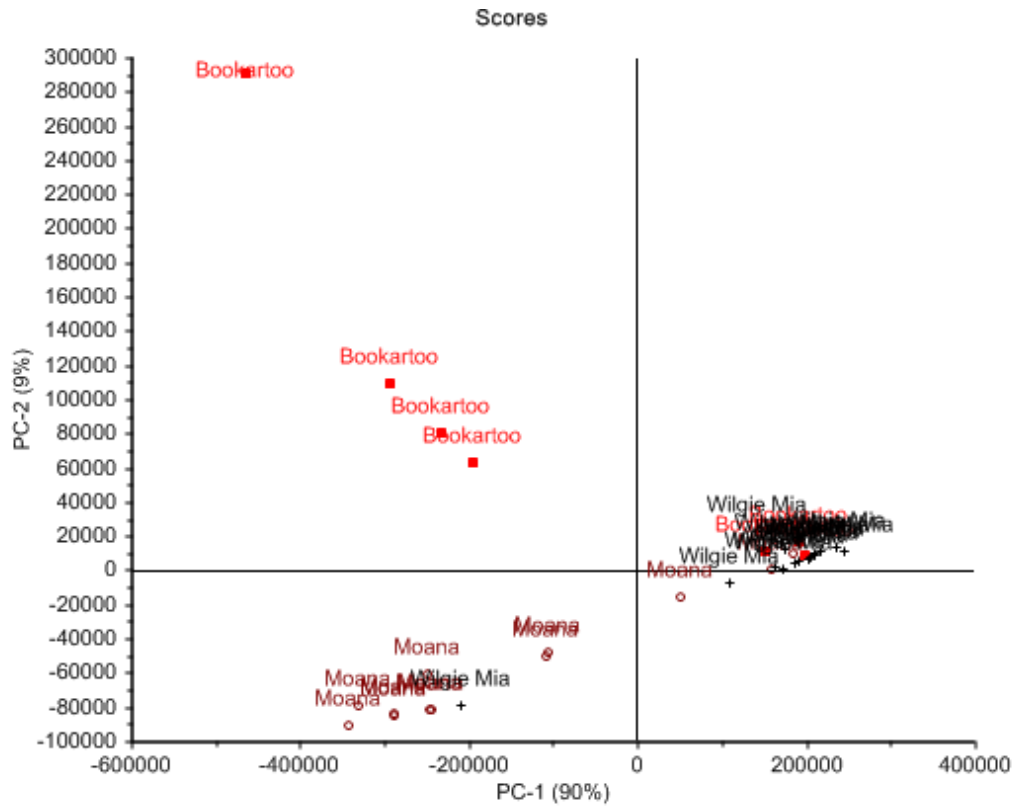
Initial PCA analysis was performed on all data. Analysis was performed using an uncentred SVD algorithm with a leverage validation method. All variables were given equal weighting. Results of this are shown in Figure 5-19 where PC1 and PC2 explain 99% of the variance.

Results of this analysis show basic grouping of samples based on location, with some overlap present. A review of the loadings plot shows that the elements Ca, Fe, Al and K dominate the influence on PC1 and PC2. Ca seems to have the greatest effect on a number of Bookartoo samples, pulling them to the upper left quadrant, whilst Fe have a similar influence over a number of Wilgie Mia samples. This analysis is also not considering sample colour. As was performed previously, the yellow and orange samples are now excluded from the analysis, with only the red samples considered. There were 34 red samples analysed, with the elemental average detected and standard deviations (population) given in

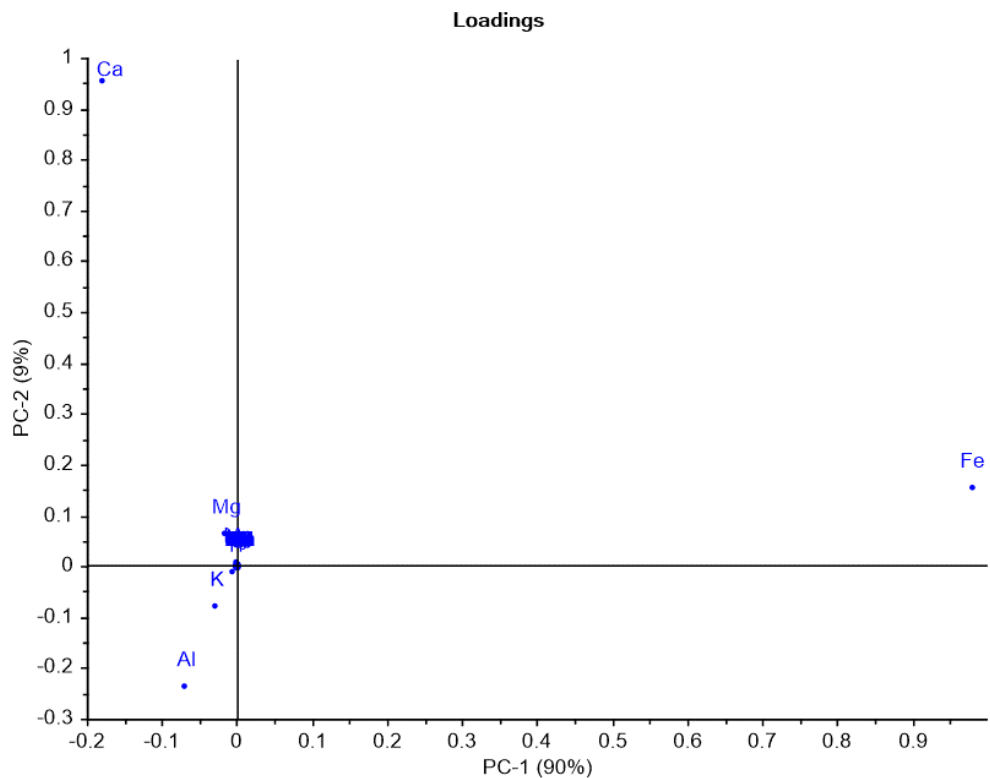
Table 5-4. Results of the PCA analysis are shown in Figure 5-21.

It can be seen from the PCA analysis, where PC1 and PC2 combine to explain 65% of the variance, that reasonable separation is achieved based on sample location. Similar to the results seen from the I1Pro colour analysis, Bookartoo appears to be more distinctly different to Wilgie Mia and Moana, which show some overlap. The loads plot shows in this case that the elements Au and Ca have the greatest impact on Bookartoo samples, pulling them to the left half, whilst Sb has the greatest influence on Wilgie Mia and K and Hg on Moana, pulling them to the upper and lower right quadrants respectively.

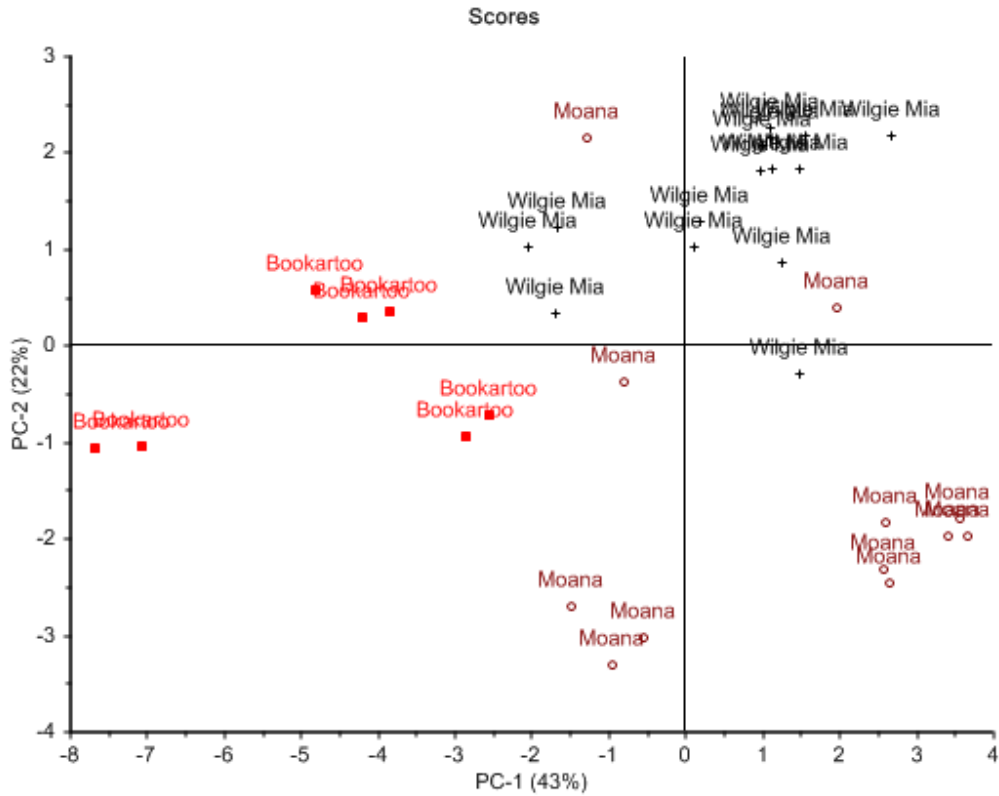
However, it can be seen from the descriptive statistics that many of these key and other elements are missing from a significant number of samples, and this may be impacting on the PCA results. In order to combat this, any elements missing from 7 or more samples (10% of the total number of samples), were excluded and analysis was repeated.



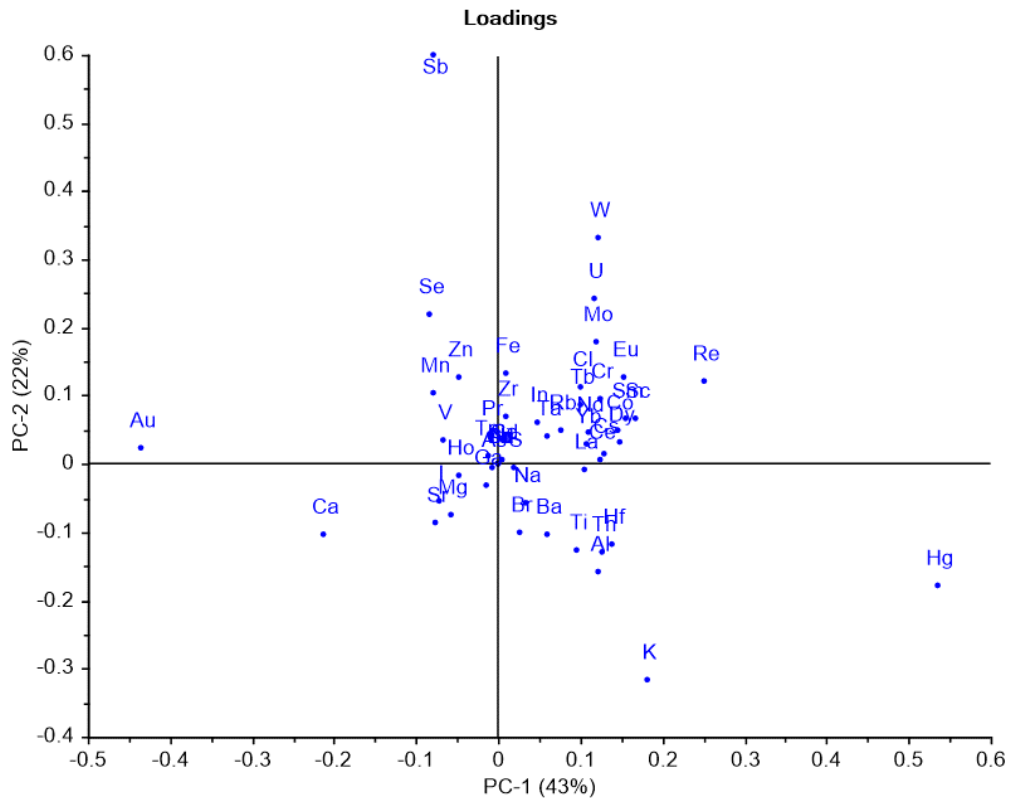
**Figure 5-19:** Results of principle component analysis for PC1 vs PC2 performed on the NAA data of all Wilgie Mia (shown in black), Bookartoo (shown in bright red) and Moana (shown in dark red) samples.



**Figure 5-20:** Loadings plot corresponding to the PCA results given in Figure 5-19.



**Figure 5-21:** Results of principle component analysis for PC1 vs PC2 performed on the NAA data of all Wilgie Mia (shown in black), Bookartoo (shown in bright red) and Moana (shown in dark red) samples classified to be red in colour.



**Figure 5-22:** Loadings plot corresponding to the PCA results given in Figure 5-21.



**Table 5-2:** Table showing the ochres utilised in NAA analysis including their database classification number, sample site and visual colour.

Ochre Number	Sample Site	Colour	Ochre Number	Sample Site	Colour
<b>OCH075</b>	Bookartoo	Red	<b>OCH275-C</b>	Moana	Red
<b>OCH076-A</b>	Bookartoo	Red	<b>OCH275-E</b>	Moana	Red
<b>OCH076-B</b>	Bookartoo	Red	<b>OCH276-C</b>	Moana	Red
<b>OCH076-D</b>	Bookartoo	Red	<b>OCH281-A</b>	Moana	Brown/Red
<b>OCH078-A</b>	Bookartoo	Red	<b>OCH283</b>	Moana	Yellow
<b>OCH079-A</b>	Bookartoo	Red	<b>OCH286</b>	Moana	Yellow
<b>OCH263</b>	Bookartoo	Red	<b>OCH287</b>	Moana	Yellow
<b>OCH302</b>	Bookartoo	Yellow	<b>OCH293</b>	Moana	Brown/Red
<b>OCH304</b>	Bookartoo	Orange	<b>OCH294</b>	Moana	Brown/Red
<b>OCH306</b>	Bookartoo	Orange	<b>OCH296</b>	Moana	Yellow
<b>OCH307</b>	Bookartoo	Orange	<b>OCH062-A</b>	Wilgie Mia	Red
<b>OCH308</b>	Bookartoo	Orange	<b>OCH063</b>	Wilgie Mia	Red
<b>OCH309</b>	Bookartoo	Yellow	<b>OCH064-A</b>	Wilgie Mia	Red
<b>OCH002-A</b>	Moana	Brown/Red	<b>OCH065-A</b>	Wilgie Mia	Red
<b>OCH019</b>	Moana	Red	<b>OCH065-B</b>	Wilgie Mia	Red
<b>OCH020-C</b>	Moana	Orange	<b>OCH067</b>	Wilgie Mia	Red
<b>OCH020-D</b>	Moana	Orange	<b>OCH117-A</b>	Wilgie Mia	Red
<b>OCH036-A</b>	Moana	Orange	<b>OCH117-E</b>	Wilgie Mia	Red
<b>OCH036-B</b>	Moana	Orange	<b>OCH117-Y</b>	Wilgie Mia	Red
<b>OCH036-C</b>	Moana	Orange	<b>OCH118-A</b>	Wilgie Mia	Red
<b>OCH037-A</b>	Moana	Red	<b>OCH119</b>	Wilgie Mia	Red
<b>OCH037-B</b>	Moana	Red	<b>OCH257</b>	Wilgie Mia	Red
<b>OCH037-C</b>	Moana	Red	<b>OCH257-A</b>	Wilgie Mia	Red
<b>OCH101-A</b>	Moana	Red/Yellow	<b>OCH258-A</b>	Wilgie Mia	Yellow
<b>OCH101-B</b>	Moana	Red/Yellow	<b>OCH260</b>	Wilgie Mia	Red
<b>OCH101-C</b>	Moana	Red/Yellow	<b>OCH260-A</b>	Wilgie Mia	Red
<b>OCH142-B</b>	Moana	Red	<b>OCH264-A</b>	Wilgie Mia	Orange
<b>OCH254-A</b>	Moana	Red	<b>OCH264-C</b>	Wilgie Mia	Orange
<b>OCH254-B</b>	Moana	Red	<b>OCH277</b>	Wilgie Mia	Red
<b>OCH254-C</b>	Moana	Red	<b>OCH277-A</b>	Wilgie Mia	Red

## CHAPTER FIVE

**Table 5-3:** Descriptive statistics obtained from the NAA analysis of the ochres given in **Table 5-2**.

	# of Missing	Mean	Max	Min	Range	Std. Deviation	Variance	RMS	Skewness	Kurtosis	Median	Q1	Q3
<b>Al</b>	0	46140.57	156900	707.1	156192.9	43885.88	1.93E+09	63429.88	1.004054	0.249516	32740	9303	73050
<b>Ar</b>	60	9.642	9.642	9.642	0	0	0	9.642	0	0	9.642	9.642	9.642
<b>As</b>	2	73.26329	555.4	2.84	552.56	109.1077	11904.49	130.6531	2.83038	8.783379	31.53	10.6	95.14
<b>Au</b>	49	5.335767	38.74	0.01821	38.72179	11.62304	135.095	12.34129	2.575762	6.873158	0.062055	0.042525	2.396575
<b>Ba</b>	24	354.4956	1703	30.6	1672.4	338.8251	114802.4	487.2031	2.453883	6.958473	261.9	181.5	371.2
<b>Br</b>	1	19.86624	124.6	0.8653	123.7347	29.38333	863.38	35.26553	2.566907	5.827109	8.5795	4.75025	16.4875
<b>Ca</b>	19	23248.49	396700	69	396631	70752.21	5.01E+09	73669.42	4.227413	19.73904	1847.5	626.8	6656.25
<b>Cd</b>	60	7.26	7.26	7.26	0	0	0	7.26	0	0	7.26	7.26	7.26
<b>Ce</b>	1	46.79449	165	1.681	163.319	40.60236	1648.551	61.73167	1.053573	0.386753	32.47	13.3425	73.0475
<b>Cl</b>	1	7974.228	55090	26.69	55063.31	12595.85	1.59E+08	14818.89	2.019671	3.360519	2342	899.25	5881.5
<b>Co</b>	0	8.760278	107.7	0.306	107.394	16.74997	280.5615	18.78043	4.690786	24.0701	5.087	2.418	7.475
<b>Cr</b>	0	97.24233	363.1	5.591	357.509	94.72739	8973.277	135.2119	1.372567	0.793686	65.44	28.78	111.5
<b>Cs</b>	29	6.408366	23.42	0.7442	22.6758	5.63869	31.79482	8.477522	1.241753	1.523717	5.9795	1.415	8.4305
<b>Cu</b>	60	247.6	247.6	247.6	0	0	0	247.6	0	0	247.6	247.6	247.6
<b>Dy</b>	5	4.707503	15.65	0.1383	15.5117	3.281204	10.7663	5.721418	0.942723	0.948364	3.7805	2.3775	7.0725
<b>Eu</b>	2	1.163319	8.787	0.07302	8.71398	1.250927	1.564818	1.700473	4.10668	23.61282	0.8871	0.4575	1.465
<b>Fe</b>	0	299909.3	695700	14830	680870	247719.5	6.14E+10	387691.4	0.490653	-1.45871	202100	100700	609400
<b>Ga</b>	36	25.59784	63.62	7.785	55.835	18.52379	343.1306	31.37935	0.991449	-0.54268	15.41	11.3	31.91
<b>Gd</b>	49	22.22433	65.38	9.982	55.39799	15.58749	242.97	26.77089	2.342206	5.60863	17.34	13.85	20.545
<b>Hf</b>	8	6.39809	31.86	0.06791	31.79209	7.00264	49.03696	9.436588	2.207837	4.796069	5.078	2.214	6.288
<b>Hg</b>	56	139.745	214.8	1.625	213.175	84.77113	7186.144	158.9899	-1.37057	1.873927	158.4	125.2	198.7
<b>Ho</b>	34	2.706922	17.1	0.6178	16.4822	3.450004	11.90253	4.335489	3.496819	12.81785	1.697	1.2365	2.5765
<b>I</b>	30	19.08809	96.75	1.649	95.101	21.3187	454.4867	28.35819	2.120989	5.023882	10.07	6.081	26.145

A STUDY INTO INTER-SITE AND INTRA-SITE VARIATION

	# of Missing	Mean	Max	Min	Range	Std. Deviation	Variance	RMS	Skewness	Kurtosis	Median	Q1	Q3
<b>In</b>	35	0.19965	0.5055	0.02104	0.48446	0.129634	0.016805	0.252845	1.274825	2.030766	0.12625	0.083265	0.355225
<b>K</b>	12	14167.21	89930	134.3	89795.7	17060.32	2.91E+08	22041.43	2.064853	6.65158	5764	1545	22710
<b>La</b>	1	23.92716	91.38	1.257	90.123	21.37026	456.688	31.96228	1.210011	0.854871	16.525	6.7	36.695
<b>Lu</b>	60	2.272	2.272	2.272	0	0	0	2.272	0	0	2.272	2.272	2.272
<b>Mg</b>	11	6085.87	87360	362.8	86997.2	12201.97	1.49E+08	13525.83	6.273768	42.23579	3949	1679	6416.75
<b>Mn</b>	0	325.893	3491	6.814	3484.186	619.2291	383444.7	695.2445	3.559747	14.15012	141.9	37.49	236.7
<b>Mo</b>	42	74.24242	216.5	4.946	211.554	78.70506	6194.486	106.679	0.879614	-1.1661	28.87	17.41	163.75
<b>Na</b>	1	4702.297	33770	70.06	33699.94	7316.403	53500000	8645.761	2.447073	5.355129	1828.5	1037.25	3785
<b>Nd</b>	19	30.07283	88.79	4.327	84.463	20.90545	437.038	36.48302	1.006721	0.718215	26.31	13.4375	39.65
<b>Ni</b>	60	98890	98890	98890	0	0	0	98890	0	0	98890	98890	98890
<b>Pr</b>	58	20.42333	24.29	15.61	8.680001	4.309168	18.56893	20.73928	-0.99086	0	21.37	18.49	22.83
<b>Rb</b>	30	132.3078	928.9	19.28	909.62	161.5662	26103.63	206.8017	4.198283	20.82349	112.6	37	165.3
<b>Re</b>	50	1.220291	3.518	0.1007	3.4173	1.406223	1.977463	1.825743	0.976421	-0.8325	0.3676	0.1437	2.233
<b>S</b>	59	56395	63990	48800	15190	10740.95	1.15E+08	56904.13	0	0	56395	52597.5	60192.5
<b>Sb</b>	9	134.2203	776.5	0.2941	776.2059	241.2742	58213.24	274.0599	1.916129	2.168741	15.625	1.01575	115.55
<b>Sc</b>	0	14.67933	67.56	0.2403	67.31969	13.95366	194.7045	20.17416	1.918648	4.081637	10.33	4.799	19.05
<b>Se</b>	51	8.726199	38.04	1.329	36.711	10.81717	117.0111	13.47267	2.648596	7.54181	4.7345	3.79375	8.98
<b>Sm</b>	0	4.652989	20.83	0.1368	20.6932	4.168554	17.37684	6.224451	1.475938	2.900784	3.64	1.56	7.183
<b>Sr</b>	45	282.6856	1877	30.88	1846.12	540.627	292277.6	594.913	2.471806	5.372114	60.865	48.44	106.525
<b>Ta</b>	31	1.01384	2.029	0.2255	1.8035	0.468356	0.219358	1.116321	0.121819	-0.21175	1.0515	0.648625	1.31575
<b>Tb</b>	20	0.874034	2.391	0.1005	2.2905	0.55755	0.310862	1.034681	0.759055	0.348017	0.8086	0.4567	1.189
<b>Th</b>	11	11.43118	30.04	0.29	29.75	9.263213	85.80711	14.65486	0.228577	-1.4707	11.565	1.70575	19.965
<b>Ti</b>	10	3930.606	15870	219	15651	3702.831	13700000	5375.107	1.245726	1.343262	1811	989.55	5672.5
<b>Tm</b>	42	0.808953	1.554	0.4293	1.1247	0.259719	0.067454	0.85669	1.320555	3.37948	0.77	0.6106	0.9509
<b>U</b>	7	16.26112	82.03	0.4255	81.6045	19.80971	392.4244	25.48692	1.319527	0.853791	4.3355	2.957	35.2425
<b>V</b>	0	321.0848	2743	21.34	2721.66	560.5047	314165.5	641.9586	3.123302	9.133474	137.8	73.9	268.1
<b>W</b>	26	33.65563	203.5	0.7489	202.7511	42.40587	1798.258	53.66176	2.081927	6.235525	11.38	3.3425	61.9
<b>Yb</b>	8	2.838187	8.773	0.2562	8.5168	1.740586	3.029641	3.321115	1.061521	1.899557	2.468	1.661	3.78

CHAPTER FIVE

	# of Missing	Mean	Max	Min	Range	Std. Deviation	Variance	RMS	Skewness	Kurtosis	Median	Q1	Q3
<b>Zn</b>	14	93.45166	996.3	8.978	987.322	154.5218	23876.98	179.1708	4.642733	25.89516	46.34	26.425	85.52
<b>Zr</b>	39	455.7454	1243	159.8	1083.2	331.1635	109669.3	558.917	1.342607	0.693003	337.8	215	594.625

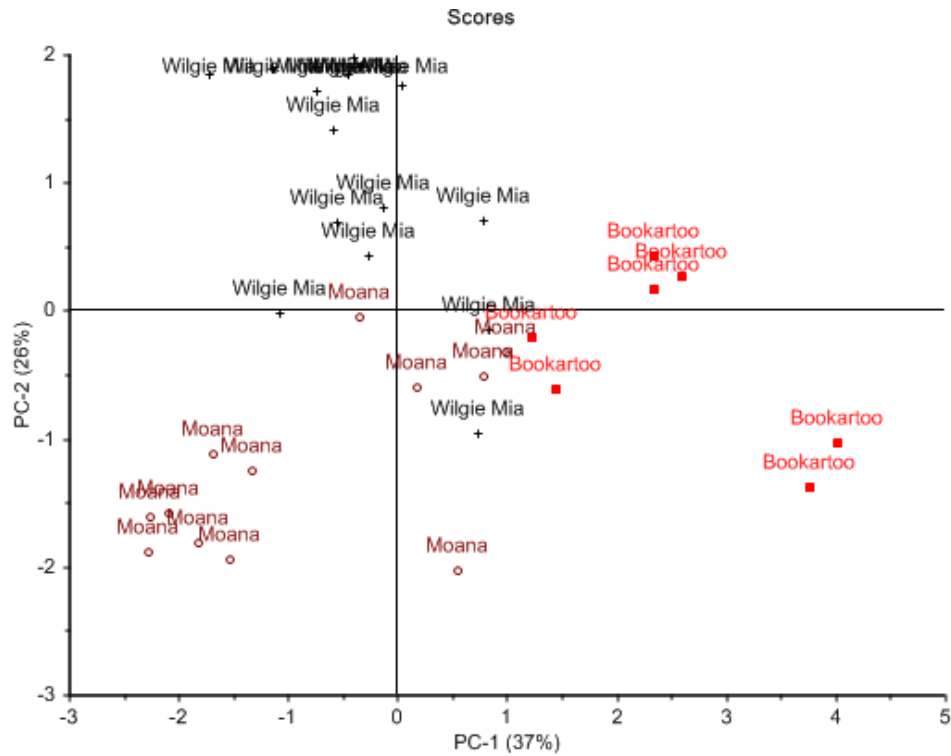
**Table 5-4:** Elemental average detected and standard deviations (population) for the 34 red samples studied.

	Average	Standard Deviation	Average	Standard Deviation	Average	Standard Deviation
	Bookartoo	Bookartoo	Moana	Moana	Wilgie Mia	Wilgie Mia
<b>Ag</b>						
<b>Al</b>	7350.0	6613.2	44143.3	25771.9	15685.1	23922.3
<b>Ar</b>			9.6	0.0		
<b>As</b>	110.8	115.8	163.6	186.0	69.6	35.9
<b>Au</b>	21.2	12.7			0.1	0.0
<b>Ba</b>	140.5	0.0	330.3	175.9	127.9	155.5
<b>Br</b>	5.9	3.8	12.9	10.6	4.5	3.1
<b>Ca</b>	143723.3	130906.7	2907.4	2215.2	3806.2	6907.8
<b>Cd</b>	7.3	0.0				
<b>Ce</b>	13.0	10.5	61.5	48.2	31.6	26.0
<b>Cl</b>	909.8	805.3	863.1	583.3	2317.7	1435.9
<b>Co</b>	1.1	0.9	14.1	20.0	12.0	25.8
<b>Cr</b>	18.5	7.9	64.3	27.2	177.4	109.6
<b>Cs</b>	1.1	0.1	5.8	2.9		
<b>Cu</b>					247.6	0.0
<b>Dy</b>	0.8	0.7	6.1	4.7	3.4	2.0
<b>Er</b>						
<b>Eu</b>	0.2	0.1	1.2	0.9	1.9	2.0
<b>Fe</b>	376262.9	231274.7	298100.0	181183.8	615793.3	105259.9
<b>Ga</b>			17.7	6.7	22.4	20.7

	Average	Standard Deviation	Average	Standard Deviation	Average	Standard Deviation
	Bookartoo	Bookartoo	Moana	Moana	Wilgie Mia	Wilgie Mia
<b>Gd</b>			16.6	3.2		
<b>Ge</b>						
<b>Hf</b>	0.9	0.9	7.2	6.8	1.3	0.6
<b>Hg</b>			1.6	0.0	174.3	35.0
<b>Ho</b>	17.1	0.0	2.8	3.3	1.8	0.9
<b>I</b>	77.3	19.4	13.8	8.1	3.9	1.7
<b>In</b>	0.2	0.0	0.1	0.0	0.3	0.2
<b>Ir</b>						
<b>K</b>	2542.1	1718.7	18640.7	12706.7	567.6	475.2
<b>La</b>	8.3	7.4	28.3	21.9	18.5	21.8
<b>Lu</b>			2.3	0.0		
<b>Mg</b>	17710.6	28751.7	3659.2	2854.1	2482.7	3573.6
<b>Mn</b>	1425.9	1185.9	191.9	212.3	242.4	276.0
<b>Mo</b>	14.3	0.9	29.5	18.0	85.2	76.5
<b>Na</b>	1439.1	1285.4	1421.4	602.8	1018.5	568.5
<b>Nb</b>						
<b>Nd</b>	7.9	2.5	36.5	22.4	30.9	25.1
<b>Ni</b>	98890.0	0.0				
<b>Os</b>						
<b>Pd</b>						
<b>Pr</b>			20.0	4.3		
<b>Pt</b>						
<b>Rb</b>	33.1	1.4	114.4	37.7		
<b>Re</b>			1.8	1.7		
<b>Rh</b>						
<b>Ru</b>						
<b>S</b>			56395.0	7595.0		
<b>Sb</b>	94.1	53.3	1.5	1.2	404.8	300.6
<b>Sc</b>	1.4	0.9	10.8	6.2	16.9	8.0

CHAPTER FIVE

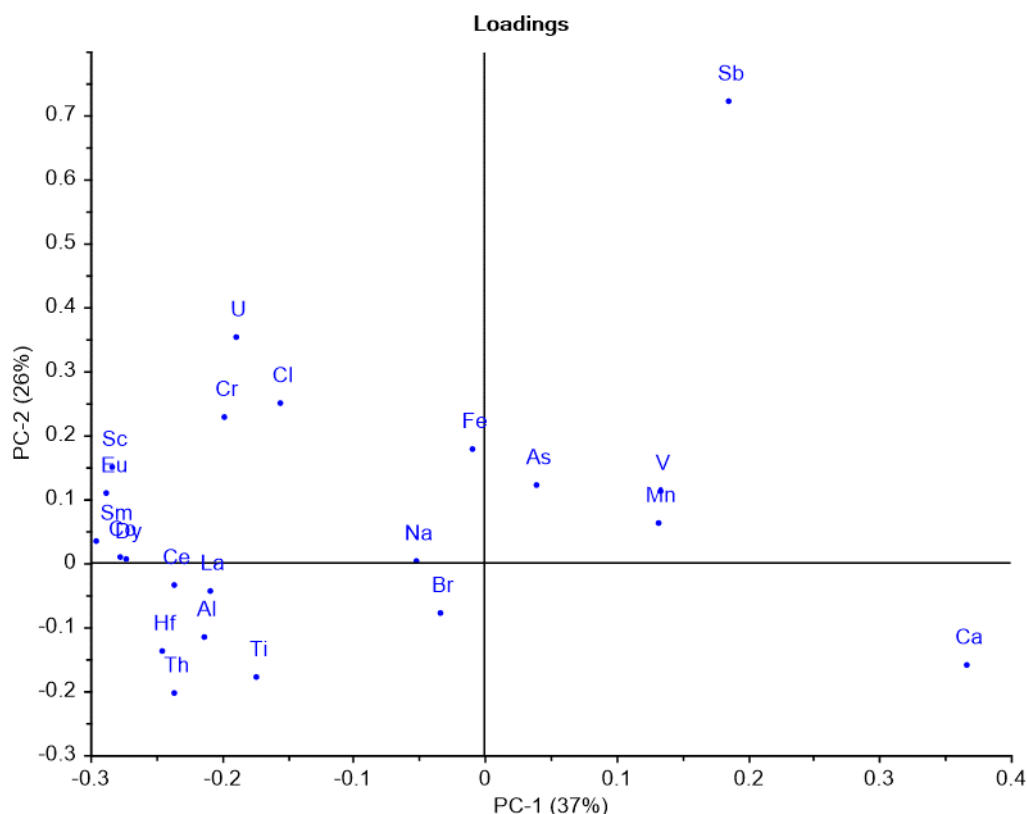
	Average	Standard Deviation	Average	Standard Deviation	Average	Standard Deviation
	Bookartoo	Bookartoo	Moana	Moana	Wilgie Mia	Wilgie Mia
<b>Se</b>			8.0	4.0	38.0	0.0
<b>Sm</b>	0.7	0.5	6.3	4.9	5.1	5.0
<b>Sn</b>						
<b>Sr</b>	311.7	206.6	496.6	719.9	72.4	38.4
<b>Ta</b>	0.2	0.0	0.8	0.2		
<b>Tb</b>	0.2	0.1	1.2	0.7	0.9	0.5
<b>Te</b>						
<b>Th</b>	1.5	1.1	12.5	8.2	1.4	0.4
<b>Ti</b>	1246.0	77.0	3109.2	2159.9	1287.2	1992.0
<b>Tm</b>			1.1	0.4		
<b>U</b>	2.3	0.9	4.6	3.1	31.7	17.0
<b>V</b>	1606.0	855.7	171.8	66.9	234.3	145.1
<b>W</b>	3.9	2.5	2.5	0.2	69.2	42.1
<b>Y</b>						
<b>Yb</b>	0.6	0.2	3.3	2.6	2.0	0.4
<b>Zn</b>	199.0	79.6	147.6	285.5	94.5	56.3
<b>Zr</b>			478.8	349.0		



**Figure 5-23:** Results of principle component analysis for PC1 vs PC2 performed on the NAA data of all Wilgie Mia (shown in black), Bookartoo (shown in bright red) and Moana (shown in dark red) samples classified to be red in colour using a reduced number of elements.

It can be seen here that the grouping is again approximately based on location. Removing the elements not contained in 90% of samples has resulted in better grouping in particular of the Moana samples, which the loadings plot now shows are heavily influenced by Th, Hf, Ti and Al, bringing the samples into the lower left quadrant. Bookartoo is drawn to the right, where the loadings plot shows it is influenced by Ca, Mn and Wilgie Mia is drawn to the upper left, influenced by U, Cr, Cl and Fe. This is reflected when examining the raw data. Consider for example, Uranium (U), where for only the red samples, Bookartoo gives an average value of 2.3, Moana of 4.6 and Wilgie Mia an order of magnitude higher at 31.7. Sb has a similar effect, with values of 94.1, 1.5 and 404.8 respectfully. The same is again seen with Ca, which has a strong influence on the lower far right region, dominated by Bookartoo, where levels are in the region of 144000 for Bookartoo and in the 2000-4000 for Moana and Wilgie Mia.

Overall, the separation between sites is good with only minor overlap. The Bookartoo samples appear more distinctly different to Wilgie Mia and Moana, especially before the number of elements was reduced. And this is interesting as it was Moana that was best separated by the i1Pro analysis seen previously. This demonstrates that traditional techniques such as NAA, where available and where experimental limitations such as sample type and size are not a strong consideration, can be used well in conjunction with the i1Pro analysis for the separation of Australian ochre samples based on site of origin.



**Figure 5-24:** Loadings plot corresponding to the PCA results given in Figure 5-23.

## 5.5. Conclusions

The i1pro instrument has been successfully applied to fifty seven ochres from Moana (28 ochres), Wilgie Mia (14 ochres) and Bookartoo (15 ochres). Samples from each site exhibited red, orange, brown and yellow hues. Spectral analysis was combined with statistical analysis utilizing principle component analysis and demonstrated that the i1Pro could successfully examine the ochres from each individual site and distinguish between the ochre based on colour.

Analysis then progressed to comparisons between sites and, despite many spectral similarities, principal component analysis yielded promising results. Clusters were successfully formed based on colour, with clear distinctions made between yellow, orange and red independent of the source.

When comparing ochres of the same colour from various sites, yellow and orange samples were able to be distinctly separated based on location. However, only a small number of samples were present for some colour/location combinations, and statistical analysis is difficult on low sample numbers. Red ochre was studied in the greatest depth due to its cultural significance as well as the large number of samples available. Both spectrally and with principle component analysis, the red ochre from Moana was shown to be significantly different



to the red ochre from Bookartoo and Wilgie Mia, and was easily distinguishable. The red ochre from Bookartoo and Wilgie Mia exhibited a number of similarities, making complete separation difficult. However, a number of subtle differences in the spectra exist, and principle component analysis highlighted these and as a result was able to achieve approximate but incomplete separation, with some overlap present between the two clusters.

Given the nature of the instrument and the limitations of traditional methods that the i1pro is able to overcome, these results are very promising. They suggest the possibility of a fast, transportable, affordable and non-destructive screening method that may be able to preliminarily identify ochre and, with statistical accuracy, exclude sites as possible source material.

Neutron activation analysis was then performed on a number of the samples tested from Wilgie Mia, Moana and Bookartoo, and the results compiled and analysed. Results of this analysis show basic grouping of samples based on colour and location, with some overlap present. Studies then focused on only the samples appearing visually red in colour. A number of attempts were made to improve the distinction between the groupings, including removing any elements not present in at least 90% of the samples. Results of NAA analysis were inconsistent with the results obtained from the i1Pro analysis, with Bookartoo samples appear more distinctly different to Wilgie Mia and Moana, especially before the number of elements was reduced. This demonstrates that traditional techniques such as NAA, where available and where experimental limitations such as sample type and size are not a strong consideration, can be used well in conjunction with the i1Pro analysis for the separation of Australian ochre samples based on site of origin.

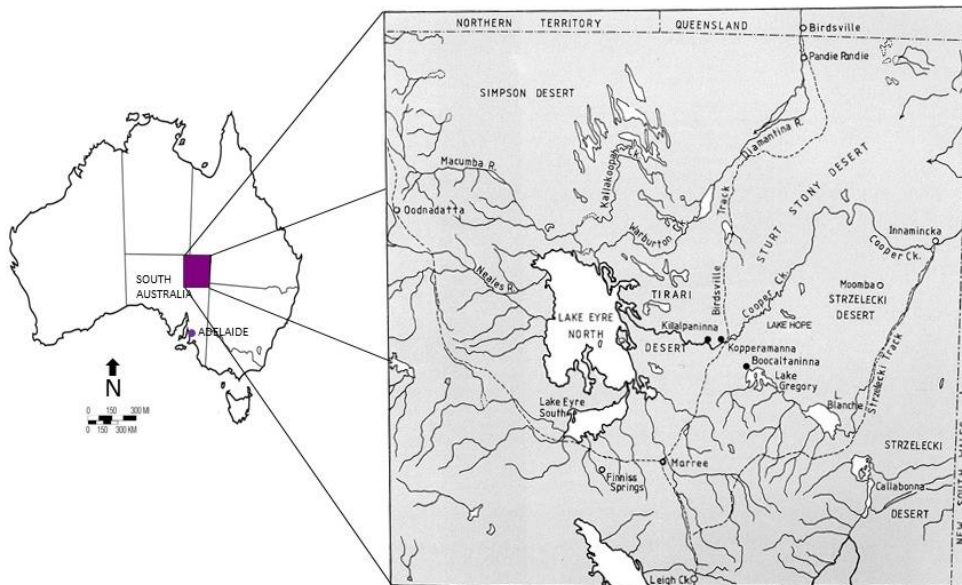


**CHAPTER SIX:  
A CASE STUDY WITH  
THE APPLICATION OF  
THE i1PRO SYSTEM  
TO TOAS**

## 6.1. Background information

Toas are small sculptures, primarily ranging from 15 to 45cm in length traditionally prepared by Australian Aboriginals [162]. They are typically wooden, and usually consist of a carved head on a cylindrical rod. The head shape varies greatly and may be represented by a boomerang-shape, an animal head, a small knob shape, hand shaped, geometrical shapes or tufted with materials such as feathers, twigs, hair or leaves. Toas are decorated with a number of materials including, but not exclusive to ochre, gypsum, and straw. The toas were placed in the ground such that they acted as signposts [163].

The toas used in this study are known as part of the Reuther Collection, as they were obtained by Pastor J.G. Reuther. The collection contains approximately 385 toas of various forms, including resin sculptures of dogs. They were made in the vicinity of the Killalpaninna Lutheran Mission in the Lake Eyre region in north-eastern South Australia between 1890 and 1905 [164]. Along with the toas, Ruther collected a set of four raw red ochre specimens. It was questioned whether these ochres were the source of ochre used on the toas he collected.



**Figure 6-1:** Map showing the location of the toas collection with respect to Australia and (insert) map of the Lake Eyre region.

Very little is known about the individual sculptors of the toas. It is not known if they were of a single gender or both, if their ages varied, and even if their locations varied. Culturally this is a great pity as it results in a lack of understanding on our behalf as to how the makers of the toas stood in relation to the specific symbols and messages on the sculptures [164]. Scientifically it is also significant because if the location of manufacture varied then the likelihood of multiple sources of ochre being used in the sculptures manufacture greatly increases.

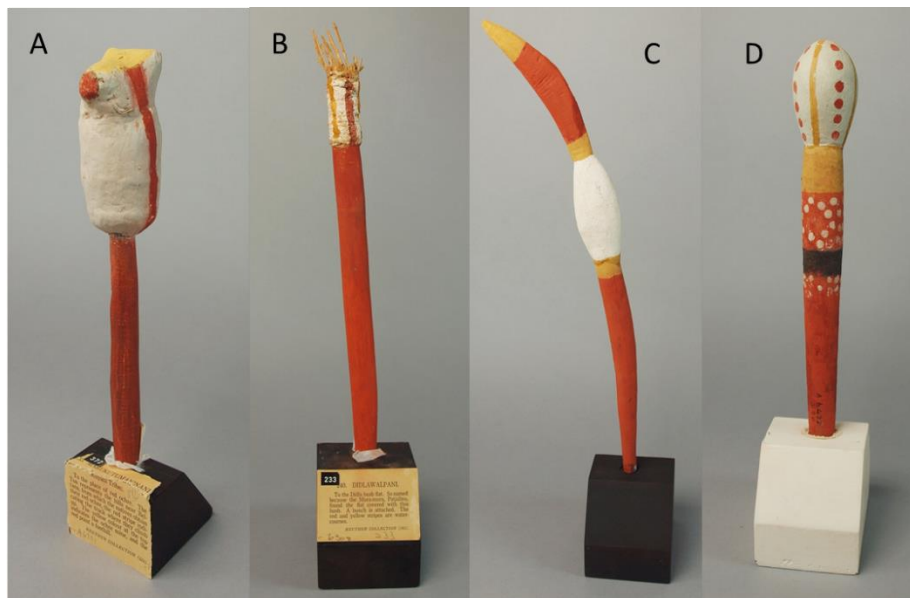
**Table 6-1:** Table showing the toas used in this study including their museum reference number and the colour components studied.

<b>Museum Reference Number</b>	<b>Red Component Examined</b>	<b>Yellow Component Examined</b>
<b>A6106</b>	Yes	Yes
<b>A6301</b>	Yes	Yes
<b>A6153</b>	Yes	
<b>A40876</b>	Yes	Yes
<b>A6190</b>	Yes	Yes
<b>A6195</b>	Yes	
<b>A6178</b>	Yes	Yes
<b>A40862</b>	Yes	Yes
<b>A68458</b>	Yes	
<b>A6222</b>	Yes	
<b>A40858</b>	Yes	
<b>A6490</b>	Yes	
<b>A6418</b>	Yes	
<b>A6419</b>	Yes	
<b>A6415</b>	Yes	
<b>A6501</b>	Yes	
<b>A6475</b>	Yes	
<b>A6172</b>	Yes	Yes
<b>A6477</b>	Yes	Yes
<b>A6308</b>	Yes	Yes
<b>A2176 (raw)</b>	Yes	
<b>A66497 (raw)</b>	Yes	
<b>A2175 (raw)</b>	Yes	
<b>A2174 (raw)</b>	Yes	
<b>A66498 (raw)</b>	Yes	
<b>A66499 (raw)</b>	Yes	

The decision to focus on the haematite chromophore was made because the collection also contains four samples of raw, powdered red ochre collected by Pastor J.G. Reuther, and it is hoped that the ochre used on the toas can be linked to one of these samples.

## **6.2. Toas investigated**

This study examines twenty of the toas and a set of six raw red ochres from the Reuther collection held by SA Museum. Museum access numbers are given in Table 6-1. The items were selected to represent a cross section of the differing styles of toas present within the



**Figure 6-2:** Photographic example of some of the toas studied (A) A6301 (B) A6308 (C) A6178 and (D) A6477.



**Figure 6-3:** Photographic example of some of the toas studies (A) A40876 (B) A40862 (C) A6190 and (D) A6172.

### 6.3. Experimental methods

UV/visible reflectance spectra were collected over the range 430–700nm using the X-Rite i1Pro. The instrument was placed at the surface of the toa and measurements acquired at 10nm intervals. Spectra for each toa was collected from a minimum of five alternate sites, with a minimum of five replicates from each site (twenty-five measurements in total). A Q-test, was applied to determine if any of the twenty-five measurements was an outlier. The spectra were

normalised to their maxima before the derivatives taken. Where appropriate, the spectra was subsequently averaged to give a single spectra per toa which is then analysed statistically utilising cluster analysis.

A subsample of approximately 0.01 grams of each of the six raw powdered sources was collected and rubbed into a single piece of Fuji Xerox 80 g/m<sup>2</sup> white laserprint paper to form a circle approximately 2.5cm in diameter, with complete and uniform coverage. As with the toas, each sample was then measured at a minimum of five alternate sites, with each sample site measured utilising the i1Pro a minimum of five times, before statistical analysis for outliers, normalisations, derivitisations and signal averaging was applied.

The statistical analysis is completed using MiniTab (Version 15.1.30.0), with multivariate single linkage Euclidean distance cluster variables analysis with separation based on the samples similarities over the region of 450-670nm, where the greatest sample variation is seen and the standard deviation has been shown to be less than half of one percent. The formation of clusters represents significant similarities in the colour of the ochres examined, such that the source of the ochre may be said to be the same.

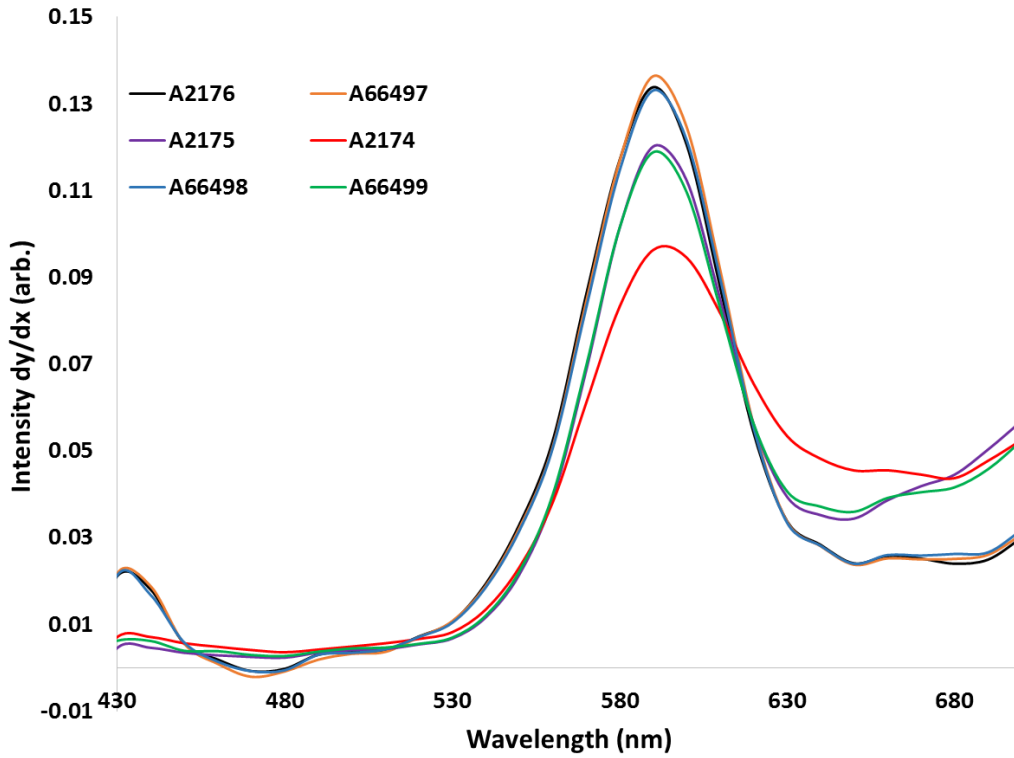
Further statistical analysis was performed using The Unscrambler version X 10.0.1. The data utilised here is the raw i1Pro data, which is then normalized and the first order derivative taken. A Q-test is then applied and any outliers removed before all subsamples are averaged to give a single data set per ochre. Statistical studies will focus on the use of principal component analysis (PCA) where a mean uncentred singular value decomposition algorithm was used. A random cross validation or leverage method was utilised incorporating twelve segments with seven component outputs requested. Variables were evenly weighted.

## **6.4. Results and discussion**

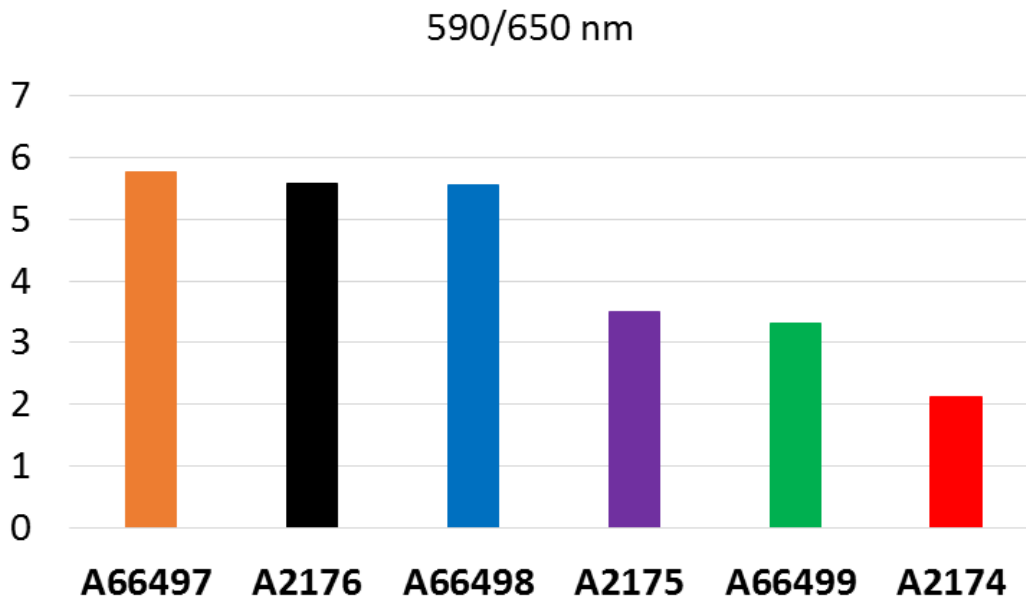
### **6.4.1. Raw ochre samples**

The reproducibility of the six individual raw ochre samples suspected of possibly being source material for some of the ochre was good. No outliers were detected for any sample. Results of the averaged derivative spectra are shown below in Figure 6-4, with preliminary statistical analysis given in Table 6-2 and Table 6-3. I

t can be seen in Figure 6-4 that three distinct groupings form within the spectra. A66497, A2176 and A66498 all display a similar peak maximum of approximately 0.13 at 590nm, A66499 and A2175 have a peak maximum of approximately 0.12, and A2174 has the lowest maxima of approximately 0.09, at the same wavelength. This trend is reversed with increasing wavelength with the same groupings but an opposite scale of intensity seen in the region of 650nm. This is highlighted by taking the ratio between the intensity at these points, and is shown graphically below in Figure 6-5.



**Figure 6-4:** The average normalised derivative spectra for each of the six raw ochre samples collected by Reuther at the same time as the Toas representing possible source material.



**Figure 6-5:** The ratio between the average normalised and derivatised spectra of the six raw ochre samples collected by Reuther at the same time as the toas representing possible source material at 590 and 650nm.



A CASE STUDY WITH THE APPLICATION OF THE i1PRO SYSTEM TO TOAS

**Table 6-2:** Preliminary statistical analysis performed on the average normalised derivative spectra for each of the six raw ochre samples collected by Reuther at the same time as the Toas representing possible source material.

<b>Toa</b>	<b>A2176</b>	<b>A66497</b>	<b>A2175</b>	<b>A2174</b>	<b>A66498</b>	<b>A66499</b>
<b>Maximum</b>	0.133805	0.136329	0.120106	0.096252	0.133054	0.118797
<b>Max at</b>	590	590	590	590	590	590
<b>Minimum</b>	-0.00081	-0.00212	0.002298	0.003534	-0.00083	0.002666
<b>Min at</b>	470	470	470	480	470	480
<b>Minimum (590-700nm)</b>	0.023956	0.023701	0.034346	0.043674	0.023925	0.035925
<b>Min (590-700nm) at</b>	680	650	650	680	650	650
<b>Median</b>	0.024895	0.025055	0.035146	0.043674	0.025949	0.037107
<b>590/470</b>	-166	-64.4444	48.91839	23.72771	-159.978	40.73755
<b>590/690</b>	5.37477	5.243098	2.388774	2.018441	5.008893	2.597525
<b>590/650</b>	5.570114	5.752014	3.496976	2.118015	5.561242	3.306838
<b>Peak width at half maxima (nm)</b>	50	50	40	40	50	40

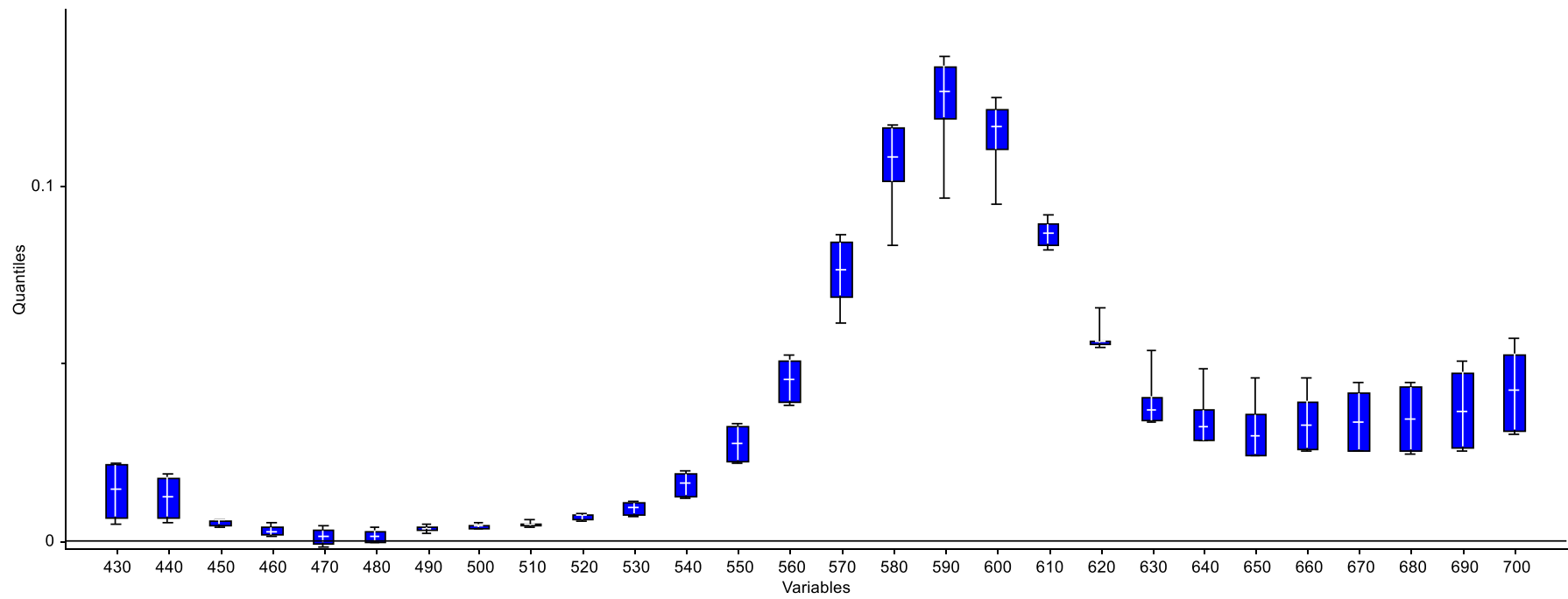
CHAPTER SIX

**Table 6-3:** Preliminary statistical analysis performed on the average normalised derivative spectra for each of the six raw ochre samples collected by Reuther at the same time as the Toas representing possible source material.

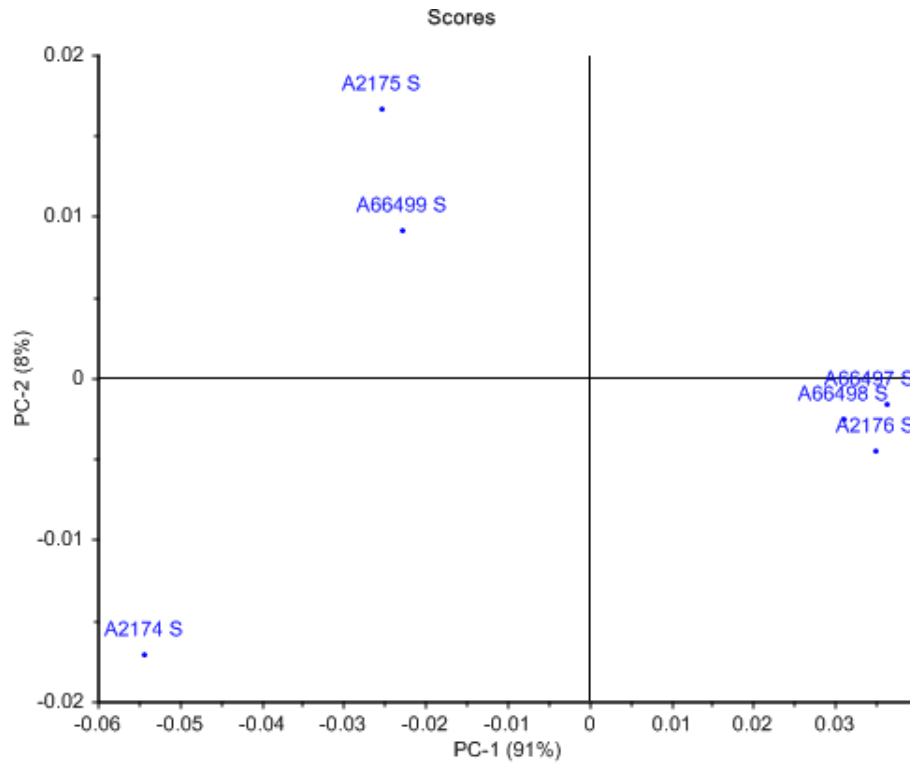
Wavelength	Mean	Max	Min	Range	Std Deviation	Variance	RMS	Skewness	Kurtosis	Median	Q1	Q3
430	0.013622	0.043096	0.006901	0.036195	0.006621	4.38E-05	0.015092	3.574547	15.78883	0.011914	0.010367	0.015788
440	0.011516	0.029726	0.007672	0.022054	0.004238	1.80E-05	0.012244	3.233819	13.38046	0.010579	0.009539	0.012029
450	0.006574	0.018466	0.004011	0.014455	0.002761	7.62E-06	0.00711	3.372796	13.68827	0.006052	0.00527	0.006838
460	0.00481	0.014513	0.002476	0.012036	0.002443	5.97E-06	0.005374	2.870613	9.733599	0.004173	0.003664	0.004896
470	0.003188	0.009537	0.00101	0.008527	0.001945	3.78E-06	0.003716	2.100769	4.833729	0.002613	0.00223	0.003795
480	0.002847	0.009026	0.000512	0.008514	0.001905	3.63E-06	0.003405	2.515326	6.701538	0.002382	0.00184	0.003209
490	0.004583	0.01304	0.002473	0.010567	0.00223	4.97E-06	0.005078	2.913882	9.047585	0.00426	0.003503	0.00466
500	0.005863	0.014706	0.003835	0.010871	0.002263	5.12E-06	0.006269	2.956466	9.607041	0.005399	0.004802	0.005852
510	0.006371	0.014568	0.004134	0.010434	0.00218	4.75E-06	0.00672	2.616789	7.912024	0.005671	0.005292	0.006649
520	0.007487	0.016029	0.005433	0.010596	0.002303	5.31E-06	0.007821	2.428157	7.025584	0.006729	0.006023	0.008025
530	0.008859	0.016458	0.006843	0.009615	0.002083	4.34E-06	0.009091	2.46649	6.835742	0.008422	0.007652	0.009055
540	0.013921	0.021601	0.011496	0.010104	0.002196	4.82E-06	0.014086	2.089075	5.065886	0.013105	0.01271	0.014363
550	0.023802	0.03184	0.019872	0.011968	0.002546	6.48E-06	0.023933	1.457047	2.853726	0.023234	0.022153	0.024744
560	0.04066	0.046082	0.033656	0.012426	0.003137	9.84E-06	0.040777	-0.2141	-0.0257	0.040837	0.038815	0.042182
570	0.069288	0.079018	0.055005	0.024013	0.005204	2.71E-05	0.069476	-1.0665	1.29168	0.071267	0.067246	0.072324

A CASE STUDY WITH THE APPLICATION OF THE i1PRO SYSTEM TO TOAS

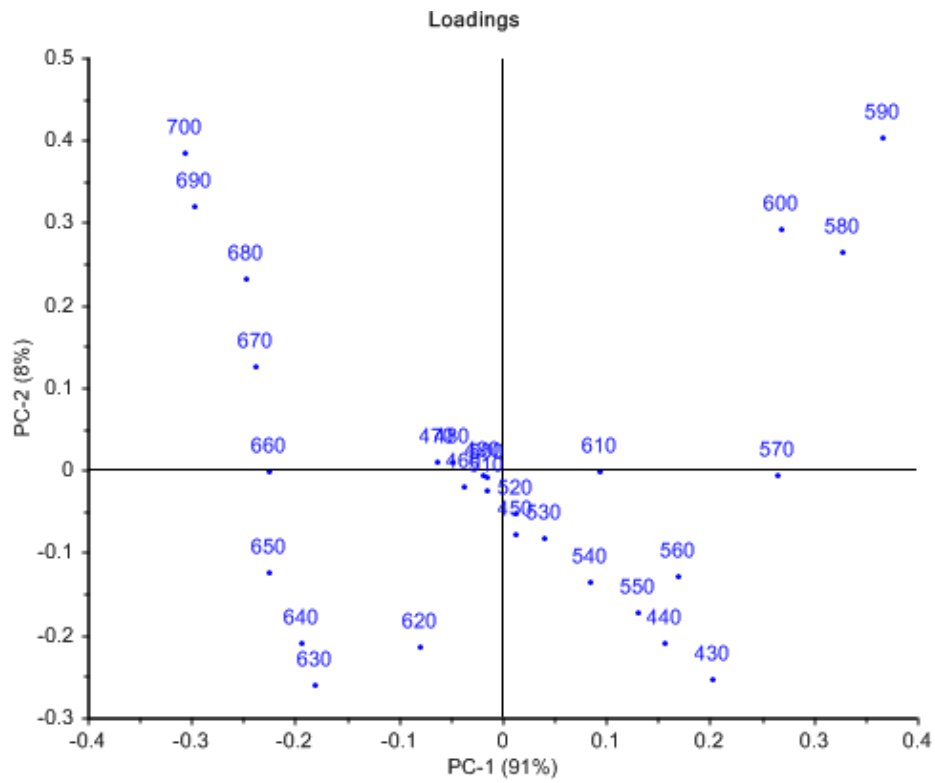
Wavelength	Mean	Max	Min	Range	Std Deviation	Variance	RMS	Skewness	Kurtosis	Median	Q1	Q3
580	0.097014	0.11141	0.0718	0.039611	0.008769	7.69E-05	0.097395	-0.99852	1.300811	0.099255	0.092638	0.102919
590	0.11138	0.124259	0.083239	0.04102	0.011408	0.00013	0.111941	-0.80664	-0.22017	0.114488	0.103624	0.121343
600	0.101847	0.114404	0.079616	0.034788	0.010424	0.000109	0.102359	-0.76312	-0.72969	0.10584	0.093214	0.110717
610	0.077093	0.084847	0.059197	0.02565	0.00637	4.06E-05	0.077346	-1.14146	0.970973	0.078158	0.075012	0.081848
620	0.053159	0.063678	0.041539	0.022138	0.004246	1.80E-05	0.053322	-0.34707	1.936552	0.054097	0.050788	0.055408
630	0.038491	0.053572	0.029235	0.024337	0.004926	2.43E-05	0.038793	0.809374	2.412172	0.038205	0.035942	0.040679
640	0.035526	0.04994	0.026297	0.023643	0.00496	2.46E-05	0.035858	0.872929	1.415502	0.034863	0.032257	0.038519
650	0.034485	0.04763	0.027516	0.020114	0.004837	2.34E-05	0.03481	0.907765	0.807802	0.034149	0.030376	0.037335
660	0.037822	0.048767	0.030965	0.017802	0.004308	1.86E-05	0.038058	0.860216	0.606923	0.037204	0.034613	0.039827
670	0.039638	0.049066	0.029454	0.019612	0.004178	1.75E-05	0.03985	0.378418	1.172124	0.038913	0.037256	0.041448
680	0.044211	0.052564	0.031096	0.021468	0.004218	1.78E-05	0.044404	-0.45518	3.088168	0.043342	0.042452	0.045732
690	0.048202	0.057203	0.029752	0.027451	0.005247	2.75E-05	0.048476	-1.32438	5.187222	0.048716	0.046191	0.050888
700	0.053349	0.064541	0.036964	0.027577	0.005095	2.60E-05	0.053583	-0.75855	3.60031	0.054235	0.05105	0.055208



**Figure 6-6:** Graphical representation of the average spectra obtained for the raw materials studied with a range and single standard deviation shown.



**Figure 6-7:** Principle component analysis results of the six raw materials studied.



**Figure 6-8:** Loadings plot generated in conjunction with the PCA results for the six raw materials studied.

The grouping of A6176, A66497 and A66498 is again repeated when examining the peak with at half maxima. Here, all three samples return a value of 50nm. The distinction between the remaining three samples is not as evident, all returning a value of 40nm despite visual differences. This is likely due to instrumental limitations where a measurement is only taken in 10nm increments.

Principal component analysis was then performed on the raw ochre material. A nonlinear iterative partial least squares (NIPALS) algorithm was utilised with a random cross-validation method requiring six segments. Data points 410 and 420 were excluded from the analysis due to previously demonstrated poor reproducibility.

When examining the principal component analysis results, shown in Figure 6-7, the three groupings discussed previously are again very clearly present. The loadings plot highlights the areas of greatest difference and influence, and this reflects well the results of spectral analysis where variation is most prominent at high wavenumbers and also in the region of 580-600nm and in the region of 630-650nm.

From these results it is possible to conclude that the six raw material samples obtained and hypothesised to be the source of the decorative material on the toas used in this study are not uniform in colour. This may be a result of large inter-site variation, or is likely due to the material not being collected from a single source.

### 6.4.2. Toas

#### 6.4.2.1. Yellow pigments

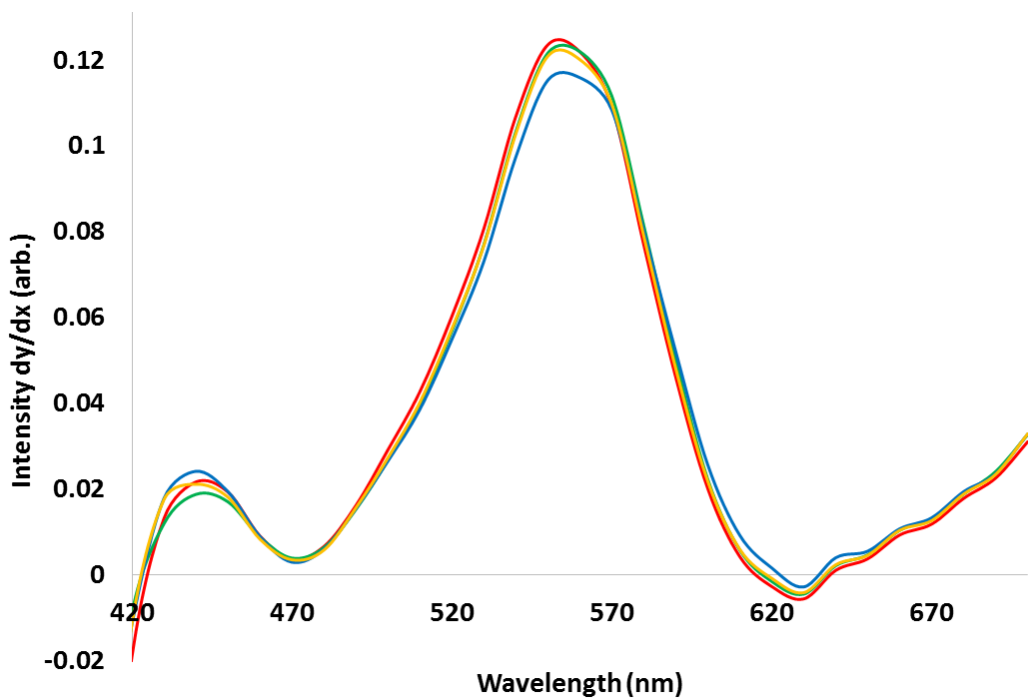
A number of the toas studied contained a yellow pigment, most likely goethite, as part of the decorate design. A small selection of these were examined using the i1pro in an attempt to determine if a single or multiple sources were used. This study was not extensive, and no possible source data exists for comparison. The number of sites studied on each toa varied based on the amount of yellow pigment present and any visually apparent differences, and is shown below in Table 6-4.

Each individual site for each toa was measured five times. Reproducibility was good and a Q-test was applied to each site with no outliers were detected. The sites within each toa were then compared, with all except three toas having every site showing good agreement between sites. An example of this good agreement within sites is shown in Figure 6-9, where each series represents the normalised and derivatised average of the five measurements taken at a single sample site on Toa A40862. All four series showing good agreement and allowing for an average to be used for this toa.

This trend of agreement continues for all the toas where the yellow pigment was examined with the exception of three, toas A6477, A40876 and toa A6190. The series representing the normalised and derivatised average of a the five measurements taken at a single sample site

**Table 6-4:** The Toas containing a yellow pigment as decoration that were examined, the number of unique sites on each toa studied, and the number of groups identified from spectral and statistical analysis.

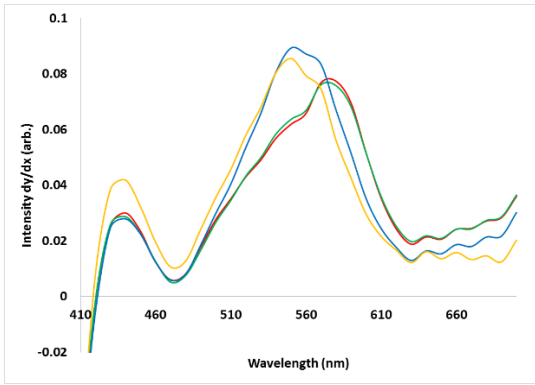
Toa Number	Number of Sites Studied	Number of Groups Identified
A40862	4	1
A6477	4	2
A6172	4	1
A6308	3	1
A6178	3	1
A6190	3	2
A6106	2	1
A40876	2	2
A6301	2	1



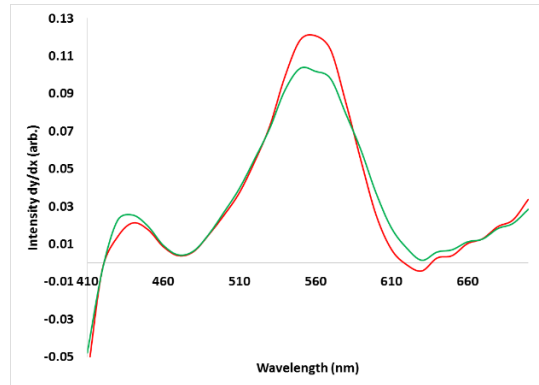
**Figure 6-9:** Each series represents the normalised and derivatised average of a the five measurements taken at a single sample site on Toa A40862, with all four series showing good agreement and allowing for an average to be used for this toa.

on each of these toas are shown below in Figure 6-10 (a), representing toa A6477, H (b), representing toa A40876 and H (c) representing toa A6190.

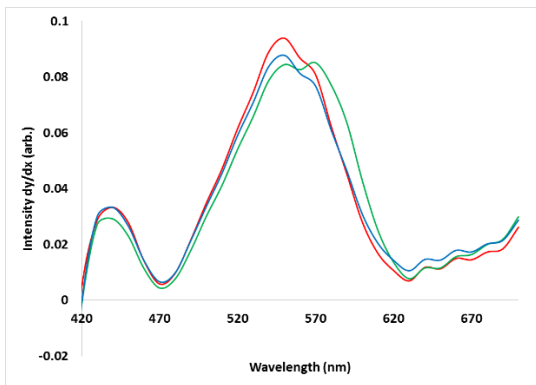
Here it can be seen that each toa exhibits two distinct groupings of spectra, and results were averaged to reflect this. For all subsequent analysis these toas will have two spectra, labelled (a) and (b) with the spectra with the highest peak maxima labelled (a).



(a)



(b)



(c)

**Figure 6-10:** Series representing the normalised and derivatised average of a the five measurements taken at a single sample site on each of these toas are shown below in Figure H (a), representing toa A6477, H (b), representing toa A40876, and H (c) representing toa A6190.

Not only are the differences within each toa apparent, but there are also clear visual differences between these toas. This is highlighted in Figure 6-12, below, where the average spectra for toas are overlaid, with statistical analysis contained in Table 6-5.

From examining Figure 6-12 and Table 6-5 and Table 6-6 it is apparent that many similarities and differences exist between the toas. All spectra demonstrate a minima of similar intensity at 430nm, and a second minima, this time of varying intensity, at 630nm. Similarly, all spectra show a peak at 430nm, and a series of small peaks trending upwards in intensity from the minima at 630nm.

Between the two minima at 470nm and 630nm is where some grouping and some significant distinctions are present within the sample set. All samples exhibit an intense maxima here, peaking between 450 and 470nm. The intensity and shape of the maxima vary greatly. Some spectra show a rounded maxima, others appear to have a double peak. The width of the peak also varies greatly. Whilst some toas group well together, for example A6308, A6172, A40862 and A40876a, there is enough variation here to suggest that multiple sources were used for the yellow decoration on the toa collection.



A CASE STUDY WITH THE APPLICATION OF THE i1PRO SYSTEM TO TOAS

**Table 6-5:** Preliminary statistical analysis on the yellow material used to decorate a selection of toas based on the normalised and derivatised average spectra per toa where statistically appropriate.

Toa	A40862	A6477a	A6477b	A6172	A6308	A6178	A6190a	A6190b	A6106	A40876a	A40876b	A6103
<b>Maximum</b>	0.120337	0.076538	0.087354	0.124371	0.126409	0.081859	0.085114	0.090829	0.134411	0.120757	0.103386	0.107478
<b>Maximum at (nm)</b>	550	570	550	560	560	550	570	550	550	560	550	550
<b>Minimum (430-700nm)</b>	-0.00426	0.005595	0.008256	-0.00573	-0.00487	0.005471	0.004397	0.006241	-0.00832	-0.00435	0.001331	-0.00261
<b>Minimum (430-700nm) at (nm)</b>	630	470	470	630	630	470	470	470	630	630	630	630
<b>Minimum (550-790nm)</b>	-0.00426	0.019278	0.012573	-0.00573	-0.00487	0.013711	0.007714	0.008766	-0.00832	-0.00435	0.001331	-0.00261
<b>Minimum (550-790nm) at</b>	630	630	630	630	630	630	630	630	630	630	630	630
<b>Median</b>	0.018584	0.027172	0.024107	0.016329	0.015654	0.025249	0.023977	0.024302	0.01579	0.018394	0.020158	0.01751
<b>Max/630</b>	-28.2255	3.970256	6.947534	-21.7053	-25.9327	5.970333	11.03403	10.36157	-16.163	-27.7524	77.69632	-41.2261
<b>560/630</b>	-28.1365	3.438955	6.619289	-21.7053	-25.9327	5.910388	10.71076	9.582329	-15.9345	-27.7524	76.53161	-36.3783
<b>560/470</b>	34.34069	11.84979	10.08074	42.98345	51.36326	14.81149	18.78899	13.45848	31.38366	32.35361	24.50104	13.61452

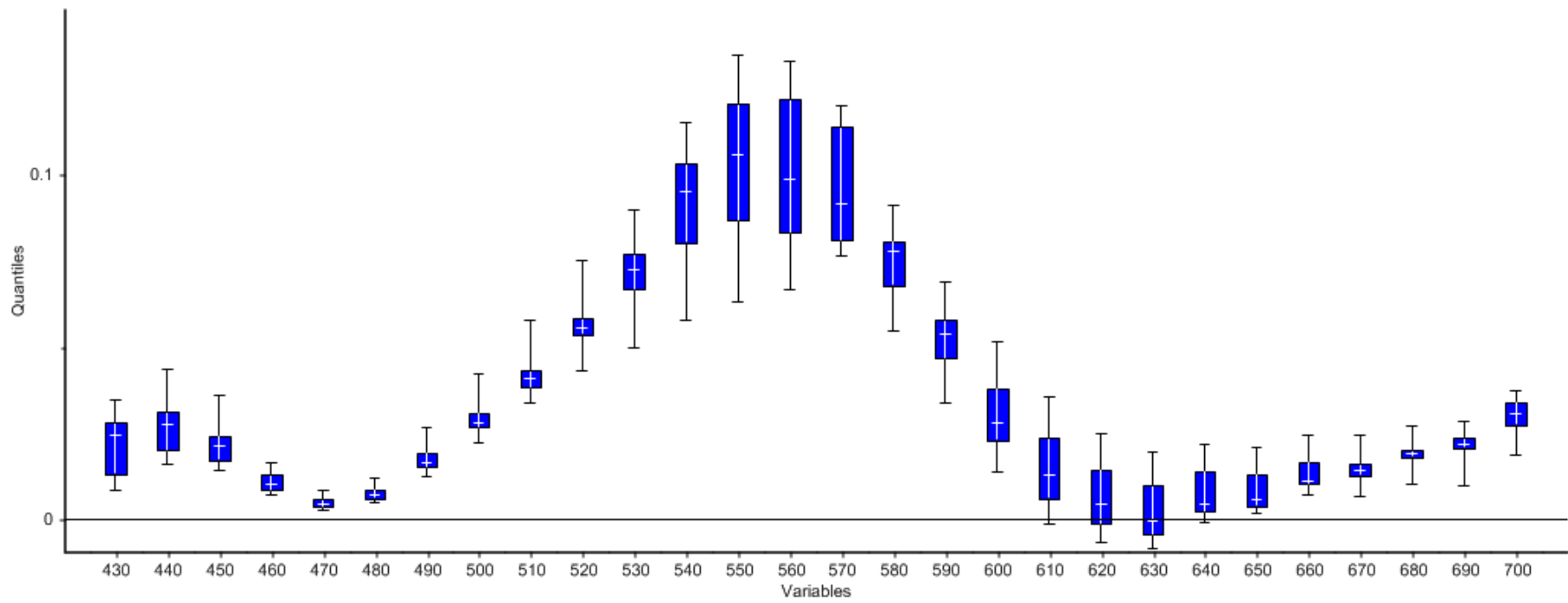
CHAPTER SIX

**Table 6-6:** Descriptive statistics on the yellow material used to decorate a selection of toas based on the normalised and derivatised average spectra per toa where statistically appropriate.

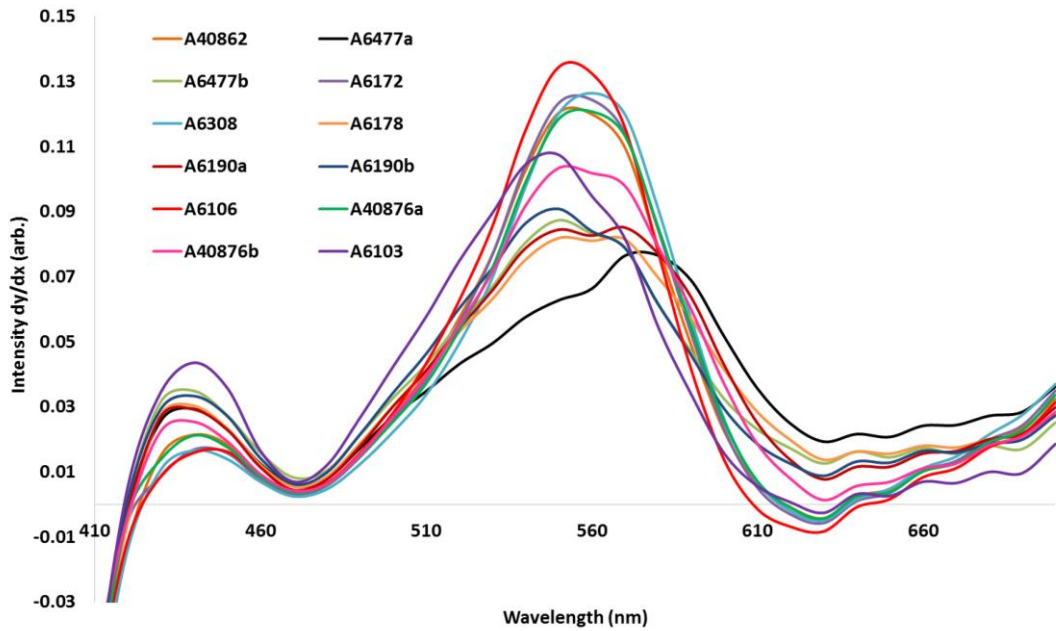
Wavelength	Mean	Max	Min	Range	Std Deviation	Variance	RMS	Skewness	Kurtosis	Median	Q1	Q3
430	0.021316	0.034595	0.008551	0.026044	0.009389	8.82E-05	0.023134	-0.18388	-1.63091	0.024221	0.013105	0.028035
440	0.026489	0.043546	0.015894	0.027652	0.008503	7.23E-05	0.027712	0.468173	-0.28591	0.027265	0.020123	0.031043
450	0.021739	0.035761	0.01392	0.021842	0.006207	3.85E-05	0.022536	0.966264	0.944796	0.021173	0.017238	0.024298
460	0.011017	0.016438	0.006949	0.009489	0.003249	1.06E-05	0.011448	0.503595	-1.07892	0.010339	0.008577	0.012898
470	0.004824	0.008256	0.002461	0.005795	0.001723	2.97E-06	0.005098	0.623134	-0.19962	0.00431	0.003673	0.005756
480	0.007623	0.011981	0.004658	0.007323	0.002172	4.72E-06	0.007901	0.74946	-0.16757	0.007106	0.006136	0.008766
490	0.017618	0.026536	0.01232	0.014216	0.0039	1.52E-05	0.018009	1.086945	1.226222	0.01645	0.015169	0.019352
500	0.029375	0.042279	0.022251	0.020027	0.005205	2.71E-05	0.029795	1.390035	2.722003	0.027724	0.026704	0.030783
510	0.041377	0.057681	0.033698	0.023983	0.006241	3.90E-05	0.041806	1.623891	3.963008	0.040701	0.038282	0.043063
520	0.05626	0.074818	0.043131	0.031687	0.007657	5.86E-05	0.056736	0.993752	2.959898	0.055403	0.053478	0.058074
530	0.071697	0.089548	0.049475	0.040073	0.010405	0.000108	0.072385	-0.32724	1.205168	0.072061	0.066641	0.076767
540	0.091084	0.114943	0.057569	0.057375	0.016012	0.000256	0.092366	-0.64509	0.209959	0.094689	0.080039	0.103025
550	0.102894	0.134411	0.062728	0.071683	0.021445	0.00046	0.104923	-0.35138	-0.75869	0.105432	0.086627	0.120181
560	0.101488	0.132511	0.066296	0.066215	0.022393	0.000501	0.103728	0.001728	-1.60024	0.098338	0.083075	0.121661
570	0.096109	0.119906	0.07643	0.043476	0.017288	0.000299	0.097524	0.197287	-2.04168	0.091508	0.080838	0.113525
580	0.074878	0.090978	0.054701	0.036277	0.010887	0.000119	0.0756	-0.5585	-0.47148	0.077449	0.06773	0.080624

A CASE STUDY WITH THE APPLICATION OF THE i1PRO SYSTEM TO TOAS

Wavelength	Mean	Max	Min	Range	Std Deviation	Variance	RMS	Skewness	Kurtosis	Median	Q1	Q3
590	0.052557	0.068841	0.033868	0.034972	0.009754	9.51E-05	0.05338	-0.24771	-0.04033	0.053454	0.046714	0.057777
600	0.030043	0.051546	0.013593	0.037953	0.0114	0.00013	0.031964	0.39869	-0.47226	0.027717	0.022906	0.038054
610	0.014904	0.035632	-0.00141	0.037042	0.011498	0.000132	0.018529	0.38279	-1.02394	0.012863	0.006128	0.023522
620	0.006877	0.024799	-0.00687	0.031665	0.010449	0.000109	0.01214	0.381	-1.30963	0.00427	-0.00127	0.014527
630	0.002769	0.019278	-0.00832	0.027594	0.009212	8.49E-05	0.009244	0.530045	-1.20344	-0.00064	-0.00448	0.009718
640	0.007862	0.021615	-0.00084	0.022452	0.007509	5.64E-05	0.010654	0.598475	-1.13587	0.004427	0.002174	0.013958
650	0.008596	0.020736	0.00161	0.019126	0.006204	3.85E-05	0.010449	0.694375	-0.73548	0.005886	0.00374	0.013245
660	0.013307	0.024166	0.006959	0.017206	0.004989	2.49E-05	0.014138	0.880611	0.36906	0.01109	0.010184	0.016634
670	0.014472	0.024377	0.006557	0.017821	0.004252	1.81E-05	0.015034	0.651358	2.626982	0.014044	0.012694	0.016039
680	0.01909	0.027219	0.009991	0.017227	0.003835	1.47E-05	0.01944	-0.3968	4.171932	0.018973	0.018124	0.020008
690	0.021572	0.028453	0.009637	0.018815	0.004876	2.38E-05	0.022072	-1.15527	2.738097	0.021665	0.020688	0.023649
700	0.030178	0.036992	0.018581	0.01841	0.005251	2.76E-05	0.030594	-0.78473	0.737869	0.03062	0.027352	0.033992

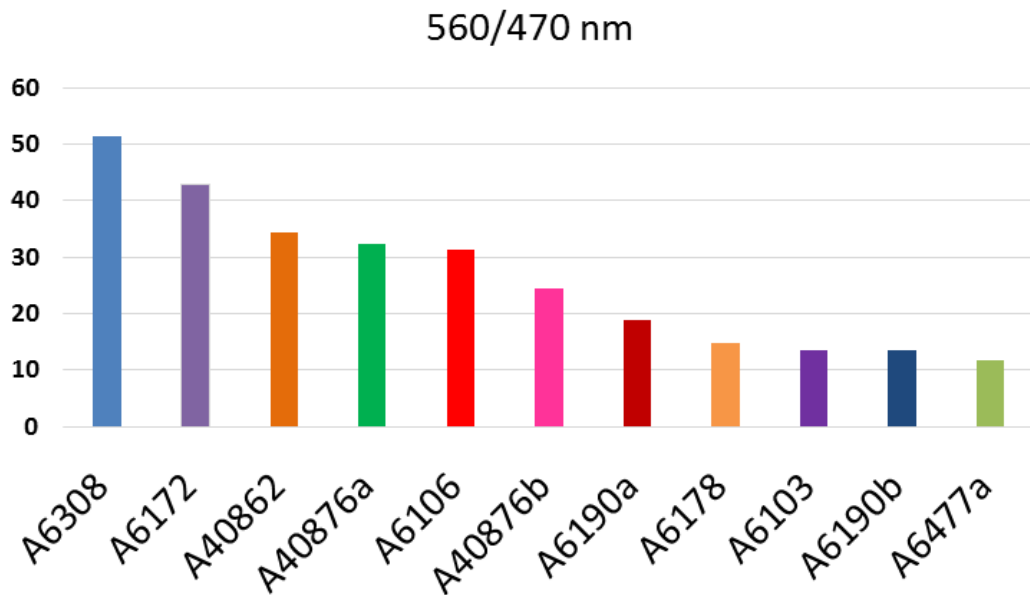


**Figure 6-11:** Graphical representation of the average spectra obtained for the yellow areas studied with a range and single standard deviation shown.



**Figure 6-12:** Series representing the normalised and derivatised average of all the measurements taken on each toa, except where statistical averaging was not applicable and multiple series exist per toa.

The groupings discussed around the maxima at 550-570nm is reflected when considering the ration between the intensity of this maxima and the minima present in all samples at 470nm. This is represented graphically in Figure 6-13.



**Figure 6-13:** The ratio of the intensities of the peak at 560nm and the minima at 470nm where the spectra underwent normalisation and derivitisation before being averaged to give a single spectra per toa where statistically appropriate.

It is clear when examining Figure 6-13 in comparison to Figure 6-12, that the groupings present using this ratio method are not entirely reflective of the visual groupings apparent in the spectra. This is most likely due to the varied shape of the spectra not being reflected in this single method. The ratio method has proved to be less accurate here than when applied to the possible source samples previously in Figure 6-5.

Results of the analysis of the yellow decorative material on the toas shows that multiple sources have been used here. It has been shown that some toas use a single source, and others suggest the use of multiple sources. There are no known raw goethite samples collected at the time of the toas for comparison.

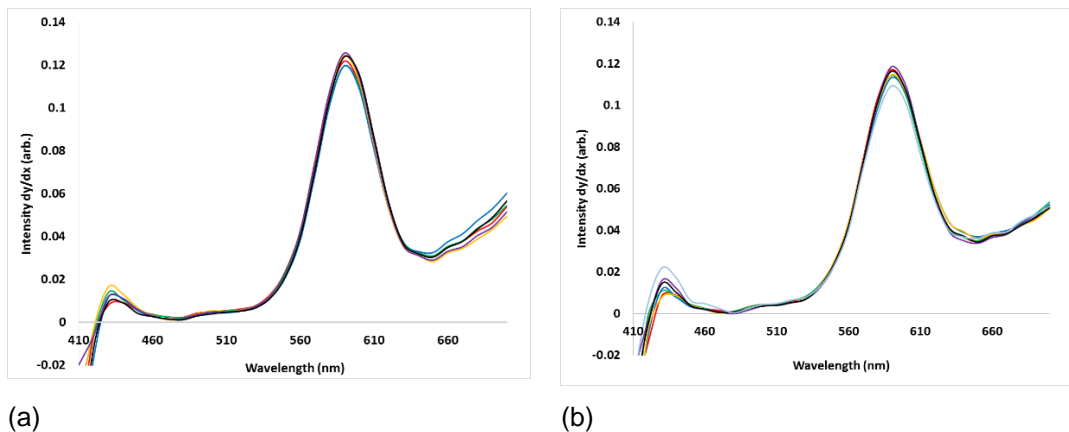
**Table 6-7:** *The Toas containing a red pigment as decoration that were examined, the number of unique sites on each toa studied, and the number of groups identified from spectral and statistical analysis.*

Toa Number	Number of Sites Studied	Number of Groups Identified
A6301	5	2
A6153	5	2
A40876	4	1
A6106	5	1
A6190	5	1
A6195	7	1
A6178	5	1
A40862	7	2
A68458	5	1
A62222	6	1
A40858	6	1
A6490	6	2
A6418	8	2
A6419	9	1
A6415	7	2
A6501	8	1
A6475	7	2
A6172	5	1
A6477	6	1
A6308	6	1

6.4.2.2. Red pigments

Studies were then focused on the red material, hypothesised to be haematite, used to decorate all the toas examined in this work. All twenty of the toas identified for this study were examined using the i1pro in an attempt to identify a single or multiple sources were used on each toa and on the collection as a whole. The number of sites studied on each toa varied based on the amount of red pigment present and any visually apparent differences, and is shown in Table 6-7.

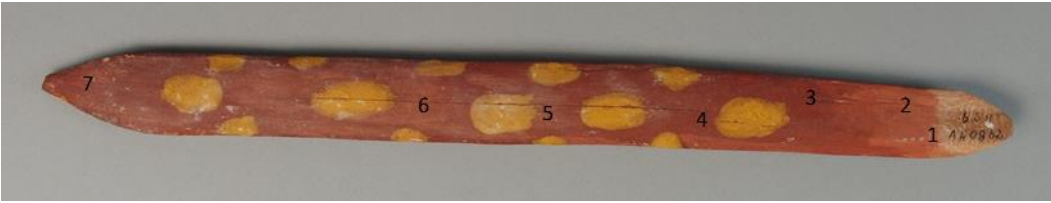
Evident in Table 6-7 is that each toa had between 5 and 9 individual sites studied, with each sites measured five times. The majority of the toas showed good grouping. Examples of this are shown below, where the normalised, derivitised and then averaged spectra for each site are shown in Figure 6-14 for two toas, A6477 shown as (a) and A6195 shown as (b). This level of agreement allows for the spectra for the whole toa to be averaged, giving a single data set per toa.



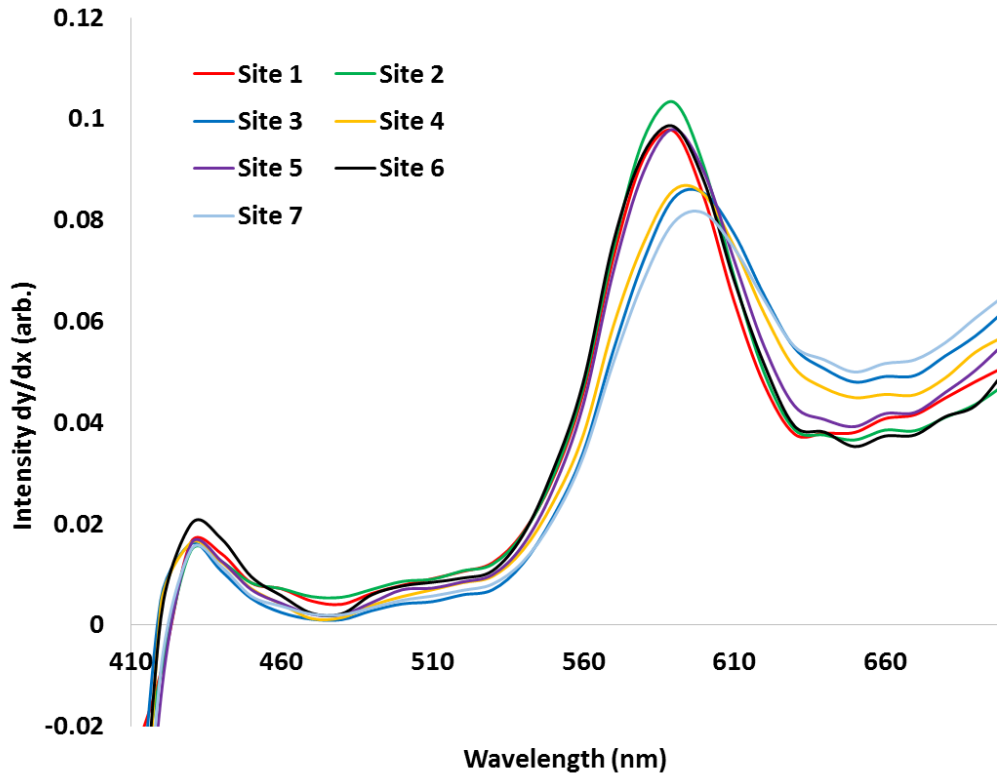
**Figure 6-14:** The normalised, derivitised and then averaged spectra for each site for two toas, A6477 shown as (a) and A6195 shown as (b), demonstrating good agreement between all sites studied on each individual toa.

Whilst the majority of the toas demonstrate this uniform trend across all sites, some show some variation with either a single site identified as an outlier or two distinct groupings present. An example of one of these cases is toa A40862, which was initially specifically chosen because the ochre, particularly the red ochre, shows significant variation in its colour. Visually, it appears as if the toa may contain multiple layers of different haematite based ochre, or may be effected by water or similar damage. Because of this variation, seven separate areas on the red coloured haematite based ochre were chosen to be sampled. These areas, along with a visual image of toa A40862, are shown in Figure 6-15.

Each of the seven sites studied was measured five times. The agreement within each site was good, allowing for the spectra to be averaged to give a single spectra per site. The normalised, derivitised and averaged spectra for each site are shown below in Figure 6-16, where the site number corresponds to the location shown visually in Figure 6-15.



**Figure 6-15:** Photographic image of toa A40862 and the seven sites studied on this toa.



**Figure 6-16:** The normalised, derivitised and averaged spectra for each site on toa A40862, where the number corresponds to the location shown visually in Figure M.

Here it can be seen that, whilst the overall trend for all spectra are similar, two distinct groups form. Sites 1, 2, 5 and 7 group together in the first of these groups and sites 3, 4 and 7 form the second group. These groups are separated clearly by a variation in both peak intensity with one group in the region of 0.1 and the other in the region of 0.8. These same groups form when examining the peak maxima location with the first group peaking at 590nm and the second at 600nm. The agreement within each grouping is statistically acceptable and a Q-test suggested no outliers.

The level of variation between groups shown here is typical of all toas identified as having two groupings, with some showing larger distinction still. In these cases, the toas will have two average spectra for further analysis, one from each grouping. These will be labelled (a) and (b) respectfully, with the series with the highest peak maxima intensity labelled (a).



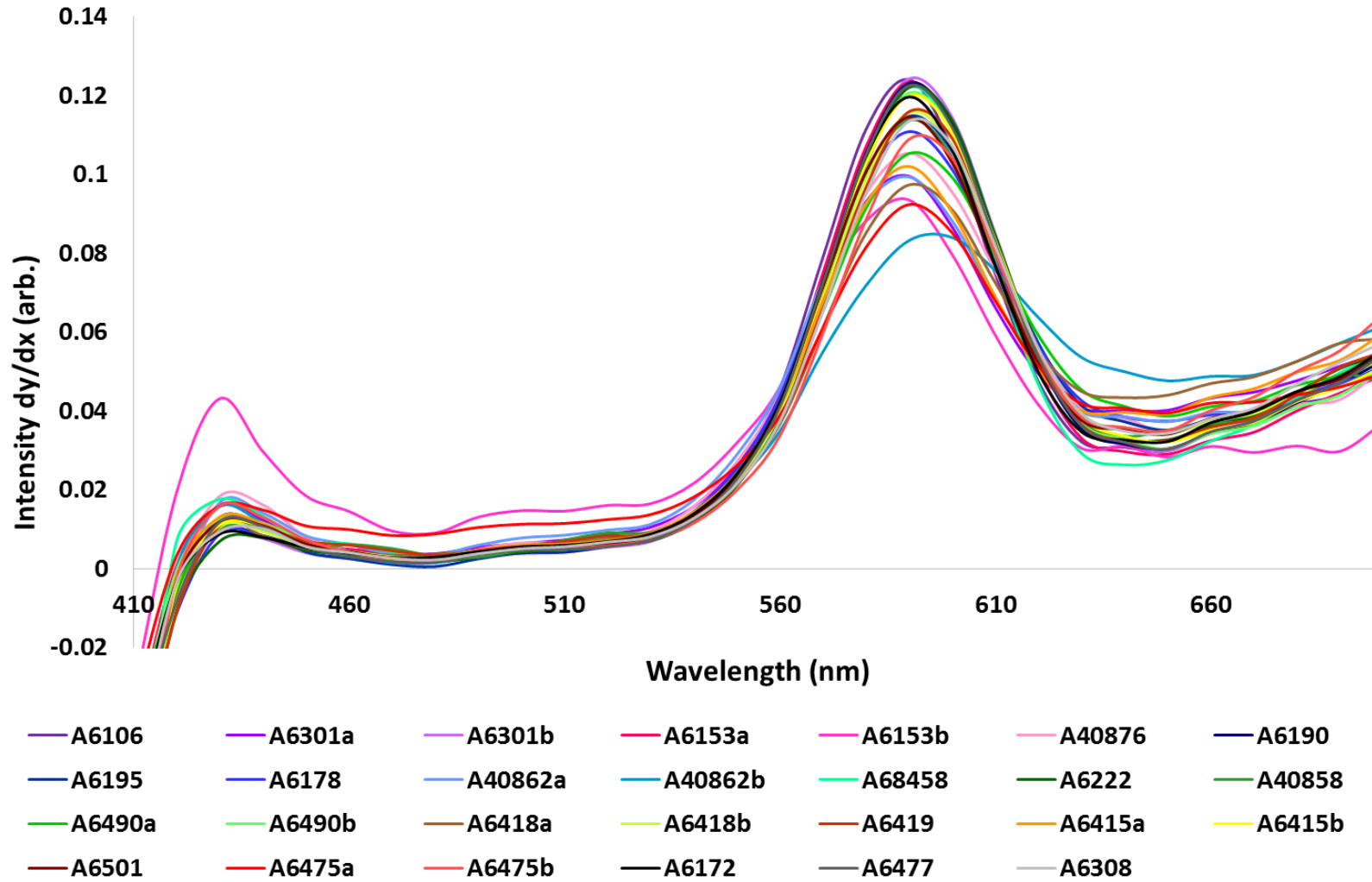


Figure 6-17: The normalised, derivitised and then averaged spectra for the red areas of all toas studied.

**Table 6-8:** Statistical analysis on the normalised, derivitised and then averaged spectra for the red areas of all toas studied.

Toa	Maximum	Maximum at (nm)	Minimum (430-700nm)	Minimum (430-700nm) at	Minimum (570-700nm)	Minimum (570-700nm) at	Median	Max/Min	590/480	590/650
<b>A6106</b>	0.124023	590	0.002198	470	0.029866	650	0.027769	56.43722	52.56696	4.031127
<b>A6301a</b>	0.099511	590	0.00376	480	0.040089	640	0.032922	26.46875	26.46875	2.482241
<b>A6301b</b>	0.124259	590	0.001315	470	0.029856	650	0.02604	94.52097	84.40966	3.956719
<b>A6153a</b>	0.123432	590	0.002749	480	0.029008	650	0.026272	44.90221	44.90221	4.159269
<b>A6153b</b>	0.093472	590	0.009026	480	0.028261	650	0.029739	10.35559	10.35559	3.013119
<b>A40876</b>	0.105368	590	0.001521	480	0.034426	650	0.030742	69.27588	69.27588	2.762855
<b>A6190</b>	0.123109	590	0.002137	480	0.030427	650	0.02683	57.61104	57.61104	3.901574
<b>A6195</b>	0.114717	590	0.000512	480	0.035125	650	0.029568	224.0838	224.0838	3.079584
<b>A6178</b>	0.110824	590	0.002382	480	0.037404	650	0.03135	46.5302	46.5302	2.878591
<b>A40862a</b>	0.099347	590	0.003442	480	0.037266	650	0.033067	28.86376	28.86376	2.577938
<b>A40862b</b>	0.08396	600	0.001503	480	0.04763	650	0.028467	55.85676	55.37734	1.666788
<b>A68458</b>	0.12206	590	0.003257	480	0.026297	640	0.024174	37.47286	37.47286	4.641607
<b>A6222</b>	0.122065	590	0.001724	480	0.032676	650	0.026862	70.81899	70.81899	3.70306
<b>A40858</b>	0.113771	590	0.002886	490	0.033607	640	0.028721	39.42382	35.99334	3.385363
<b>A6490a</b>	0.105255	590	0.001828	480	0.038662	650	0.030614	57.56795	57.56795	2.559152
<b>A6490b</b>	0.120625	590	0.002315	480	0.030325	650	0.026614	52.11051	52.11051	3.676401
<b>A6418a</b>	0.097324	590	0.003354	470	0.043363	640	0.029354	29.01514	26.49094	2.244399
<b>A6418b</b>	0.115677	590	0.002422	480	0.034149	650	0.028297	47.76791	47.76791	3.283559
<b>A6419</b>	0.115904	590	0.0034	480	0.032481	640	0.026955	34.09402	34.09402	3.56837

A CASE STUDY WITH THE APPLICATION OF THE i1PRO SYSTEM TO TOAS

Toa	Maximum	Maximum at (nm)	Minimum (430-700nm)	Minimum (430-700nm) at	Minimum (570-700nm)	Minimum (570-700nm) at	Median	Max/Min	590/480	590/650
A6415a	0.101993	590	0.002534	480	0.039301	650	0.031746	40.24517	40.24517	2.573558
A6415b	0.119961	590	0.001852	480	0.032054	650	0.027433	64.77631	64.77631	3.572199
A6501	0.114488	590	0.002456	480	0.034076	650	0.028811	46.61782	46.61782	3.249242
A6475a	0.092345	590	0.008377	470	0.039475	650	0.032483	11.02361	10.5299	2.270287
A6475b	0.108883	590	0.001858	470	0.034999	650	0.026764	58.58856	56.71345	3.041092
A6172	0.119637	590	0.002726	470	0.032234	650	0.028124	43.88674	42.09801	3.667121
A6477	0.122488	590	0.001642	480	0.030275	650	0.026492	74.58323	74.58323	3.823808
A6308	0.113487	590	0.002202	480	0.034312	650	0.027894	51.54462	51.54462	3.255206

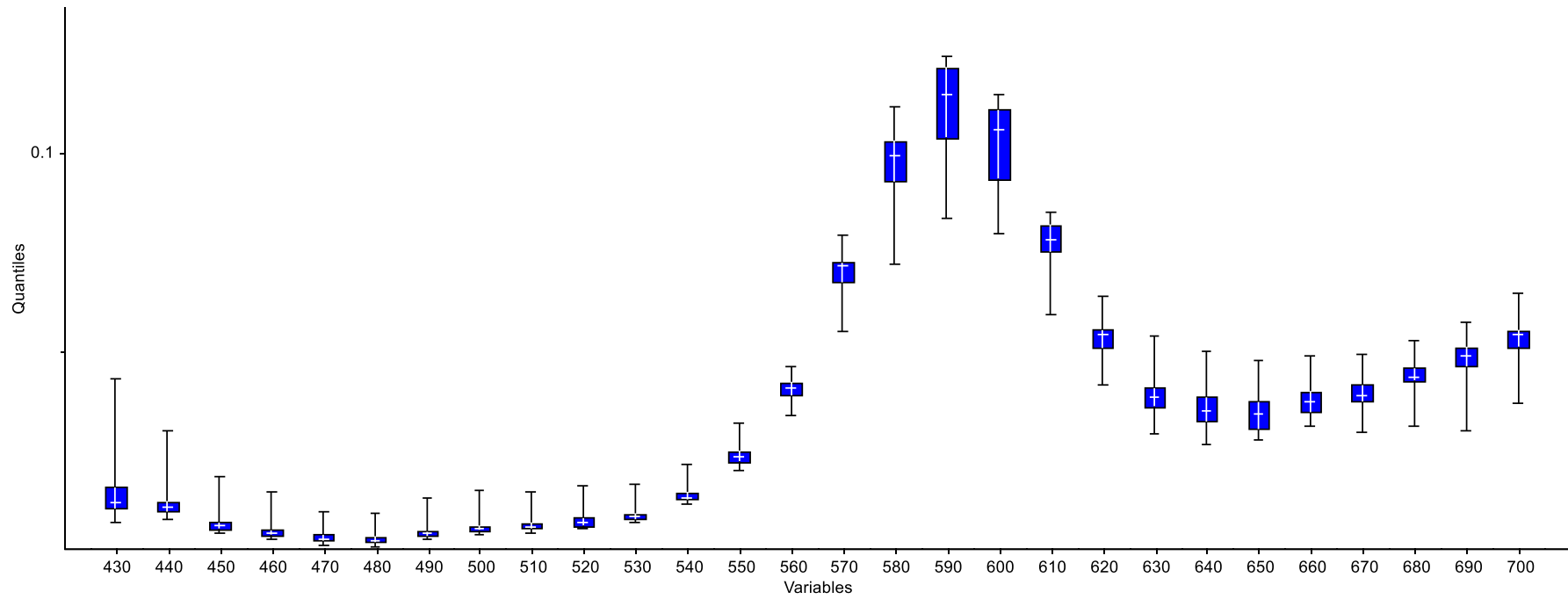
**Table 6-9:** Descriptive statistics for the normalised, derivitised and then averaged spectra for the red areas of all toas studied.

	Mean	Max	Min	Range	Std Deviation	Variance	RMS	Skewness	Kurtosis	Median	Q1	Q3
430	0.013622	0.043096	0.006901	0.036195	0.006621	4.38E-05	0.015092	3.574547	15.78883	0.011914	0.010367	0.015788
440	0.011516	0.029726	0.007672	0.022054	0.004238	1.80E-05	0.012244	3.233819	13.38046	0.010579	0.009539	0.012029
450	0.006574	0.018466	0.004011	0.014455	0.002761	7.62E-06	0.00711	3.372796	13.68827	0.006052	0.00527	0.006838
460	0.00481	0.014513	0.002476	0.012036	0.002443	5.97E-06	0.005374	2.870613	9.733599	0.004173	0.003664	0.004896
470	0.003188	0.009537	0.00101	0.008527	0.001945	3.78E-06	0.003716	2.100769	4.833729	0.002613	0.00223	0.003795
480	0.002847	0.009026	0.000512	0.008514	0.001905	3.63E-06	0.003405	2.515326	6.701538	0.002382	0.00184	0.003209
490	0.004583	0.01304	0.002473	0.010567	0.00223	4.97E-06	0.005078	2.913882	9.047585	0.00426	0.003503	0.00466
500	0.005863	0.014706	0.003835	0.010871	0.002263	5.12E-06	0.006269	2.956466	9.607041	0.005399	0.004802	0.005852

CHAPTER SIX

	Mean	Max	Min	Range	Std Deviation	Variance	RMS	Skewness	Kurtosis	Median	Q1	Q3
<b>510</b>	0.006371	0.014568	0.004134	0.010434	0.00218	4.75E-06	0.00672	2.616789	7.912024	0.005671	0.005292	0.006649
<b>520</b>	0.007487	0.016029	0.005433	0.010596	0.002303	5.31E-06	0.007821	2.428157	7.025584	0.006729	0.006023	0.008025
<b>530</b>	0.008859	0.016458	0.006843	0.009615	0.002083	4.34E-06	0.009091	2.46649	6.835742	0.008422	0.007652	0.009055
<b>540</b>	0.013921	0.021601	0.011496	0.010104	0.002196	4.82E-06	0.014086	2.089075	5.065886	0.013105	0.01271	0.014363
<b>550</b>	0.023802	0.03184	0.019872	0.011968	0.002546	6.48E-06	0.023933	1.457047	2.853726	0.023234	0.022153	0.024744
<b>560</b>	0.04066	0.046082	0.033656	0.012426	0.003137	9.84E-06	0.040777	-0.2141	-0.0257	0.040837	0.038815	0.042182
<b>570</b>	0.069288	0.079018	0.055005	0.024013	0.005204	2.71E-05	0.069476	-1.0665	1.29168	0.071267	0.067246	0.072324
<b>580</b>	0.097014	0.11141	0.0718	0.039611	0.008769	7.69E-05	0.097395	-0.99852	1.300811	0.099255	0.092638	0.102919
<b>590</b>	0.11138	0.124259	0.083239	0.04102	0.011408	0.00013	0.111941	-0.80664	-0.22017	0.114488	0.103624	0.121343
<b>600</b>	0.101847	0.114404	0.079616	0.034788	0.010424	0.000109	0.102359	-0.76312	-0.72969	0.10584	0.093214	0.110717
<b>610</b>	0.077093	0.084847	0.059197	0.02565	0.00637	4.06E-05	0.077346	-1.14146	0.970973	0.078158	0.075012	0.081848
<b>620</b>	0.053159	0.063678	0.041539	0.022138	0.004246	1.80E-05	0.053322	-0.34707	1.936552	0.054097	0.050788	0.055408
<b>630</b>	0.038491	0.053572	0.029235	0.024337	0.004926	2.43E-05	0.038793	0.809374	2.412172	0.038205	0.035942	0.040679
<b>640</b>	0.035526	0.04994	0.026297	0.023643	0.00496	2.46E-05	0.035858	0.872929	1.415502	0.034863	0.032257	0.038519
<b>650</b>	0.034485	0.04763	0.027516	0.020114	0.004837	2.34E-05	0.03481	0.907765	0.807802	0.034149	0.030376	0.037335
<b>660</b>	0.037822	0.048767	0.030965	0.017802	0.004308	1.86E-05	0.038058	0.860216	0.606923	0.037204	0.034613	0.039827
<b>670</b>	0.039638	0.049066	0.029454	0.019612	0.004178	1.75E-05	0.03985	0.378418	1.172124	0.038913	0.037256	0.041448
<b>680</b>	0.044211	0.052564	0.031096	0.021468	0.004218	1.78E-05	0.044404	-0.45518	3.088168	0.043342	0.042452	0.045732
<b>690</b>	0.048202	0.057203	0.029752	0.027451	0.005247	2.75E-05	0.048476	-1.32438	5.187222	0.048716	0.046191	0.050888
<b>700</b>	0.053349	0.064541	0.036964	0.027577	0.005095	2.60E-05	0.053583	-0.75855	3.60031	0.054235	0.05105	0.055208

A CASE STUDY WITH THE APPLICATION OF THE i1PRO SYSTEM TO TOAS



**Figure 6-18:** Graphical representation of the average spectra obtained for the red areas studied with a range and single standard deviation shown.

## CHAPTER SIX

All the toas studied will now be visually and statistically compared. Shown in Figure 6-17 is the normalised, derivitised and then averaged spectra for all toas studied (with multiple spectra present for toas with distinct groups). The statistical analysis of this data is presented in Table 6-8

When examining Figure 6-17 it is apparent that visually the spectra all appear similar in many ways with only a few easily identifiable outliers. Whilst there is no distinct grouping present, there is large variation present across the board when comparing two individual samples. At both the low and high wavelengths, toa A6153b (shown in pink) appears visually distinct in intensity compared to the other toas.

Statistical analysis in Table 6-9 shows that all spectra except toa A40862b, which has a peak maxima at 600nm, exhibit a peak maxima at 590nm. Similarly, they all exhibit an initial minima at 470-480nm and a second minima at 540-550nm. Visually the shapes of the peaks are different, and this combined with the instrument limitations of measurements only taken every 10nm, gives the appearance of some peak shifting.

Principal component analysis was then performed on the data using The Unscrambler software. A NIPALS algorithm was utilised with a random cross-validation method with six segments used. Data points 410 and 420 were excluded due to previously demonstrated poor reproducibility. Results of this analysis are shown in Figure 6-19, with the loadings plot shown in Figure 6-20.

Principal component analysis confirms lack of grouping seen previously. PCA highlights the distinct difference in the spectra of toa A6153b, with the loadings plot confirming this is mostly due to variation in the region of 430-440nm. The other toa showing significant variation to the group is A40862b. The remaining toas form a large, mostly even spread across the PC2 axis.

Using the ratio method applied previously and comparing the wavelengths of 590nm (maxima) and 650nm (minima) confirm that no grouping is present and instead a gentle change across the samples exist. This is demonstrated visually in Figure 6-21. The outlier of A68458 (which exhibits the lowest intensity at the maxima) demonstrates the lowest ratio at 1.66. The remaining toas demonstrate subtle changes between samples, despite an overall range from 2.25 to 4.60. Toa A6153b, identified previously as having the most distinctly different spectra, is present towards the middle of the spread. This is most likely due to the spectral differences being observed at the extreme ends of the wavelengths, and therefore not considered in this simple ratio calculation.

It is impossible to say from the data if a single source has been used on all the toas and the variation is due to aging, damage to the toas, mixing or application processes, or if a number of similar sources were used on the collection. Further analysis will now be completed in an attempt to obtain an accurate comparison between the toa samples and the raw ochre samples hypothesised to be sources of the material.

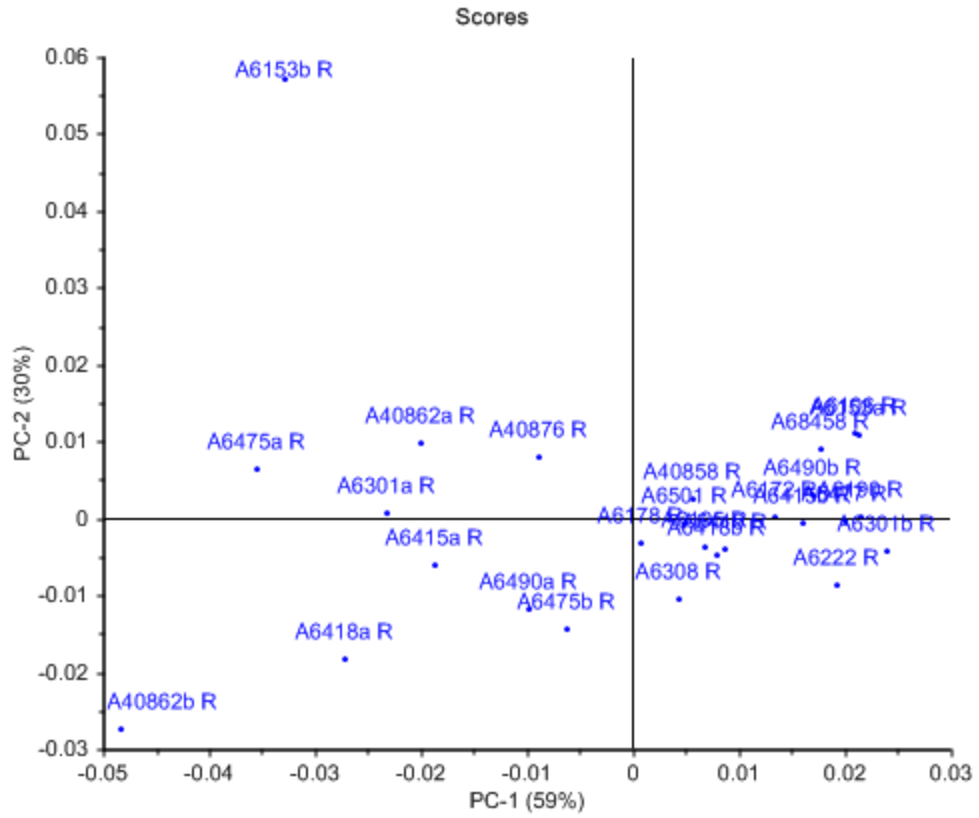
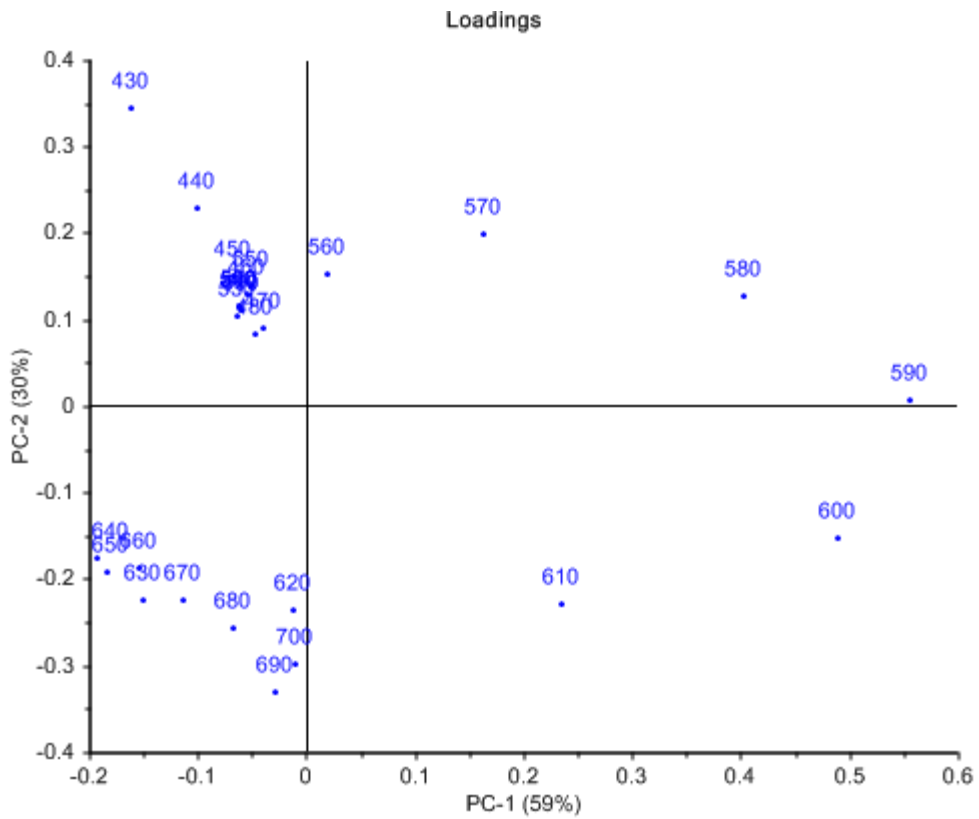
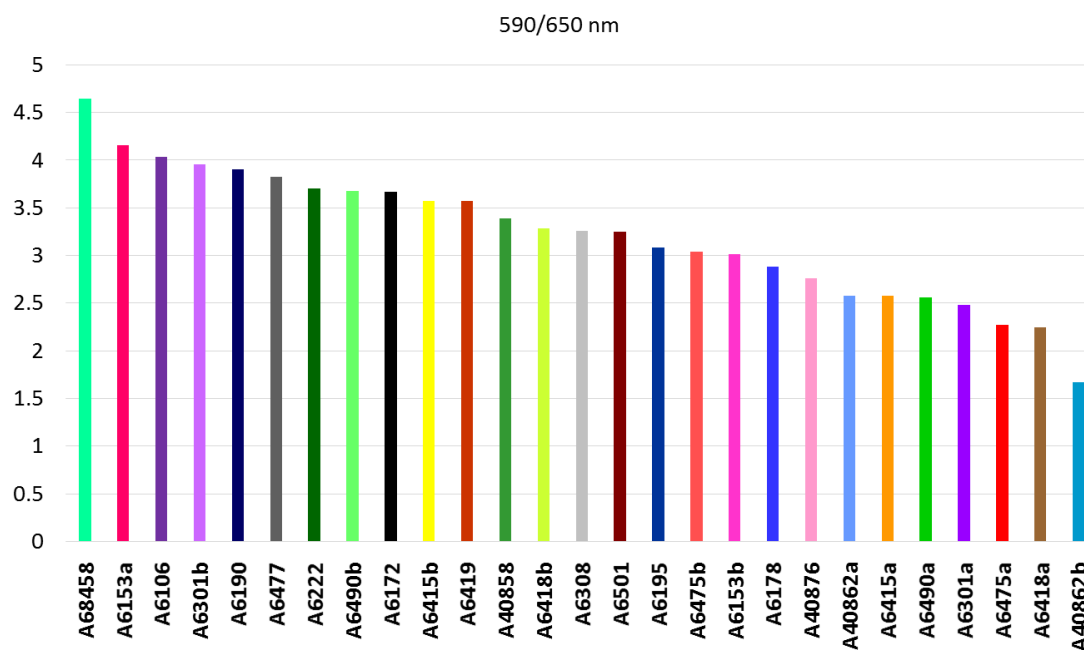


Figure 6-19: Principle component analysis results of the red material on the toas.



**Figure 6-20:** Loadings plot generated in conjunction with the PCA results for the red material on the toas.



**Figure 6-21:** The ratio of the peak intensities at 590/650nm of the normalised, derivitised and then averaged spectra for all toas studied.

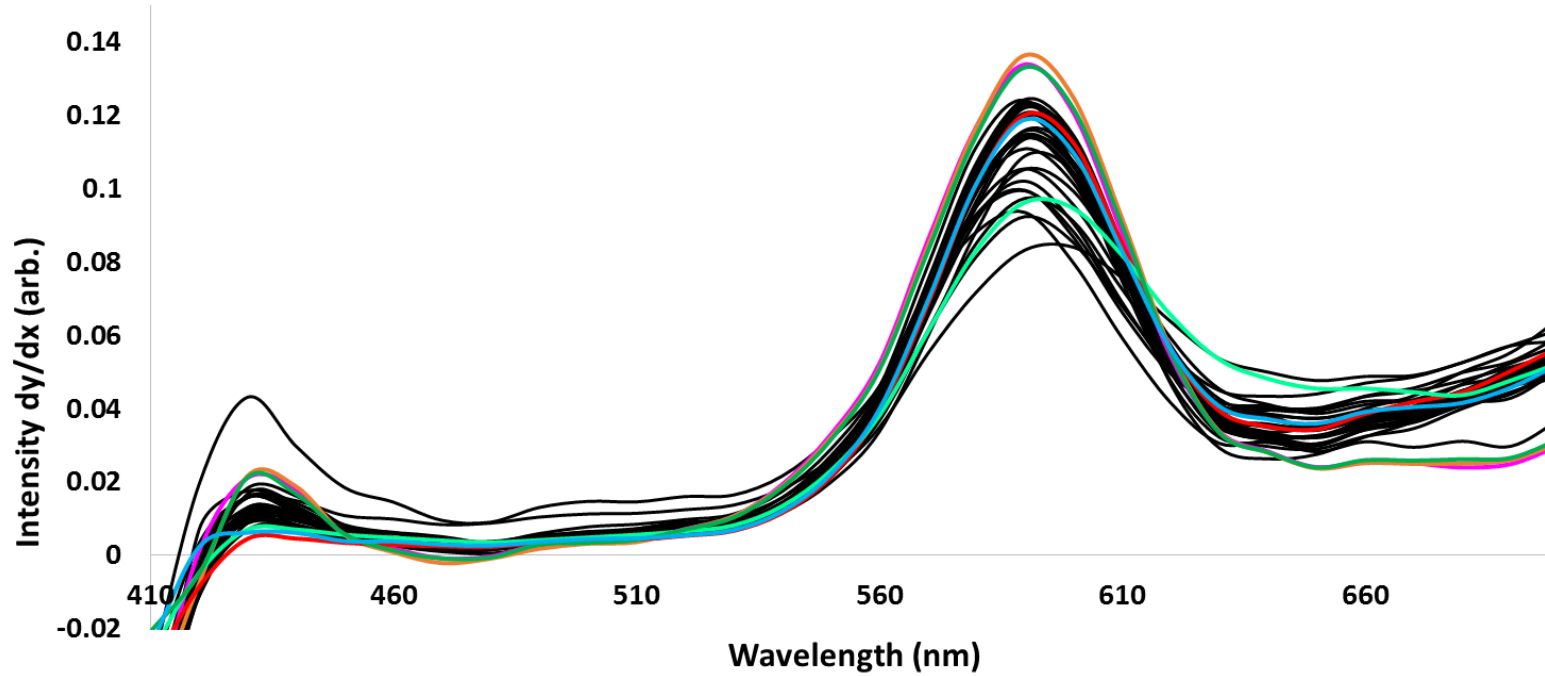
#### 6.4.3. Comparison between the raw samples and the toas

Studies now focus on comparisons between the toas and the raw ochre material collected at the same time as the toas to test the hypothesis that the raw material is the source material for the decorative works. Shown below in Figure 6-22 is spectra for the toas and raw material discussed previously, overlaid, with the toas all represented in black and the individual raw materials spectra highlighted.

Previously, three groupings were identified within the raw material, and it is visually apparent when examining *Figure 6-22* that two of these groupings overlay well with the toas, whilst one grouping is distinctly different. The distinctly different group displays a larger peak intensity at the maxima, and a lower minima at higher wavenumbers. This is confirmed when comparing the 590/650nm ratios previously examined, shown in *Figure 6-23*, with three of the raw materials falling within the range of the toas and three distinctly outside the range.

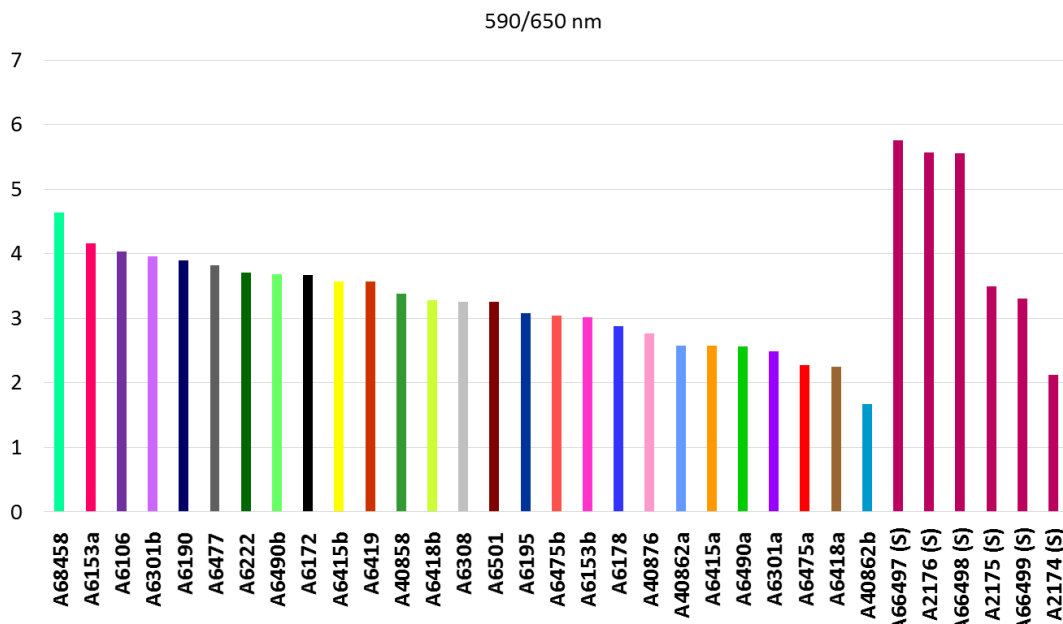
Of note is that the three raw materials showing spectral and ratio results consistent with the toas are A2174, A2175 and A66499, which themselves do not appear overly similar and in fact were identified as belonging to two distinctly different groups. It is this clustering and single group containing A2176, A66497 and A66498 that show statistically significant variation from the toas. This confirms that the range of results present from the materials used to decorate the toas in large.





- |           |            |           |           |            |            |          |          |          |
|-----------|------------|-----------|-----------|------------|------------|----------|----------|----------|
| — A6106   | — A6301a   | — A6301b  | — A6153a  | — A6153b   | — A40876   | — A6190  | — A6195  | — A6178  |
| — A40862a | — A40862b  | — A68458  | — A6222   | — A40858   | — A6490a   | — A6490b | — A6418a | — A6418b |
| — A6419   | — A6415a   | — A6415b  | — A6501   | — A6475a   | — A6475b   | — A6172  | — A6477  | — A6308  |
| — A2176 S | — A66497 S | — A2175 S | — A2174 S | — A66498 S | — A66499 S |          |          |          |

**Figure 6-22:** Normalised derivative i1Pro spectra for the toas and raw material, overlaid, with the toas all represented in black and the individual raw materials spectra highlighted.



**Figure 6-23:** The 590/650nm ratios for the toas (shown in colours) and the toas (shown in pink/purple), with three of the raw materials falling within the range of the toas and three distinctly outside the range.

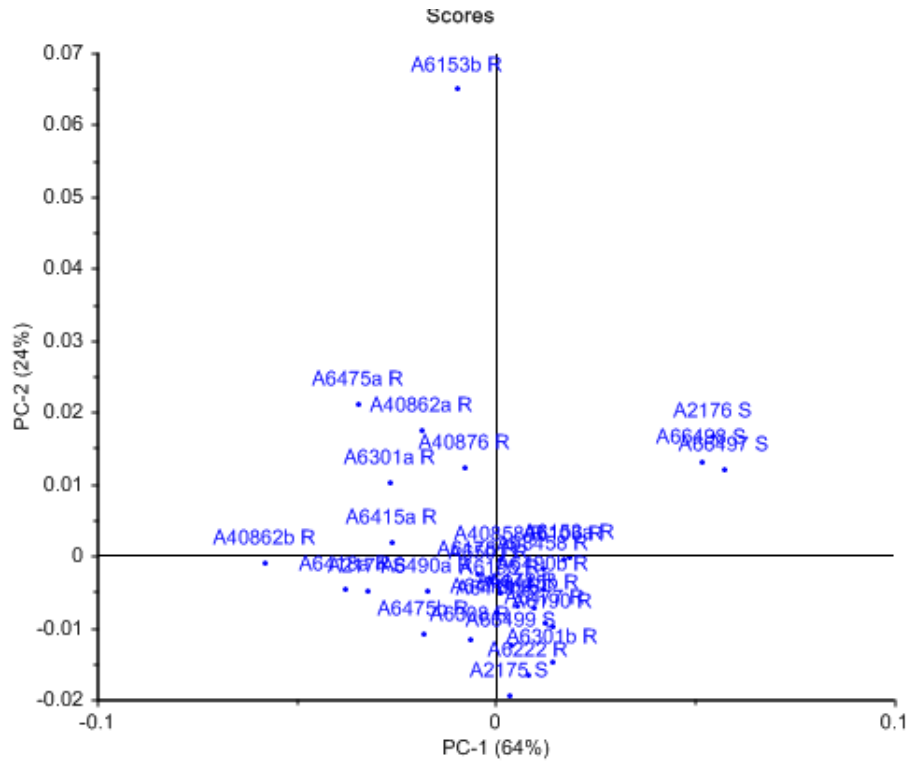
Principal component analysis was then performed on the data using The Unscrambler software. A NIPALS algorithm was utilised with a random cross-validation method with six segments used. Data points 410 and 420 were excluded due to previously demonstrated poor reproducibility.

When examining Figure 6-24 it can be seen that one large group exists with a second small cluster and a further single outlier. The outlier is toa A6153b, which has been previously discussed. The secondary cluster contains raw materials A2176, A66497 and A66498. The main grouping shows the remaining toas and raw materials. These results are consistent with the results seen from spectral and ratio analysis.

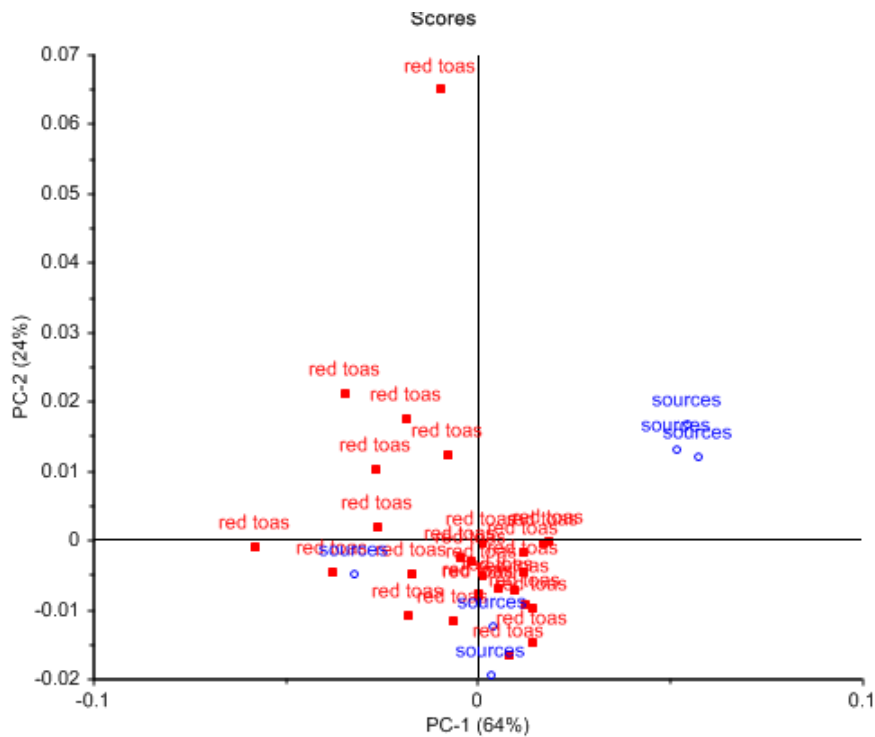
Toa A6153b was then removed from the data set and additional PCA analysis performed. This was due to the large influence the outlier was having on the results.

Removing toa A6153b from the analysis makes the spread easier to examine. This confirms that the raw materials of A2176, A66497 and A66498 show no overlap with the toas and can be excluded as a possible source. Raw materials A2174, A2175 and A66499 show consistent similarities with the toas and, despite the differences present in the raw materials, cannot be excluded as possible source material.

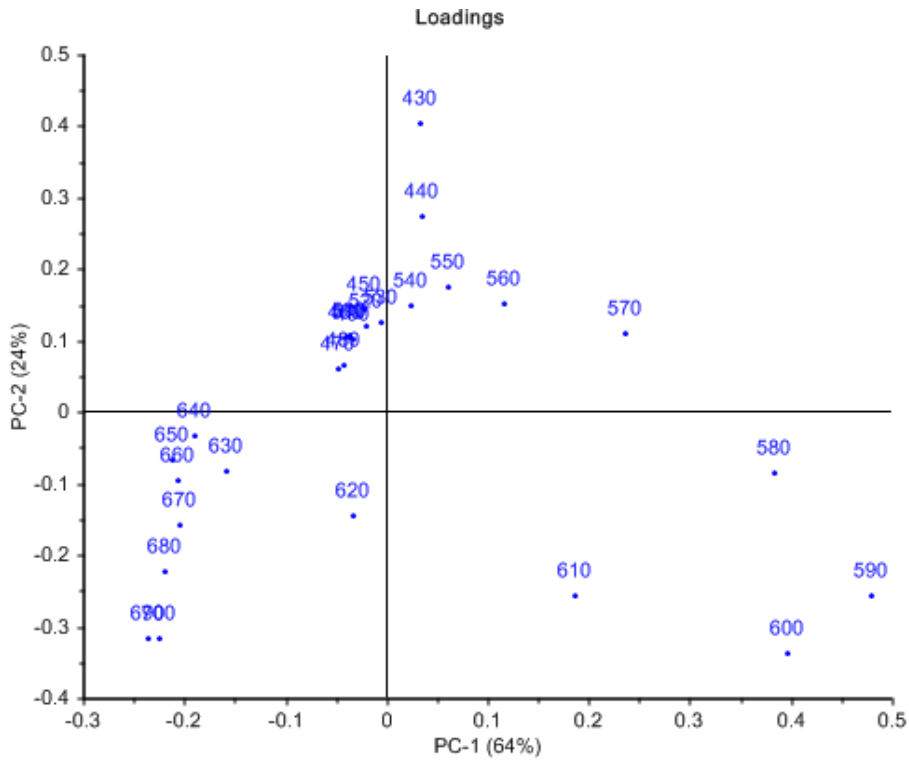
It is hypothesised that multiple sources were used in the creation of the toas. It is also possible that some of the toas have been damaged with age, weather, and water or similar, or that a single source or haematite was used but was mixed with other substances prior to its application to the toas impacting on its colour and therefore the results of this analysis.



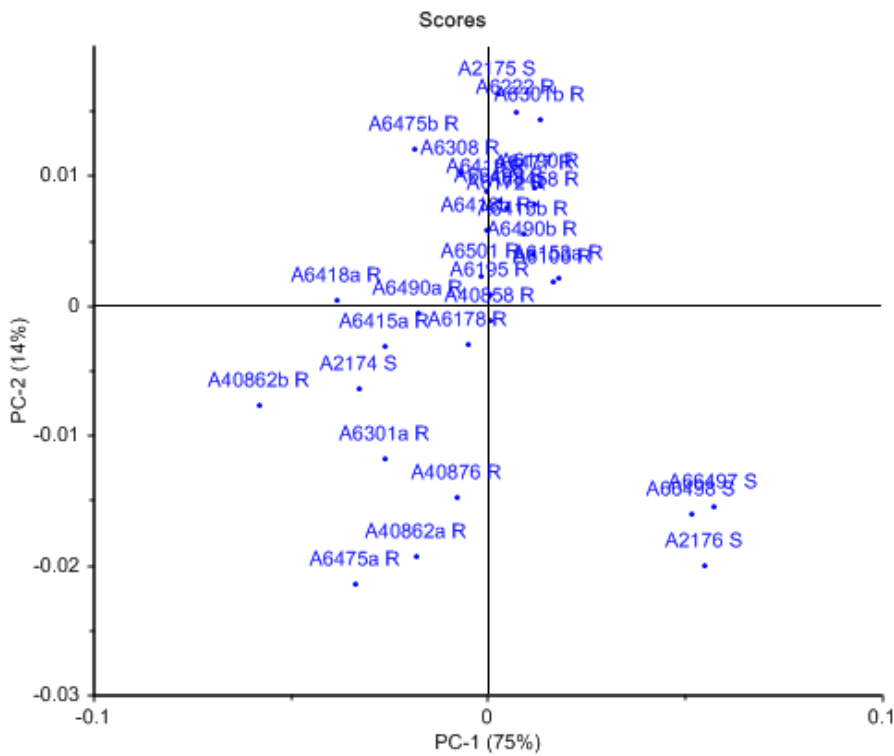
**Figure 6-24:** Principal component analysis on the red material on the toas and the raw samples collected as possible sources with the individual sample numbers shown.



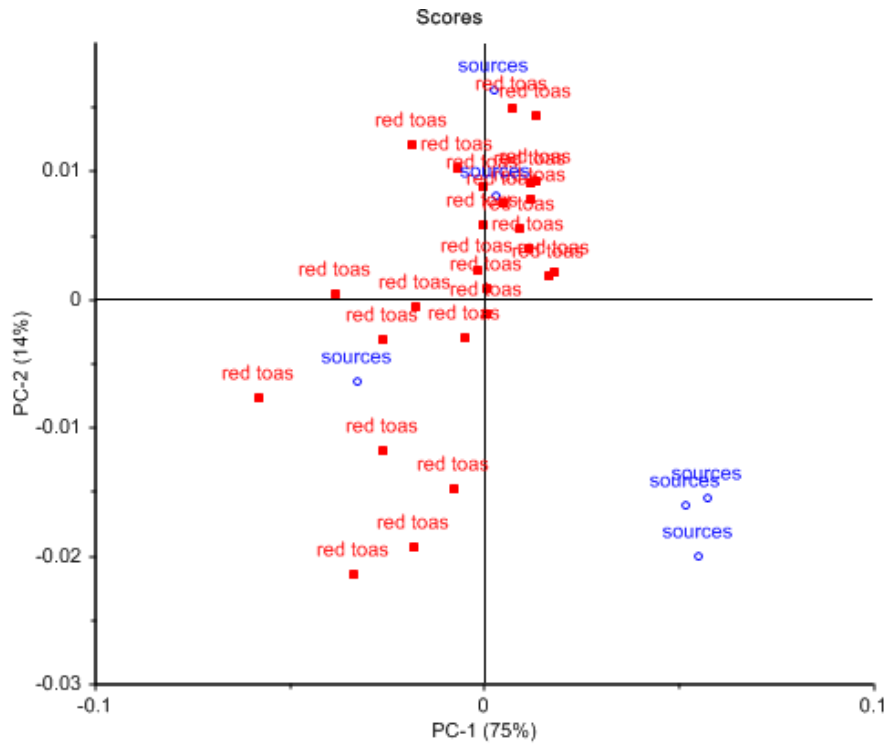
**Figure 6-25:** Principal component analysis on the red material on the toas and the raw samples collected as possible sources with the toas shown in red and the sources in blue.



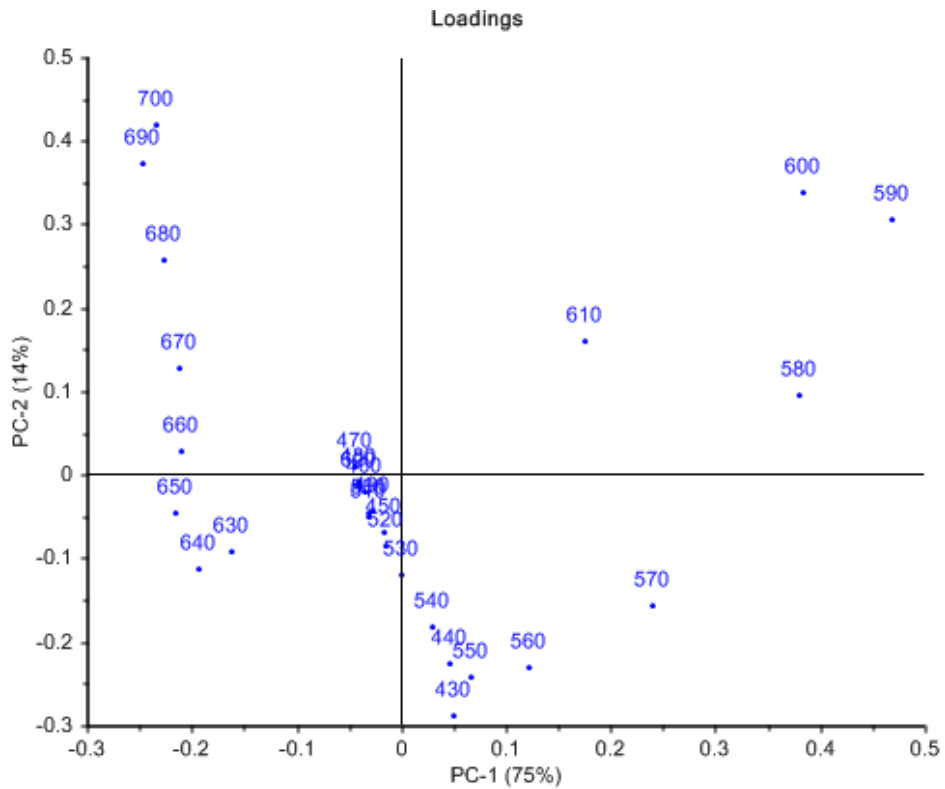
**Figure 6-26:** Loadings plot for principal component analysis on the red material on the toas and the raw samples collected as possible sources.



**Figure 6-27:** Principal component analysis on the red material on the toas (excluding toa A6153b) and the raw samples collected as possible sources with the individual sample numbers shown.



**Figure 6-28:** Principal component analysis on the red material on the toas (excluding toa A6153b) and the raw samples collected as possible sources with the toas shown in red and the sources in blue.



**Figure 6-29:** Loadings plot for principal component analysis on the red material on the toas (excluding toa A6153b) and the raw samples collected as possible sources.

#### **6.4.4. Comparison between the raw material from the Reuther collection and the Bookartoo, Wilgie Mia and Moana samples studied previously**

Principal component analysis was performed on all of the data from the haematite samples from Moana, Wilgie Mia and Bookartoo samples (previously discussed in Chapter 5), and the six raw material samples collected with the Reuther collection. A NIPALS algorithm was utilised with a random cross-validation method with six segments used. Data points 410 and 420 were excluded due to previously demonstrated poor reproducibility. Results of this are shown in Figure 6-30, with Moana samples shown in black, Wilgie Mia in maroon, Bookartoo in red and the Reuther collection raw material in blue. The corresponding loadings plot is shown in Figure 6-31.

Examining Figure 6-30 shows that A2176, A66497 and A66498 cluster well with the Bookartoo samples. These Reuther collection samples are the samples that did not group well with the toas, and this suggests that the Reuther collection samples were not from Bookartoo. Interestingly, both Bookartoo and Killalpaninna Lutheran Mission, where the Reuther collection was collected, are both in the far north-east of South Australia.

Raw materials A2174, A2175 and A66499, which have previously been shown to demonstrate some overlap with the toas, do not cluster with any of the Bookartoo, Wilgie Mia or Moana sites. Greater similarities are shown with Wilgie Mia and Moana, but it is difficult to draw any conclusions for these samples from the results obtained here.

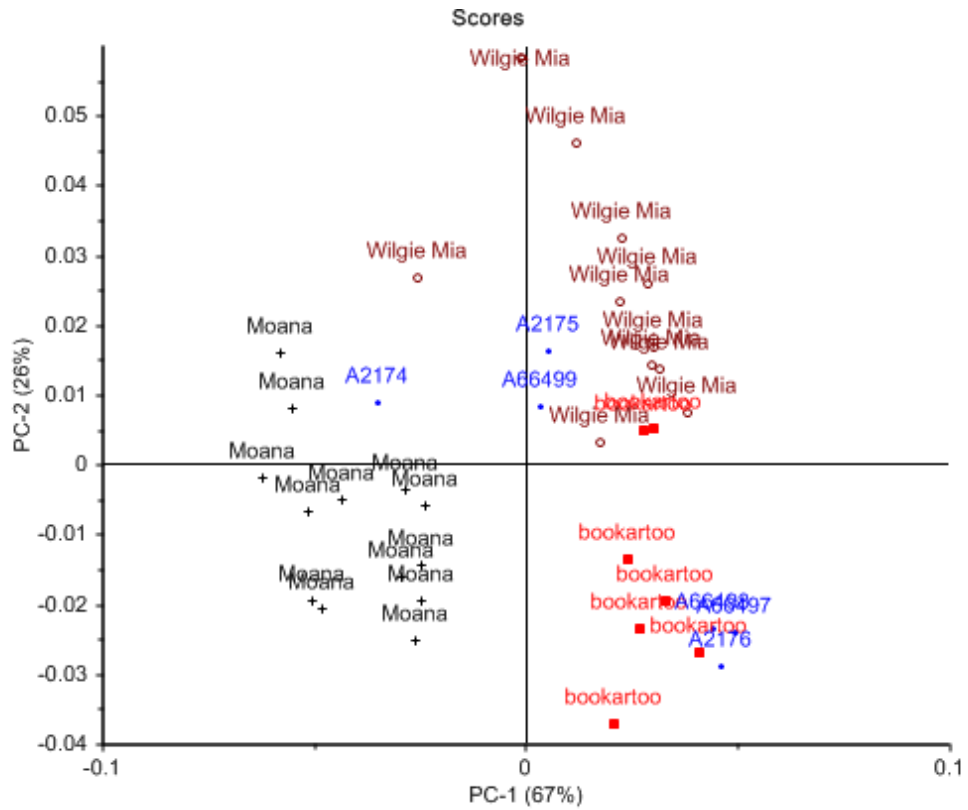
It is therefore reasonable to hypothesise that the raw samples collected by Reuther are in fact from multiple sources, one of which may have been the nearby Bookartoo mine.

### **6.5. Conclusions**

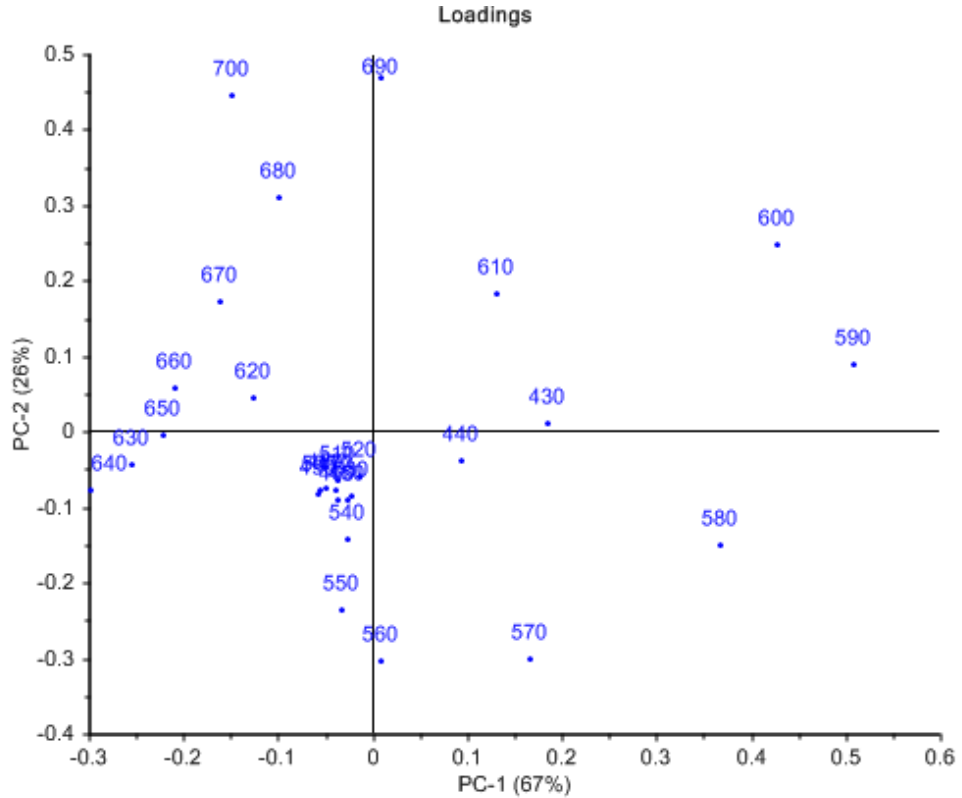
This chapter has presented a case study into twenty toas and six raw samples held by the SA Museum from the Reuther collection. Examination of the raw samples, hypothesised to be the source of the red decoration on the toas, highlighted a number of differences in the samples. It is proposed that either a high level of inter-site variation is present, or, more likely that these raw samples are not from a single source.

Studies then moved to the yellow areas of decoration on a select few of the toas. Results of the analysis of the yellow decorative material on the toas shows that multiple sources have been used here. It has been shown that some toas use a single source, and others suggest the use of multiple sources. There are no known raw goethite samples collected at the time of the toas for comparison.

Studies were then focused on the red material, hypothesised to be haematite, used to decorate all the toas examined in this work. The majority of the toas showed uniform results across all sites studied, with a small number showing spectra with two distinctly different trends.



**Figure 6-30:** Principal component analysis on the raw material collected from the Reuther Collection and the Moana, Bookartoo, Wilgie Mia samples.



**Figure 6-31:** Loadings plot for the principal component analysis on the raw material collected from the Reuther Collection and the Moana, Bookartoo, Wilgie Mia samples.

## CHAPTER SIX

Comparison of the spectra for each toa and subsequent statistical analysis showed a range of results with no clear clustering present and a small number of outliers were identified. It is impossible to say from the data if a single source has been used on all the toas and the variation is due to aging, damage to the toas, mixing or application processes, or if a number of similar sources were used on the collection.

Comparisons were then made between the raw samples collected and the red material examined on the toas. Three of the raw materials, A2176, A66497 and A66498, which had previously grouped together, show distinct variation from the toas. The remaining raw materials, A2174, A2175 and A66499, which themselves do not appear overly similar and in fact were identified as belonging to two distinctly different groups, all fall within the range of the material on the toas. This confirms that the range of results present from the materials used to decorate the toas is large. It is hypothesised that multiple sources were used in the creation of the toas. It is also possible that some of the toas have been damaged with age, weather, and water or similar, or that a single source of haematite was used but was mixed with other substances prior to its application to the toas impacting on its colour and therefore the results of this analysis.

The raw material collected with the Reuther collection were then compared to the Bookartoo, Wilgie Mia and Moana samples studied previously in Chapter 5. Results show that Reuther collection samples A2176, A66497 and A66498, which were previously shown to not group well with toas, cluster well with the Bookartoo samples. Raw materials A2174, A2175 and A66499, which have previously been shown to demonstrate some overlap with the toas, do not cluster with any of the Bookartoo, Wilgie Mia or Moana sites



**CHAPTER SEVEN:  
CONCLUSIONS AND  
FUTURE WORK**

## 7.1. Conclusions

Chapter one investigated the history of pigments across the globe. It identified a number of mineral pigments and studied their chemistry, their colour and their common uses. Prehistoric pigments were examined in context, along with a look at the use of pigments in different cultures and time periods. Pigments significant to Aboriginal Australians were identified and studied, in particular red and yellow ochre, and factors influencing their varied colour were identified. This chapter also identified many of the previous studies undertaken to examine Ochre both locally and across the globe. This chapter identified many of the techniques utilised, including but not exclusive to XRD, TGA, IR, NAA, Raman Spectroscopy and other spectroscopic based methods. Limitations and advantages of each technique were examined and it was determined that a multidisciplinary approach is necessary for complete provenancing of ochre.

Chapter two identified ten mining samples of interest. The basis of experiments completed on these samples were identified and experimental methods detailed here. This chapter also details the samples to be studied, before presenting the results obtained for analysis utilising the methods previously discussed. Results of XRD analysis confirm that many components are able to be successfully identified and often their ratio determined, but the accuracy of the technique is sometimes questionable. Results of Raman analysis showed that each sample has a significantly different spectra with trends apparent based on sample colour and therefore composition, but fluorescence as a result of the soil medium was an issue and accurate conclusions were not able to be drawn. Results of TGA on the standards confirmed that pure haematite exhibited no mass loss with heating and that the heating of goethite resulted in a chemical transformation to haematite and subsequent change in colour and loss of mass. Analysis of the mining samples containing predominantly goethite also all exhibited a loss of mass, however the volume of mass lost and the temperature at which transformation occurred varied for each sample with no discernible pattern obvious. Results of the IR were varied and whilst comparisons are able to be made, no significant trend exists to the extent required for characterisation and provenancing. Autocorrelation analysis was not able to accurately distinguish between samples based on their colour and composition, and as a result would not be suitable for the provenancing aims of this project. NAA was the most successful of the techniques used and results are able to successfully characterize and distinguish between the ten mining samples studied. Not only are the concentrations of the studied elements different, but there is also significant variation in the ratios between these elements. This allows for easy comparison of unknowns and possible successful identification. A larger sub-set of data needs to be established for further conclusions to be drawn regarding this technique, but limitations include cost, time and the destructive nature of analysis. Overall, results of experiments presented in this chapter examining the traditional methods utilised were mixed. An overall characterization picture was able to be obtained by combining the techniques, but no single technique was completely successful and without limitations.

Chapter three presented the results of a preliminary study into the use of a new, portable, handheld, UV-vis based spectrometer in the X-Rite i1Pro and its application to ochre material. This chapter detailed the instruments technical aspects, before applying it to standards of known compositions. The X-Rite i1Pro was successfully able to distinguish between goethite and haematite standards across a range of 400-700nm. The reproducibility of these measurements was investigated and on average the error in the measurement across all the wavelengths was  $\pm 0.002$  for goethite and  $\pm 0.001$  for haematite, well within the manufacturer's specifications. The X-Rite i1 Pro system was then shown to be capable of distinguishing between twenty one samples, each varying in goethite and haematite composition by approximately five percent. Statistical analysis showed complete and accurate separation, with clusters formed based on sample composition. The X-Rite i1 Pro system was then compared to a traditional, lab based UV-vis instruments and the data obtained for both instruments observes the same trend and the peak maxima in located at the same wavelength.

Chapter three also explored the X-Rite i1 Pro systems ability to group samples based on their compositions at a variety of sample thicknesses. Results of this showed that each thickness exhibited similar trends. Studies then focused on the X-Rite i1 Pro systems ability to group samples based on their composition when the samples being studied are of different sample thicknesses. This separation was achieved, and it was shown that samples needed to be equal to or greater than 10mg/approx.2cm<sup>2</sup> for samples of different thicknesses to be accurately compared. The effect of different application methods was then examined, as well as the effects of different binders (such as water, emu oil and orchid sap) and substrates (such as various woods and stones). Results of this showed that, with the exception of natural sandstone, complete and accurate separation was achieved for every method studied, and the samples were able to be distinguished between and ordered based on the goethite composition. However, the X-Rite i1 Pro system proved unable to group samples based on composition when different substrates, application methods, or binders were compared. Limited success was achieved with high goethite concentrations on some substrates, but overall the instrument showed that comparisons need to be made where all samples are treated identically with respect to binders and substrates.

Chapter three also compared the results of a number of models established in an attempt to accurately determine the sample composition of unknowns by applying the models to blind standard sample compositions. The first of these models was based on the analysis of a single wave length. Of the wavelengths investigated, 530nm was found to be the most accurate with an error of less than 2% on all ten samples analysed when applied to paper. The second model studied formed predictions based on  $\Delta E$ . The  $\Delta E$  model of prediction is significantly less accurate than the previously described 530nm model and was deemed to be unsuitable. The final model to be investigated is MLR analysis. When the samples were applied to paper, variation between the samples was, in most cases, less than 1%, with the maximum variation being less than 2%.

Chapter four presented an investigation into the effect of the substrate on the spectra obtained from the i1Pro as it was hypothesised that factors such as surface roughness and colour would influence the results. Results proved promising at low goethite concentrations (25% w/w and less) and for pure haematite, but showed some variation at other compositions. The single wavelength and MLR models established in chapter three were then applied to the results obtained from the unknown samples on alternate substrates. The single wavelength model showed that the error was significantly larger and up to 8% when samples were applied to alternate substrates, thus limiting its application to artefacts. The MLR model was then applied and results show good agreement for all compositions on all three wood surfaces, and for high goethite compositions on stone surfaces, with the majority of results showing a variation of less than 2%, and the maximum variation being less than 3%. For stone surfaces with low goethite composition the variation is significantly larger, and outside acceptable limits. In order to investigate this, a second MLR model was created using results obtained from a slate substrate, however this did not improve the accuracy of sample composition predictions.

Chapter five presents a case study into the inter-site and intra-site variation across a number of culturally significant Australian ochre sites. The i1pro instrument was successfully applied to fifty seven ochres from Moana (28 ochres), Wilgie Mia (14 ochres) and Bookartoo (15 ochres). Samples from each site exhibited red, orange, brown and yellow hues. Spectral analysis was combined with statistical analysis utilizing principle component analysis and demonstrated that the i1Pro was successfully examine the ochres from each individual site and distinguish between the ochre based on colour. Analysis then progressed to comparisons between sites and, despite many spectral similarities, principal component analysis yielded promising results. Clusters were successfully formed based on colour, with clear distinctions made between yellow, orange and red independent of the source. When comparing ochres of the same colour from various sites, yellow and orange samples were able to be distinctly separated based on location. However, only a small number of samples were present for some colour/location combinations, and statistical analysis is difficult on low sample numbers. Red ochre was studied in the greatest depth due to its cultural significance as well as the large number of samples available. Both spectrally and with principle component analysis, the red ochre from Moana was shown to be significantly different to the red ochre from Bookartoo and Wilgie Mia, and was easily distinguishable. The red ochre from Bookartoo and Wilgie Mia exhibited a number of similarities, making complete separation difficult. However, a number of subtle differences in the spectra exist, and principle component analysis highlighted these and as a result was able to achieve approximate but incomplete separation, with some overlap present between the two clusters. Given the nature of the instrument and the limitations of traditional methods that the i1pro is able to overcome, these results are very promising. They suggest the possibility of a fast, transportable, affordable and non-destructive screening method that may be able to preliminarily identify ochre and, with statistical accuracy, exclude sites as possible source material.

Neutron Activation Analysis (NAA) was performed on a number of the samples tested from Wilgie Mia, Moana and Bookartoo, and the results compiled and analysed. Results of this analysis show basic grouping of samples based on colour and location, with some overlap present. Studies then focused on only the samples appearing visually red in colour. A number of attempts were made to improve the distinction between the groupings, including removing any elements not present in at least 90% of the samples. Results of NAA analysis were inconsistent with the results obtained from the i1Pro analysis, with Bookartoo samples appear more distinctly different to Wilgie Mia and Moana, especially before the number of elements was reduced. This demonstrates that traditional techniques such as NAA, where available and where experimental limitations such as sample type and size are not a strong consideration, can be used well in conjunction with the i1Pro analysis for the separation of Australian ochre samples based on site of origin.

Chapter six is a case study into twenty toas and six raw samples from the held by the SA Museum from the Reuther collection. Examination of the raw samples, hypothesised to be the source of the red decoration on the toas, highlighted a number of differences in the samples. It is proposed that either a high level of intra-site variation is present, or, more likely that these raw samples are not from a single source. Studies then moved to the yellow areas of decoration on a select few of the toas. Results of the analysis of the yellow decorative material on the toas shows that multiple sources have been used here. There are no known raw goethite samples collected at the time of the toas for comparison. Studies were then focused on the red material, hypothesised to be haematite, used to decorate all the toas examined in this work. The majority of the toas showed uniform results across all sites studied, with a small number showing spectra with two distinctly different trends. Comparison of the spectra for each toa and subsequent statistical analysis showed a range of results with no clear clustering present and a small number of outliers were identified. It is impossible to say from the data if a single source has been used on all the toas and the variation is due to aging, damage to the toas, mixing or application processes, or if a number of similar sources were used on the collection.

Comparisons were then made between the raw samples collected and the red material examined on the toas. Three of the raw materials, A2176, A66497 and A66498, which had previously grouped together, show distinct variation from the toas. The remaining raw materials, A2174, A2175 and A66499, which themselves do not appear overly similar and in fact were identified as belonging to two distinctly different groups, all fall within the range of the material on the toas. This confirms that the range of results present from the materials used to decorate the toas in large. It is hypothesised that multiple sources were used in the creation of the toas. It is also possible that some of the toas have been damaged with age, weather, and water or similar, or that a single source or haematite was used but was mixed with other substances prior to its application to the toas impacting on its colour and therefore the results of this analysis.

The raw material collected with the Reuther collection were then compared to the Bookartoo, Wilgie Mia and Moana samples studied previously in Chapter 5. Results show that Reuther collection samples A2176, A66497 and A66498, which were previously shown to not group well with toas, cluster well with the Bookartoo samples. Raw materials A2174, A2175 and A66499, which have previously been shown to demonstrate some overlap with the toas, do not cluster with any of the Bookartoo, Wilgie Mia or Moana sites.

Overall, this thesis has presented results obtained towards to characterisation of Australian Aboriginal ochre materials and attempts made to establish a data base of materials of known locations to aid in the provenancing of artefacts. This thesis has focused on the development of a new, portable, non-destructive technique that requires no sample preparation and this has applications to artefacts of all shapes, sizes and locations. The accuracy of the instrument has been proven and the potential for application to a wide range of specialties demonstrated.

### **7.2. Future work**

This project is part of a collaboration between Flinders University, Artlab and the South Australian Museum. As such, work into Aboriginal Australian ochres is ongoing in a number of capacities.

Specifically relating to work presented here, scope exists for expansion in a number of areas. The number of samples studied and this the data base will be expanded. This will include analysis using a number of the techniques presented here, including but not limited to neutron activation analysis and the i1Pro spectrometry. Specifically, there exists number of well provenanced sites still to be studied, and comparisons made to the existing data. In addition to this, only a small percentage of the toas have been studied, and this work could be expanded.

There also exists scope to further test the i1Pro instrument. Whilst work was completed into a number of application techniques, studies into the effect of things such as natural aging, or water damage to samples are yet to be undertaken.

# REFERENCES

## REFERENCES



1. Barnett, J.R., S. Miller, and E. Pearce, *Colour and art: A brief history of pigments*. Optics & Laser Technology, 2006. **38**(4–6): p. 445-453.
2. Baranyovits, F.L.C., *Cochineal carmine: an ancient dye with a modern role*. Endeavour, 1978. **2**(2): p. 85-92.
3. Nassau, K., *The Physics and Chemistry and Colour : The Fifteen Causes of Colour*. second edition ed. 1983: Wiley-Interscience. 504.
4. Hradil, D., et al., *Clay and iron oxide pigments in the history of painting*. Applied Clay Science, 2003. **22**(5): p. 223-236.
5. Nassau, K., *The Physics and Chemistry of Color: The Fifteen Causes of Color* 1983: John Wiley & Sons.
6. Withnall, R., et al., *Achieving structured colour in inorganic systems: Learning from the natural world*. Optics & Laser Technology, 2011. **43**(2): p. 401-409.
7. Scherrer, N.C., et al., *Synthetic organic pigments of the 20th and 21st century relevant to artist's paints: Raman spectra reference collection*. Spectrochimica Acta Part A: Molecular and Biomolecular Spectroscopy, 2009. **73**(3): p. 505-524.
8. Hunt, D. and R. Chenciner, *Colour symbolism in the folk literature and textile tradition of the Caucasus*. Optics & Laser Technology, 2006. **38**(4–6): p. 458-465.
9. Tite, M.S., M. Bimson, and M.R. Cowell, *Technological Examination of Egyptian Blue*, in *Archaeological Chemistry III*. 1984, American Chemical Society. p. 215-242.
10. Kaczmarczyk, A., *The source of cobalt in ancient Egyptian pigments*. Proceedings of the 24th International Archaeometry Symposium 1986: p. 369-376
11. Riederer, J., *Recently Identified Egyptian Pigments*. Archaeometry, 1974. **16**(1): p. 102-109.
12. Rosalie David, A., et al., *Raman Spectroscopic Analysis of Ancient Egyptian Pigments*. Archaeometry, 2001. **43**(4): p. 461-473.
13. Caley, E.R., *Ancient Greek Pigments from the Agora*. Hesperia: The Journal of the American School of Classical Studies at Athens, 1945. **14**(2): p. 152-156.
14. Caley, E.R., *Ancient Greek pigments*. Journal of Chemical Education, 1946. **23**(7): p. 314.
15. Kafetzopoulos, C., N. Spyrellis, and A. Lympelopoulou-Karaliota, *The Chemistry of Art and the Art of Chemistry*. Journal of Chemical Education, 2006. **83**(10): p. 1484.
16. Burgio, L., R.J.H. Clark, and K. Theodoraki, *Raman microscopy of Greek icons: identification of unusual pigments*. Spectrochimica Acta Part A: Molecular and Biomolecular Spectroscopy, 2003. **59**(10): p. 2371-2389.

## REFERENCES

17. Richter, E.L.H., Heide *A nineteenth century collection of pigments and painting materials*. Studies in conservation 1974. **19**(2): p. 76-82
18. Gettens, R.J.F., Robert L.; Chase, W.T., *Vermilion and cinnabar*. Studies in conservation 1972. **17**(2).
19. Mazzocchin, G.A., et al., *Analysis of pigments from Roman wall paintings found in Vicenza*. Talanta, 2003. **61**: p. 565-572.
20. Mioč, U.B., et al., *Ochre decor and cinnabar residues in Neolithic pottery from Vinča, Serbia*. Journal of Raman Spectroscopy, 2004. **35**(10): p. 843-846.
21. Augusti, S. *Analysis of the material and technique of ancient mural paintings*. in *Application of science in examination of works of art. Proceedings of the seminar: September 7-16, 1965, conducted by the research laboratory, Museum of Fine Arts, Boston, Massachusetts*. 1965. Museum of Fine Arts.
22. Eastaugh, N., et al., *Pigment compendium: a dictionary of historical pigments*. 2012: Routledge.
23. Robin, J., *Raman microscopy: application to the identification of pigments on medieval manuscripts*. Chemical Society Reviews, 1995. **24**(3): p. 187-196.
24. Feller, R.L., *Artist's pigments: a handbook of their history and characteristics*. Vol. 1. Vol. 1. 1986: Cambridge University Press and National Gallery of Art.
25. Doménech-Carbó, A., M.T. Doménech-Carbó, and X. Mas-Barberá, *Identification of lead pigments in nanosamples from ancient paintings and polychromed sculptures using voltammetry of nanoparticles/atomic force microscopy*. Talanta, 2007. **71**(4): p. 1569-1579.
26. Méndez, J., et al., *Color quality of pigments in cochineals (*Dactylopius coccus* Costa). Geographical origin characterization using multivariate statistical analysis*. Journal of agricultural and food chemistry, 2004. **52**(5): p. 1331-1337.
27. Schweppe, H. and H. Roosen-Runge, *Carmine-cochineal carmine and kermes carmine*, in *Artists' pigments; A handbook of their history and characteristics*. 1986, National Gallery of Art. p. 255-283.
28. Farnsworth, M., *Ancient pigments: Particularly second century BC pigments from Corinth*. Journal of Chemical Education, 1951. **28**(2): p. 72.
29. Arieli, D., D. Vaughan, and D. Goldfarb, *New synthesis and insight into the structure of blue ultramarine pigments*. Journal of the American Chemical Society, 2004. **126**(18): p. 5776-5788.
30. Gettens, R.J., *Lapis lazuli and ultramarine in ancient times*. Alumni, 1950. **19**(3-4): p. 342-357.

31. Plesters, J., *Ultramarine blue, natural and artificial*. Studies in conservation, 1966. **11**(2): p. 62-91.
32. Gettens, R.J. and E.W. Fitzhugh, *Malachite and green verditer*. Studies in conservation, 1974. **19**(1): p. 2-23.
33. Hendry, G., *Plant pigments*. LEA. PJ, LEEGOOD, RC Plant biochemistry and molecular biology. Great Britain: Bookcraft, 1993: p. 181-196.
34. Siegel, A. and W. Struve, *The chemistry of organic pigments*. American paint journal, 1956. **41**(10): p. 90-107.
35. Roy, A. and B.H. Berrie, *A new lead-based yellow in the seventeenth century*. Studies in Conservation, 1998. **43**(Supplement 1): p. 160-165.
36. Santamaria, U., P. Muioli, and C. Seccaroni, *Some remarks on lead-tin yellow and Naples yellow*, in *Art et chimie, la couleur: actes du congrès*. 2000, CNRS Editions. p. 38-42.
37. Barnes, N.F., *Color characteristics of artists' pigments*. JOSA, 1939. **29**(5): p. 208-210.
38. Berke, H., *The invention of blue and purple pigments in ancient times*. Chemical Society Reviews, 2007. **36**(1): p. 15-30.
39. Farrar, W., *Synthetic dyes before 1860*. Endeavour, 1974. **33**(120): p. 149-155.
40. Mimani, T. and S. Ghosh, *Combustion synthesis of cobalt pigments: Blue and pink*. Current Science, 2000. **78**(7): p. 892-896.
41. Kühn, H., *Zinc white*, in *Artists' pigments; A handbook of their history and characteristics*. 1986, National Gallery of Art. p. 169-186.
42. Jansen, M. and H. Letschert, *Inorganic yellow-red pigments without toxic metals*. Nature, 2000. **404**(6781): p. 980-982.
43. Boon, H., *A brief general history of the UK paint industry: Part 2. After the Start*. Pigment & Resin Technology, 1985. **14**(2): p. 13-15.
44. Clapp, A.F. and R.D. Buck, *Emerald green and ultramarine*. Ica newsletter, 1963. **1**(1): p. 4-5.
45. Fiedler, I. and M.A. Bayard, *Emerald green and Scheele's green*. Artists' pigments: a handbook of their history and characteristics, 1997. **3**: p. 219-272.
46. Laurie, A., *The identification of pigments used in painting at different periods, with a brief account of other methods of examining pictures*. Analyst, 1930. **55**(648): p. 162-179.
47. Stevens, A. and B. Chalk, *Pigments and minerals*. Theory and practice of histological techniques. Edinburgh: Churchill Livingstone, 1990: p. 245-6.

## REFERENCES

48. Cornell, R.M. and U. Schwertmann, *The iron oxides: structure, properties, reactions, occurrences and uses*. 2003: Wiley. com.
49. Matijevic, E., W.P. Hsu, and M.R. Kuehnle, *Synthetic, monodispersed color pigments for the coloration of media such as printing inks, and method and apparatus for making same*. 1994, Google Patents.
50. Potter, M.J., *Iron oxide pigments*. Journal, v, 1994. **78**(32): p. 43-46.
51. Walter, D., *Characterization of synthetic hydrous hematite pigments*. Thermochemica acta, 2006. **445**(2): p. 195-199.
52. Marshall, L.-J.R., et al., *Analysis of ochres from Clearwell Caves: the role of particle size in determining colour*. Spectrochimica Acta Part A: Molecular and Biomolecular Spectroscopy, 2005. **61**(1-2): p. 233-241.
53. Ruan, H.D., et al., *Far-infrared spectroscopy of alumina phases*. Spectrochimica Acta Part A: Molecular and Biomolecular Spectroscopy, 2002. **58**(2): p. 265-272.
54. Bell, I.M., R.J.H. Clark, and P.J. Gibbs, *Raman spectroscopic library of natural and synthetic pigments (pre- [approximate] 1850 AD)*. Spectrochimica Acta Part A: Molecular and Biomolecular Spectroscopy, 1997. **53**(12): p. 2159-2179.
55. Bikiaris, D., et al., *Ochre-differentiation through micro-Raman and micro-FTIR spectroscopies: application on wall paintings at Meteora and Mount Athos, Greece*. Spectrochimica Acta Part A: Molecular and Biomolecular Spectroscopy, 2000. **56**(1): p. 3-18.
56. Sagona, A., *Bruising the Red Earth*. 1994: Melbourne University Press.
57. Jercher, M., et al., *Rietveld X-Ray Diffraction and X-Ray Fluorescence Analysis of Australian Aboriginal Ochres*. Archaeometry., 1998. **40**(2): p. 383-401.
58. David, B., et al., *The Maytown Ochre Source*. Memoirs of the Queensland Museum, 1995. **38**(2): p. 441-445.
59. Bowler, J.M. and A.G. Thorpe, *Human Remains for Lake Mungo: Discovery and Excavation of Lake Mungo*, in *The Origin of Australians*, R.L. Kirk and A.G. Thorpe, Editors. 1976, Australian Institute of Aboriginal Studies: Canberra, Australia. p. 127-138.
60. Smith, M.A. and S. Pell, *Oxygen-Isotope Ratios in Quartz as Indicators of the Provenance of Archaeological Ochres*. Journal of Archaeological Science, 1997. **24**(9): p. 773-778.
61. Clarke, J., *Two Aboriginal Rock Art Pigments from Western Australia: Their Properties, Use and Durability*. Studies in Conservation, 1976. **21**: p. 134-142.

62. Jones, P., *Ochre and Rust: Artefacts and Encounters on Australian Frontiers*. 2007, Adelaide: Wakefield Press.
63. Roberts, K. *Clearwell Caves - Ancient Iron Mines. Near Coleford, Royal Forest of Dean*. 2007 [cited 2007].
64. Mortimore, J.L., et al., *Analysis of red and yellow ochre samples from Clearwell Caves and Catalhoyuk by vibrational spectroscopy and other techniques*. *Spectrochimica Acta Part A: Molecular and Biomolecular Spectroscopy*, 2004. **60**(5): p. 1179-1188.
65. Ohkawa, M., et al., *Hematite in pyrophyllite ore deposits, Shobara district, southwestern Japan*. *Mineralogy and Petrology*, 2002. **70**(Volume 70, Numbers 1-2 / August, 2000): p. 15-23.
66. Elias, M., et al., *The colour of ochres explained by their composition*. *Materials Science and Engineering B*, 2006. **127**: p. 70-80.
67. Greenwood, N.N. and A. Earnshaw, *Chemistry of the Elements*. 1984: Pergamon Press.
68. Schwertmann, U. and R.M. Cornell, *Iron Oxides in the Laboratory: Preparation and Characterisation*. Second Complete and Revised ed. 1991: Wiley-VCH.
69. Faria, d. and Lopes. *Natural Hematite or Heated Goethite: Can Raman Microscopy Differentiate Them?* in *Eighteenth International Conference on Raman Spectroscopy (ICORS 2002) : proceedings of the Eighteenth International Conference on Raman Spectroscopy : 25-30 August, 2002*. 2002. Budapest, Hungary: John Wiley and Sons.
70. Wang, J., W.B. White, and J.H. Adair, *Optical Properties of Hydrothermally Synthesized Hematite Particulate Pigments*. *Journal of the American Ceramic Society* 2005. **88**(12): p. 3449-3454.
71. Weinstein-Evron, M. and S. Ilani, *Provenance of Ochre in the Natufian Layers of el-Wad Cave, Mount Carmel, Israel*. *Journal of Archaeological Science*, 1994. **21**(4): p. 461-467.
72. Guinier, A., *X-ray diffraction: in crystals, imperfect crystals, and amorphous bodies*. 1994: Courier Dover Publications.
73. Klug, H.P. and L.E. Alexander, *X-ray diffraction procedures*. 1954.
74. Klug, H.P. and L.E. Alexander, *X-ray diffraction procedures: for polycrystalline and amorphous materials*. *X-Ray Diffraction Procedures: For Polycrystalline and Amorphous Materials*, 2nd Edition, by Harold P. Klug, Leroy E. Alexander, pp. 992. ISBN 0-471-49369-4. Wiley-VCH, May 1974., 1974. **1**.
75. Zachariasen, W., *A general theory of X-ray diffraction in crystals*. *Acta Crystallographica*, 1967. **23**(4): p. 558-564.

## REFERENCES

76. Warren, B.E., *X-ray Diffraction*. 1969: DoverPublications. com.
77. Whittig, L., W. Allardice, and A. Klute, *X-ray diffraction techniques*. Methods of soil analysis. Part 1. Physical and mineralogical methods, 1986: p. 331-362.
78. Zachariasen, W.H., *Theory of X-ray Diffraction in Crystals*. 2004: DoverPublications. com.
79. Bartels, W., *Characterization of thin layers on perfect crystals with a multipurpose high resolution x-ray diffractometer*. Journal of Vacuum Science & Technology B: Microelectronics and Nanometer Structures, 1983. **1**(2): p. 338-345.
80. Cole, H., *Bragg's law and energy sensitive detectors*. Journal of Applied Crystallography, 1970. **3**(5): p. 405-406.
81. Moore, D.M. and R.C. Reynolds Jr, *X-ray diffraction and the identification and analysis of clay minerals*. 1989: Oxford University Press (OUP).
82. Wiles, D.t. and R. Young, *A new computer program for Rietveld analysis of X-ray powder diffraction patterns*. Journal of Applied Crystallography, 1981. **14**(2): p. 149-151.
83. Pflugrath, J., *The finer things in X-ray diffraction data collection*. Acta Crystallographica Section D: Biological Crystallography, 1999. **55**(10): p. 1718-1725.
84. Beck, L., et al., *PIXE characterisation of prehistoric pigments from Abri Pataud (Dordogne, France)*. X-Ray Spectrometry, 2011. **40**(3): p. 219-223.
85. Calza, C., et al., *Characterization of Brazilian artists' palette from the XIX century using EDXRF portable system*. Applied Radiation and Isotopes, 2010. **68**(4–5): p. 866-870.
86. Creagh, D.C., M.E. Kubik, and M. Sterns, *On the feasibility of establishing the provenance of Australian Aboriginal artefacts using synchrotron radiation X-ray diffraction and proton-induced X-ray emission*. Nuclear Instruments and Methods in Physics Research Section A: Accelerators, Spectrometers, Detectors and Associated Equipment, 2007. **580**(1): p. 721-724.
87. David, B., E. Clayton, and A. Watchman, *Initial Results of PIXE Analysis on Northern Australian Ochres*. Australian Archaeology, 1993. **36**: p. 50-57.
88. Erlandson, J.M., J.D. Robertson, and C. Descantes, *Geochemical Analysis of Eight Red Ochres from Western North America*. American Antiquity, 1999. **64**(3): p. 517-516.
89. Gil, M., et al., *Yellow and red ochre pigments from southern Portugal: Elemental composition and characterization by WDXRF and XRD*. Nuclear Instruments and Methods in Physics Research Section A: Accelerators, Spectrometers, Detectors and Associated Equipment, 2007. **580**(1): p. 728-731.

90. A.Manasse and M.Mellini, *Iron (hydr)oxide nanocrystals in raw and burnt sienna pigments*. Eur. J. Mineral, 2006. **18**: p. 845-853.
91. MacDonald, B.L., et al., *Geochemical characterization of ochre from central coastal British Columbia, Canada*. Journal of Archaeological Science, 2011. **38**(12): p. 3620-3630.
92. O'Neil, J.R. and B.W. Chappell, *Oxygen and hydrogen isotope relations in the Berridale Batholith*. Journal of the Geological Society, London, 1977. **133**: p. 559-571.
93. Ortega, M., et al., *Analysis of prehispanic pigments from "Templo Mayor" of Mexico city* Journal of Materials Science, 2001. **36** (3): p. 751-756.
94. Popelka-Filcoff, R.S., et al., *Trace element characterization of ochre from geological sources*. Journal of Radioanalytical and Nuclear Chemistry, 2007. **272**(1): p. 17-27.
95. Prasada, P.S.R., et al., *In situ FTIR study on the dehydration of natural goethite*. Journal of Asian Earth Sciences, 2006. **27**: p. 503-511.
96. Reiche, I., et al., *An external PIXE study: Mughal painting pigments*. X-Ray Spectrometry, 2004. **34**(1): p. 42-45.
97. Valdez, B.C., Juan; Schorr, Michael; Zlatev, Roumen and Cota, Leonel, *Characterisation of Materials and Techniques Used in Mexican Rock Paintings* Rock Art Research: The Journal of the Australian Rock Art Research Association (AURA), 2008. **25**(2): p. 131-135.
98. Juliá, C.G. and C.P. Bonafé, *The use of natural earths in picture: study and differentiation by thermal analysis*. Thermochemica Acta, 2003. **413**: p. 185-192.
99. Calligaro, T., J.C. Dran, and M. Klein, *Application of photo-detection to art and archaeology at the C2RMF*. Nuclear Instruments and Methods in Physics Research Section A: Accelerators, Spectrometers, Detectors and Associated Equipment, 2003. **504**(1-3): p. 213-221.
100. Genestar Juliá, C. and C. Pons Bonafé, *The use of natural earths in picture: study and differentiation by thermal analysis*. Thermochemica Acta, 2004. **413**(1-2): p. 185-192.
101. Castro, K., et al., *Micro-Raman analysis of coloured lithographs* Analytical and Bioanalytical Chemistry, 1994. **379**(4): p. 674-683.
102. Edwards, H.G.M., *Illumination of a mediaeval mystery: the FT-Raman spectroscopic analysis of red pigment from a mediaeval corbel in the church St Clement of Rome, Fiskerton*. Journal of Molecular Structure, 2003. **661-662**: p. 271-277.
103. Helwig, K., *The characterisation of iron earth pigments using infrared spectroscopy*. Postprints. **11**: p. 83-91.

## REFERENCES

104. Perardi, A., A. Zoppi, and E. Castellucci, *Micro-Raman spectroscopy for standard and in situ characterisation of painting materials*. Journal of Cultural Heritage, 2000. **1**, **Supplement 1(0)**: p. S269-S272.
105. Blanch, A.J., et al., *Autocorrelation infrared analysis of mineralogical samples: The influence of user controllable experimental parameters*. Analytica Chimica Acta, 2007. **590(2)**: p. 145-150.
106. Edreira, M.C., et al., *Spectroscopic analysis of roman wall paintings from Casa del Mitreo in Emerita Augusta, Mérida, Spain*. Talanta, 2003. **59**: p. 1117-1139.
107. Edreira, M.C., et al., *Roman wall paintings characterization from Cripta del Museo and Alcazaba in Mérida (Spain): chromatic, energy dispersive X-ray fluorescence spectroscopic, X-ray diffraction and Fourier transform infrared spectroscopic analysis*. Analytica Chimica Acta, 2001. **434**: p. 331-345.
108. Edreira, M.C., et al., *Roman wall paintings characterization from Cripta del Museo and Alcazaba in Mérida (Spain): chromatic, energy dispersive X-ray fluorescence spectroscopic, X-ray diffraction and Fourier transform infrared spectroscopic analysis*. Analytica Chimica Acta, 2001. **434(2)**: p. 331-345.
109. Lazic, V., et al., *Characterisation of lustre and pigment composition in ancient pottery by laser induced fluorescence and breakdown spectroscopy*. Journal of Cultural Heritage, 2003. **4**, **Supplement 1(0)**: p. 303-308.
110. Mirti, P. and P. Davit, *New developments in the study of ancient pottery by colour measurement*. Journal of Archaeological Science, 2004. **31(6)**: p. 741-751.
111. Smith, K., et al., *Detecting art forgeries using LA-ICP-MS incorporating the in situ application of laser-based collection technology*. Talanta, 2005. **67(2)**: p. 402-413.
112. Russell, J.D. and A.R. Fraser, *Infrared methods*, in *Clay Mineralogy: Spectroscopic and Chemical Determinative Methods*, M.J. Wilson, Editor. 1994, Springer Netherlands. p. 11-67.
113. Schrader, B., *Infrared and Raman spectroscopy: methods and applications*. 2008: John Wiley & Sons.
114. Stenberg, B., et al., *Chapter five-visible and near infrared spectroscopy in soil science*. Advances in agronomy, 2010. **107**: p. 163-215.
115. Stewart, J.E., *Infrared spectroscopy: Experimental methods and techniques*. 1970: M. Dekker.
116. Suetaka, W., *Surface Infrared and Raman Spectroscopy: Methods and Applications*. Vol. 3. 1995: Springer.
117. Klocek, P., *Handbook of infrared optical materials*. 1991: CRC Press.



118. Williams, D., I. Fleming, and E. Pretsch, *Spectroscopic Methods*. Organic Chemistry, 1989(1989).
119. Griffiths, P.R. and J.A. De Haseth, *Fourier transform infrared spectrometry*. Vol. 171. 2007: John Wiley & Sons.
120. Allen, S.D.M., et al., *Infrared spectroscopy of the mineralogy of coprolites from Brean Down: evidence of past human activities and animal husbandry*. Spectrochimica Acta Part A: Molecular and Biomolecular Spectroscopy, 2002. **58**(5): p. 959-965.
121. Hug, S.J. and D. Bahnemann, *Infrared spectra of oxalate, malonate and succinate adsorbed on the aqueous surface of rutile, anatase and lepidocrocite measured with in situ ATR-FTIR*. Journal of Electron Spectroscopy and Related Phenomena, 2006. **150**(2-3): p. 208-219.
122. Colthup, N.B., L.H. Daly, and S.E. Wiberley, *Introduction to infrared and Raman spectroscopy*. 1990: Academic press.
123. Gardiner, D.J., P.R. Graves, and H.J. Bowley, *Practical Raman Spectroscopy*. Vol. 21. 1989: Springer-Verlag Heidelberg,, Germany.
124. Bloembergen, N., *The stimulated Raman effect*. American Journal of Physics, 1967. **35**: p. 989.
125. Koningstein, J.A., *Introduction to the Theory of the Raman Effect*. 1972: Reidel Dordrecht.
126. Loudon, R., *Theory of the first-order Raman effect in crystals*. Proceedings of the Royal Society of London. Series A. Mathematical and Physical Sciences, 1963. **275**(1361): p. 218-232.
127. Loudon, R., *The Raman effect in crystals*. Advances in Physics, 1964. **13**(52): p. 423-482.
128. Halvorson, R.A. and P.J. Vikesland, *Surface-Enhanced Raman Spectroscopy (SERS) for Environmental Analyses*. Environmental Science & Technology, 2010. **44**: p. 7749-7755.
129. Grasselli, J.G. and B.J. Bulkin, *Analytical Raman Spectroscopy*. 1991: Wiley.
130. Long, D.A. and D. Long, *Raman spectroscopy*. 1977: McGraw-Hill New York.
131. McCreery, R.L., *Raman spectroscopy for chemical analysis*. Vol. 225. 2005: Wiley.com.
132. De Faria, D., S. Venâncio Silva, and M. De Oliveira, *Raman microspectroscopy of some iron oxides and oxyhydroxides*. Journal of Raman spectroscopy, 1997. **28**(11): p. 873-878.
133. Schrader, B., *Infrared and Raman spectroscopy*. 2008: Wiley.com.

## REFERENCES

134. Mazzeo, R., et al., *Characterization of mural painting pigments from the Thubchen Lakhang temple in Lo Manthang, Nepal*. Journal of Raman Spectroscopy, 2004. **35**: p. 678-685.
135. Helmke, P.A., *Neutron activation analysis*. Methods of Soil Analysis: Part 3, Chemical Methods, 1996: p. 141-160.
136. Bieber, A.M., *Neutron-Activation Analysis*. Bulletin of the American Schools of Oriental Research. Supplementary Studies, 1974: p. 141-147.
137. De Soete, D., *Neutron activation analysis*. 1972.
138. David, B., *Initial Results of PIXE Analysis on Northern Australian Ochres*. Australian Archaeology, 1993. **36**: p. 50.
139. Watling, R.J. and R.L. Green, *Submission to the Parliamentary Inquiry into Australia's Indigenous Visual Arts Sector*. 2006, Centre for Forensic Science University of Western Australia. p. 1-23.
140. Frost, R., Z. Ding, and H. Ruan, *Thermal analysis of goethite*. Journal of Thermal Analysis and Calorimetry, 2003. **71**(3): p. 783-797.
141. Green, R.L. and R.J. Watling, *Trace Element Fingerprinting of Australian Ocher Using Laser Ablation Inductively Coupled Plasma-Mass Spectrometry (LA-ICP-MS) for the Provenance Establishment and Authentication of Indigenous Art\**. Journal of Forensic Sciences, 2007. **52**(4): p. 851-859.
142. Iriarte, E., et al., *The Origin and Geochemical Characterisation of Red Ochres from the Tito Bustillo and Monte Castillo Caves (Northern Spain)\**. Archaeometry, 2009. **51**(2): p. 231-251.
143. Montagner, C., et al., *Ochres and earths: Matrix and chromophores characterization of 19th and 20th century artist materials*. Spectrochimica Acta Part A: Molecular and Biomolecular Spectroscopy, 2013. **103**(0): p. 409-416.
144. Mooney, S.D., C. Geiss, and M.A. Smith, *The Use of Mineral Magnetic Parameters to Characterize Archaeological Ochres*. Journal of Archaeological Science, 2002. **29**: p. 000-000.
145. Mooney, S.D., C. Geiss, and M.A. Smith, *The use of mineral magnetic parameters to characterize archaeological ochres*. Journal of Archaeological Science, 2003. **30**(5): p. 511-523.
146. Colombini, M.P., et al., *Integrated analytical techniques for the study of ancient Greek polychromy*. Talanta, 2004. **63**: p. 839-848.
147. Bennett, J., *Commissioning of NAA at the new OPAL reactor in Australia*. Journal of radioanalytical and nuclear chemistry, 2008. **278**(3): p. 671-673.

148. Von Orelli, A.Z., (CH), Lanker, Michael (Pfäffikon, CH), Frick, Beat (Buchs, CH), Kunz, Thomas (Dällikon, CH), Offermann, Mario (Buchs, CH), *Handheld colour measurement device*, C. X-Rite Europe GmbH (Regensdorf, Editor. 2010: United States.
149. X-Rite Incorporated. *X-Rite: Right on Color*. 2010 [cited 2010 01/12/2010]; Available from: <http://www.xrite.com/>.
150. DataColor. *Datacolor Spectrocolorimeter Model #1005 Specification Comparison*. 2011 05/11/2011]; Available from: <http://spyder.datacolor.com/product-compare1005.php>.
151. Finney, M.D.C., (IL, US), Lamfers, Robert A. (Hudsonville, MI, US), Beukema, Steven M. (Grand Rapids, MI, US), *Color measurement instrument and base unit*, I.G. X-Rite, MI, US), Editor. 2006: United States.
152. Newman, D., *The Distribution of Range in Samples from a Normal Population, Expressed in Terms of an Independent Estimate of Standard Deviation*. *Biometrika*, 1939. **31**(1/2): p. 20-30.
153. Technology, A., *Uses of Derivative Technology*, A.J. Owen, Editor. 1995.
154. Tsai, F. and W. Philpot, *Derivative Analysis of Hyperspectral Data*. *Remote Sensing of Environment*, 1998. **66**(1): p. 41-51.
155. Dubrovkin, I.M., *Theory of quantitative multicomponent analysis from differential spectra*. *Journal of Applied Spectroscopy*, 1983. **38**(6): p. 686-689.
156. O'Connell, J., P. Latz, and P. Barnett, *Traditional and modern plant use among the Alyawara of central Australia*. *Economic Botany*, 1983. **37**(1): p. 80-109.
157. *Talyala Emu Farm, Mt. Charles Rd, Keith, South Australia 5268*. 2007.
158. Blee, A.J., Walshe, K.A., Pring, A., Quinton, J.S., & Lenehan, C.E., *Towards the Identification of Plant and Animal Binders on Australian Stone Knives*. *Talanta*, 2010. **82**(2): p. 745-750.
159. Casadio, F., et al., *Electron energy loss spectroscopy elucidates the elusive darkening of zinc potassium chromate in Georges Seurat's;A Sunday on La Grande Jatte—1884*. *Analytical and Bioanalytical Chemistry*, 2011. **399**(9): p. 2909-2920.
160. *Allstone Pty Ltd, 207-211 Devonport Tce Prospect, South Australia 5082*. 2009.
161. Davidson, D.S., *Notes on the pictographs and petroglyphs of Western Australia and a discussion of their affinities with appearances elsewhere on the continent*. *Proceedings of the American Philosophical Society*, 1952: p. 76-117.
162. Kerwin, D., *Aboriginal Dreaming Paths and Trading Routes: The Colonisation of the Australian Economic Landscape*. 2012: Sussex Academic Press.

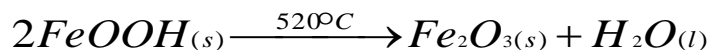
## REFERENCES

163. Hillier, H.J., *Letters to the Director of the Queensland Museum*. 1916: Petersburg S.A. Queensland Museum Archives.
164. Jones, P. and P. Sutton, *Art and Land: Aboriginal Sculptures of The Lake Eyre Region*. 1986, Adelaide: South Australian Museum and Wakefield Press.
165. Watchman, A.L., and R. Jones, *Dating rock images in the tropical monsoon region of northern Australia*. Australian Aboriginal Studies, 1998. **1998.2**: p. 64.
166. Morwood, M., *Handy household hints for archaeological excavations at rock art sites*. Rock art research, 1994. **11**(1): p. 10-12.
167. *Bushwalking in Flinders Rangers National Park*, D.f.E.a. Heritage, Editor. 2007: Hawker, SA.
168. Klaassen, N. *Flinders Rangers Research: Art In The Flinders Rangers*. 2007.
169. Birt, P., *A report for the Department of Environment and Heritage and the Aboriginal Heritage Branch, Aboriginal Affairs and Reconciliation Division*. 2007, Aboriginal Heritage Branch: Adelaide, SA. p. 7.

**APPENDIX A:  
AN INVESTIGATION  
INTO THE GOETHITE  
DEHYDRATION  
MECHANISM**

## 9.1. Background information and motivations

The percentage by weight of both the goethite and haematite components of ochres is of interest as it is known that goethite can be easily converted to haematite via a dehydration process at a temperature between 260°C and 550°C, such as roasting at a camp fire, as shown by the equation below [69-71].



**Equation 9-1:** *The dehydration mechanism for the conversion of Goethite to Haematite.*

This suggests that the heat treatment of yellow ochre can result in the characteristic red colour associated with haematite, whilst still maintaining the predominant structure and majority composition of goethite.

However, some debate exists over the temperature at which this dehydration occurs, and if Indigenous Australians were dehydrating goethite to create a red coloured ochre for use in rituals and the creation of objects. This study hopes to confirm the temperature at which this dehydration occurs to see if it would in fact be possible to achieve this colour change by treating the goethite with resources available to Indigenous Australians, such as a bonfire. It also aims to determine if it is scientifically possible to distinguish between natural haematite and haematite created from the dehydration of goethite, so that samples collected from within aboriginal communities can be studied to identify if this practice was in use.

## 9.2. TGA Studies: Variation of temperature

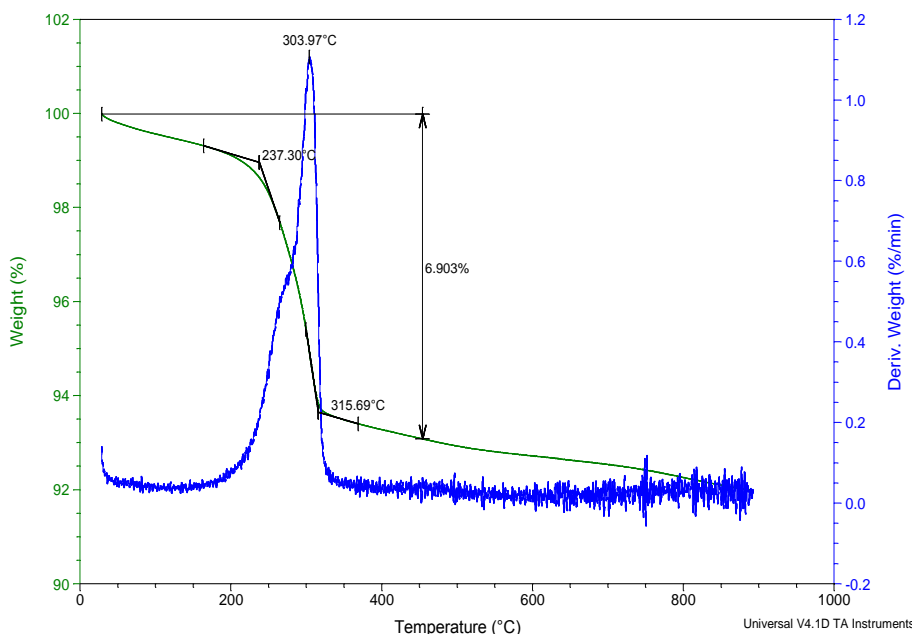
### 9.2.1. Experimental methods

Initial studies focus on TGA with the variation of temperature to establish the temperature at which the onset of this transition occurs, as well as the optimum temperature. Also of interest is the percentage of mass of the sample lost.

A sample of pure Fluka goethite 71063 of approximately 24.5mg in weight is placed into an Auto TGA 2950HR version 6.1A and heated to 900°C at a rate of 10°C per minute. Heating occurs under air at a rate of 50mL/min. Results are then presented as both a function of temperature, and a derivative function of temperature to highlight change.

### 9.2.2. Results

Results of this TGA analysis show an onset of the dehydration at 237.30°C, reaching its maximum at 303.97°C, and continuing to loose mass to a temperature of approximately 316°C. The total percentage of mass lost during this dehydration is 6.903%, with small volumes of mass lost until the maximum temperature is reached with a total mass loss of approximately 8%.



**Figure 9-1:** TGA results obtained from the heating of pure goethite to 900°C in air.

In order to confirm that this loss of mass is due to the conversion of goethite to haematite, XRD studies are completed.

### 9.3. X-Ray diffraction

XRD analysis was completed at the Commonwealth Scientific and Industrial Research Organisation (CSIRO), aided by Peter Self from the Mineralogical and Geochemical Services group at the CSIRO Land and Water in Adelaide South Australia.

Due to the nature of the equipment involved, the majority of the data collection was completed by Peter Self, and as such the following description of experimental methods is largely his wording. Some heating was completed at Flinders University, as well as the analysis of the results and as such the discussion contained here is a result of the candidates work.

#### 9.3.1. Experimental methods

##### 9.3.1.1. Sample type

Due to availability, two alternate types of goethite were used as reference material. One being pigment-grade, Hattrick goethite Y163, and the other being Fluka goethite 71063.

##### 9.3.1.2. Heating

###### a) Ex-suit: CSIRO

The heating of samples was carried out in such a way that the weight loss of a sample as a result of the heating could be measured with reasonable accuracy. The weight of a glass weighing jar and lid was measured accurately. Approximately and half grams of Hattrick

goethite was added to the jar and the weight of the jar, lid and sample accurately measured. The jar containing the sample and the lid (removed from jar) were placed in an oven set to the required temperature. Most samples were heated for 24 hours; some were heated for 72 hours. After the required time interval, the oven was opened and the lid immediately placed on the weighing jar whilst the jar was still in the oven. The closed jar containing the sample was then removed from the oven and allowed to cool to room temperature. The weight of the closed jar was accurately measured and the weight loss calculated.

The majority of heating was carried out in air in an oven that allowed for some air flow through the heating chamber. A limited number of heating experiments were carried out using a vacuum oven. The method for heating under vacuum was the same as for heating in air with the exception that before opening the vacuum oven the oven was brought to atmospheric pressure by filling the heating chamber with dry nitrogen gas.

### **b) Ex-suit: Flinders University**

The heating of samples completed on site at Flinders University was carried out in an attempt to confirm the dehydration was occurring at a number of temperatures, and made no allowances to measure the weight lost.

Samples of approximately 1.5grams in size were placed in glass crucibles into ovens and heated at a variety of temperatures from 100°C to 220°C across a time frame of 24 hours to 72 hours to one complete week.

### **c) In-suit: CSIRO**

The sample, in this case Fluka goethite 71063, was run initially at room temperature, and then heated to 300°C at 30°C/min. Once the temp reached 300°C an initial pattern was collected, and then a pattern collected every hour.

#### **9.3.1.3. Quantitative XRD**

Samples for XRD examination were micronized under ethanol using a McCrone micronising mill. Micronisation ensures that the particles in the sample are of a size suitable for quantitative XRD analysis. The micronized samples were dried in an oven set to a temperature of 60°C. Dried samples were back-pressed into XRD sample holders. XRD patterns were recorded with a PANalytical X'Pert Pro multi-purpose diffractometer using Fe-filtered Co K<sub>α1</sub> radiation, automatic divergence slit, 2° anti-scatter slit and fast X'Celerator Si strip detector. The diffraction patterns were recorded in steps of 0.017° 2 theta with a 0.5 second counting time per step, and logged to data files for analysis.

Quantitative XRD determinations were obtained using Reitveld analysis as implemented by the TOPAS software package (Bruker AXS). The quantitative XRD results present make no allowance for non-crystalline materials in the samples.



### 9.3.2. Results

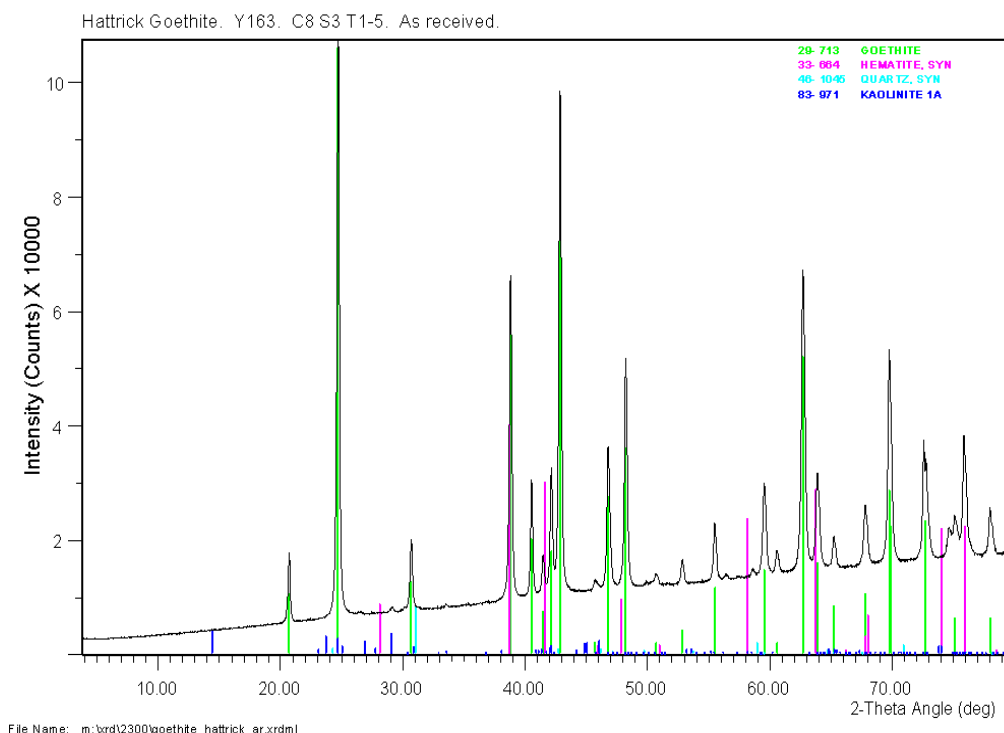
#### 9.3.2.1. Standards

Due to availability, two alternate types of goethite were used as reference material. One being pigment-grade, Hattrick goethite Y163, and the other being Fluka goethite 71063. XRD analysis was performed on both original 'pure' samples in order to confirm that neither sample contained any haematite prior to heating, and this is shown in Figure 9-2 and Figure 9-3 respectively.

It is important to note that whilst some variation exists between the two goethite standards, neither contains haematite, and as this study focuses only on the formation of haematite, the minor compositions of the standard are irrelevant and thus both standards are acceptable for use.

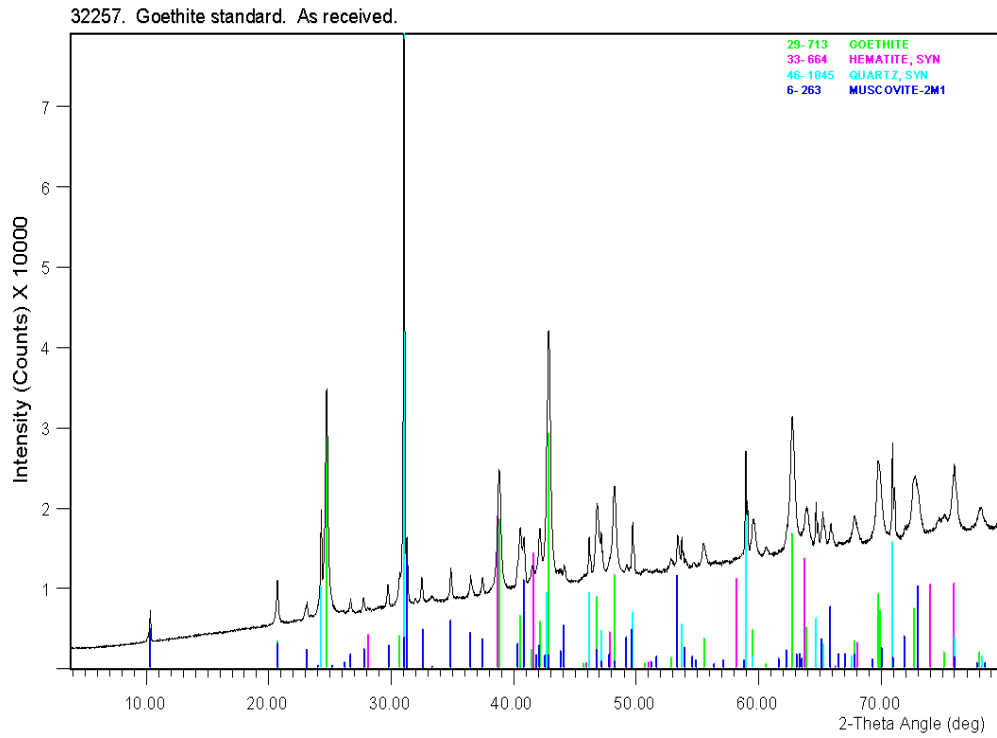
#### 9.3.2.1. Variation of temperature

Following this, the Hattrick goethite Y163 was then heated in air at temperatures ranging from 105°C - 300°C, as previously described. The resulting XRD patterns are shown in Figure 9-4. When examining these results, it can be seen that the XRD patterns of heated Hattrick goethite Y163 show no measurable changes for temperatures up to 200°C. At a heating temperature of 250°C the sample can be seen to contain a significant amount of hematite. For example, note the peaks at two-theta angles of approximately 28 °C and 58 degrees in the XRD pattern of the 250°C heated Hattrick goethite Y163 sample as shown in Figure 9-4. Quantitative XRD analysis calculates the hematite to goethite weight ratio in the 250°C heated sample as 23 to 77. At a heating temperature of 300°C there has been total conversion of goethite to hematite.

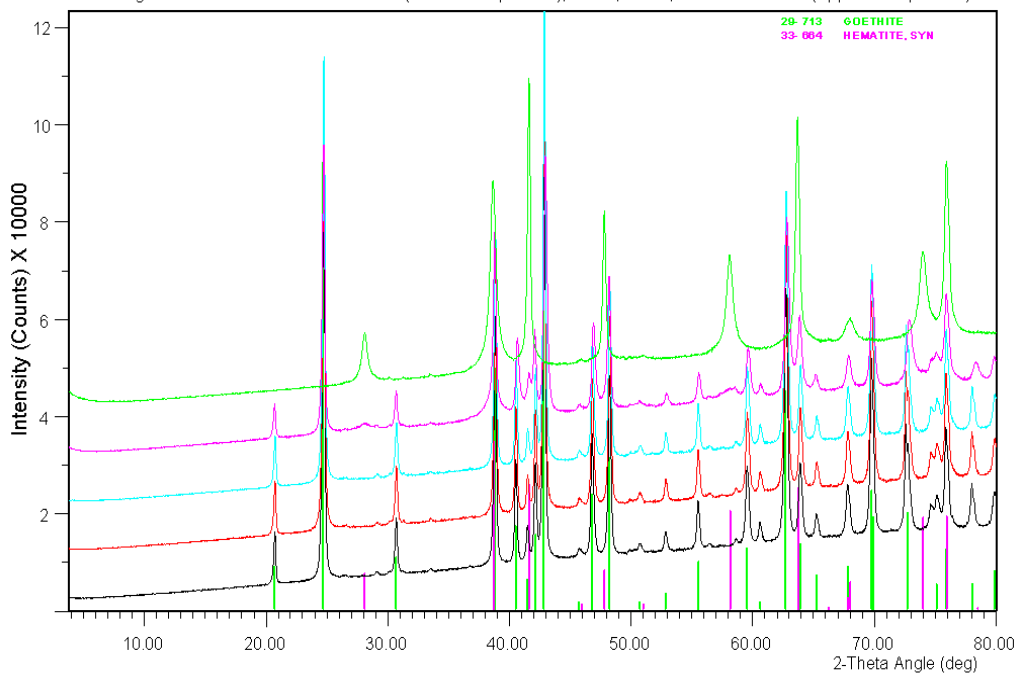


**Figure 9-2:** XRD pattern of as-received Hattrick goethite Y163.

APPENDIX A



**Figure 9-3:** XRD pattern of as-received Fluka goethite 71063.

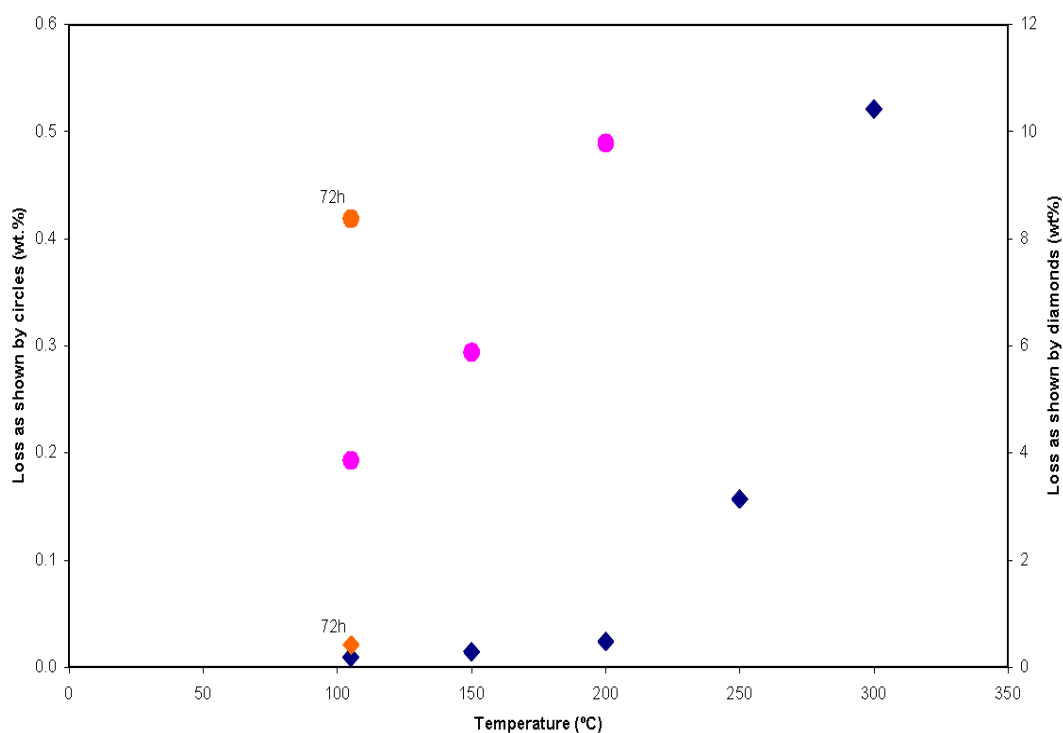


**Figure 9-4:** XRD patterns of Hattrick goethite Y163 heated at 105°C (shown in black), 150°C (shown in red), 200°C (shown in blue), 250°C (shown in purple) and 300°C (shown in green) for 24 hours in air.

The weight losses for heated Hattrick goethite Y163 are listed in Table 9-1 and plotted in Figure 9-5. The maximum weight loss in a sample where there was no transformation of goethite to hematite was at a temperature of 200°C. The weight losses at temperatures of

**Table 9-1:** Weight loss of Hattrick goethite Y163 after heating at the shown temperatures for the shown times.

Temp (°C)	Time (h)	Loss (wt.%)
105	24	0.19
105	72	0.42
150	24	0.29
200	24	0.49
250	24	3.14
300	24	10.43

**Figure 9-5:** Weight loss of Hattrick goethite Y163 after heating. Heating was in air for a time of 24 hours unless otherwise indicated. The data is plotted on two scales to better show the measured weight loss at temperatures below 250°C.

105°C and 150°C were significantly lower than the weight loss at 200°C. Heating Hattrick goethite Y163 at 105°C for 72 hours gave a similar weight loss to that after heating at 200°C for 24 hours.

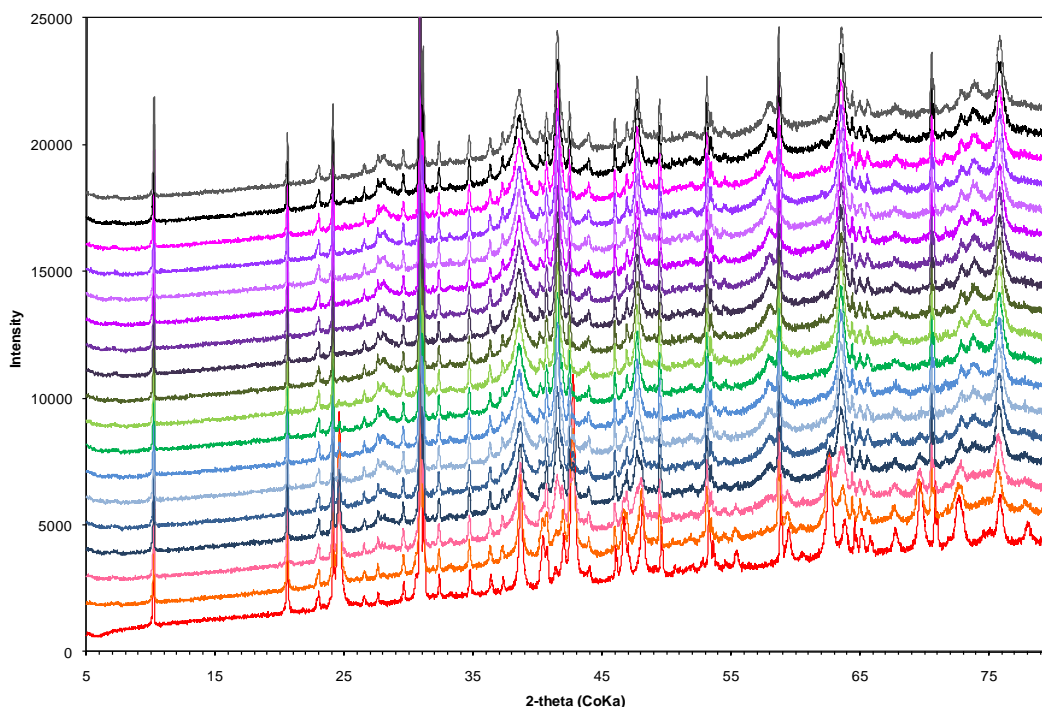
From the data obtained it is not possible to draw any conclusion about the true value of the non-structural water content of Hattrick goethite Y163. However, as it is well documented that the transition for goethite to haematite does result in a mass loss, and the presence of haematite has been confirmed via XRD analysis, it can be said that after a period of 24 hours

at 250°C partial transformation has occurred, with complete transformation occurring at a temperature of 300°C after a period of 24 hours. Further studies into the mass lost with this transition will be carried out utilizing TGA and will be discussed in a later section.

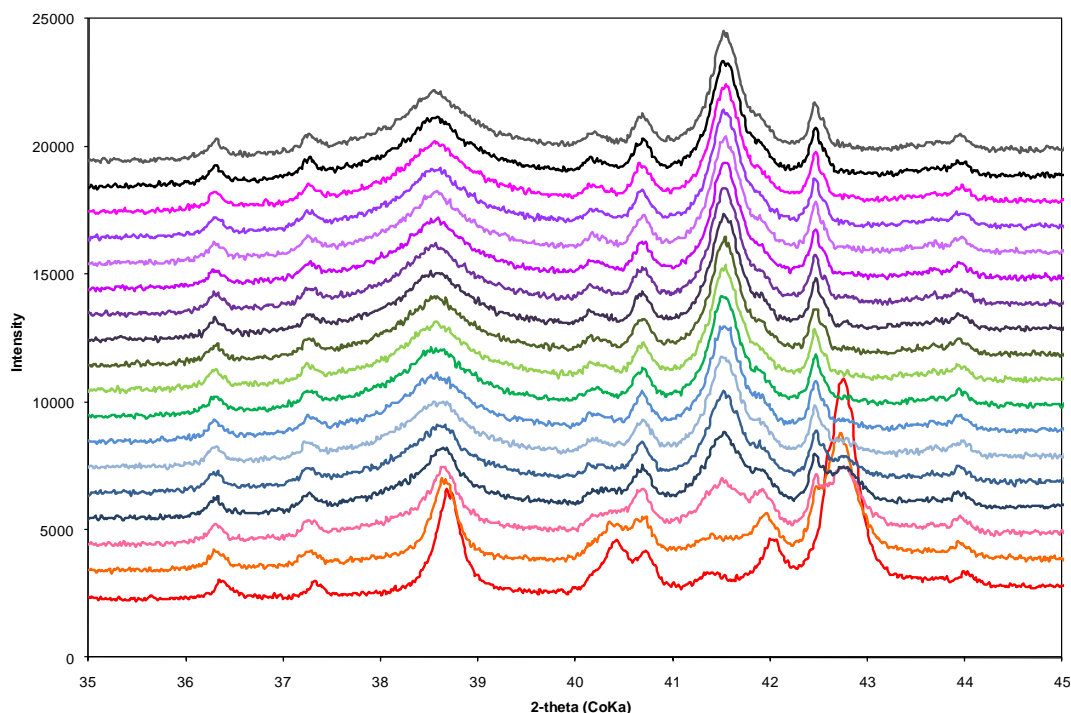
#### 9.3.2.2. Variation of time

Following the establishment that the dehydration does in fact occur at 300°C after a period of 24 hours, the XRD apparatus was converted to in-situ heating mode to allow for the monitoring of this transformation as both a function of temperature and time. This was not done initially as it was not known if this transformation would be achievable within the limitations of the instrument as previous TGA studies (see Figure 9-1) suggested a temperature of 303.43°C, slightly higher than the instruments maximum temperature of 300°C. It is also a lengthy and complicated process to convert the instrument, and time on this instrument is in great demand.

The sample, in this case Fluka goethite 71063, was run initially at room temperature, and then heated to 300°C at 30°C/min. The room temperature measurement of the standard is shown, then once the temp reached 300°C an initial pattern was collected, and then a pattern collected every hour. Results of this are shown in Figure 9-6. When examining this figure, it can be seen that the spectra appear very busy, and little variation is immediately apparent. The same spectra are shown in Figure 9-7, centred on the area where the goethite and haematite peaks dominate.



**Figure 9-6:** Spectra obtained (offset) from the heating of goethite, with the original spectra shown in red obtained at room temperature, the second spectra shown in orange obtained as the temperature reached 300°C, and each following spectra being an additional one hour into heating.



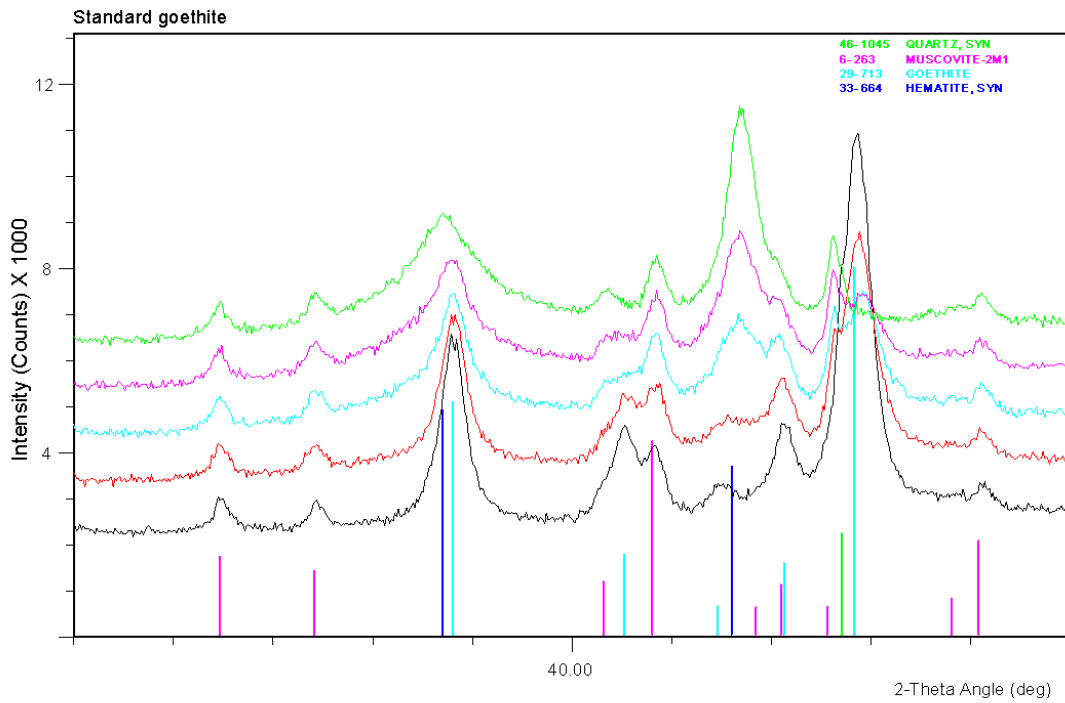
**Figure 9-7:** Spectra obtained (offset) from the heating of Goethite, with the original spectra shown in red obtained at room temperature, the second spectra shown in orange obtained as the temperature reached 300°C, and each following spectra being an additional one hour into heating, with only theta angles 35 to 45 shown.

It can be seen from this that, with time, at 300°C significant changes does occur. Of note is the reduction in the peaks present at approximately 2-theta 38.5° and 42.5°, and a formation of a peak at 41.5°. It appears that this change occurs quickly and is complete within the first six hours of heating, however this will be confirmed in a later section with the aid of weight loss analysis via TGA.

It is proposed that this change in spectra is due to the conversion of goethite to haematite, and this is confirmed in Figure 9-8, where the areas of interest shown in Figure 9-7 are overlaid with the known peak locations. To aid with visualisation, only the spectra collected at room temperature, the spectra obtained when the sample initially reached 300°C, the spectra obtained for the first two hours following this, and the final spectra taken at 16 hours of heating, are shown.

When comparing the peaks present with the overlaid known patterns of peak locations (with haematite shown in dark blue and goethite shown in light blue), it can be confirmed that this transition is in fact occurring with heating, and that complete transformation does occur within the specified 16 hour heating time.

APPENDIX A



**Figure 9-8:** Spectra obtained (offset) from the heating of Goethite, obtained at room temperature (shown in black), as temp reached 300°C (shown in red), with one and two hours heating (shown in blue and purple), and 16 hours heating (shown in green). Only 2-theta angles 35 to 45 are shown.

**APPENDIX B:  
ARKAROO ROCK -  
A CASE STUDY**

Arkaroo Rock, an important Aboriginal art site located in the Flinders Ranges National Park, South Australia, features a range of artworks created using red, yellow and white ochre along with charcoal. The site is widely promoted to tourists and, during peak season, attracts more than fifty visitors each day.

Whilst the ochre pigments used at this site are relatively inert and sustainable, rock art is susceptible to damage from a variety of sources, both natural and anthropogenic. These include subsidence (rock fall), vandalism, weathering and exposure to transported aerosols and airborne dusts.

It has been reported that dusts, whether airborne or from trampling of the floor sediment, can be a contributing factor in the deterioration of rock art, and accumulates in sheltered locations [165, 166]. In mid-2007, local Aboriginal people noted that the art was covered with a dust-like substance, the nature of which was unknown. It was hypothesised that the substance was the result of local soil adhering to the surface of the artwork with the morning dew. In order to preserve the site, cleaning and conservation work began in early 2008. This study presents an investigation into the source of the particulate matter covering the artworks.

### 10.1. Site location

This study focuses on the characterization of dust-like particulate matter found coating rock paintings at Arkaroo Rock, a site within the Flinders Ranges National Park, located approximately four hundred and fifty kilometres north of the Adelaide in South Australia and shown in Figure 10-1.



**Figure 10-1:** Map showing the location of Arkaroo Rock relative to South Australia's capital city, Adelaide.



Arkaroo Rock is an Adnyamathanha (meaning 'hills people') art site named for Akurra, the Dreaming serpent responsible for the creation of the Flinders Ranges, and more specifically, Wilpena Pound. The ochre and charcoal paintings present at the site depict this Dreaming story [167, 168]. The site is heavily promoted to tourists and has undergone extensive remodelling since the mid 1980's, including the erection of a cage/protective fence and boardwalk surrounding the art in an attempt to protect it from its thousands of annual visitors [168, 169].

## 10.2. Samples

In mid-2007, dust-like particles covering the surface of the artwork at Arkaroo Rock were identified by, a local Adnyamathanha man and employee of the Aboriginal Partnerships Section, Department for Environment and Heritage (DEH). Photographs taken at this time clearly show the presence of this particulate.

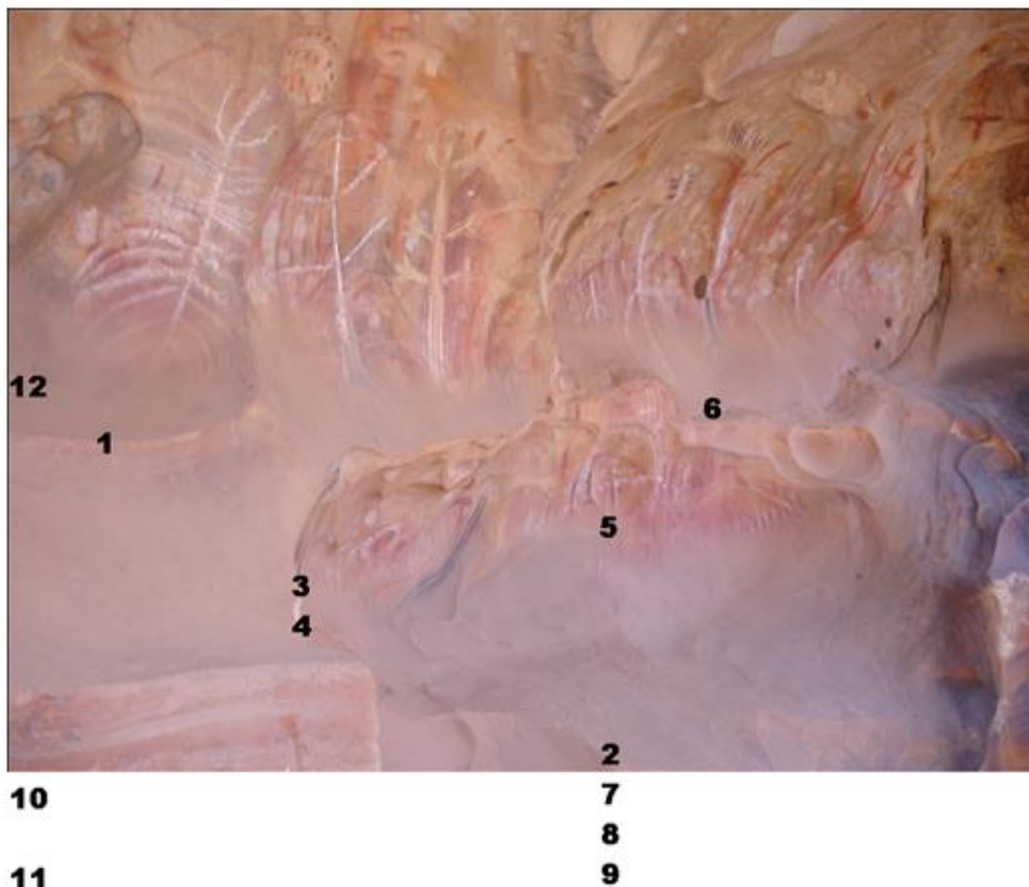
Samples were collected and analysis undertaken in an attempt identify the particulate and its origin, and to confirm the hypothesis that the fine particles collecting on the surface are being blown into the area with the breeze and are adhering to the surface of the rock when dew is present, and are not a result of soil disturbance in and around the caged area.

During conservation work in April 2008, samples were collected from the areas shown in Figure 10-2. Samples 1-6 and 12 are of the dust-like particles collected from the surface of the rock art and were collected with an artist's brush and sanitary glass containers, collecting as much sample as was obtainable from within an area of approximately 5 cm<sup>2</sup> (approximately 2 grams). Samples 3-4 were collected as they were from an area on the rock art showing suspected salt leaching. Samples 7-10 are also approximately 2 grams in weight, and are composed of soil collected from within the protective fence and surrounding area, and sample 11 is various plant material, including small leaves and stems, collected from a plant growing within the protective fence.

## 10.3. Experimental methods

A number of experimental techniques were applied to the samples collected. Optical microscopy was performed using a Lietz orthopol 12 petrographic microscope, with magnification between 50 and 200 times. Samples were prepared with approximately 0.3 grams of sample in Canadian Balsam and analysis was performed at the South Australian Museum.

X-ray diffraction (XRD) was performed on samples approximately 0.0025 grams in weight, ground in a mortar and pestle, then adhered to Mylar film with acetone following the addition of approximately 10% silicon powder as a phase standard with an exposure time of 120 minutes. Powder X-ray diffraction patterns were collected on a Huber Guinier Imaging Plate G670 with Co K<sub>α1</sub> radiation ( $\lambda=1.78892 \text{ \AA}$ ) generated at 35 kV and 34 mA, and processed



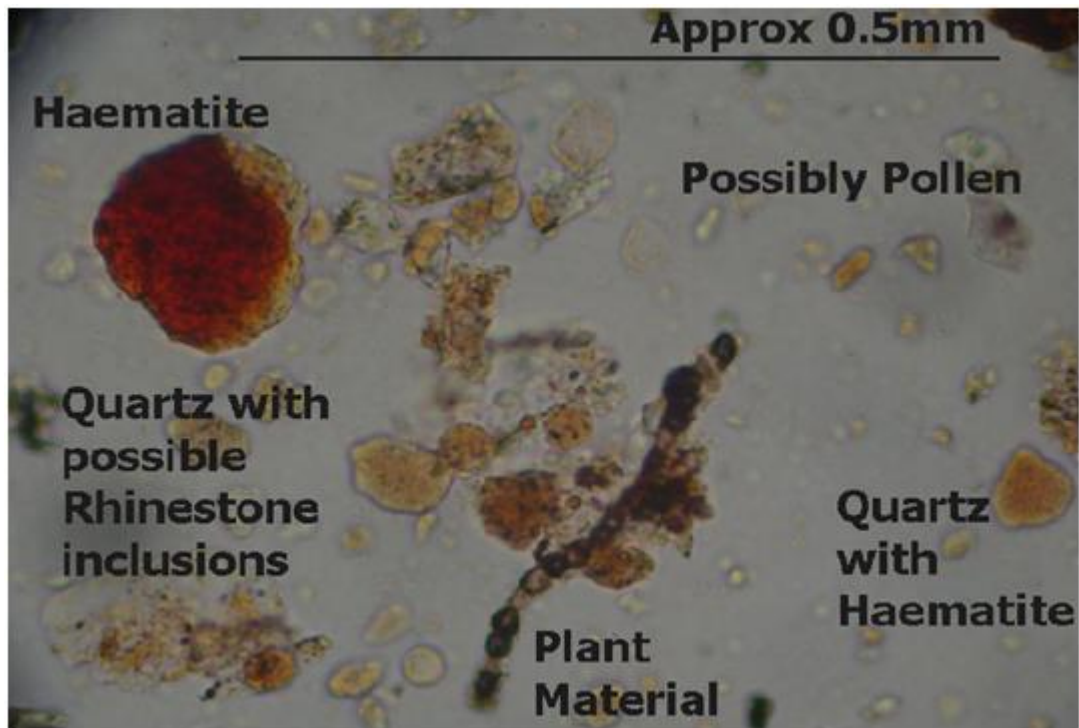
**Figure 10-2:** Photograph showing the dust- like particles collecting on the surface of the artwork, and the areas where samples were collected both from the rock surface (samples 1-6, 12) and from ground within the protective fence (samples 7-11).

using Jade software. Quantitative phase analyses were performed using the Rietveld method with the aid of a computer program called Rietica for Windows (v1.7.7)

Thermal gravimetric analysis (TGA) was performed on an Auto TGA 2950HR version 6.1A. Samples were ground but otherwise un-treated, and sample size is in the range of tens of milligrams. Samples were analysed under compressed air and heated from room temperature (approximately 25°C) to 900°C at a rate of approximately 10°C per minute. The weight is constantly monitored and is given spectroscopically as a function of temperature.

The EFI-ES1000 is a hand-held spectrophotometer with a tungsten source capable of performing measurements in the region of 380-730nm. The instrument was developed for the printing industry and its application to ochre and natural samples is novel. It is of particular interest for this project as it is non-destructive and portable, and work previously discussed has focused on this instrument.

Samples of approximately 0.05 grams are pressed under 10 tons of force for 120 seconds to obtain a disk approximately 1 cm in diameter with a flat and uniform surface. Analysis is then performed using EFI Colour Profiler for Printers and ColorPort 1.0.1. software (EFI Colour



**Figure 10-3:** Photograph taken on medium magnification utilizing a Lietiz orthopol 12 petrographic microscope showing a number of the species present in sample number 5 of the dust like particulate removed from the rock surface.

Profiler for Printers Windows XP 2004 v1.5.9.5). Data was then analysed using single linkage dendrogram routines in MINITAB (Minitab v15.1.30.0, Minitab Inc).

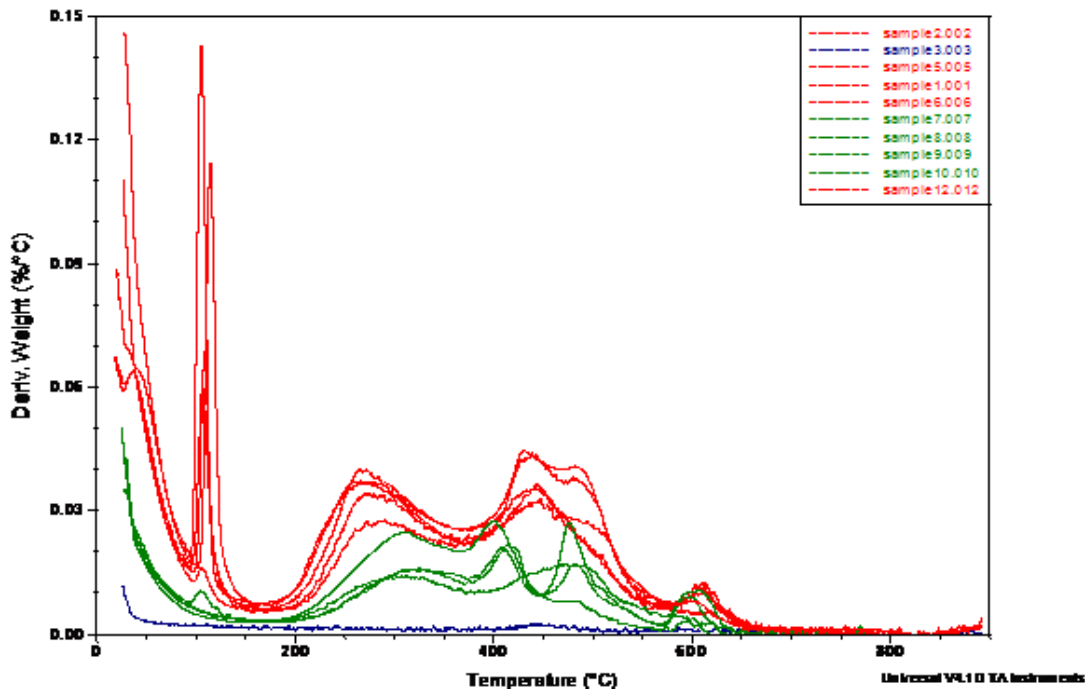
## 10.4. Results

### 10.4.1. Microscopy

When the dust-like particles collecting on the rock surface were examined microscopically, a number of components were identified. These components included quartz (both pure and with inclusions including rhinestone and haematite), pure haematite, a variety of plant material, and particles that possibly represent a variety of pollen species shown in Figure 10-3. Whilst Figure 10-3 is a singular representation of the composition of many of the samples, the microscopy study identified a large variety in particle size and composition, between and within samples. This considerable variation makes conclusions difficult to draw based only on the microscopy study.

### 10.4.2. X-ray diffraction

X-ray diffraction analysis identified the presence of quartz in all samples. However, no other mineral components were able to be identified with this method. This was not unexpected, but is valuable as it confirms that the samples being analysed are not contaminated with any ochre material from the surface of the rock. Unfortunately, as only quartz and silicon were detected,



**Figure 10-4:** Results of the TGA analysis of the fine particles collected from Arkaroo Rock. The plot shows the derivative weight (percent) as a function of temperature.

and the silicon was added as a standard and is not naturally present, Rietveld quantitative phase analysis is not able to be applied.

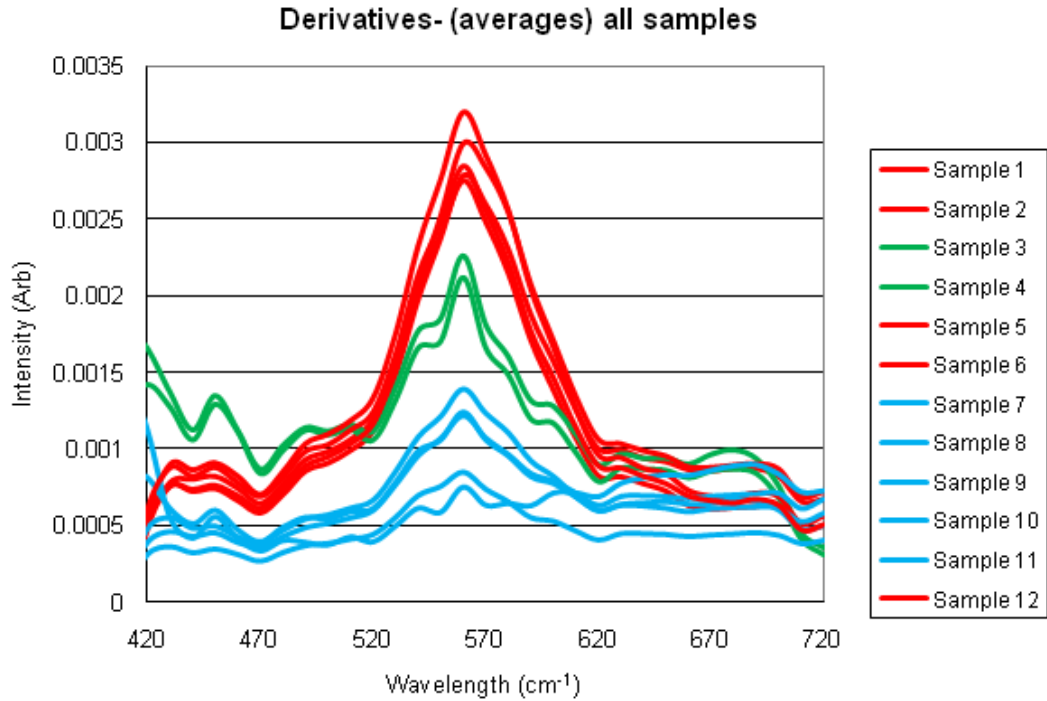
#### 10.4.1. Thermal gravimetric analysis:

Thermal gravimetric analysis results are presented in the form of a derivative weight loss curve as this allows observation of the temperature at which the most significant changes take place Figure 10-4.

Visual examination of the trends indicated substantial variation between sample types. The spectra can be loosely separated into three groups: (1) those showing no mass loss (blue), which are suspected of being salt leached from the rock; (2) those showing three peaks of high intensity at 100 °C, 250-275 °C and 425-450 °C (red) are samples collected from the surface of the rock; and (3) those showing 2-3 peaks of medium intensity at 300 °C, 400 °C and 475-500 °C (green) which are soil and plant samples collected from the caged and surrounding areas.

#### 10.4.2. Colour analysis utilising the EFI ES-1000:

The EFI ES-1000 produces a number of characteristic spectroscopic results for each sample analysed, of which the most relevant to this project is the spectral output. Figure 10-5 displays the first derivative of these spectra, which was chosen because it highlights subtle variations between the spectra of samples that otherwise appear very similar.



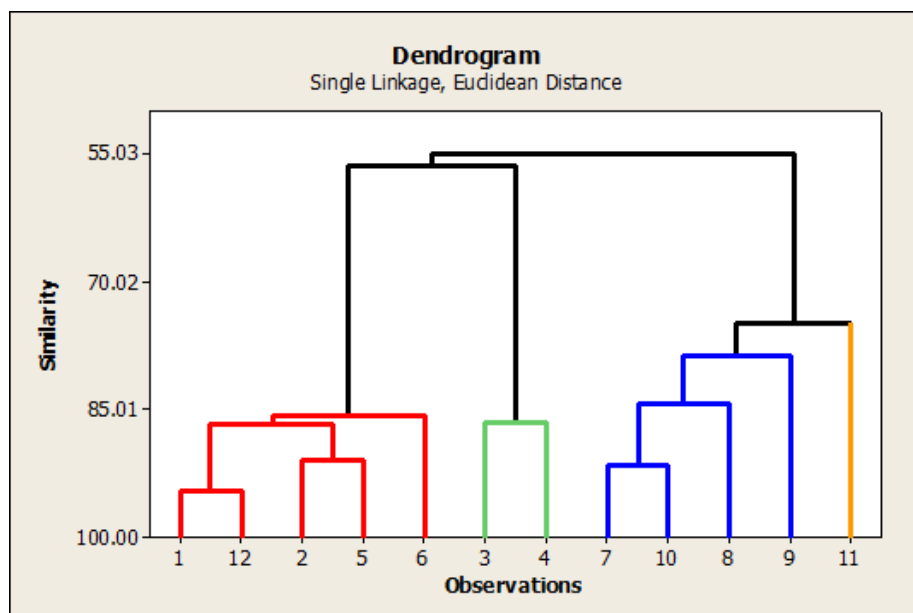
**Figure 10-5:** The derivative of the spectra obtained for all samples collected from both the surface of the rock and the ground within the caged area, using the EFI ES-1000 hand-held spectrophotometer.

Upon inspection of Figure 10-5, three distinct and separate groups are apparent. The distinction is most noticeable when examining the area between 520nm and 620nm. The group of samples with the greatest intensity in this area (samples 1, 2, 5, 6 and 12) correspond to those samples collected from the rock surface, shown in red. The ground of samples with the lowest intensity in this area (samples 7, 8, 9, 10 and 11) correspond to those samples, both soil and plant material, collected from ground within the caged area and are shown in blue, and the samples with intensities in the middle (samples 3 and 4) correspond to those samples collected from the surface of the rock from the area suspected to be contaminated by salt leaching and are shown in green.

#### 10.4.3. Statistical analysis

Whilst three distinct groupings of sample types have been shown to be present in the results of both TGA and the EFI ES-1000 analyses, interpretation was carried out by visual inspection of the result and as such, may be susceptible to human error. In an attempt to eliminate this, statistical analysis and grouping was undertaken to validate the interpretation.

Statistical analysis in this study was carried out utilising the cluster analysis routines in MINITAB software to produce dendrograms. These are visual illustrations that produce a hierarchical arrangement of sample clusters based on how similar (or dissimilar) objects under analysis (in this case samples) are. Analysis was performed using a multivariate approach with the spectroscopic results presented in Figure 3, using data in the region of 520-600 cm<sup>-1</sup>.



**Figure 10-6:** Dendrogram from statistical analysis using the MINITAB software of the derivatives of the spectra obtained for the samples collected (numbering shown in figure 2) and analysed using the EFI ES-1000.

The method was single linkage, Euclidean distance, and the results of the statistical analysis are shown in Figure 10-6.

Analysis of the dendrogram reveals four distinct groups of samples, shown in red, green, blue and orange. Further investigation shows that these groups correspond to samples removed from the rocks surface, samples removed from the rock surface in an area suspected to be contaminated by salt leaching, samples collected from the ground within the caged area, and plant material, respectfully. These are the distinctions that were visually apparent in Figure 10-4 and Figure 10-5.

## 10.5. Conclusions

Results of the microscopy and XRD studies, whilst valuable in confirming a number of similarities between the samples, and in identifying a number of expected components, proved to be of little value statistically and were unable to support or discount the original hypothesis that that the substance found on the surface of the rock-art was the local soil adhering to the surface of the artwork with the morning dew.

The TGA study, however, proved to be of more value. The peak featured at 100°C is unusual because it is a result of the sample drying and water being lost, and as it is only present on those samples collected from the surface of the rock. It's presence supports the hypothesis that that the fine particles collected are adhering to the surface of the rock when dew is present.

In addition, TGA analysis was able to separate the samples into three distinct groups; (1) those collected from the surface of the rock, (2) those collected from the floor within the protective

fence and surrounding area and (3) those suspected of being effected by salt leaching. These results support the hypothesis that the particulate matter adhering to the surface of the rock art is not the same as the material found within the caged area. This is significant and it supports the hypothesis that the dust-like particles adhering to the rock surface are being carried in on the breeze from an alternative location and are not a result of soil disturbance from within the protective fence area.

The colour analysis results obtained from the EFI ES-1000 also proved to be valuable and visually confirmed the presence of three distinct groups: (1) those collected from the surface of the rock, (2) those collected from the floor within the protective fence and surrounding area and (3) those suspected of being effected by salt leaching. Importantly, these are the same three groups as the TGA study showed, and this again supports the hypothesis that the dust-like particles present on the surface of the rock are not from within the protective fence but are in fact from an alternative location.

Statistically, these three groups were confirmed with the production of a dendrogram from MINITAB. Results of this also resulted in further separation with the plant material able to be distinctly separated from the soil samples collected from within the protective fence area.

This statistical analysis supports the hypothesis that the dust-like particles collected from the surface of the rock are not a result of the soil within the caged area being disturbed and adhering to the surface of the rock. The dendrogram shows that these two categories of samples vary by approximately 45% in the region studied.

It is also significant to note that statistical analysis was able to further separate the particles adhering to the surface of the rock based on the location of collection, with samples adhering to the south side of the rock able to be statistically separated to those adhering to the north. This is significant as it suggests that the particles are not uniform across the surface, and perhaps are being blown in on the wind from a number of alternate locations with varying wind direction. This requires further investigation.

With all the techniques applied showing consistent results, it is concluded that the dust-like particles that are accumulating on the surface of Arkaroo Rock in the Flinders Ranges have not resulted from the removal of plant life and construction of the boardwalk, nor a result of visitors or nature having disturbed the soil from within the caged area. Instead, the particles have travelled in on the breeze from at least one other (unknown) location and adhere to the surface of the rock when dew is present.

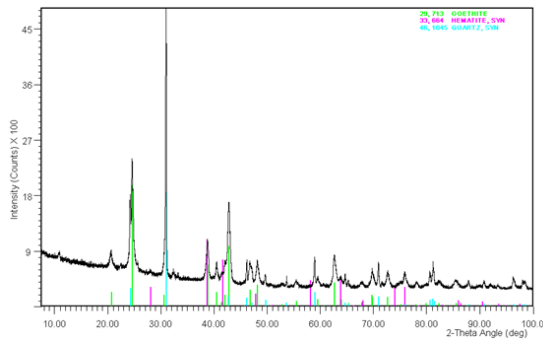




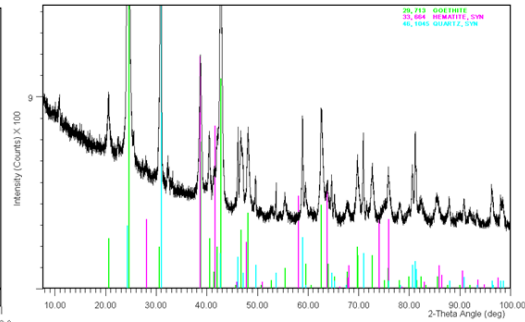
**APPENDIX C:  
SUPPORTING DATA**

### 11.1. Results of the XRD analysis of the ten mining samples

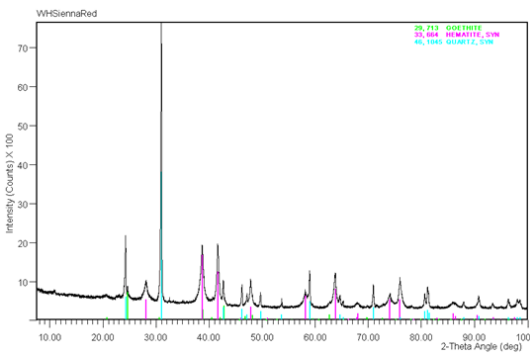
The data contained here related to work completed in section 2.4.1, where all discussion of results can be found.



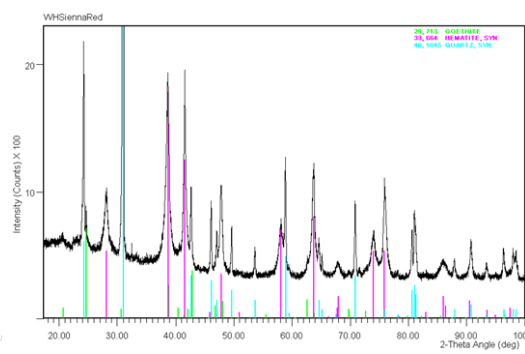
(a) Ochre 3696



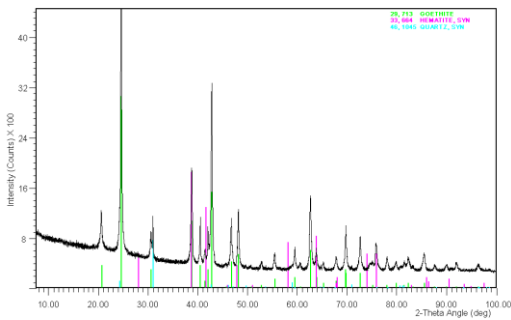
(b) Ochre 3696 low intensities



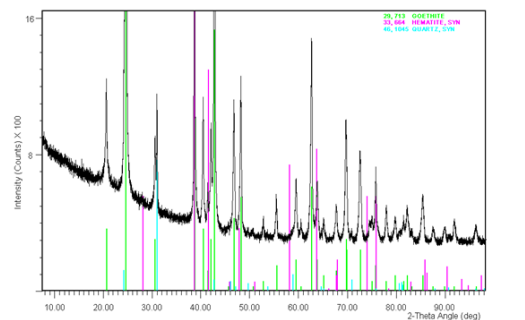
(c) Ochre 1150



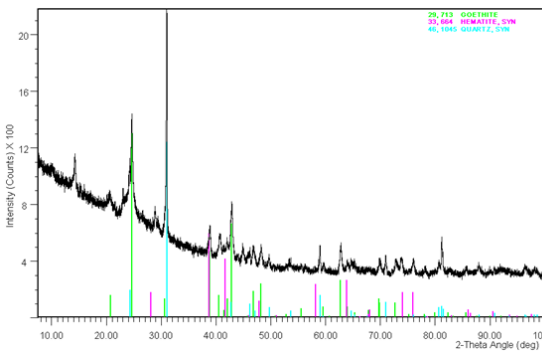
(d) Ochre 1150 low intensities



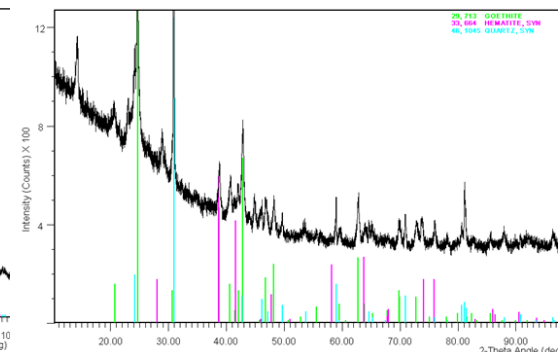
(e) Ochre 1285



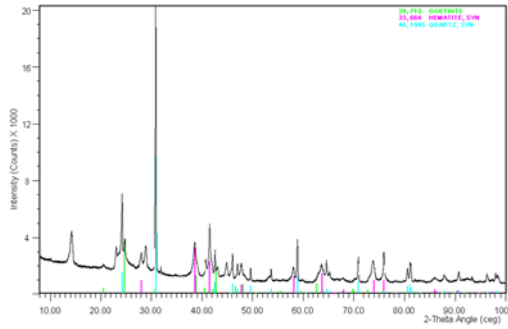
(f) Ochre 1285 low intensities



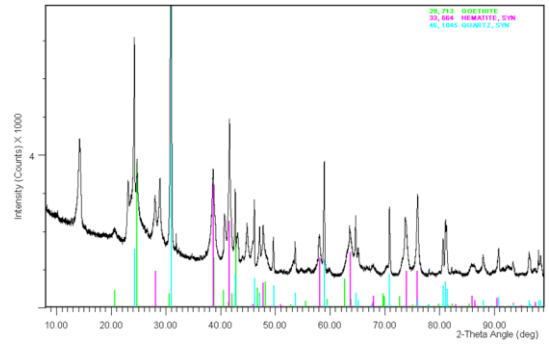
(g) Ochre 3742



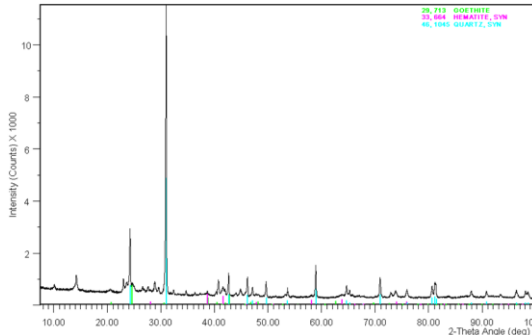
(h) Ochre 3742 low intensities



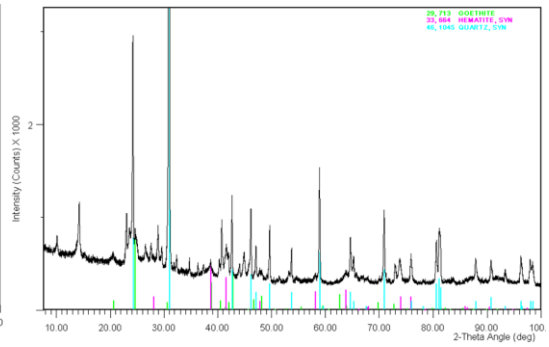
(i) Ochre 1337



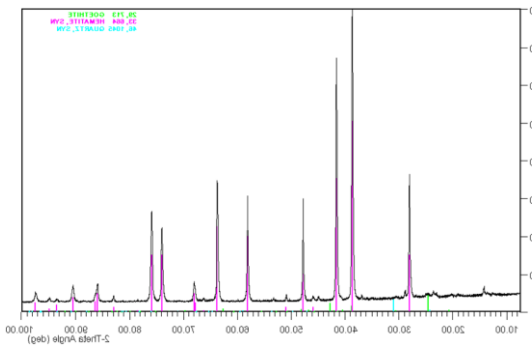
(j) Ochre 1337 low intensities



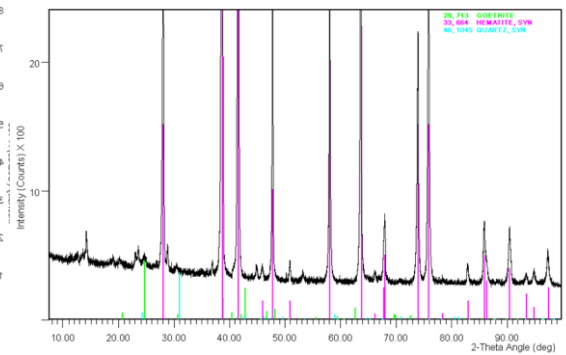
(k) Ochre 1137



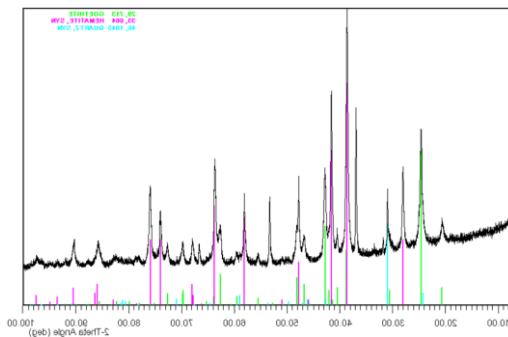
(l) Ochre 1137 low intensities



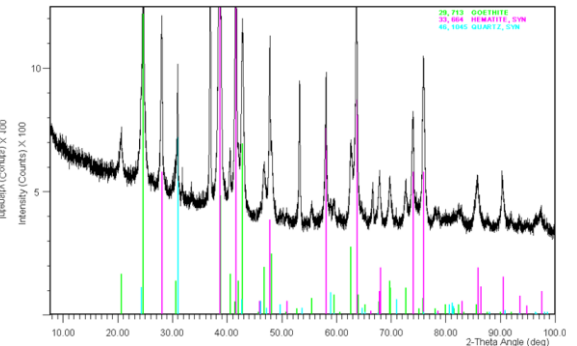
(m) Ochre 1139



(n) Ochre 1139 low intensities

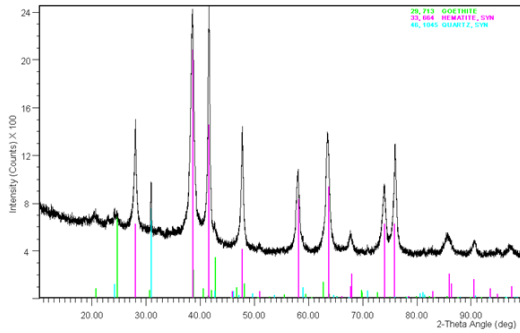


(o) Ochre 1293



(p) Ochre 1293 low intensities

APPENDIX C

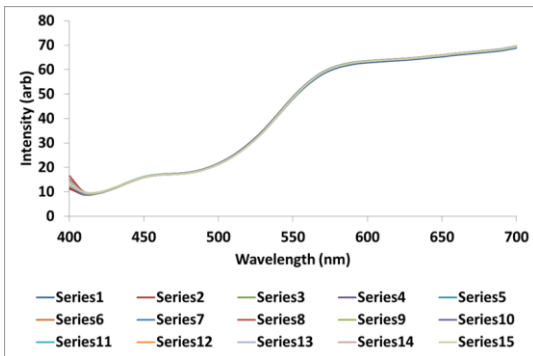


(q) Ochre 1323

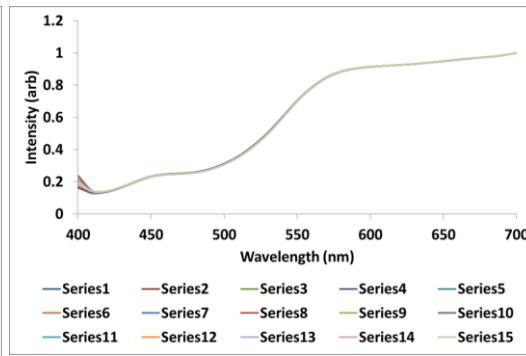
**Figure 11-1:** XRD analysis of mining sample ochres with ICDD overlap of goethite (green), haematite (purple) and quartz (blue). Samples (a) – (h) appear yellow in colour and (i) -

**11.2. Results of the analysis of the ten mining samples utilising the i1Pro, both raw and normalised**

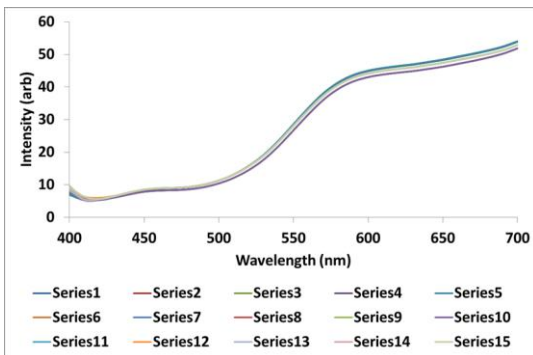
The data presented in the following spectra related to work detailed in section 3.3.2.



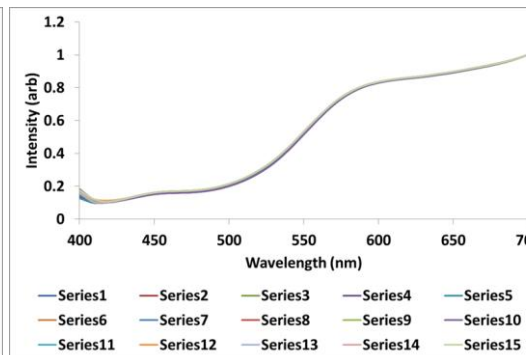
(a) Ochre 3742



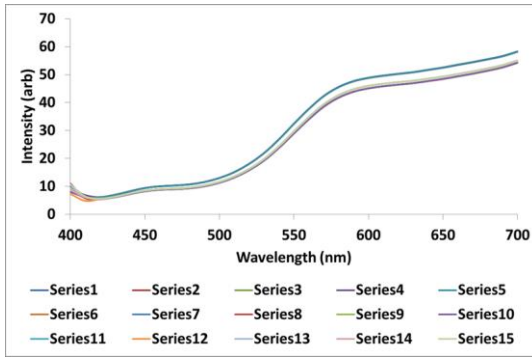
(b) Ochre 3742 normalised



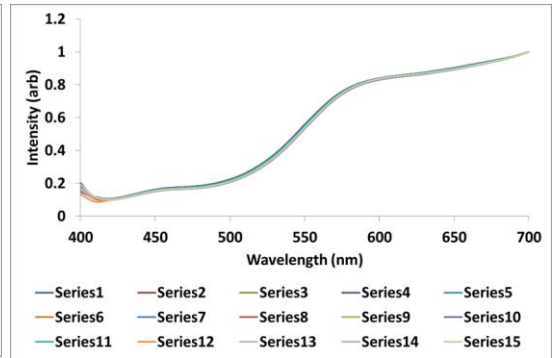
(c) Ochre 3696



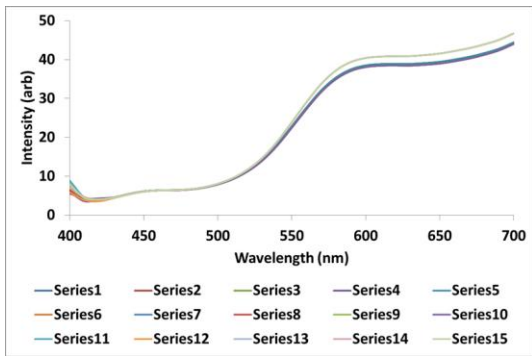
(d) Ochre 3696 normalised



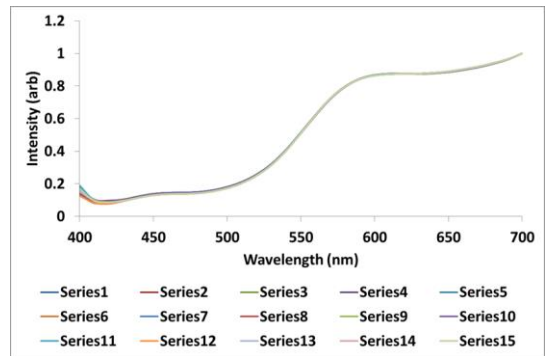
(e) Ochre 1286



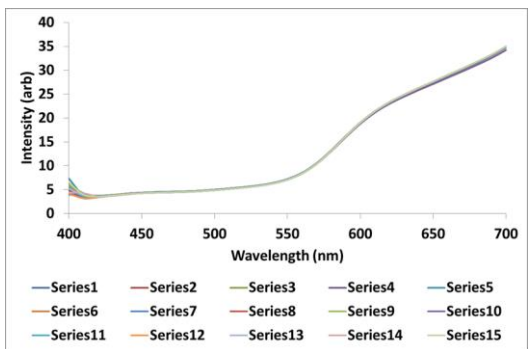
(f) Ochre 1286 normalised



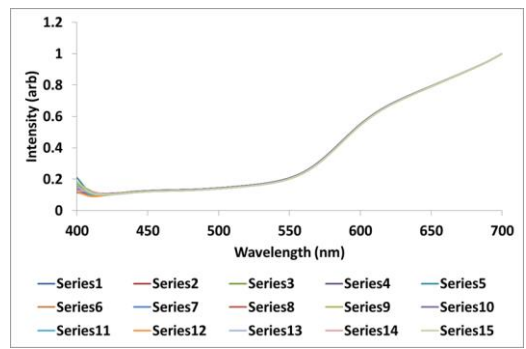
(g) Ochre 1285



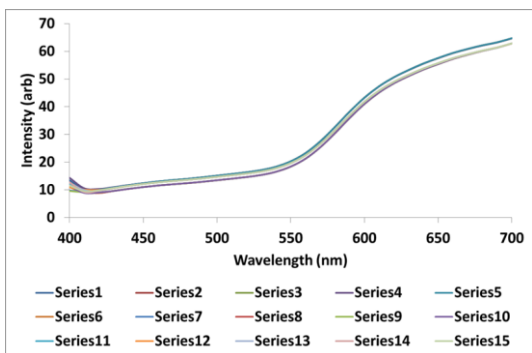
(h) Ochre 1285 normalised



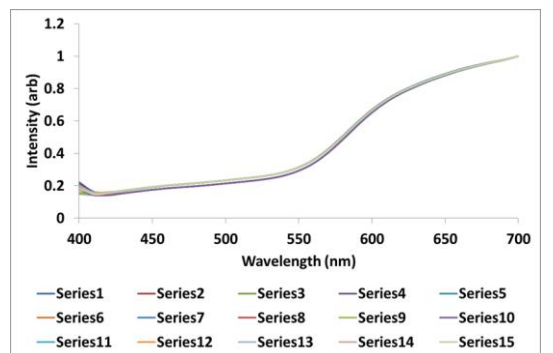
(i) Ochre 1293



(j) Ochre 1293 normalised

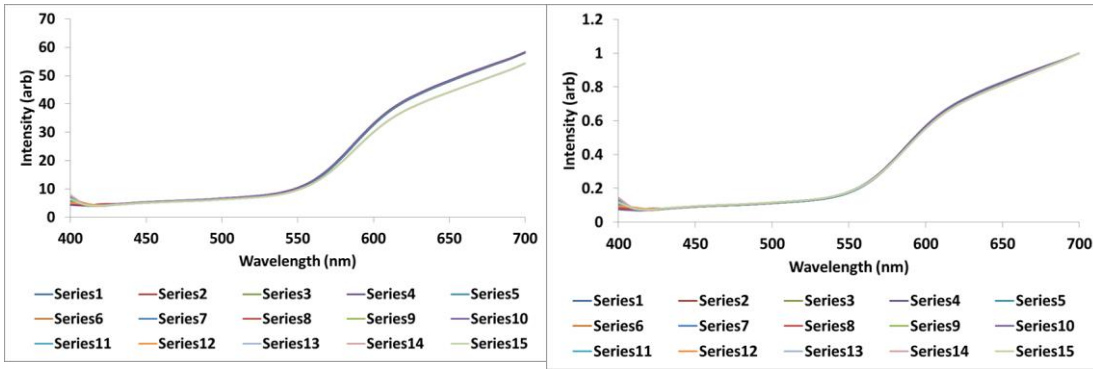


(k) Ochre 1137



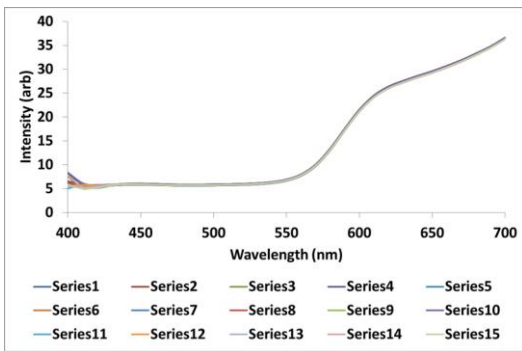
(l) Ochre 1137 normalised

APPENDIX C

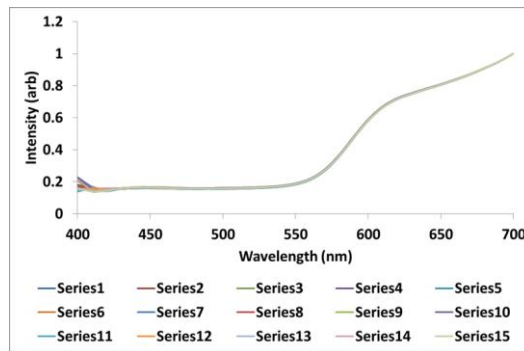


(m) Ochre 1337

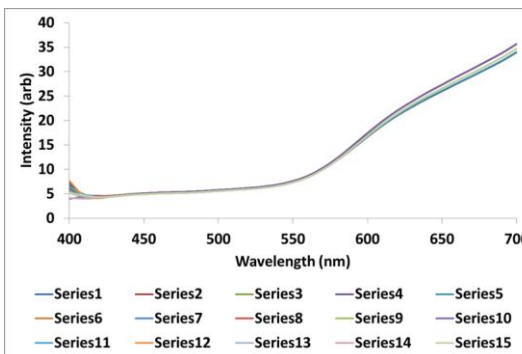
(n) Ochre 1337 normalised



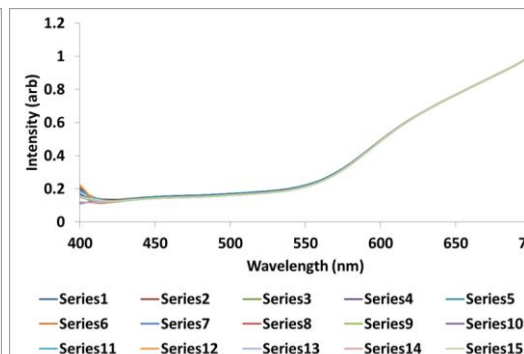
(o) Ochre 1139



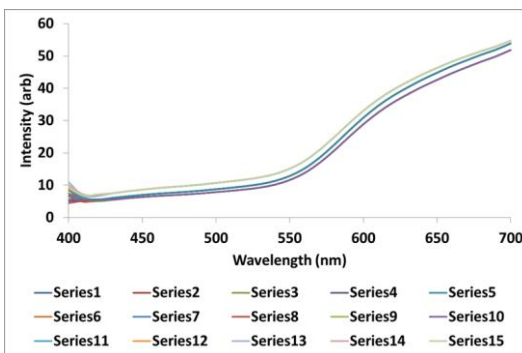
(p) Ochre 1139 normalised



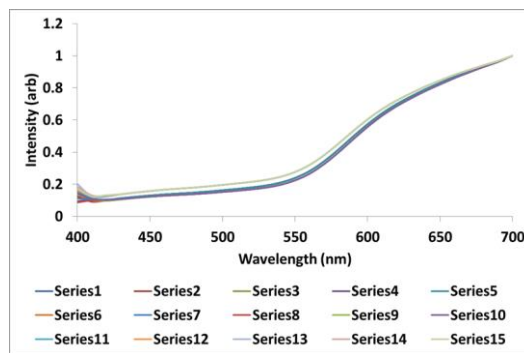
(q) Ochre 1323



(r) Ochre 1323 normalised



(s) Ochre 1150

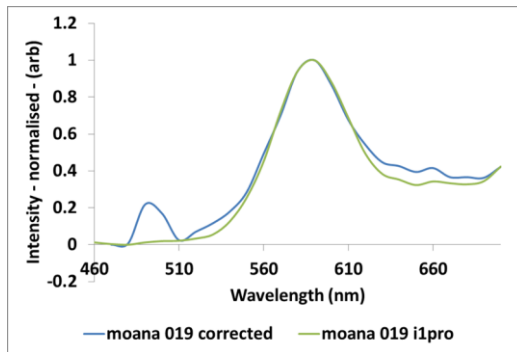


(t) Ochre 1150 normalised

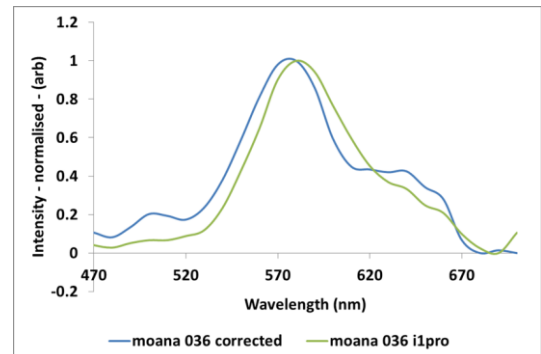
**Figure 11-2:** Results of *i1Pro* analysis of the ten mining samples measured at three spots five times consecutively.

### 11.3. Results of the analysis of Moana and Bookartoo ochres utilising both the i1Pro system and the Perkin-Elmer Lambda 950 bench top grade equipment

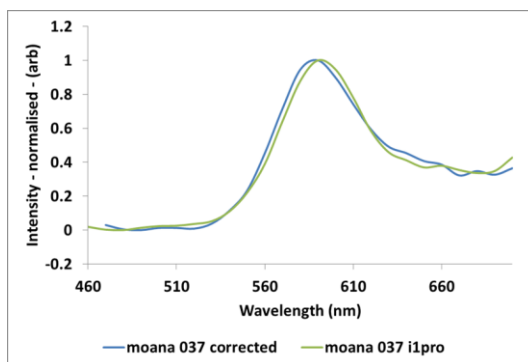
The data presented here is additional supporting data for the comparison between the i1Pro system and the Perkin-Elmer Lambda 950 bench top system. Discussion surrounding this data can be seen in section 3.3.2.



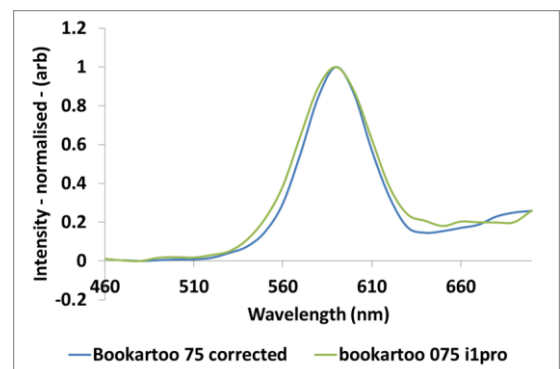
(a) Moana ochre 019



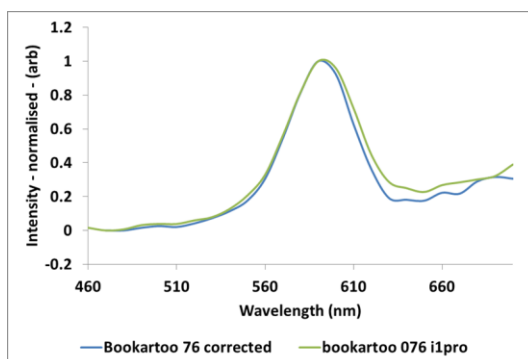
(b) Moana ochre 036



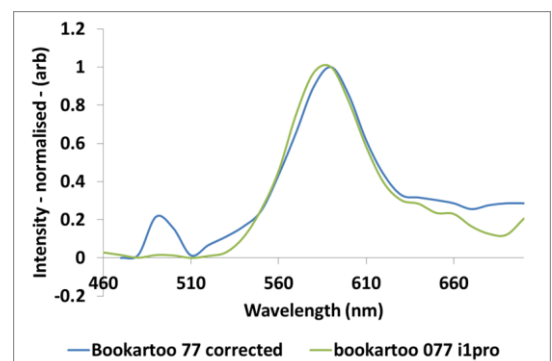
(c) Moana ochre 037



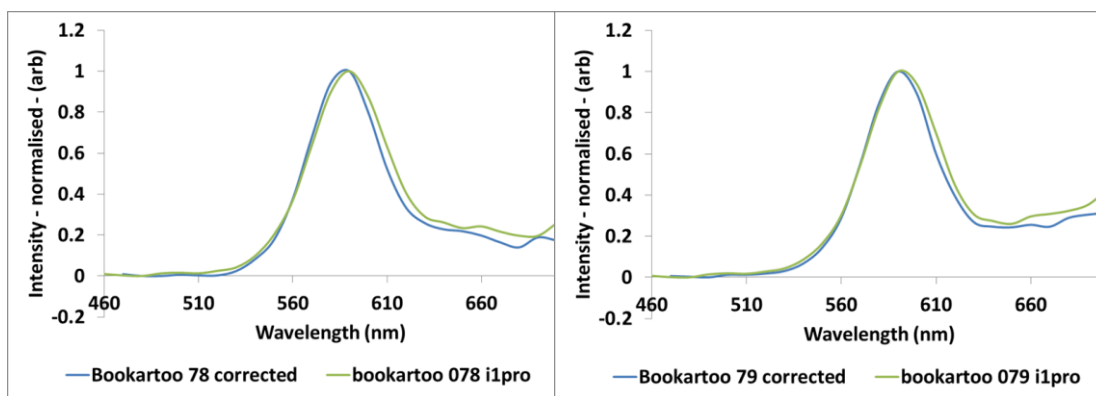
(d) Bookartoo ochre 075



(e) Bookartoo ochre 076



(f) Bookartoo ochre 077



(g) Bookartoo ochre 078

(h) Bookartoo ochre 079

**Figure 11-3 :** Comparison of the derivatives of the spectra obtained for Bookartoo and Moana ochres utilising both the i1Pro system (shown in green) and the Perkin-Elmer Lambda 950 (shown in blue).

### 11.4. Results of the analysis of the internal standards utilised in neutron activation analysis

The data contained in the following table relates to the NIST standards used in the NAA analysis experiments detailed in section 2.4.5.

**Table 11-1:** Results of NAA on the NIST internal standards.

	NIST279			NIST689		
mg/kg	Conc.	Unc.	LD	Conc.	Unc.	LD
Na	37840	1611	29.36	16250	651.1	0
Mg	2306	310.4	1142	50530	1905	1184
Al	77430	2715	47.96	92610	3246	67.34
S			113500			151700
Cl	635.6	40.7	167			162.2
Ar			18.3			18.31
K	34430	2021	3687	1597	237.9	682.5
Ca	7354	457.8	626.1	86330	3616	1335
Sc	5.221	0.1851	0.004105	37.37	1.316	0.01458
Ti	1759	159.3	751.7	6944	300.1	814.9
V	8.032	1.659	3.789	260.6	10.03	4.617
Cr	7.941	0.4066	1.079	320.9	11.73	4.14
Mn	402.4	14.19	1.799	1274	44.67	1.807
Fe	14310	505.6	60.5	70700	2479	192.6
Co	1.482	0.05836	0.0647	48.08	1.703	0.2211
Ni			10660			13900
Cu			92.09			21.23

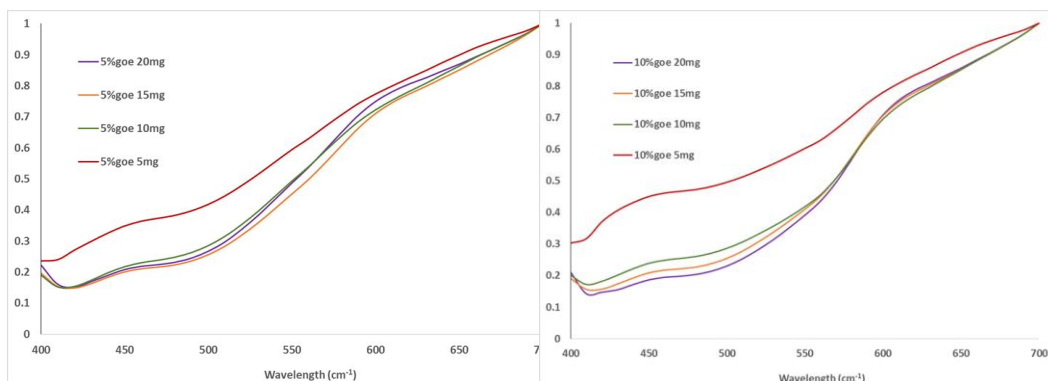


	NIST279			NIST689		
Zn	52.25	2.273	2.462	83.96	5.674	8.642
Ga			0.000753			8.93E-05
Ge			4758			6192
As	4.552	1.05	3.994			1.655
Se			1.209			3.298
Br			3.048			3.313
Rb	133.5	5.06	5.096			20.1
Sr			50.13			180.2
Y			26010			33860
Zr	353.7	19.71	95.41			420.4
Nb			5427			5031
Mo			16.67			11.11
Ru			0.7351			3.108
Rh			119.3			160.3
Pd			845.3			221.7
Ag			1.099			3.576
Cd			41.62			18.27
In			0.401			0.1528
Sn			111.6			417.6
Sb	1.441	0.06835	0.2443			0.2267
Te	4.453	0.6832	2.624			8.393
I			17.76			23.66
Cs	4.894	0.1786	0.2041			0.8519
Ba	890.7	32.19	40.37	275.2	25.86	132.2
La	31.52	1.575	0.7075	5.115	0.2067	0.185
Ce	65.82	2.329	0.5761	11.33	0.5699	2.13
Pr			120.1			46.56
Nd	26.08	1.042	1.841	7.136	1.108	6.03
Sm	5.987	0.3652	0.2286	2.076	0.08916	0.05866
Eu	0.7131	0.02537	0.0186	0.8752	0.03261	0.05825
Gd			2.264			8.017
Tb	0.9327	0.03413	0.07037	0.4623	0.04654	0.2567
Dy	6.483	0.4826	1	3.127	0.3111	1.125
Ho	94.49	21.2	3.455			1.936
Er			171.5			215
Tm	0.4854	0.06943	0.2671			0.9127
Yb	4.139	0.146	0.1646	2.113	0.08867	0.2876
Lu			35.9			43.54

	NIST279			NIST689		
<b>Hf</b>	8.312	0.3318	0.09217	1.427	0.1126	0.3307
<b>Ta</b>	1.248	0.05303	0.07809			0.3808
<b>W</b>			3.433			4.321
<b>Re</b>	0.1889	0.02669	0.1023			0.1202
<b>Os</b>			0.1518			0.5484
<b>Ir</b>			22.63			2.587
<b>Pt</b>			6.718			6.063
<b>Au</b>			0.01939			0.01214
<b>Hg</b>			0.3438			1.334
<b>Th</b>	12.29	0.4336	0.1098			0.3006
<b>U</b>			3.381			1.398

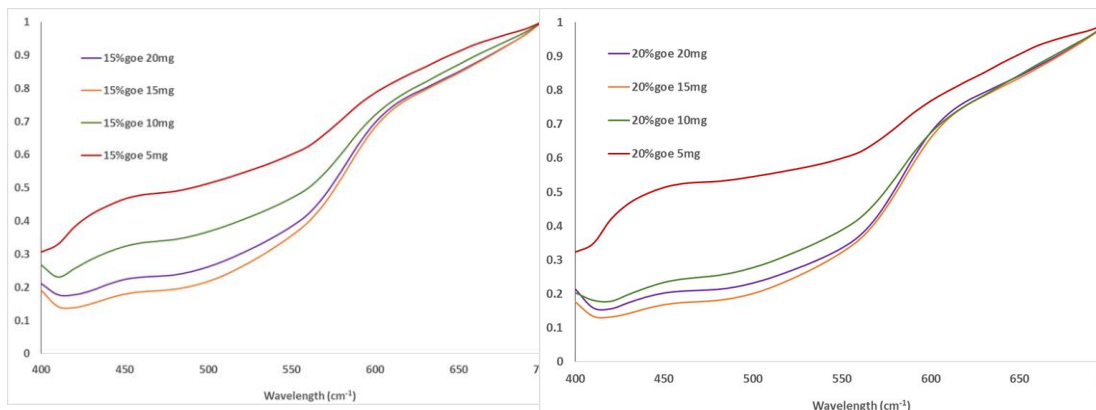
### 11.5. Visual comparisons of spectra obtained for samples of various standard compositions at four known thicknesses utilizing the i1-Pro

The data contained here is pertinent to section 3.3.3, where experimental parameters, additional data and all discussion is contained.



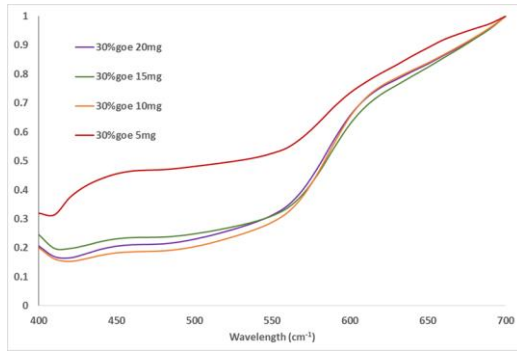
(a) 5/95% w/w goethite/haematite

(b) 10/90% w/w goethite/haematite

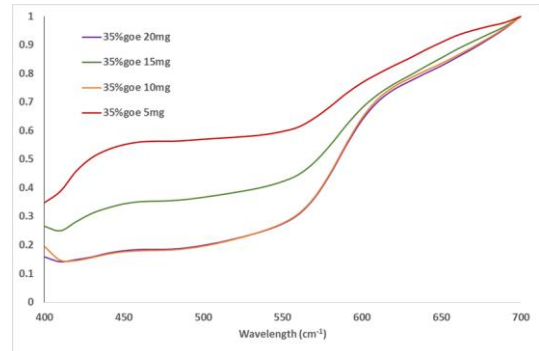


(c) 15/85% w/w goethite/haematite

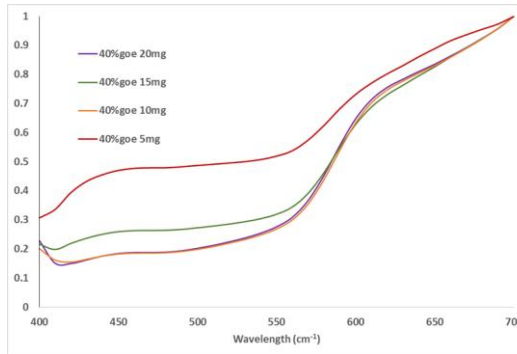
(d) 20/80% w/w goethite/haematite



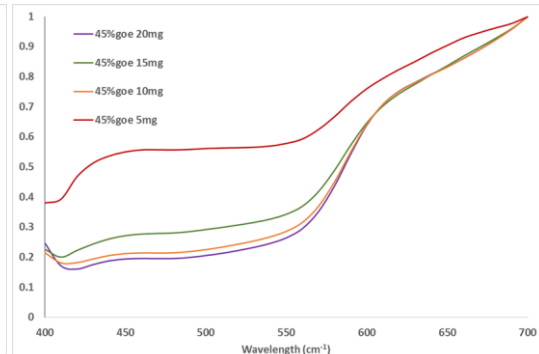
(e) 30/70% w/w goethite/haematite



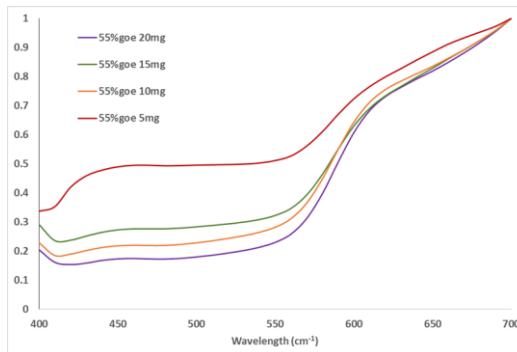
(f) 35/65% w/w goethite/haematite



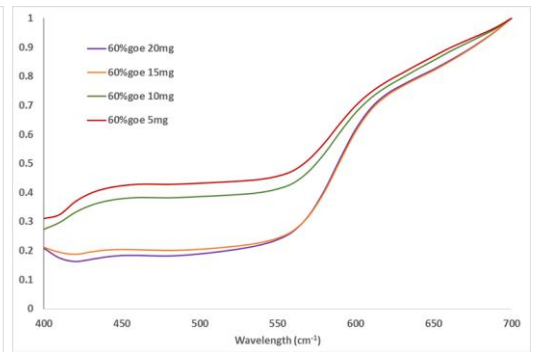
(g) 40/60% w/w goethite/haematite



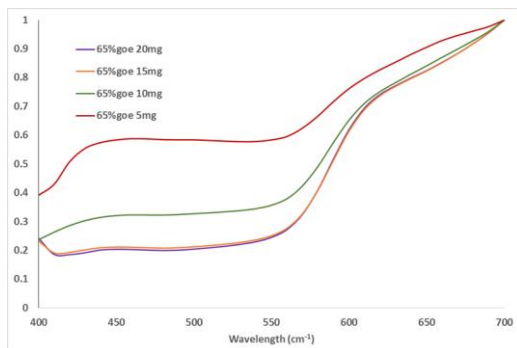
(h) 45/55% w/w goethite/haematite



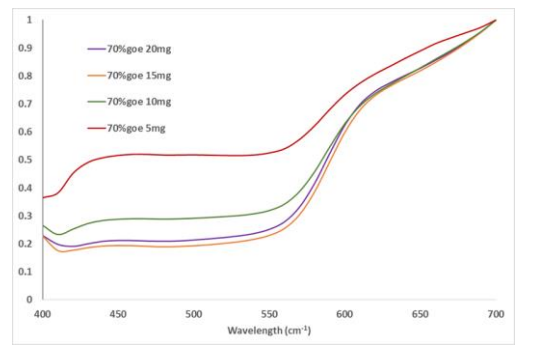
(i) 55/45% w/w goethite/haematite



(j) 60/40% w/w goethite/haematite

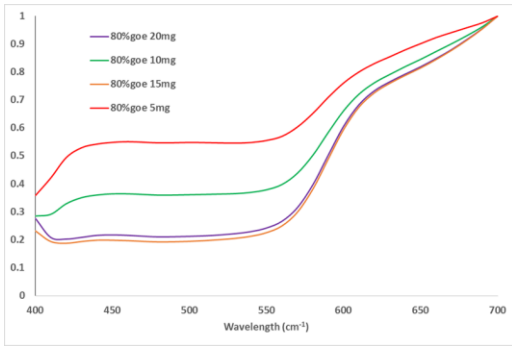


(k) 65/35% w/w goethite/haematite

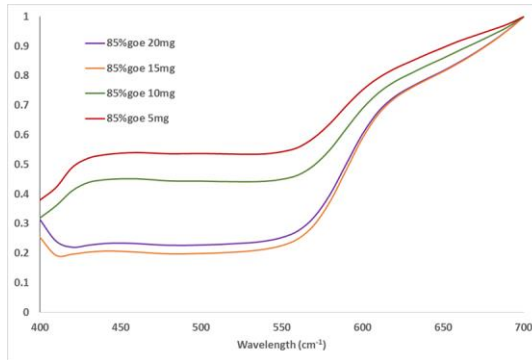


(l) 70/30% w/w goethite/haematite

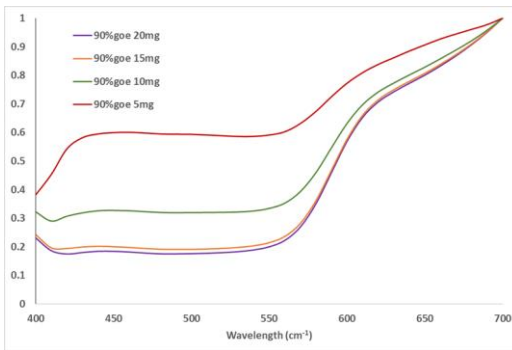
APPENDIX C



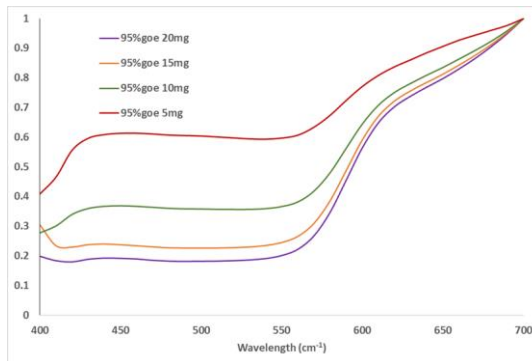
(m) 80/20% w/w goethite/haematite



(n) 85/15% w/w goethite/haematite



(o) 90/10% w/w goethite/haematite



(p) 95/5% w/w goethite/haematite

**Figure 11-4:** Results of the analysis of various composition goethite/haematite standard at four various sample thicknesses, 20mg (shown in purple), 15mg (shown in yellow), 10mg (shown in green) and 5mg (shown in red). Spectra are normalised but not derivitised.